FACULTY OF ELECTRICAL
ENGINEERING
AND COMMUNICATION

Department
of Electrical and Electronic
Technology

20th ABAF

BRNO 2019

Advanced Batteries, Accumulators and Fuel Cells

INTERNATIONAL CONFERENCE

August 25th - August 28th 2019

Organised by:

Department of Electrical and Electronic Technology,
Faculty of Electrical Engineering and Communication,
Brno University of Technology

Organizing committee:
Jiří Vondrák
Marie Sedlaříková

co-sponsored by

ISE
ECS
Shmuel De-Leon Energy Ltd

Honourary Scientific Committee:

- Petr Vanýsek, *Northern Illinois University, DeKalb, Illinois, USA*
- Jaroslav Cihlář, *FME BUT, Brno, Czech Republic*
- Arnaldo Visintin, *INIFTA, La Plata, Argentina*
- Günter Fafilek, *TU Wien, Vienna, Austria*
- Tatjana Kulova, *IPCE RAS, Moscow, Russia*
- Vito Di Noto, *University of Padova, Padova, Italy*
- Alexei Kornyshev, *Imperial College, London, UK*
- Boris Markovsky, *Bar-Ilan University, Tel Aviv, Israel*
- Philipp Adelhelm, *Friedrich Schiller University, Jena, Germany*
- Laurence Hardwick, *University of Liverpool, Liverpool, UK*
- Renata Oriňáková, *UPJŠ, Košice, Slovakia*
- Grzegorz Lota, *Poznan University of Technology, Poznan, Poland*
- Mariusz Walkowiak, *Institute of Non-Ferrous Metals, Poznan, Poland*

Organisation Committee:

- Marie Sedlaříková, *FEEC BUT, Brno, Czech Republic*
- Tomáš Kazda, *FEEC BUT, Brno, Czech Republic*
- František Klein, Brno, *Czech Republic*
- Vítězslav Novák, *FEEC BUT, Brno, Czech Republic*
- Miroslav Zatloukal, *FEEC BUT, Brno, Czech Republic*
- Lucie Šimonová, *FEEC BUT, Brno, Czech Republic*
- Jiří Libich, *FEEC BUT, Brno, Czech Republic*
- Josef Máca, *FEEC BUT, Brno, Czech Republic*
- Tomáš Binar, *University of Defence, Brno, Czech Republic*
- Jiří Švarc, *University of Defence, Brno, Czech Republic*

Program Committee:

- Marie Sedlaříková, *FEEC BUT, Brno, Czech Republic*
- Mariusz Walkowiak, *Institute of Non-Ferrous Metals, Poznan, Poland*
- Arnaldo Visintin, *INIFTA, La Plata, Argentina*
- Petr Vanýsek, *Northern Illinois University, DeKalb, Illinois, USA*
- Günter Fafilek, *TU Wien, Vienna, Austria*
- Boris Markovsky, *Bar-Ilan University, Tel Aviv, Israel*
- Tatjana Kulova, *IPCE RAS, Moscow, Russia*
- Alexei Kornyshev, *Imperial College, London, UK*
- Philipp Adelhelm, *Friedrich Schiller University, Jena, Germany*
- Laurence Hardwick, *University of Liverpool, Liverpool, UK*
- Josef Máca, *FEEC BUT, Brno, Czech Republic*
- Vítězslav Novák, *FEEC BUT, Brno, Czech Republic*
- Petr Bača, *FEEC BUT, Brno, Czech Republic*
- Tomáš Kazda, *FEEC BUT, Brno, Czech Republic*
- Helena Polsterová, *FEEC BUT, Brno, Czech Republic*
- Miroslav Zatloukal, *FEEC BUT, Brno, Czech Republic*
- Andrea Fedorková-Straková, *UPJŠ, Košice, Slovakia*
- Jiří Libich, *FEEC BUT, Brno, Czech Republic*
- Jiří Tichý, *FEEC BUT, Brno, Czech Republic*
- Tomáš Binar, *University of Defence, Brno, Czech Republic*
- Jiří Švarc, *University of Defence, Brno, Czech Republic*

ISBN 978-80-214-5774-4

Contents

Lithium batteries and related systems

Supercapacitors

Fuel Cells

Aqueous Batteries

New systems of Batteries

Photovoltaics

Other Technology, Applications and Simulations

We would like to express our thanks to the Brno University of Technology, Faculty of Electrical Engineering and Communication for support and help with organising 20th ABAF conference.

Structural and Electrochemical Aspects of Ni-Rich Electrodes for Lithium-Ion Batteries

B. Markovsky[a], S. Francis Amalraj[a], J. Liu[b], L. Burstein[c], M. Dixit[a], D. Kovacheva[d],
Y. Grinblat[a], M. Talianker[e], O. Haik[a], A. I. Frenkel[f], D. T. Major[a], and D. Aurbach[a]

[a]Department of Chemistry, Bar-Ilan University, Ramat-Gan 52900, Israel

[b]Department of Physics, Manhattan College, Riverdale, New York 10471, United States

[c]The Wolfson Applied Materials Research Centre, Tel-Aviv University, Tel-Aviv 69978

[d]Institute of General and Inorganic Chemistry, Academy of Sciences, Sofia 1113, Bulgaria

[e]Department of Materials Engineering, Ben-Gurion University of the Negev,
Beer-Sheva 84105, Israel

[f]Department of Materials Science and Chemical Engineering, Stony Brook University,
Stony Brook, New York 11794, United State

The most promising cathode materials for lithium ion batteries (LIBs) are the lithium intercalation transition metal oxides of layered structure (*R-3m*), $Li[Ni_xCo_yMn_z]O_2$ (x+y+z=1) (NCM). NCM materials can exhibit specific capacity > 200 $mAhg^{-1}$ at Ni-content of ≥80 %. They can also demonstrate high rate capability and may reach relatively low costs (1). However, these materials have disadvantages like low electronic and ionic conductivities and structural instability; their capacity also decays fast upon cycling (2). In this presentation, we summarize our recent studies of $Li[Ni_xCo_yMn_z]O_2$ for electrodes of LIBs. We focus on a family of Ni-rich (x=0.5 – 0.8) materials with various content of Co and Mn. The main questions studied were lattice doping with Al^{3+}, Zr^{4+} and Mo^{6+} cations of the above materials in relation to the electrode behavior, structural stability, electronic properties, and thermal reactions with battery solutions. We elucidated also possible structural transformations of these electrode materials upon Li-intercalation/deintercalation.

Results and Discussion

For $LiNi_{0.5}Co_{0.2}Mn_{0.3}O_2$ lithiated oxides (NCM523), using density functional theory calculations, we have shown that aluminum doping is preferred at Ni sites over Co sites, and the thermodynamic preference for Al^{3+} doping follows the order: Ni>Co>Mn (3). The lower capacity fading of the Al-doped electrodes upon cycling and aging in a charged state (4.3 V) at 60 ^{0}C, as well as lower resistances of the surface film and charge-transfer are likely related to the chemical and structural modifications of the electrode/solution interface. It was concluded from XPS studies that the modified stable and less resistive interface on the Al-doped particles comprised the Li^+-ion conducting centers like $LiAlO_2$, AlF_3, etc., which promote, to some extent, the Li^+ transport to the bulk and therefore facilitate the electrochemical reactions. In molybdenum doped $LiNi_{0.5}Co_{0.2}Mn_{0.3}O_2$ (1 mol.% Mo^{6+}) materials Mo replaces Ni-ions at *3b* sites and even *minor* Mo-doping increases the amount of Ni^{2+} ions in NCM523 at the cost of Ni^{3+} ions, due to charge compensation (4). Analysis of both Ni K-edge EXAFS and XANES data and DFT calculations led us to a conclusion that doping affects Ni oxidation states and Ni-O bond lengths. These findings are consistent with a model of partial substitution of Ni by Mo^{6+}. Further, an important finding is that the dopant tends to segregate at the surface, a phenomenon we established for the first time in NCM523 materials (4). We established lower capacity fading of Mo-doped electrodes during cycling to 4.3 V and to higher cut-off potentials of 4.4 - 4.6 V both at 30^0C and at the elevated temperature of 45^0C. It was shown that Mo-doped electrodes exhibited ~20 – 30% higher rate capability at 1C – 4C rates, which may be attributed to faster kinetics of these cathode materials. This was confirmed, in particular, by analysis of the charge-transfer resistance values calculated from impedance spectra of undoped and doped electrodes during consecutive cycling (up to 100 cycles). This kinetic parameter was shown to increase rapidly with cycling of undoped electrodes, whereas it changed only slightly for Mo-doped ones. This can be ascribed to the modified stable interface comprising segregated Mo^{6+} ions. Indirect evidence of the modified interface was also obtained from studies of thermal behaviour of NCM523 materials. They allow us to approve that NCM523 Mo-doped samples demonstrate ~2 times lower total heat evolved in reactions with EC-EMC/$LiPF_6$ battery solution (Q_t=116 Jg^{-1}) in comparison with the undoped ones (Q_t=210 Jg^{-1}). This reduced heat evolution implies less interactions with the solution species such as trace H_2O, PF_5, HF (contaminants related to $LiPF_6$) and the alkyl carbonate solvents in the temperature range of 30 – 300^0C. By analyzing the nano-beam electron diffraction patterns of several individual particles of the cycled NCM523 electrode materials, we established that both undoped and Mo-doped samples form cubic spinel phases. These were detected in discharged and charged electrodes and are likely $Li(TM)_2O_4$ or delithiated Mn_2O_4, respectively. The above partial structural layered-to-spinel transformation was detected mainly at the periphery of the grains and it progresses towards the bulk of the particles. Surface sensitive XPS studies of cycled Mo-doped electrodes terminated in a discharged state, revealed presence of Mo^{5+} ions in addition to Mo^{6+}. This fact can be ascribed to Mo^{6+} reduction related to electrode cycling and agrees with the DFT calculations, which showed Molybdenum conduction band states located near the Fermi level. In a combined computational and experimental study, we have established that Zr-doped $LiNi_{0.6}Co_{0.2}Mn_{0.3}Zr_xO_2$ electrodes possess faster electrochemical kinetics, much lower surface film and charge-transfer resistances measured from impedance spectra in the potential range of 3.7–4.3 V (5). These electrodes also exhibited higher discharge capacities during cycling at 45^0C, especially at high rates.

We synthesized a family of five high Ni-rich oxides $LiNi_{0.80-x}Mo_xCo_{0.1}Mn_{0.1-y}O_2$ (x=0.01 – 0.03; y=0.01), in which Ni or both Ni and Mn were partially substituted with a minor amount of the molybdenum Mo^{6+}-dopant. From the Rietveld refinement analysis of XRD patterns of 1 mol. % doped sample $LiNi_{0.79}Mo_{0.01}Co_{0.1}Mn_{0.1}O_2$, it was concluded that two models provide similar results for the Mo-ions residing either in the Li-layer or occupying the transition metal sites (6). In contrast, for the dopant content of 3 mol. %, we concluded that Mo ions more likely occupy the 3*b* position (lithium layer) in the crystal structure. DFT calculations revealed that Mo^{6+} cations preferably substitute Ni in the oxide structure due to the lowest substitution energy compared to Li, Co, and Mn. This conclusion agrees with the relatively low crystallographic mismatch between ionic radii of Ni-host (rNi^{2+}=69 pm) and Mo-guest (rMo^{6+}=59 pm). Analysis of the unit cell parameters *a* and *c* of the undoped and Mo-doped materials that increase with increasing the substituting level, allowed us to conclude on a successful incorporation of the dopant into the lattice. This was supported by the calculated values of the radial distribution functions for "TM(3a) – Oxygen" and "Li(3b) – Oxygen" distances in NCM811 materials that clearly show the increased bond lengths for the Mo-doped samples. It was shown that Mo-doped electrodes exhibited much lower the irreversible capacity loss in the 1-st cycle and lower the remaining currents developed during the potentiostatic steps followed the initial charging to 4.3 V. We concluded therefore on the formation of a more stable electrode/solution interface and lesser side reactions of doped materials with the solution species. This is evident also from lower the charge-transfer resistance of the above electrodes as well as from decreased the total heat evolved during chemical reactions of undoped and 1% Mo-doped materials (433 Jg^{-1} and 299 Jg^{-1}, respectively) with the battery solutions, similarly to doped NCM523 electrodes (4). The above findings correlate well with the segregation of transition metals and the Mo-dopant at the surface (15 – 20 Å) established experimentally, for the first time, in the above Ni-rich materials. We have demonstrated that doped electrodes exhibited higher by 12 – 20% discharge capacities compared to undoped ones, especially at high rates of 4C. This is in agreement with our previous results for Zr and Mo-doped NCM622 and NCM523 electrodes, respectively. It was shown also that Mo-doped NCM811 electrodes demonstrated higher capacity retention and lower the voltage hysteresis during cycling at 30 and 45^0C. The results of the electrochemical studies were attributed to the fact that incorporation of highly-charged Mo^{6+} dopant leads to the re-distribution of charge among transition metal cations resulting in decreasing the relative number of Ni^{3+} ions and increasing the number of Ni^{2+} ions and electrochemically active Ni^{2+}/Ni^{3+} redox couples responsible mainly for the electrode capacity. The above materials are structurally stable since the initial rhombohedral *R-3m* structure was mainly preserved upon cycling of both the undoped and doped samples. However, it was suggested the formation of a cubic spinel phase detected by electron diffraction on a few selected particles of cycled electrodes, due to the layered-to-spinel transition in agreement with the literature data.

To summarize, in this study we address questions related to structural, surface, electronic characteristics, and electrochemical performance of undoped and doped $Li[Ni_xCo_yMn_z]O_2$ cathodes. We conclude that doping of these cathode materials with the highly charged cations (Zr^{4+}, Mo^{6+} even at a *minute* level) is a promising path towards enhanced electrochemical activity in advanced lithium-ion batteries.

References

1. H. H. Ryu et al., *Chem. Mater.,* **30**, 1155–1163 (2018).
2. W. Liu et al., Angew. Chemie Int. Ed., **54**, 4440–4457 (2015).
3. M. Dixit et al., J. Electrochem. Soc., **164 (1)** A6359-A6365 (2017).
4. O. Breur et al., ACS Appl. Mater. Interfaces, **10**, 29608−29621(2018).
5. F. Schipper et al., J. Mater. Chem. A, **4**, 16073 (2016).
6. F.S. Amalraj et al., ACS Appl. Energy Mater., **2**, 4521−453 (2019).

Innovating Binder Free Silicon Based Electrode is Promising Anode for Stable and Safer Lithium-Sulfur Batteries.
Technology & Equipment for production. Electrochemical Properties. Electromagnetic Non-Destructive testing

Elena Shembel[a,b] , Volodymyr Redko[a], Timothy Pastushkin[a], Alexander Markevych[b],
Andrea Straková Fedorková[c], Volodymyr Khandetskyy[a]

[a] Enerize Corporation, Coral Springs, FL, 33067,USA

[b] Scientific-Research Laboratory of Chemical Power Sources, Ukrainian State
University of Chemical Technology, Dnipro, 49005, Ukraine

[c] Pavol Jozef Safarik University, Kocice, SK-04154, Slovak Republic

Electrode based on the composition of silicon and graphite is very attractive for battery with cathode based on sulfur. Both electrodes: based on silicon for negative electrode and based on sulfur for positive electrode have high level of energies. As result the materials balance for Si – S battery is more promising than, for example, for Si – LiCoO2 battery. As compare with the Li-S battery system Si - S is also greatly promising, because Si based anode don't generate the dendrites during cycling, is safe and environmentally friendly unlike from Li. However the problem to using the Si based anode is connected with destruction the Si based anode during cycling. For avoid these problem we developed advantaged process of the Gas Detonation Deposition (GDD) [1]

Introduction

The Gas Detonation Deposition (GDD) Process for fabricating the silicon & graphite composition on the current collector has numerous advantages [1], including:

1. High adhesion of deposited layer of Si-Graphite composition to substrate of the current collector
2. Ability to vary the GDD process parameters and obtain the layers of Silicon - graphite possessing the required properties
3. Low cost, low power-consumption, high throughput of GDD equipment, and, as a result, low cost of the fabricated layers
4. Control of deposition layer for various thickness depending on application - from a few microns to a few millimetres
5. Increasing safety during battery cycling due to the absence of dendrite formation and cathode/anode short circuits

In the current abstract are presented also the following information:

1. Structure of the composite silicon-graphite layer of the positive electrode

2. Galvanostatic characteristics of the binder free positive electrode based on the composition silicon and graphite.

More detailed information will be presented in our speech during ABAF Conference

Experimental

Following methods have been used for investigation the binder free composition of silicon and graphite, which produced by method GDD: Scanning Electron Microscope "Vega3" (Tescan) for evaluation the structure of silicon-graphite composition Electromagnetic impedance testing for non-contact non-destructive evaluation of the interface resistance between current corrector and the binder free composition of the silicon & graphite. Electrochemical investigation, including the impedance and galvanostatic cycling have been realizing using the VoltaLab PGZ 301. As electrolyte the EC:DMC (1:1), 1M $LiClO_4$ has been used.

Results and its discussion

Structure of the composite silicon-graphite layer of positive electrode is presented on the Figure 1

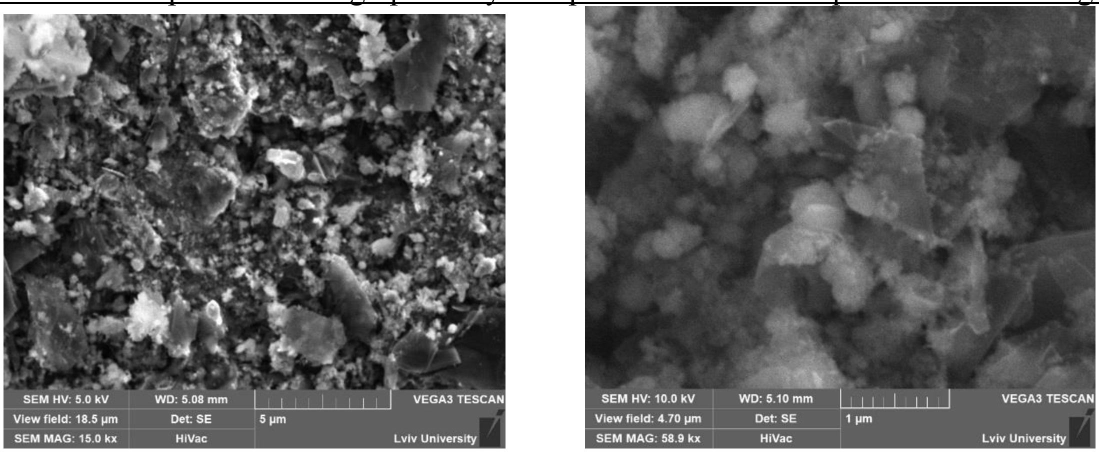

Figure 1. *Scanning electron microscopy of the surface of a silicon-graphite electrode. A: Magnification 30,000. B: Magnification 80,000*

The structure of the composite silicon-graphite layer contains micron, submicron, and nanosized particles of silicon.

The results of a study of the structure of the silicon-graphite composite obtained by SDD confirm that this structure includes graphene. The presence of graphene provides unique properties of an electrode based on a silicon-graphite composite: high electrochemical characteristics, structural stability during cycling, high adhesion to a metal current lead, and high cohesion between silicon and graphite particles in the electrode layer.

Galvanostatic characteristics of the binder free positive electrode that is based on the composition the silicon and graphite

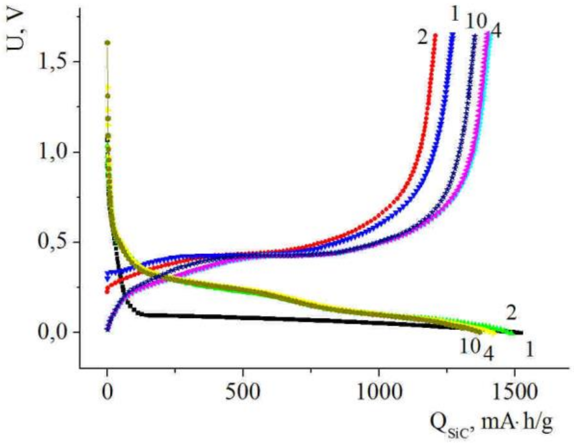

Figure 2. *Charge-discharge curves of electrode No. 210. The current of the cycling is 0.1 C (0.19 mA). Figures on curves - cycle numbers. Electrode size is 1,5 x 1,5 cm*

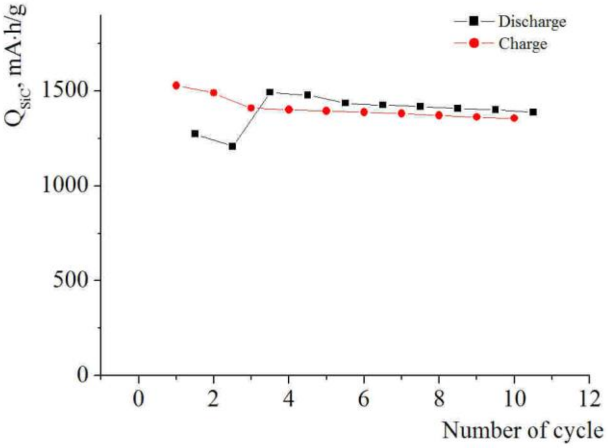

Figure 3. *The dynamics of changes in the charging and discharge capacity for electrode No. 210 in the process of cycling*

Presented results confirm, that

1. The film of binder free silicon & graphite compositions that produced using the Gas Detonation Deposition (GDD) Process has a nanostructure
2. Discharge capacity during cycling has high level that is near 1500 mA.h/g
3. High efficiency of binder free silicon based electrode is realizing due to the high level of adhesion between the electrode layer and current collector and due to the high level of cohesion between silicon and graphite particles.

More detailed following information will be presented during our speech in ABAF Conference:

1. Advantages Gas Detonation Deposition (GDD) Process. Perspective the scaling up the process fabrication the binder free silicon based electrodes
2. Interface resistant between the film of composition the silicon & graphite and various types of the current collectors. This resistance have been tested using the innovating

electromagnetic impedance non-destructive non-contact method. These evaluations were conducted under different frequencies of the magnetic field. [2]

3. Dynamic the changing impedance of binder free silicon based electrodes, and the impedance of the cell based on Silicon negative electrode – Sulfur based positive electrodes
4. Results of the galvanostatic cycling of high energy cell that is based on the Silicon & graphite negative electrode – Sulfur positive electrode

Acknowledgments

This investigations have been carried out in cooperation of Company Enerize Corporation, USA, and the SRLCPS of USUCT, Ukraine. Investigation and tested have been done also under framework of NATO SPS 985148 project "Development of New Cathodes for Stable and Safer Lithium-Sulfur Batteries"/ Science for Peace and Security Programme. Enerize Corporation is industrial partner under NATO SPS 985148 project. Prof. E. Shembel is the Head of SRLCPS USUCT and Partner country-Ukraine Director of this NATO project

References

1. E. Shembel, ; N Klyui (Kliui); I. Maksyuta etc *US Patent Appliation* No.068480 (2011)
2. V. Redko, V. Khanderskyy, E. Shembel, etc. *US Patent* No.7,982,457.(2011)
3. V. Redko, E. Shembel, T. Pastushkin, A. Markevych, A. Straková Fedorková, O. Girin, O. Kolomoyets, Yu. Polishchuk. *ECS Transactions*, 87 (1) (2018).

Strategies to improve Lithium Sulfur batteries performance

S. Bodoardo, C. Francia, J. Amici, U. Zubair, D. Versaci, and M. Alidoost

[a] Department of Applied Science and Technology, Politecnico di Torino, c.so Duca degli Abruzzi 24, 10129 Torino, Italy

Lithium sulfur batteries are promising very high theoretical energy density which can change the performance of batteries for automotive applications. Unfortunately, Sulfur cathodes encounter many issues mainly arising because of the low conductivity of Sulfur, the solubility of polysulfide intermediates, shuttling of dissolved polysulfides. Here some strategies to overcome these issues are presented and are mainly based on the use of oxides and conductive layers to trap polysulfides highly increasing the capacity and the cycle life of LiS cells.

Introduction

Lithium ion battery (LIB) is the most widely employed energy storage technology for portable devices and a few electrical vehicles.

Energy density of LIBs is practically limited to 250-300Wh/kg at pack level. In this respect, sulfur is emerged as a promising cathode material to outperform LIB cathodes in terms of availability, sustainability, cost and theoretical specific capacity (1672mA h/g).

Sulfur cathodes encounter lower sulfur utilization, low Coulombic efficiency, fast capacity decay and narrow cycle life. These limitations mainly arise because of the low conductivity of S8 (5 Å~ 10−18 S cm−1), the solubility of polysulfide intermediates, shuttling of dissolved polysulfides, and a general lack of morphological restoration of the sulphur-containing host material during long term cycling. Several methodologies were proposed to make sulfur, Li2S and LiPS available for electrochemical reactions in a stable, efficient and reversible manner. The first innovation for the Li-S system focused on engineering the design of the cathode host materials, where sulfur is typically embedded into ionically and electrically conductive matrices such as porous graphitic carbons. Carbon matrices are lightweight, conductive and provide the scaffold to fix the reaction products, prevent shuttling while making sulphur accessible to electrochemical reactions for charging and discharging. The most commonly reported carbon matrices are microporous, mesoporous carbons, carbon nanotubes and arrangements of graphene.

Metal oxides can interact with LiPS via chemisorption, acid-base interactions, or form a surface bound active redox mediators that mimic spatially localized impregnation approaches into porous carbons.

In this work, we demonstrate multiple integrated design strategies to form a cost effective and sustainable sulfur-containing electrode of carbon and Magnéli phase TinO2n-1, that offers exceptional long life and good rate performance with high sulphur loading for Li-S batteries. Electrically conductive Magnéli phase TinO2n-1 nanoparticle-loaded carbon matrices (TinO2n-1@C/S) were synthesized by simple heat treatment of the mixture of TiO2 nanotubes and polyvinyl alcohol (PVA) at 1000 °C in inert environment. Carbon from PVA enables carbothermal reduction of TiO2 to several TinO2n-1 Magnéli phases, which have a chemical binding affinity for LiPS. The approach also suppresses the sintering and grain growth in TinO2n-1 nanoparticles ensuring high surface area for LiPS docking that mitigates shuttling effect for a high capacity.

A second strategy consists on a simple and novel one-pot synthetic strategy to accomplish vanadium oxide nitride (VOxNy) nanoparticles in nitrogen reduced graphene aerogel (VONNG) via concurrent in-situ nitridation and carbonization processes. Metal oxide nitride particles have been achieved without involving external ammonia source. For the purpose, polycondensation reactions involved in accomplishment of C3N4 have been exploited to generate on-site active nitrogen species to realize porous vanadium oxide nitride nanoscales particles in nitrogen doped rGO aerogel. Remarkable performances have been observed using VONNG as host material for sulfur cathodes that can be attributed to the interface between V-O and V-N linkages to offer stronger binding interaction and fast electrocatalytical conversion of LiPS. The interaction mechanism between VONNG and LiPS has been probed by in-operando Raman spectroscopy, XPS and electrochemical methods. By modifying the chemical environment of vanadium oxide, we are enabling to tune the redox potential to facilitate thiosulfate formation that in turn form polythionate complexes to limit LiPS shuttle. Secondly, the V-N linkage offer an opportunity to improve the kinetics of the redox reactions along with strong binding interactions.

Other strategies are also presented including the use of use of C3N4 based layers.

Results and discussion

As a first example here the results achieved on the insertion of titanium oxides in the Magneli phase are here reported.

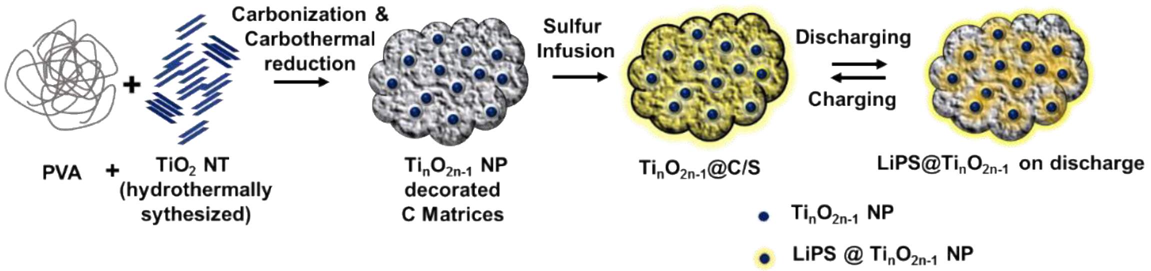

Figure 1. *Schematic illustration of the synthesis strategy for carbothermal reduction of TiO2 nanotubes to Magnéli phase TinO2n-1 nanoparticle-embedded carbon host matrices (TinO2n-1 NP@C).*

The synthesis of sulfur-infused TinO2n-1@Ccomposite, i.e. TinO2n1@C/S, is schematically summarised in Fig. 1. This approach is useful for single-pot cathode material synthesis, using the scalable robustness of hydrothermal synthesis and the technical superiority of simultaneous carbonization and carbothermal reduction to the required Magnéli phase from TiO2 directly. Initially, TiO2 nanotubes were produced by hydrothermal synthesis. In the procedure, the commercial TiO2 powder was treated with highly concentrated NaOH solution at 120 °C in a Teflon lined autoclave under autogenerated pressure to prepare sodium titanate (Na2Ti6O13) nanosheets. These nanotubes were first sonicated, and then interspersed into the dispersion of PVA under mechanical stirring. The dried mass of PVA wrapped TiO2 nanotubes was heated at 1000 °C in quartz glass tube under nitrogen flux, to get the carbothermal reduction of TiO2.

To test the electrochemical performance of sulfur-infused TinO2n-1@C/S composite, CR2032-type coin cells were assembled. The as-prepared composite was cast on Al foil by mixing with PVDF and Shawinigan Black AB50 (CSW) carbon in ratio of 8:1:1 with sulfur loading of 2-2.3 mg cm-2. The electrolyte to sulfur (E/S) ratio was kept 5-6 µL mg-1.

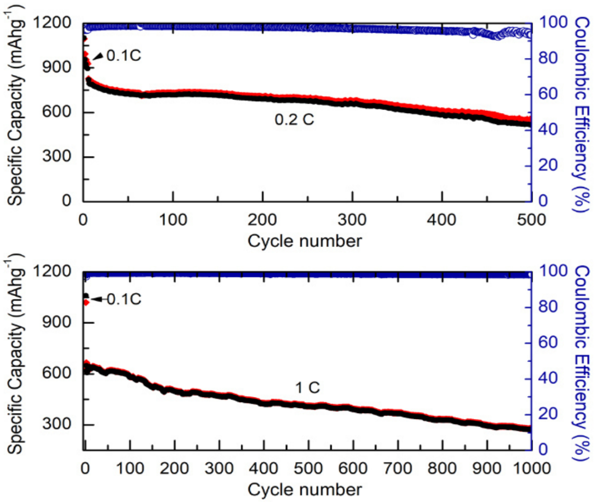

Figure 2. *TinO2n-1@C/S NP Corresponding discharge-charge. (e) 500 cycle performance and Coulombic efficiency at 0.1 an 0.2 C and (f) Long term cycling behaviour at a high C-rate of 1 C for 1000 cycles.*

Figure 2 shows the galvanostatic charging and discharging behaviour of the cathodes at specific current of 334 mA g-1, 836 mA g-1, and 1672 mA g-1 (0.2 C, and 1 C, respectively) for 1000 cycles.

The long cycle performance of the cathode material was also evaluated at the higher rate of 1C for 1000 cycles as shown in Fig. 6f. At 1C, cathode material exhibited initial capacity of 700 mA h g-1 with less than 0.06% capacity loss per cycle for 1000 cycles with Coulombic efficiency close to 99%.

Thus, the cathode synthesis strategy is very efficient in supressing LiPS dissolution and shuttling by trapping LiPS both physically and chemically, and is capable of long cycle life stable operation with high capacity, and excellent response to faster rates.

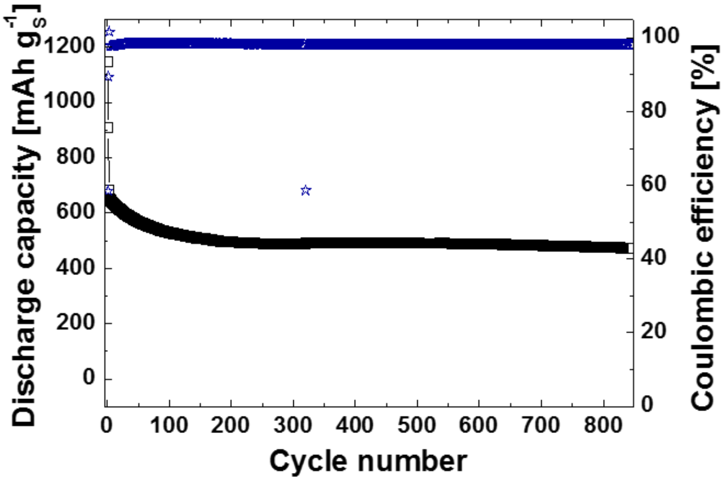

Figure 3 *Vox in NP sulfur electrod Corresponding discharge-charge at 1 C. Long term cycling behaviour. (DME:DIOX (1:1) v/v; 1M LiTFSI; 0.25M* $LiNO_3 1^{st}$ *Cycle at C/10, Onward cycling at C/5)*

Figure 3 shows the electrochemical long term behavior of a sulfur electrode prepared embedding vanadium oxides. These oxides show a very good capability to entrap polysulfides guaranteeing very good cyclability and high capacity retention.

Acknowledgments

H2020 ALISE project is kindly acknowledged

References

1. U. Zubair J. Amici[a], C. Francia[a], D. McNulty, S. Bodoardo, and C.O'Dwyer, *ChemSusChem..*, 10.1002/cssc.201800484 (2019).

Effect of used separator on the electrochemical properties of an LFP battery

T. Kazda[a], P. Řehák[a], J. Tichý[a]

[a] Department of Electrical and Electronic Technology, Faculty of Electrical Engineering and Communication, BUT, Technická 10, 616 00 Brno, Czech Republic

Lithium-ion batteries are the second most popular battery system (after lead-acid batteries). The range of their application is very wide from small electronic devices through electromobility to big energy storage systems. One of the major parts of the batteries, together with cathodes and anodes, are separators, which create a physical barrier between the electrodes and prevent electrical short circuit. The material and structure of the separator can have a big influence on the properties of the lithium-ion batteries. This article discusses the influence of five types of the separators to electrochemical properties of a cell with $LiFePO_4$ cathode.

Introduction

Lithium-ion batteries are essential for many applications nowadays. In the future, their importance will become more and more significant, mainly due to the increase in electromobility. Separators are an integral part of these batteries. They prevent electrical short circuit of electrodes and retain the electrolyte which serves for ion transport between the electrodes. The structure and composition of the separator can influence cycle life, energy density, power density or safety of the battery. Separators for lithium-ion batteries must fulfill several requirements as good chemical and electrochemical stability in combination with electrolyte and material of the electrodes [1]. Other requirements are good wettability, good thermal and dimensional stability, thickness under 30 μm and enough porosity. Separators can be divided into several groups based on their structure. Separators based on microporous membranes, modified microporous membranes, non-woven materials, and composite membranes. [2] Most commonly used materials for separators are based on microporous membranes made from polyethylene (PE), polypropylene (PP) and their combinations as PE/PP and PP/PE/PP [3]. These microporous membranes are made by two manufacturing methods: by a wet process and a dry process. Preparation for the dry process of separator production is easier and the structure of pores is different compared to the pores of separators prepared by the wet process. Open and straight porous structures are more suitable for high power batteries. Membranes prepared by the wet process have interconnected pores and disordered structure which is more suitable for long cycle life because it prevents dendrites grow during cycling [4]. The influence of five types of separators on electrochemical properties of the cell with LFP ($LiFePO_4$) will be studied in this article. The separators will be: Celgard 2400, Celgard 3401, Separion S240P20, Treofan, and glass fiber).

Experimental

The electrode slurry was based on an LFP active material consisting of NMP (N-Methyl-2-pyrrolidone) (solvent), PVDF (Polyvinylidenfluorid) (binder) and carbon Super P. The weight ratio of the materials was: active material 80 %, Super P 10 %, PVDF 10 %. The resulting mixture was subsequently deposited by a 200 µm coating bar on an Al foil, dried and pressed. A disk with the diameter of 18 mm was cut out of the coated aluminum foil and inserted into an electrochemical test cell El-Cell© ECC-STD. The assembly was done in a glove box filled with an argon atmosphere. Metal lithium foil was used as a material for the anode and 1mol/l $LiPF_6$ EC:DMC 1:1 w/w as the electrolyte. Five types of materials listed in table 1were used as the separators. We can see a comparison of capacities during cycling at 0.5 C and 1 C of all tested cells with different separators in figure 1.

Table 1. *Selected types of separators*

Separator name	Thickness	Separator type
Celgard 2400	25 µm	Microporous PP based separator
Celgard 3401	25 µm	Microporous PP based separator with surface modification
Separion S240P20	21 µm	Non-woven PET core with a ceramic surface layer
Treofan	20 µm	Nanostructured PP mesh
Glass fiber	120 µm	Glass fiber separator

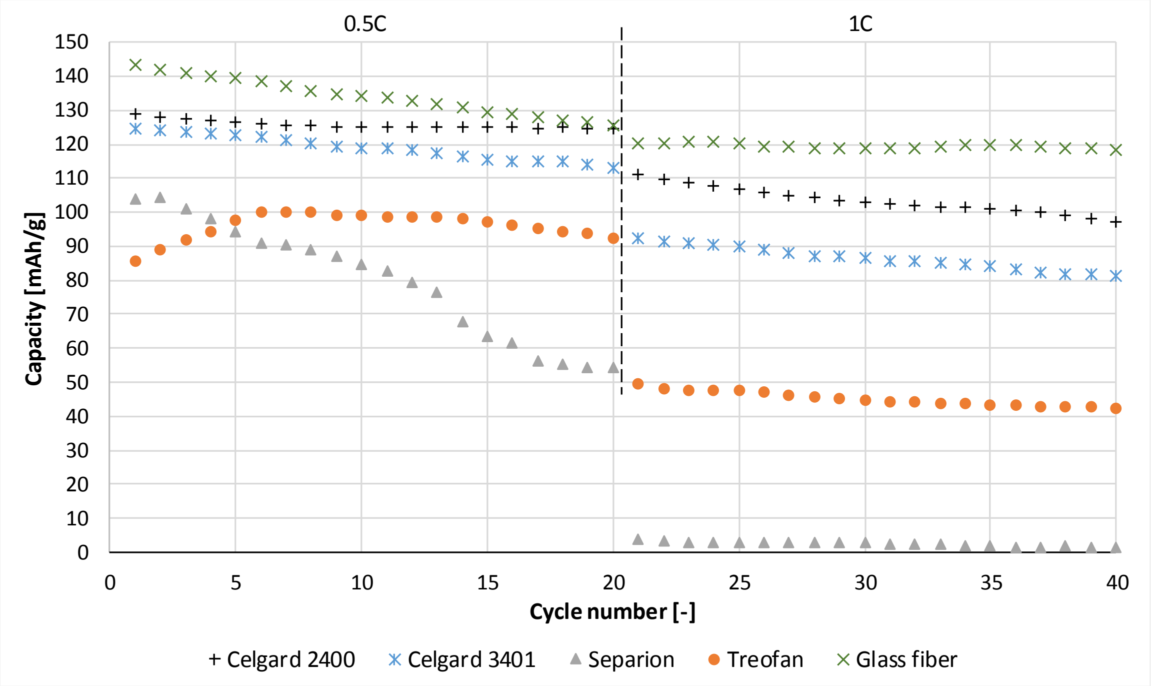

Figure 1. *Comparison of the capacities during cycling at 0.5 C and 1 C for the cells with separators Celgard 2400, Celgard 3401, Separion S240P20, Treofan, and glass fiber*

Conclusion

The highest capacity was reached by the cell with the glass fiber separator (143.3 mAh/g), however, this capacity at the 0.5 C load was not as stable as the capacity of the cell with the separator Celgard 2400. The cell with the separator Celgard 2400 lost only 3.1 % of its capacity after 20 cycles at 0.5 C. On the other hand, the cell with the separator Separion lost almost 50 % of its capacity after the first 20 cycles at 0.5 C. The most stable cell during cycling at the higher C-rate was the cell with the glass fiber separator which lost 17.4 % of its capacity. The cell with the separator Celgard 2400 had an overall capacity loss of 24.4 %. The most unstable cell was the cell with the separator Separion which lost almost 99 % of its capacity, and after cell disassembly, the separator was completely melted and stuck on the cathode surface.

Acknowledgments

Authors gratefully acknowledge the financial support from the Ministry of Education, Youth and Sports of the Czech Republic under project No. LTT19001, BUT specific research programme (project No. FEKT-S-17-4595).

References

1. Arora P, Zhang Z (2004) Battery Separators. Chemical Reviews 104:4419–4462. doi: 10.1021/cr020738u
2. Lee H, Yanilmaz M, Toprakci O, Fu K, Zhang X (2014) A review of recent developments in membrane separators for rechargeable lithium-ion batteries. Energy & Environmental Science 7:3857-3886. doi: 10.1039/c4ee01432d
3. Johnson M, Wilkes G (2002) Microporous membranes of isotactic poly(4-methyl-1-pentene) from a melt-extrusion process. I. Effects of resin variables and extrusion conditions. Journal of Applied Polymer Science vol. 83:2095-2113. doi: 10.1002/app.10164
4. Weber C, Geiger S, Falusi S, Roth M (2014) Material review of Li ion battery separators. Review on Electrochemical Storage Materials and Technology 1597:66-81. doi: 10.1063/1.4878480
5. Wu F, Chen J, Chen R, Wu S, Li L, Chen S, Zhao T (2011) Sulfur/Polythiophene with a Core/Shell Structure: Synthesis and Electrochemical Properties of the Cathode for Rechargeable Lithium Batteries. The Journal of Physical Chemistry C vol. 115:6057-6063. doi: 10.1021/jp1114724

The Study of New Non-Crystallizing Solvents and Lithium Electrolytes

M. Kasprzyk [a,*], A. Zalewska [a], M. Tymejczyk [a], A. Pajkowska [a], B. Świątkowska [a], M. Pyzik [a], M. Broszkiewicz [a], E. Żero [a], W. Wieczorek [a]

[a] Faculty of Chemistry, Warsaw University of Technology, Warsaw 00 664, Poland

The new non-crystallizing solvent mixtures and lithium electrolytes are presented in this study. The mixtures of poly(ethylene glycol)'s (PEG) with propylene carbonate (PC) have never been reported before. Both solvents exhibit melting temperatures but when mixed together in proper ratio the mixtures show neither melting nor crystallization signals. The mixtures exhibit glass transitions only and at temperatures as low as -100°C and below. Moreover, after lithium salt addition the non-crystallizing electrolyte formation is observed. The glass transition temperatures are also very low - below -80°C. In this work we present full study of physical and electrochemical properties of these new systems.

Introduction

The lithium-ion batteries are still developing very fast. There are not only portable electronic devices that are powered by lithium-ion batteries, but also electric cars have been introduced into the market. Standard batteries need electrolyte that works at ambient temperatures and the working temperature window do not have to be very wide.

Most lithium electrolytes exhibit crystallization point below -20°C. Very few electrolytes show crystallization point at temperature around -50°C, but most of them are quaternary, complex systems [1]. In the last few years new binary non-crystallizing solvent systems have been introduced. Those are mixtures of PEG with ethylene carbonate (EC) [2]. The glass transition temperatures in these systems may be even below -80°C.

The non-crystallizing electrolytes with such low glass transition temperatures (around -100°C) may be applicable in future systems required to operate at extremely low temperatures. Among these systems are: systems for polar expeditions, high mountain expedition systems (e.g. GPS, emergency, communication, electronic devices, etc.), electronics for stratospheric (weather) balloons, planes power storage (for auxiliary systems, ignition, maybe propulsion in the future, etc.), space probes/satellites, etc.

Experimental and results

Herein the physical and electrochemical study of these new non-crystallizing systems is presented. DSC (differential scanning calorimetry), MDSC (modulated DSC) of chosen solvent mixtures are presented. Lithium electrolytes based on various lithium salts are introduced. The conductivity measurements, lithium cation transference numbers, cyclic voltammetry and cycling results are presented. Two salts have been chosen for detailed study: commonly used $LiPF_6$ (lithium hexafluorophosphate) and LiTDI (lithium 4,5-dicyano-2-(trifluoromethyl)imidazolate). In both systems the lack of crystallization was observed. Three various PEGs were investigated: PEG250, PEG500 (poly(ethylene glycol) dimethyl ethers with average 250 and 500 $g \cdot mol^{-1}$ molar mass, respectively) and PEG350 (methoxy poly(ethylene glycol) ether with average 350 $g \cdot mol^{-1}$ molar mass).

All electrolytes show satisfying conductivity results not only at ambient temperatures (above 1 $mS \cdot cm^{-1}$) but also at low temperatures. The good electrochemical stability is observed (even above 4.5 V vs Li), despite using ethylene glycols. The chosen systems have been cycled in full cell Gr/LFP systems as well (graphite | electrolyte | $LiFePO_4$) and the results are presented in this work.

Acknowledgments

This work was financially supported by Faculty of Chemistry, Warsaw University of Technology (thanks to Dean's Project for Young Scientists addressed to Marta Kasprzyk).

This work was financially supported by National Science Centre on the basis of a decision nr: DEC-ODW1/2013/09/N/ST5/00875

References

1. M.C. Smart, B.V. Ratnakumar, S. Surampudi, *J. Electrochem. Soc.*, **149(4)**, A361 (2002).
2. M. Kasprzyk, A. Zalewska, L. Niedzicki, A. Bitner, M. Marcinek, W. Wieczorek, *Solid State Ionics*, **308**, 22 (2017).

Nanosized Electrode Materials for Lithium-Ion Batteries Obtained By Means of a Citric Acid Aided Route: Advantages and Shortcomings

S. A. Kirillov[a], A. V. Potapenko[a,b], I. V. Romanova[c]

[a] Joint Department of Electrochemical Energy Systems, Kyiv 03142, Ukraine

[b] School of Energy Science and Engineering, University of Electronic Science and Technology of China, Chengdu 611731, PR China

[c] Institute for Sorption and Problems of Endoecology, Kyiv 03134, Ukraine

State-of-the-art in obtaining nanosized electrode materials for lithium-ion batteries by means of a citric acid aided route is presented. An optimal synthetic procedure elaborated by the authors is described. It enables on to obtain electrode materials of the lowest possible particle size and high-rate electrochemical properties overwhelming those of known commercial samples. Based on our and literature data, criteria of an ideal electrode material are suggested, the theoretical high-rate limit of it is established, and shortcomings of nanosized electrode materials lying in their high reactivity are especially stressed.

Possible advantages of nanosized materials for batteries were first articulated by Aricó *et al.* in 2005 (1). It was suggested that subdivision would lead to greater specific surface, increased area of contact with the electrolyte, and shortening pathways for the diffusion of lithium ions and electrons in electrode materials, thereby enabling one to increase the specific power of a battery. This could be especially beneficial for applications requiring short charge/discharge times of a battery (electric cars on the first place). Since that time, numerous nanochemistry-specific approaches, like self-assembly, template synthesis, microencapsulation, etc., were probed in order to obtain such materials. However, industrial production relies, first of all, on precipitation and sintering, which lead to microsized samples, and the prospects of commercialization of nanochemistry-specific approaches remain unclear.

The aim of this presentation is a short review of the so-called citric acid aided route which appears a convenient alternative nanochemistry-specific approaches in obtaining nanosized electrode materials for lithium-ion batteries. An idea of this route goes back to Pechini (2) who has shown that evaporating solutions of mixtures of metal salts, citric acid, and ethylene glycol gives a transparent substance (presumably gel). Its pyrolysis leads to target materials. In spite of the major drawback to this method consisting in the low yield of the product in question and great amount of evolved gases, its advantages are associated with the absence of segregation of the components due to the complex formation of metal ions with citric acid and polymerization of the chelates obtained upon the polycondensation of the acid and ethylene glycol. The Pechini method has been successfully commercialized, at least, on a SME level (3).

At the beginning of our works in the field, we put forward the following unresolved problems (4): (i) the optimal metal-acid-glycol ratio was not determined; (ii) the very nature of precursors (gels?) was unknown; (iii) conditions of obtaining materials of the smallest particle size were not specified. Our further efforts were concentrated around these problems.

The composition of glasses and all types of precursors obtained at all stages of the synthesis and in the course of the thermal treatment has been determined; these are stoichiometric citrates containing several crystallization water molecules (5, 6). Adjustment of the pH of the synthesis solution by adding ammonia is not recommended (5). It has been shown that the transparent substance formed upon evaporation of the citrate solutions demonstrates no Tyndall cone and hence should be considered a glass but not a sol or gel (6). Glycols are shown to evaporate from reaction mixture without decomposition, so that their presence in the formulation is hardly required (6). It has been found that the optimal ratio between metal salt and citric acid is 1:2; just this ratio guarantees the reaction product (single or mixed oxide) of the lowest possible particle size and greatest specific surface area (6). The thermal decomposition of citrate precursors is a self-propagating exothermic process (7). The presence of combustion products of the citric acid leads to quite specific red-ox processes upon the thermal decomposition; these have been uncovered by means of thermodynamic analysis (8).

By means of this method, numerous nanosized electrode materials have been synthesized, characterized and subjected to comparative electrochemical tests along with respective commercial materials. The list of cathode materials includes lithium-manganese spinels $Li[Li_xMn_{2-x}]O_4$ (9), lithium-nickel-manganese spinel $LiNi_{0.5}Mn_{1.5}O_4$ (10), surface modified lithium ferrous phosphate – carbon composite $LiFePO_4/C$ (11) and lithium-manganese spinel with a shell of $LiNi_{0.5}Mn_{1.5}O_4$ (12), as well as a lithium-manganese rich $0.5Li_2MnO_3 \cdot 0.5LiNi_{0.5}Mn_{0.3}Co_{0.2}O_2$ material (submitted). The list of cathode materials comprises titanium oxide TiO_2 (13,14), lithiated titanium oxide $Li_4Ti_5O_{12}$ (15), and Co_3O_4 (7).

It is of great interest to stress that the citric acid aided route is quite advantageous for controlling properties of materials obtained. For example, in Ref. 9 we managed to decrease the size of $Li[Li_xMn_{2-x}]O_4$ spinels performing pyrolysis in an inert atmosphere thus retarding the oxidation of manganese and “dressing” the particles in a carbon “coat”. Similar approach has been explicitly employed for obtaining $LiFePO_4/C$ composite (11), core-shell $LiMn_2O_4$/ $LiNi_{0.5}Mn_{1.5}O_4$ material (12) and lithiated titanium oxide $Li_4Ti_5O_{12}$ (15).

Testing results reveal that maximal current loads for these nanosized materials exceed 10 A/g, i.e. they overwhelm respective microsized high-rate materials existing on the market. It should be mentioned that in order to compare different materials tested in non-similar conditions, a method based on the comparison of the capacity loss per unit discharge current (dQ/dI) proposed in Ref. 10 could be of great help.

The data on high-rate spinel electrode materials have been extensively reviewed in Ref. 16, where criteria of an ideal electrode material are suggested and the theoretical high-rate limit of it is estimated. Specifically, it is stressed that high-rate properties and high specific capacity of an electrode material should be functions not only of crystal size but also of the perfection of the crystals and their ability to aggregation or, in other words, nanodimensionality is not obligatory for attaining high-rate properties. The theoretical high-rate limit of an ideal electrode material is formulated in terms of the Frenkel kinetic theory of diffusion. It appears that in a material consisting of nanosized perfect crystals, lithium ions pass the distance of 50 nm by ~0.21 s, and this time corresponds to currents of ~4000 C, or to specific power of 10^5 W/kg.

Among disadvantages of nanosized electrode materials, their high reactivity should be stressed on the first place. This problem has been uncovered in overdischarge (overlithiation) studies of spinel cathode materials. It has been found that in microsized commercial materials, superlithiated phases reversibly transform to mother spinel, whereas in nanosized materials irreversibly such phases readily degrade at reduced voltages (17).

A more detailed description of these and related questions including an analysis of the molecular composition of battery electrolytes can be found in a recent review by one of the authors (18).

References

1. A. S. Aricò, P. Bruce, B. Scrosati, J.-M. Tarascon and W. van Schalkwijk, *Nature Mater.*, **4**(5), 366 (2005).
2. M. P. Pechini, US Pat. 3330697A, August 16, 1963.
3. C. Bluthardt, C. Fink, K. Flick, A. Hagemeyer, M. Schlichter and A. Volpe, Jr, *Catal. Today*, **137**(1),132 (2008).
4. S. A. Kirillov, I. V. Romanova, and I. A. Farbun, in *New Carbon Based Materials for Electrochemical Energy Storage Systems*, C. Johnson, V. G. Barsukov, and I. V. Barsukov, Editors, p. 473, Springer, Dordrecht (2006).
5. I. A. Farbun, I. V. Romanova, and T. E. Terikovskaya, D. I. Dzanashvili and S. A. Kirillov, *Russ. J. Appl. Chem.*, **80**(11), 1798 (2007).
6. I. A. Farbun, I. V. Romanova and S. A. Kirillov, *J. Sol-Gel Sci. Technol.*, **68**(3), 411 (2013).
7. Yu. V. Shmatok, N. I. Globa and S. A. Kirillov. *Electrochim. Acta*, **245**, 88 (2017).
8. I. V. Romanova and S. A. Kirillov, *J. Therm. Anal. Calorim.*, **132**(1), 503 (2018).
9. A. V. Potapenko, S. I. Chernukhin and S. A. Kirillov, *Mater. Renew. Sustain. Energy*, **3**(1), 40 (2014).
10. A. V. Potapenko, S. I. Chernukhin, I. V. Romanova, M. M. Gafurov, K. Sh. Rabadanov and S.A. Kirillov, *Electrochim. Acta*, **134**, 442 (2014).
11. V. V. Kosilov, S. I. Chernukhin, I. V. Romanova and S.A. Kirillov, *Chem., Phys. and Techn. Surface*, **5**(1), 99 (2014) (in Ukrainian).
12. A. V. Potapenko and S. A. Kirillov, *Electrochim. Acta*, **258**, 9 (2017).
13. S. A. Kirillov, T. V. Lisnycha and S. I. Chernukhin, *J. Power Sources*, **196**(4), 2221 (2011).
14. T. V. Lisnycha, A. V. Potapenko and S. A. Kirillov, *Int. Nano Lett.*, **6**(2), 111 (2016).
15. S. A. Kirillov, T. V. Lisnycha, I. V. Romanova and A. V. Potapenko, *Electrochim. Acta*, **286**, 163 (2018).
16. A. V. Potapenko and S. A. Kirillov, *J. Energy Chem.* **23**(5), 543 (2014).
17. V. V. Kosilov, A. V. Potapenko and S. A. Kirillov, *J. Solid State Electrochem.*, **21**(11), 3269 (2018).
18. S. A. Kirillov, *Theor. Exp. Chem.*, **55**(2), 73 (2019).

Advanced Anode and Cathode Materials for 48 V Lithium Accumulators

M. Zukalová[1], K. Mocek[1], A. Zukal[1] and J. Procházka[2]

[1]J. Heyrovský Institute of Physical Chemistry, v.v.i., AS CR, Dolejškova 3, Prague 8, Czech Republic

[2]HE3DA, s.r.o., Beranových 130, Prague 9, Czech Republic

HE3DA® battery concept represents a unique technological platform based on three-dimensional electrodes using lithium nano-materials (patented HE3DA® technology). The basic unit of HE3DA accumulator represent graphite anode, ceramic separator and $LiNi_{1/3}Mn_{1/3}Co_{1/3}O_2$ cathode. The layered $LiNi_{1/3}Mn_{1/3}Co_{1/3}O_2$ (NMC 111) is a promising cathode material and represents environmentally acceptable replacement of widely used $LiCoO_2$(1). NMC 111 is isostructural to layered $LiCoO_2$, its Co content is only 1/3 of that in $LiCoO_2$ and exhibits impressive stability upon cycling, reasonable specific capacity (150 mAh/g) and good high rate capability. Due to relatively low Li^+ diffusion coefficients of the order of 10^{-10}- 10^{-15} cm^2/s (2) NMC 111 material consisting of nanocrystals with well-developed structure represents the best candidate for stable and fast Li-ion battery. NMC 111 for the basic unit of 48 V accumulator - 4 V cell is prepared by optimized procedure producing stable material providing charge capacity of 141 mAh/g (cyclic voltammetry) and 144 and 135 mAh/g (galvanostatic chronopotentiometry) at 1 and 10C, respectively(3). Evaluation of 103 Wh battery module containing optimized cathode NMC 111 material proved its stability and availability of 89% theoretical charge capacity after 5 formatting cycles. Battery passed successfully Audi battery test. In all 10 cycles of 3x15 s 100 A discharge the value of battery potential after 3rd discharging pulse did not decrease below 2.4 V limit. The first prototype of 48 V accumulator consisting of 12 particular basic modules was completed and tested. It passed successfully both load test and Audi battery test. To decrease further the production expenses and to minimize the amount of toxic Co, 4 V HE3DA cells with Ni rich cathode material (NMC 622 and 532) were assembled and tested. However, in contrary to expectations, their charge capacity did not exceed the values of the cell with NMC 111.

Although graphite is a cheap and frequently used anode material, its layered structure exhibiting volume expansion of ca 13% in a fully lithiated state(4) represents a safety issue for Li-ion batteries. In contrary, TiO_2 polymorphs are known as environmentally friendly and safe anode materials. We tried to develop easily scalable preparation of TiO_2 anatase and TiO_2(B) with reasonable charge capacity and cycling stability. Electrochemical measurements of optimized products proved charging capacities of 170-220 mAh/g for both anatase and TiO_2(B) with a capacity drop less than 3% after 50 cycles at 1C charging rate.

Acknowledgments

This work was supported by the Ministry of Industry and Trade of the Czech Republic (contract TRIO FV20471).

References

1. P. K. Nayak, J. Grinblat, M. Levi, B. Markovsky and D. Aurbach, *J Electrochem Soc*, **161**, A1534 (2014).
2. O. Capron, R. Gopalakrishnan, J. Jaguemont, P. Van Den Bossche, N. Omar and J. Van Mierlo, *Materials (Basel)*, **11** (2018).
3. M. Zukalova, J. Prochazka, B. Pitna Laskova, A. Zukal and L. Kavan, *ECS Trans*, **87**, 67 (2018).
4. S. Schweidler, L. de Biasi, A. Schiele, P. Hartmann, T. Brezesinski and J. Janek, *The Journal of Physical Chemistry C*, **122**, 8829 (2018).

Features of Influence the Temperature on the Electrochemical Parameters of Li-Battery With Cathode Based on Polymer Sulfur. Impedance and Galvanostatic Cycling

Irina Kirsanova[a], Yuliya Polishchuk[a], Elena Shembel[a,b], Andrea Straková Fedorková[c], and Vlad Redko[b]

[a] Scientific Research Laboratory of Chemical Power Sources of Ukrainian State University of Chemical Technology, Dnipro, 49005, Ukraine

[b] Enerize Corporation, Coral Springs, FL, 33067, USA

[c] Pavol Jozef Safarik University, Košice, SK-04154, Slovak Republic

The effect of temperature on 1) impedance and discharge –charging characteristics of Li-S cells during cycling, and 2) the conductivity of non-aqueous electrolyte that is used in this system have been investigated. Particular attention is paid to the hysteresis of the conductivity in the temperature range from minus 25 °C to plus 60 °C and then back to plus 25 °C.

Introduction

Lithium-sulfur (Li-S) batteries are currently promising for use due to their high specific energy, low cost and environmental friendliness. Therefore Li-S batteries have received great attention and have achieved significant success over the past few years [1, 2]. However, there are problems that prevent their commercialization: high self-discharge, possible flammability of electrolyte under high temperature, and low operation voltage of discharge under minus temperatures, etc.

Experimental

As electrolyte has been used 0.7 M bis(trifluoromethylsulfonyl)lithium imide (LiIm) ($LiN(CF_3SO_2)_2$) and 0.25 M lithium nitrate ($LiNO_3$) (Fisher Chemical, anhydrous) dissolved in mixture of in dimethoxyethane (DME) (Aldrich, anhydrous, 99.9%) and 1,3-dioxolane (DOL) (Sigma Aldrich, anhydrous, 99.8%) in relation 1:2.

The assembly of electrochemical cells and the preparation of the electrolytes were carried out in a hermetically glove box, in dry argon atmosphere.

Conductivity measurements of electrolyte have been carried out in a 2-electrode glass cell with platinum electrodes. Testing was carried out from -25 °C to +60 °C. The electrochemical measurements of the electrolyte and electrochemical cells were carry out using a computer-controlled measurement system (Analytical Radiometer Voltalab PGZ 301). The frequency range in which the impedance spectrum was obtained is 100 kHz - 100 Hz. The amplitude of the voltage is 10 mV.

To calculate the specific ionic conductivity (χ, $Ohm^{-1} \cdot cm^{-1}$) of electrolyte solutions, the cell constant (K, cm^{-1}) was determined as the product of the value of ionic conductivity of a 0.1 M KCl aqueous solution.

The resistance (R, Ohm) of the non-aqueous electrolyte determined from the impedance hodographs as a segment on the axis of the active resistance obtained by extrapolating the impedance spectrum to high frequencies. The value of the specific ionic conductivity of the investigated electrolyte has been calculated by formula: $\chi = K / R$.

Electrochemical tests of Li-S cells have been carried out in hermetic coin cells 2325 size. The polymer sulfur based electrode used as working electrode. Electrode area 2 cm^2. As current collector was used aluminum foil and aluminum foil that modified by carbon [3]. The metallic lithium was the auxiliary electrode. Celgard 2300 CGR (25 micron) was used as a separator. Electrochemical properties of Li-S system was carried out in electrochemical cells using the galvanostatic cycling method in the potential range of 2.7 V to 1.5 V.

Li- S cells with three electrodes have been used for investigation the impedances of cathode (positive electrode) based on the sulfur, and anode (negative electrode) based on lithium. The second lithium electrode was used as a reference electrode. These cells have the prismatic pouch design. Investigation conducted in a wide range of temperatures.

Results and its discussion

Ionic conductivity of electrolyte

The temperature dependence of the electrolyte conductivity of 0.7 M LiIm, 0.25 M $LiNO_3$, DOL: DME = 1: 2 is shown in Figure 1. The sequence of temperature changes in measuring the conductivity of a non-aqueous electrolyte was follows: +25; +7; 0; -15; -25; +25; +40; +60 °C. Direction of change the temperature is shown in Figure 1 by arrows.

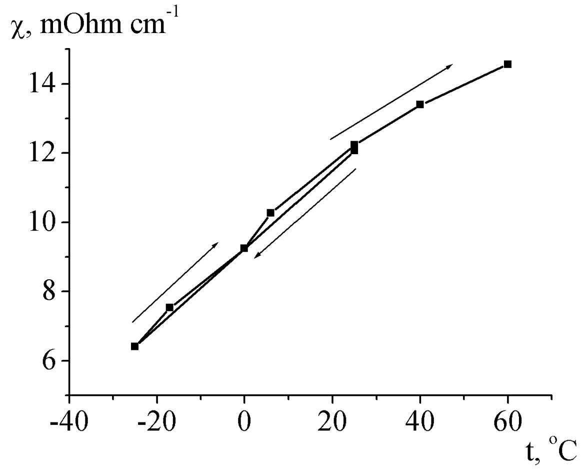

Figure 1. *Temperature dependence of the ionic conductivity 0.7 M LiIm, 0.25 M $LiNO_3$, DOL:DME=1:2 electrolyte.*

Obviously, the increasing the temperature leads to increasing the mobility of ions, which in turn leads to increasing the ionic conductivity of electrolyte. The obtained values of ionic conductivity are in the range of 6 ÷ 14 $mOhm^{-1}\cdot cm^{-1}$ in the specified temperature range.

Our results indicate the absence of conductivity hysteresis with changing the temperature. The electrolyte retains high values of conductivity in a wide temperature range.

Impedance of Li-S cells

Below are presented the results of the study: 1) the dynamics of change in the impedance of Li-S cell by the temperature and 2) the correlation between the effect of temperature on the electrolyte conductivity and the effect of temperature on the impedances of the Li-S cell.

When the temperature drops to -25 °C, the impedance of the Li-S system increases dramatically compared with the temperature of +25 °C (Figure 2 and 3).

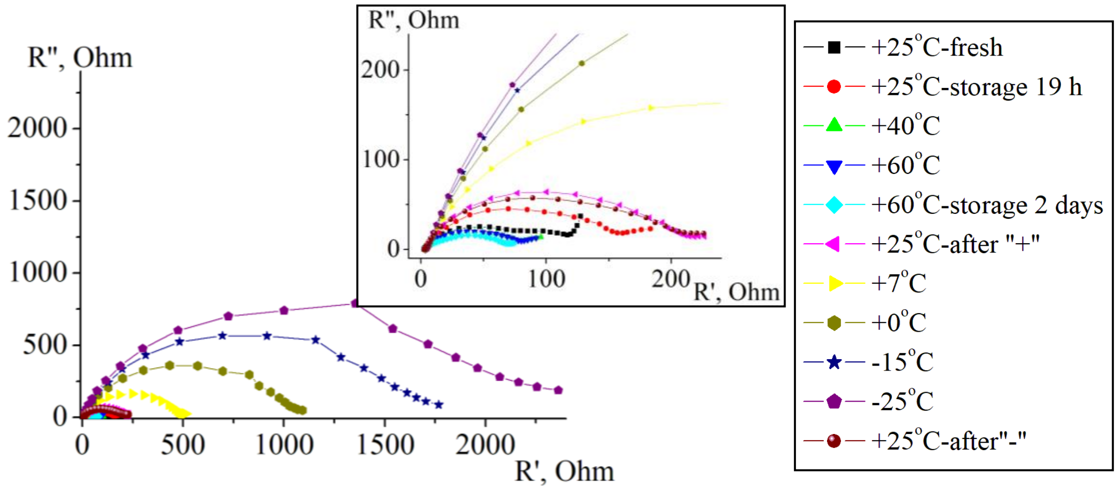

Figure 2. *Temperature dependence impedance of Li-S systems from -25 to +60 °C. Electrolyte: 0.7 M LiIm, 0.25 M $LiNO_3$, DOL:DME=1:2. Cell #18. Current collector – aluminum foil.*

The positive effect of modifying the Al current collector (Figure 3) appears at temperature +25 – +60 °C: summary impedance of cell, in which used the Al modified be carbon, in 1.5 times lower than Al (Figure 2).

At the negative temperatures the dependence of the cell impedance on the modification Al current collector is changed. We associate this with the peculiarities the current distribution in the porous macro structure of positive electrode (cathode). With a decrease in temperature, the conductivity of the electrolyte decreases, as well the electrochemical reaction constants decrease. These factors have a more influence of impedance as compared with the influence of the transition resistance of the electrode mass and the current collector. As will be shown below, the features of the formed films on the lithium electrode are also significant increased at negative temperatures.

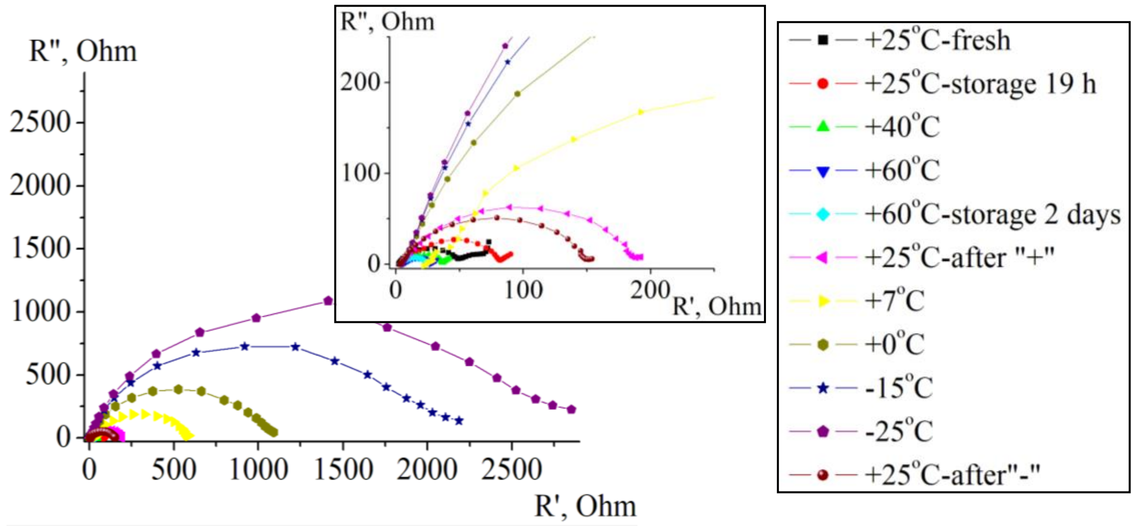

Figure 3. *Temperature dependence impedance of Li-S systems from -25 to +60 °C. Electrolyte – 0.7 M LiIm, 0.25 M $LiNO_3$, DOL:DME=1:2. Cell #20. Current collector – aluminum foil modified by carbon.*

The change in impedance hodographs obtained in 3-electrode Li-S-Li cells is shown below. Hodographs obtained for two electrodes connectivity scheme: S - working electrode, Li - reference and Li - auxiliary electrode (Figure 4); Li - working and Li reference electrode, S - auxiliary electrode (Figure 5). In this case, we can identify "individual" hodographs for each electrode separately. The sequence of temperature changes was as follows: +25; 0; -15; +25; +40; +60 °C.

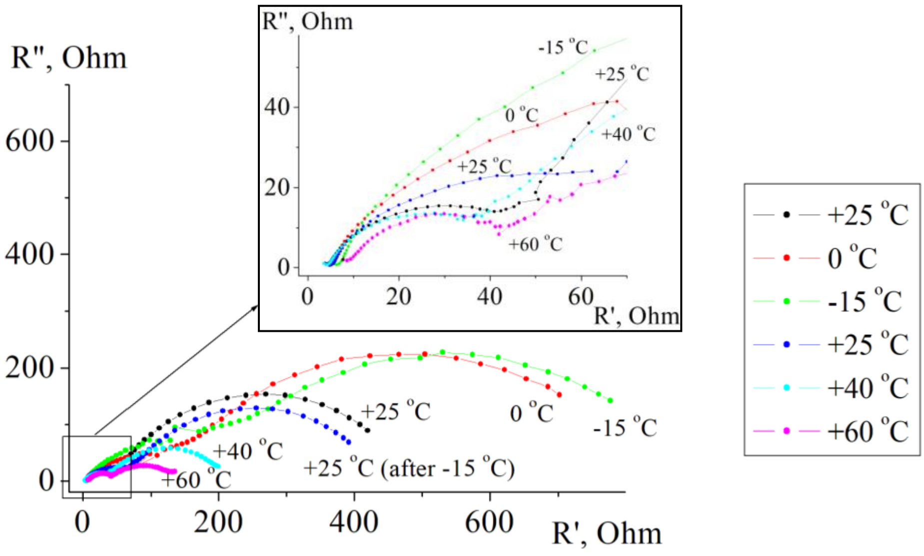

Figure 4. *Impedance spectra of S electrode in Li-S-Li cell. Electrode area 2 cm^2. Electrolyte: 0.7M LiIm, 0.25M $LiNO_3$, DME : DOL = 2:1. Content of sulfur in electrode is 75%.*

The obtained data allow us to conclude that a significant contribution to the total impedance of the system is made by changes at the negative lithium electrode.

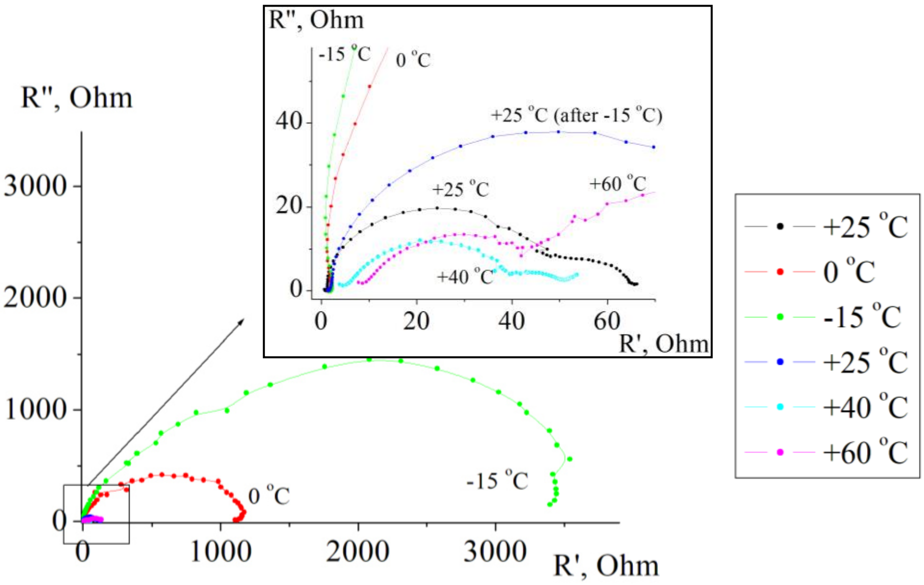

Figure 5. *Impedance spectra of Li electrode in Li-S-Li cell. Electrode area 2 cm^2. Electrolyte: 0.7M LiIm, 0.25M LiNO$_3$, DME : DOL = 2:1.*

It should be noted that the influence of high and low temperatures does not lead to degradation of the Li-polymer S system. Figure 6.a shows that the impedance spectra of the Li-S system under +25 °does not changed when 1) returning to +25 °C after -25 °C and 2) returning to +25 °C after +60 °C. The fact that the impedance hodographs at +25 °C does not changed confirm that the system Li – polymer S is stable.

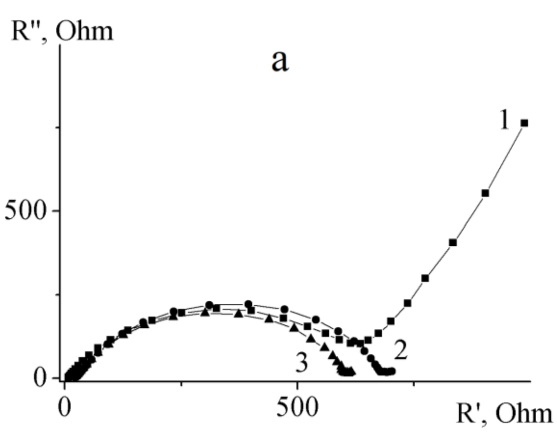

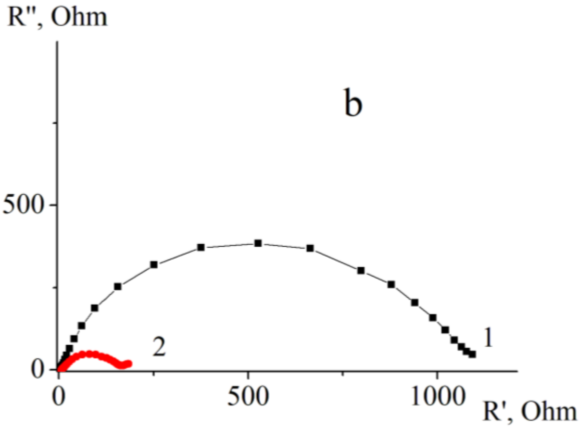

Figure 6.a. *Hodographs of impedance Li-S cell at +25 °C. Status of Li-S system: 1 – "fresh"; 2 – after +60 °C; 3 – after -25 °C.*

Figure 6.b. *Hodographs of impedance Li-S cell at 0 °C. Status of Li-S cell: 1 – after keeping the cell at 0 °C before cycling; 2 – after 10 charge at 25 °C and keeping the cell at 0 °C. Electrolyte – 0.7 M LiIm, 0.25 M LiNO$_3$, DOL:DME=1:2.*

Electrochemical characteristics of Li - S cells

The performance of Li-S batteries after keeping the cell at low temperatures (-25 °C) and high temperatures (+60 °C) is also confirmed by the data of galvanostatic cycling (Figure 7).

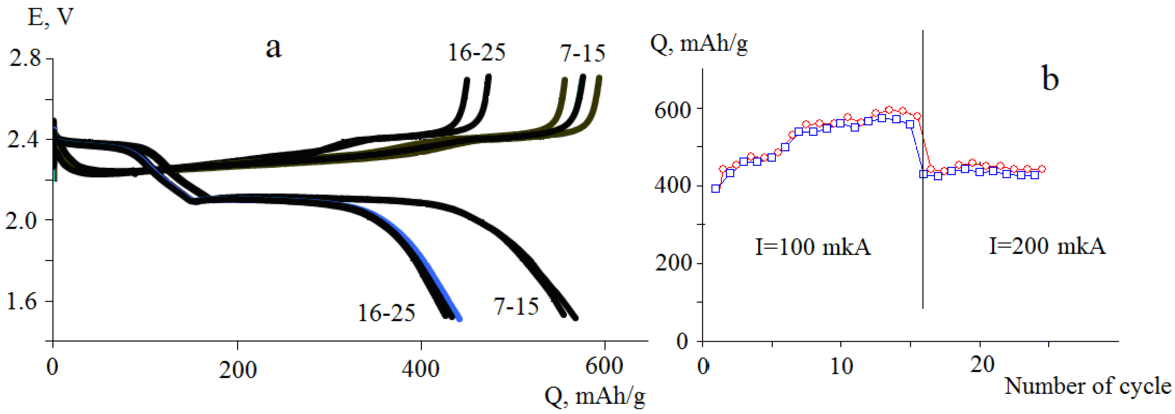

Figure 7. Discharge-charge curves (a) and changing the specific discharge capacity (b) of Li-S cell # 21. Electrolyte: 0.7 M LiIm, 0.25 M $LiNO_3$, DOL:DME=1:2. Charge current – 100 mkA. Discharge current: for 1-15 cycles - 100 mkA, for 16-25 cycles - 200 mkA. Numbers on curves are the cycle number. Discharge current density i =50 mkA/cm^2 and 100 mkA/cm^2 – 0.001C, charge current density i=100 mkA/cm^2 – 0.001C.

Starting from the 7th cycle, the system stabilizes at a capacity value of 540-600 mAh/g with discharge current 100 mkA. Increase the current at two time leads to a decrease in the capacity to 410-425 mAh/g with maintaining stable cycling.

After cycling, the cell impedance at low temperatures decreases, for example, at 0 ^{o}C (Figure 6, b). These data confirm that the developed power source can operate at low temperatures.

Acknowledgments

This investigations have been carried out in cooperation the Ukrainian State University of Chemical Technology, Scientific Research Laboratory of Chemical Power Sources and company Enerize Corporation, USA under framework of NATO SPS 985148 project “Development of New Cathodes for Stable and Safer Lithium-Sulfur Batteries”/ Science for Peace and Security Programme. Enerize Corporation is industrial partner under NATO SPS 985148 project. Prof. E. Shembel is the Head of SRLCPS USUCT and Partner country-Ukraine Director of this NATO project.

References

1. Xiaofei Yang, Xia Li, Keegan Adair, Huamin Zhang, Xueliang Sun, *Electrochemical Energy Reviews,* **1**, p. 239 (2018).
2. *Lithium–Sulfur Batteries*, First Edition. Mark Wild and Gregory J. Offer, Editors, Published by John Wiley & Sons Ltd (2019).
3. V. Redko, E. Shembel, T. Pastushkin, A. Markevych, A. Straková Fedorková, O. Girin, O. Kolomoyets, Yu. Polishchuk. *ECS Transactions*, **87** (1) (2018).

GarnetT-PEO Composite Solid Electrolytes: A Multiscale View on Li$^+$ Transport

Jakub Zagorski[(a)*], Juan Miguel Lopez del Amo[(a)], Frederic Aguesse[(a)], Anna Llordes[(a,b)]

[(a)] CIC Energigune, Parque Tecnologico de Alava,01510 Miñano, Spain

[(b)] IKERBASQUE, The Basque Foundation for Science, María Díaz de Haro 3, 48013 Bilbao, Spain

*E-mail of the Corresponding Author: jzagorski@cicenergigune.com

The fast-expanding sector of portable electronics and electric vehicles look for new solutions to overcome safety and performance limitations of liquid electrolyte-based Li-ion batteries. A promising new technology is the so-called Li metal Solid State Battery (SSB), which aims to replace the flammable liquid electrolyte by solid electrolyte materials, such as ceramics or polymers. Ceramic electrolytes are the best candidates for SSB in terms of high Li$^+$ conductivity, though they are strongly limited by their interfacial mechanical stability with Li metal anode [1]. An alternative is to combine the desirable properties of ceramic and polymeric electrolytes into a composite concept. Generating knowledge about interactions between composite components and their influence on Li-ion mobility, electrochemical stability and Li electrodeposition properties is thus, essential to progress towards practical applications.

In this contribution, we focus on the composite solid electrolyte system based on PEO-LiTFSI polymeric matrix enriched with $Li_{6.55}La_3Zr_2Ga_{0.15}O_{12}$ garnet fillers [2].To accurately investigate the Li-ion transport properties and avoid the typical segregation issues of these immiscible mixtures, we apply a new processing method that ensures a high degree of structural and chemical homogeneity, even at the local scale, and across a broad range of ceramic filler content. Solid-state NMR and Electron microscopy were used to locally characterize the structure of the composites. The local mobility of Li-ion was investigated by 2D NMR to understand and propose possible transport mechanism. The effect of garnet filler on salt dissociation, ions interactions and correlation between local and global ion nobilities were reconsidered. The impact of garnet filler content on the macroscopic Li-ion conductivity will be discussed as well as their influence on mechanical behavior and the polymer matrix stability with metallic Li anode. Finally, the implementation of these composite electrolytes in Li metal all-solid-state full cell device will be presented. All in all, in this work we show how the combination of hard-soft electrolyte materials can enhance the interfacial stability with Li metal anode upon cycling, offering new opportunities to prevent Li dendrite formation in solid-state batteries.

References

1. W. Manalastas, J. Rikarte, R. Chater, R. Brugge, A. Aguadero, L. Buannic, A. Llordes, F. Aguesse, J. Kilner, Mechanical Failure of Garnet Electrolytes during Li Electrodeposition Observed by In-Operando Microscopy. *J. Power Sources*, 412 (2019), 287–293.
2. J. Zagorski, J.M. Lopez del Amo, M.J. Cordill, F. Aguesse, L. Buannic, A. Llordes. Garnet-Polymer Composite Electrolytes: New Insight on Local Li-ion Dynamics and Electrodeposition Stability with Li Metal Anodes. *ACS App. Energy Mater.* Just accepted DOI: 10.1021/acsaem.8b01850 https://pubs.acs.org/doi/10.1021/acsaem.8b01850

Innovating Cathode Based on Polymer Sulfur for Stable and Safer Lithium-Sulfur Batteries.

Yuliya Polishchuk[a], Elena Shembel[a,b], Andrea Straková Fedorková[c], Vlad Redko[b], Nellya Zaderey[a], Tatyana Vergun[d], Evgeny Zaginayko[d]

[a] Scientific Research Laboratory of Chemical Power Sources of Ukrainian State University of Chemical Technology, Dnipro, 49005, Ukraine

[b] Enerize Corporation, Coral Springs, FL, 33067, USA

[c] Pavol Jozef Safarik University, Kocice, SK-04154, Slovak Republic

[d] Dniepropetrovsk Research Forensic Center, Dnipro, 49033, Ukraine

Comparative characteristics of sulfur allotropes (orthorhombic and polymeric) in Li –S cells are given. The difference in the structure and physic-chemical properties of the initial material has been shown. The electrochemical properties of S-based cathodes in non-aqueous liquid electrolyte (0.7 M LiIm, 0.25 M $LiNO_3$, DME: DOL (2:1) in lithium rechargeable batteries has been investigated.

Introduction

Sulfur is the active cathode material with a theoretical capacity of 1672 mAh/g and an average discharge potential of 2.2 – 2.4 V versus lithium. The advantage of lithium-sulfur batteries: high capacity and high energy density up to 500 Wh/kg, low price, environmental compatibility. But the biggest problem of the sulfur cathode is self-discharge due to the formation of polysulfides. This problem can be avoided by using an electrolyte in which sulfur is insoluble or using sulfur with structure different from natural material. Our solution to the problem is the use of insoluble sulfur with a specific polymer structure.

The choice of polymer sulfur was due to its insolubility in organic solvents. Some compounds for example, pine oil, tar, etc. are used for stabilize polymer sulfur. For rubber vulcanization, the tire industry uses a composite material that contains up to 80% of polymeric sulfur and 20% organic additive titled binder. The sulfur, which is used for vulcanization, has a special polymer structure. It should be noted that the presence of additives are electrochemically inactive and will act as a ballast component in the electrode of the current source. To remove excess binder component, we used a special method of “washing” sulfur in acetone. The results of comparative studies of the characteristics of natural elemental and sulfur with a polymeric structure are presented below.

Experimental

We used three type of sulfur: initial polymeric insoluble sulfur Crystex (TM) HD OT 20; “washed” polymeric insoluble sulfur Crystex (TM) HD OT 20 without excess binder component and natural elemental sulfur. The positive electrodes have been fabricated by coating the slurry. As the current collector has been used the aluminum foil with modification by fusion of graphite into aluminum [1]. Disk electrodes based on sulfur have the following parameters: d – 1.6 cm, working surface – 2.0 cm^2. Cathode mass has the following composition: Sulfur - 75% wt.; Carbon black-10% wt.; Graphite with high conductivity - 10%; PVdF (6020/1001, Solef) - 5% wt. The drying of the cathode was under at 60 °C for 6 h under vacuum.

The cells with pouch design have been used for testing. All procedures were carried out in an Ar-filled glove box. The negative electrodes were made of lithium foil. The microporous polypropylene Celgard®2300 with a thickness of 25 mkm was used as the separator. Electrolyte composition: 0.7M bis(triuoromethanesulfone)imide (LiIm), 0.25M $LiNO_3$, DME: DOL (2:1).

The following measurements was used: Scanning electron microscopy (SEM), XRD analyze, Electromagnetic non-contact testing of conductivity the powedered materials, Gas-liquid chromatography, FTIR spectroscopy, Impedance spectroscopy (IS) and Cycling voltammograms (CV) S based electrode in Li-S-Li cell and galvanostatic cycling Li-S batteries. The measurements have been conducted under temperature 25 °C.

The electromagnetic non-contact non-destructive testing [2, 3] was used for investigation the conductivities and densities of: 1) powders of carbon materials that included in electrode mass based on sulfur, and 2) powder of cathode mass based on mixture of sulfur and carbon. Porosity and density of electrode based on the sulfur also have been testing. Based on these results the composition and technology of fabrication the sulfur based cathode have been optimized.

Impedance spectra and cyclic voltammograms were obtained using VoltaLab PGZ 301 analytical radiometer. Diffractometer DRONE-3 in monochromatized Cu-Kα-radiation was used for evaluation the phase composition of sulfur powder. Gas-liquid chromatography Agilent Technologies 6890N / 5975 with mass-selective detection in the conditions of the registration of chromatograms of full ion current (m / z = 8-600) and Infrared Imaging Microscope Nicolet IN10FX with module Nicollet iZ10, Smart ITX accessory and diamond ATR crystal was used.

Results

Scanning electron microscopy of the elemental and polymer “washed” sulfur illustrates that the powder of elemental sulfur preferably consists of particles from 10 to 35 microns. Small particles combined into agglomerates (Figure 1, a) up to 80 microns.

The powder of “washed” polymer sulfur preferably consists of spherical particles with average size 3 microns (Figure 1, b). The fact that the polymer sulfur does not organizes the agglomerates.

Natural elemental sulfur has an orthorhombic crystal lattice (01-478). In the powder of initial polymer sulfur (20-1225), the content of the orthorhombic allotrope (01-478) is about 20% and after “washing” it rises to ~ 40%.

The presence of orthorhombic sulfur in the samples is partially confirmed by the chromatogram. Also, the data confirm that the special method we used allows us to remove a significant part of the organic additive (binder) from initial powder of polymer sulfur.

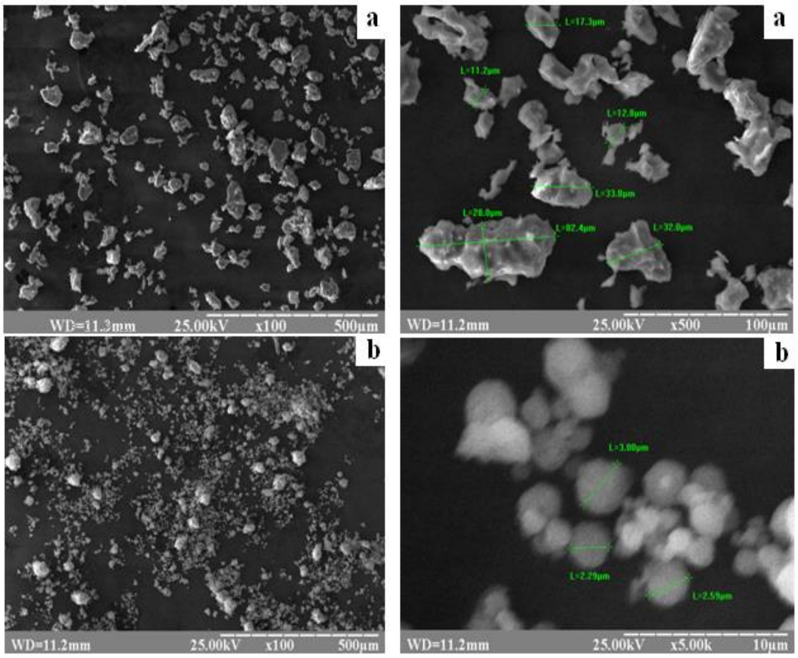

Figure 1. *Scanning electron microscopy of elemental (a) and polymer "washed" (b) sulfur.*

The hodographs of different type of sulfur based electrodes have two semicircles (fig. 2).

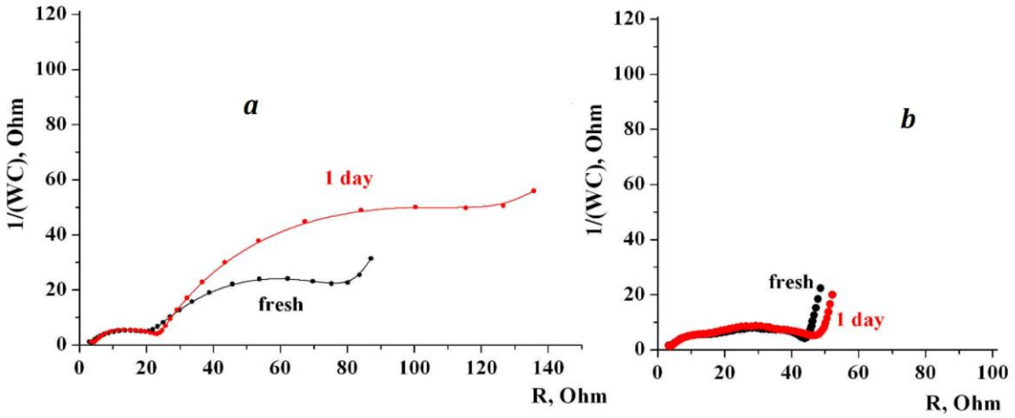

Figure 2. *Impedance spectra of S-based electrode in Li-S-Li cell. Electrode area 2 cm^2. Electrolyte: 0.7M LiIm, 0.25M LiNO3, DME : DOL = 2:1. Cathode based on natural elemental (a) and polymer "washed" (b) sulfur.*

In the case of the polymer "washed" sulfur (Fig. 2 b), two semicircles overlap each other. In general, the summary impedance of cathodes based on natural sulfur is higher than that of polymer S.

Fig. 3 shows the CV of S-based electrodes in lithium batteries. Two cathodic peaks are observed at potentials 2.2-2.3 V and 1.9-2.0 V for electrodes based on polymer "washed" S (fig. 3b). The first cathodic peak corresponds to the transformation from elemental sulfur to long chain polysulfides. The second traditionally is associated with the reduction of higher-order polysulfides to Li_2S_2 and Li_2S. For elemental sulfur based cathode at these conditions we observe only one cathodic peak at 2.0-2.1 V. During cycling this peak degrades (fig. 3a).

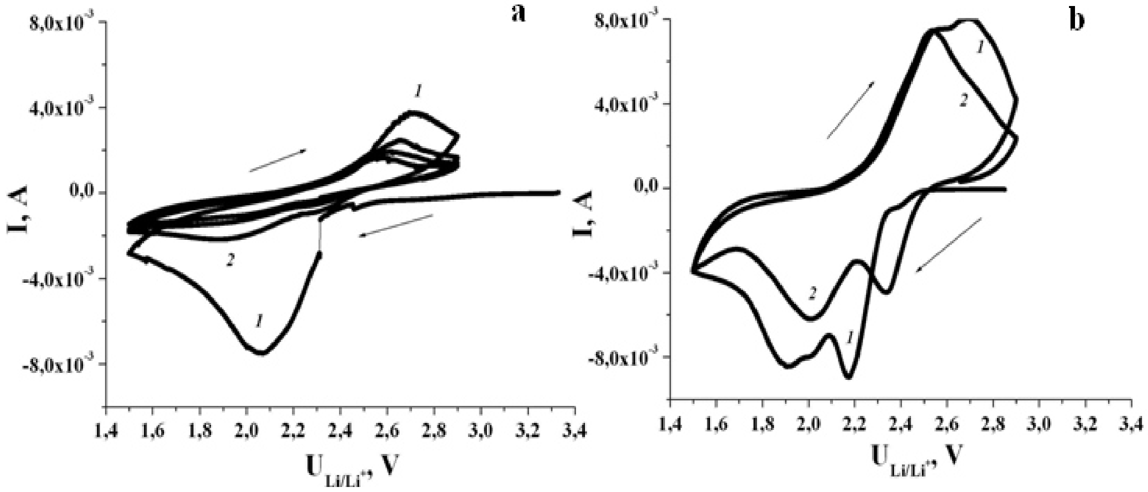

Figure 3. *CV characteristics S-based electrode in Li-S-Li cell obtained in the potential range of 1.5 - 2.9 V. The potential scan rate is 0.5 mV/s. Electrode area 2 cm^2. Electrolyte: 0.7M LiIm, 0.25M LiNO$_3$, DME: DOL (2:1). Cathode based on natural elemental (a) and polymer "washed" (b) sulfur.*

The charge/discharge characteristics of the S-based electrodes are presented in Fig. 4. Two discharge plateaus are observed in the discharge profiles of for electrodes based on polymer "washed" sulfur.

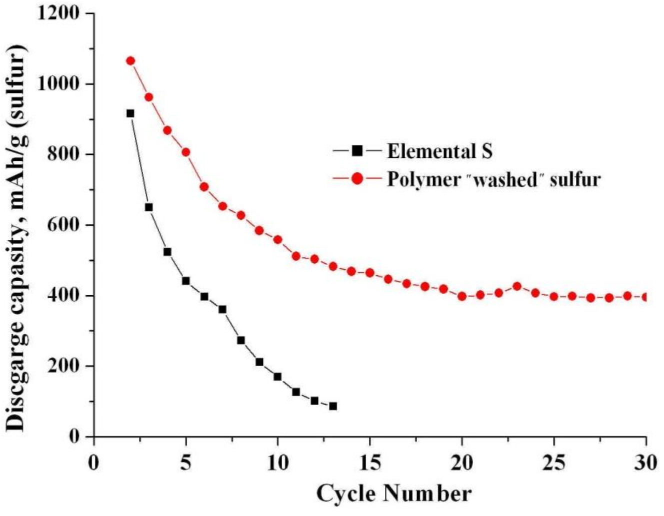

Figure 4. *Change of specific discharge capacity during cycling for Li-S cell. Electrolyte: 0.7M LiIm, 0.25M LiNO$_3$, DME: DOL (2:1). Sulfur content in cathode is 75%. Discharge current – 0.2 mA; charge current – 0.1 mA.*

The discharge capacity for elemental sulfur extremely decreases during cycling. For cell with polymer "washed" sulfur based cathode after 10 cycles, the capacity is stabilized at about 500 mAh/g of S.

The complex of research, in summary, allows us to conclude that the features of the structure and physical parameters of sulfur with a polymer structure can significantly stabilize the discharge capacity lithium-sulfur batteries during of cycling.

All results described in this study indicate that the sulfur with polymer structures is a promising cathode material for high-performance and safer lithium-sulfur batteries.

Acknowledgments

This investigations have been carried out in cooperation the Ukrainian State University of Chemical Technology**,** Scientific Research Laboratory of Chemical Power Sources of and Enerize Corporation, USA. Technologies and materials that are presented in this article are developed also under framework of NATO SPS 985148 project "Development of New Cathodes for Stable and Safer Lithium-Sulfur Batteries". Enerize Corporation is industrial partner under NATO SPS 985148 project. Prof. E. Shembel is the Head of SRLCHS USUCT and Partner country-Ukraine Director of this NATO project.

References

1. V. Redko, E. Shembel, T. Pastushkin, A. Markevych, A. Straková Fedorková, O. Girin, O. Kolomoyets, Yu. Polishchuk. *ECS Transactions*, **87** (1) (2018).
2. V. Redko, E. Shembel, etc. *US Patent* No. 7,288,941 Method and Apparatus for Measuring Conductivity of Powder Materials Using Eddy Currents.
3. V. Redko, E. Shembel, T. Pastushkin, etc. *US Patent* No. 8,102,181. Method and Device for Rapid Non - Destructive Quality Control of Powdered Materials.

Improving the Electrochemical Performance of Spinel Cathode Materials for High Voltage Li-ion Batteries

Moustafa M.S. Sanad[1*], Ayat N. Shazly[1], Atef Y. Shenouda[1*], G. Topalov[2], B. Oberschachtsiek[2]

[1]Central Metallurgical Research & Development Institute, P.O. Box: 87, Helwan, Cairo, Egypt

[2]Fuel Cell Research Center ZBT GmbH, Carl-Benz-Str. 201 (Universitätscampus) -
D-47057 Duisburg - Germany

Lithium ion batteries (LIBs) are regarded as a promising energy storage solution for transport and stationary applications like electric vehicles, uninterrupted power supply or photovoltaics and have drawn increasing attentions. In this regard, pure spinel nanopowders of $LiNi_{0.5}Mn_{1.5}O_4$ (LNMO) and $LiNi_{0.25}M`_{0.25}$ $Mn_{1.5}O_4$ (M` = V, Cr or Co) have been prepared via sol-gel auto-combustion method as high voltage cathode materials. The changes in the crystallographic symmetry and space group were detected by X-ray diffraction technique (XRD). The surface morphology and particle size of the as-prepared materials were characterized by field emission scanning-electron microscopy (FE-SEM). Moreover, the magnetic properties of the as-prepared materials have been comparatively demonstrated using the vibrating sample magnetometer (VSM). The ionic conductivity of Li^+ ions in both bulk materials and assembled model electrodes were measured using electrochemical impedance spectroscopy analysis (EIS) at room and high temperatures. The obtained results indicated a remarkable improvement in both electronic and ionic conductivies of metal ions-doped LNMO spinel materials, showing lower charge transfer resistance and higher lithium ion diffusion coefficient, leading to better electrochemical kinetics. Finally, the galvanostatic cycling tests have been carried for the assembled batteries in the potential range of 3.0–4.8 V (vs. Li^+/Li).

Keywords: Lithium ion batteries, Spinel Cathodes, Sol-gel auto-combustion, Specific capacity.

***Contact person**: mustafa_sanad2002@yahoo.com, phone 00201068320472

References

1. L. Zhang, X. Lv, Y. Wen, F. Wang, and H. Su, “Carbon combustion synthesis of LiNi0.5Mn1.5O4 and its use as a cathode material for lithium ion batteries,” *J. Alloys Compd.*, vol. 480, no. 2, pp. 802–805, 2009.
2. N. D. Rosedhi, N. H. Idris, M. M. Rahman, M. F. M. Din, and J. Wang, “Disordered spinel LiNi0.5Mn1.5O4cathode with improved rate performance for lithium-ion batteries,” *Electrochim. Acta*, vol. 206, pp. 374–380, 2016.
3. Z. Zhu, L. Qi, W. Li, and X. Liao, “Preparation and Electrochemical Performance of 5 V LiNi0. 5Mn1. 5O4 Cathode Material by the Composite Co-Precipitation Method for High Energy/High Power Lithium Ion Secondary Batteries,” *Wuli Huaxue Xuebao*, vol. 30, no. 4, pp. 669–676, 2014.
4. R. Amin and I. Belharouk, “Part I: Electronic and ionic transport properties of the ordered and disordered LiNi0.5Mn1.5O4 spinel cathode,” *J. Power Sources*, vol. 348, pp. 311–317, 2017.

Innovating Sulfur Based Electrode and Modified Lithium Electrode for Stable and Safer Lithium-Sulfur Batteries. Cycling, Impedance, Non-Destructive Testing, Construction

Alexander Markevych [a], Elena Shembel[a,b], Andrea Straková Fedorková[c], Vlad Redko[b]

[a] Scientific-Research Laboratory of Chemical Power Sources, Ukrainian State
University of Chemical Technology, Dnipro, 49005, Ukraine

[b] Enerize Corporation, Coral Springs, FL, 33067,USA

[c] Pavol Jozef Safarik University, Kosice, SK-04154, Slovak Republic

In the article the results of galvanostatic cycling of electrochemical cells with sulfur electrodes, prepared by the innovative saturation method of the carbon matrix with sulfur, previously dissolved in an organic solvent are presented. Studies of Li-S cells were carried out in two types of electrochemical cells: 1) 2-electrode coin cells (size 2016) and 2) 3-electrode flat pouch cells, with a lithium reference electrode. The effects of 1) the sulfur content in the cathode on the specific reversible electrochemical capacity of sulfur, as well as 2) the effect of the capacity per cm^2 of the electrode surface during lithium cycling on the stability of the electrochemical system as a whole are shown. The process of self- discharge of the sulfur electrode during storage and the change of the impedance of the sulfur electrode during storage are investigated.

Advantages of innovating method production the sulfur based cathode

In our previous publication the technology of manufacturing innovative sulfuric electrode by the method of saturation was described [1]. This technology includes the following stages:

- the formation of a porous carbon matrix on the surface of the current collector;
- Preparation of a solution of sulfur in an organic solvent;
- Saturation of the carbon matrix with sulfur solution;
- Evaporation of the solvent and filling the pores of the carbon matrix with sulfur; The advantages of this technology compared to the traditional, based on the
- preparation of slurry, are as follows:
- The lower temperature of the formation of the sulfur electrode allows reducing the evaporation rate of sulfur and maintaining the active electrode material in the structure of the electrode;
- Ability to use a more efficient binder component that forms the structure of the porous carbon matrix at a higher temperature. Evaporation of the solvent from the electrode, saturated with sulfur, is carried out at a lower temperature at which sulfur does not evaporate. This makes it possible to stabilize the electrode structure during a long cycling process and to increase the specific electrochemical capacity of the cathode and the Li-S cell in general;
- Low content of polymer binder in the electrode, because of the binder is used to form only the carbon matrix. It allows to reduce the binder content from the traditional 10% to 3%

in general electrode composition, which is important from an environmental point of view.

Cycling sulfur based cathode produced by saturation method

The following methods were used to study sulfur electrodes: galvanostatic cycling, impedance spectroscopy, innovative non-destructive electromagnetic testing methods [2].

The electrochemical characteristics of the sulfur electrodes obtained by the saturation method were studied in electrochemical cells of 2 types: 2-electrode coin cells (2016 size), and 3-electrode pouch cells of a flat design, with a lithium reference electrode. Composition of electrolyte: Dimethoxyethane + dioxolane (2: 1), 0.7 M LiIm, 0.25 M $LiNO_3$.

The charge-discharge characteristics of sulfur electrodes in coin and pouch electrochemical cells and the dynamics of changing of the specific electrochemical capacitance during the cycling process are presented in Fig. 1 and 2.

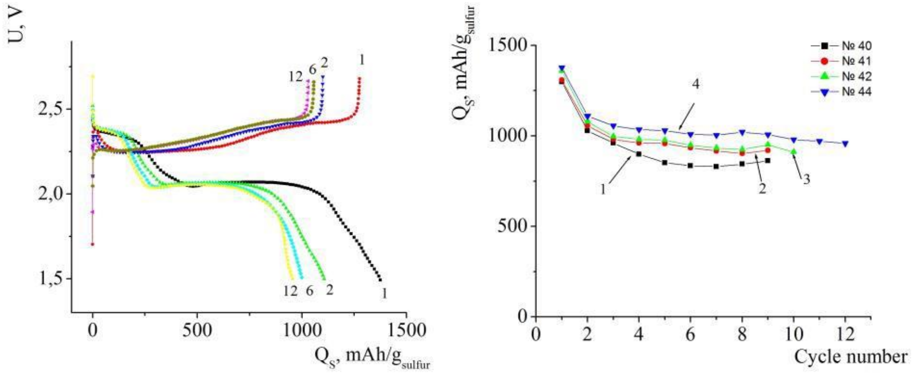

A B

Figure 1. *A - Charge-discharge characteristics of the electrode No. 44. Sulfur weight 4.1 mg/cm^2. Cycling current 0.1 C (0.41 mA/cm^2). The sulfur content in the cathode is 70%. Coin cell with 2016 size. B - the dynamics of changes of the specific electrochemical capacity of sulfur electrodes № 40, 41, 42 and 44 for cycling.*

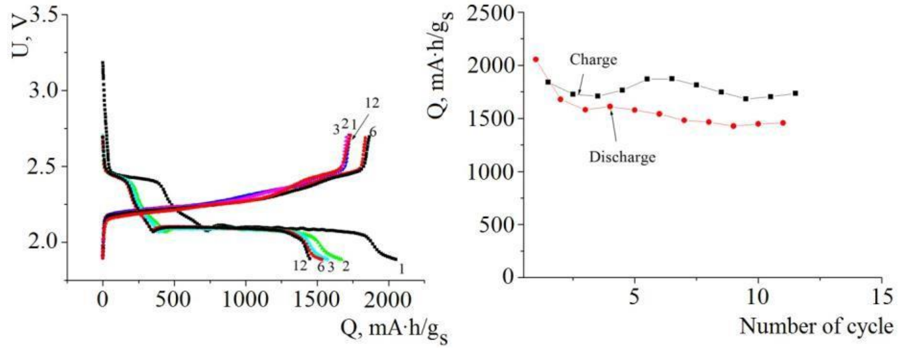

A B

Figure 2. *A - Charge-discharge characteristics of the electrode No. 95. Sulfur weight 1 mg/cm^2. Cycling current 0.1 C (0.1 mA/cm^2). The sulfur content in the cathode is 20%. Pouch cell. B - the dynamics of changes of the specific electrochemical capacity of the electrode No. 95 for cycling.*

In the coin cells (Fig. 1), Li-S cells with a high sulfur content in the cathode were investigated: 4.1 mg/cm^2. This corresponded to 70% sulfur containing in the cathode.

It was found that the limit on the number of charge-discharge cycles in an electrochemical system, where sulfur electrodes with a high sulfur content were used, may be due not only to the sulfur electrode electrochemistry, but also to the following factors:

1. Electrochemical reduction of non-aqueous electrolyte on the surface of the carbon matrix in the process of cathode discharge. To reduce this process, we carried out a discharge of the current source in the potential range not lower than 1.8 V. The use of carbon materials, which are inhibitors of the electrochemical decomposition of non- aqueous electrolyte, is also promising.

2. Redistribution of non-aqueous liquid electrolyte between components of Li-S cells. This process is due to the fact that under conditions of high sulfur content in the cathode, high values of discharge and charging capacity are realized during system cycling. As a result, a lithium bulk precipitate with a developed structure is formed on the surface of the lithium anode. This structure is filled with non-aqueous electrolyte. At this, the amount of free (buffer) electrolyte in the cell decreases, the amount of electrolyte in the porous structure of the cathode and the separator also decreases [3]. Such a process can be called the “drying” of the electrode structure.

With the goal to reduce the electrochemical capacity per unit of the surface of the lithium electrode, and as a consequence of reducing the rate of “drying” of the electrode structure, electrodes with a low sulfur content were used in electrochemical pouch cells: 1 mg/cm^0 or 20% in the cathode.

From fig. 1 and 2, it can be seen that the sulfur electrodes obtained by the saturation method have a rather high specific reversible electrochemical capacity. The specific reversible discharge capacity of electrodes with 70% sulfur content reaches 900-1000 mA·h/g of sulfur (Fig. 1).

Electrodes with low sulfur content (20%, Fig. 2) have a significantly higher specific reversible discharge capacity, which reaches 1400 mA·h/g of sulfur with the same rate of cycling (0.1 C).

The impedance characteristics of the sulfur electrode after cycling for 65 charge- discharge cycles in a charged state during storage have been investigated. The presentation will present the impedances of the sulfur electrode storage process and the results of the study of the process of self-discharge of the current source during storage.

Cycling of lithium with a sulfur electrode

One of the reasons for limitation the number of charge-discharge cycles of lithium-sulfur batteries is the redistribution of non-aqueous electrolyte in the structure of the Li-S cell. One of the factors of decomposition of a liquid electrolyte is the process of interaction of its components on the surface of a lithium electrode in the process of cycling.

For a more detailed study of this effect, the electrochemical cells of the lithium- sulfur system after cycling were opened, and the surface of lithium was investigated visually. In fig. 3 shows photographs of the surface of the lithium electrode after cycling together with a sulfur electrode, from a different angle.

A B C

Figure 3. *Photograph of the electrode structure of the cell after cycling electrode No.86b. A - the outer surface of lithium. B - the inner surface of lithium. C - side view.*

Dark spots on the surface of lithium, which are friable through formations, are probably the product of the interaction of lithium and components of the liquid electrolyte. Thus, the process on the surface of the lithium electrode during the cycling of the power source contributes to the decomposition of the electrolyte.

Thus, on the basis of the conducted research the following conclusions can be made:

- Specific reversible electrochemical capacity of sulfur electrodes with high sulfur content (70%) when cycling with a current of 0.1 C reaches 1000 mAh/g;
- Specific reversible electrochemical capacity of sulfur electrodes with low sulfur content (20%) when cycling with a current of 0.1 C reaches 1400 mAh/g;

The limitation of cycling of the electrochemical system of lithium-sulfur is due to several factors:

- redistribution of electrolyte in the electrode structure of Li-S cells;
- interaction of metallic lithium with electrolyte components during cycling;
- electrochemical decomposition of electrolyte on the surface of the carbon matrix in the discharge process at relatively low potentials.

Acknowledgments

This work has been done in the framework of NATO SPS 985148 project “Development of New Cathodes for Stable and Safer Lithium-Sulfur Batteries” / Science for Peace and Security Programme. Enerize Corporation is an industrial partner under NATO SPS 985148 project. Prof. E. Shembel is the Head of SRLCPS USUCT and Partner country- Ukraine Director of this NATO project.

References

1. A.V.Markevych, E.M. Shembel, V. Redko*, J. ECS Transactions.*, **81**(1), p. 115-122 (2018).
2. V. Redko, V. Khanderskyy, E. Shembel, etc. US Patent № 7,982,457. (2011).
3. Guoxing Li, Yue Gao, Xin He, *J. Nat. Communications.*, Vol. **8**, Article number*:* 850 (2017).

Anion Structure Influence on Li-Ion Electrolyte Properties. Model Electrolytes, New Salts, Non-Fluorine Electrolytes

L. Niedzicki[a], M. Broszkiewicz[a], J. Szydłowski[a], M. Kasprzyk[a] and T. Trzeciak[a]

[a] Faculty of Chemistry, Warsaw University of Technology,
Noakowskiego 3, 00-664 Warszawa, Poland

In the present work a detailed analysis of anion structure influence on electrochemical and other properties of the lithium-ion cell electrolyte are presented. The subject of the investigation are two analog salts – LiTDI and LiPDI, which both comply with all requirements of the battery industry and differ only with perfluoroalkyl side chain length (CF_3 and C_2F_5, respectively). Resulting information were applied in the design and synthesis of new anions tailored for the lithium-ion cell electrolyte application, but potentially can be also used in other cells such as Li-S, Na-ion and/or as anions for ionic liquid synthesis.

Introduction

For the last almost 30 years of lithium-ion cells on the market, they were dominated with only one electrolyte technology – the one based on $LiPF_6$ salt. $LiPF_6$ have been widely known for low thermal stability, chemical stability and sensitivity as well as susceptibility to the most common traces, such as H_2O and HF (HF both residual from $LiPF_6$ manufacturing and produced through contact with water traces). Other salts were tried by numerous teams around the world (over 200 suggested anions throughout last 30 years), with only around a dozen passing through most basic tests. Among those, $LiClO_4$ fails due to thermal instability – explosive properties, $LiAsF_6$ due to its toxicity, $LiBF_4$, LiDFOB (lithium difluoro(oxalato)borate) and LiBOB (lithium bis(oxalato)borate) due to formation of instable SEI layer on the anode, LiTFSI (lithium bis(trifluorosulfonyl)imide) and LiFSI (lithium bis(fluorosulfonyl)imide) due to their corrosive properties towards aluminum (current collector of cathode) and LiFAP (lithium trifluorotris(pentafluoroethyl)phosphate) due to expensive manufacturing. LiTDI (lithium 4,5-dicyano-2-trifluoromethylimidazolide) and LiPDI (lithium 4,5-dicyano-2-pentafluoroethylimidazolide), as well as LiHDI (lithium 4,5-dicyano-2-(*n*-heptafluoropropyl)imidazolide) introduced by Warsaw University of Technology team of Prof. Wieczorek – L. Niedzicki *et al.* (1)(2)) to the field few years ago were more robust than most of aforementioned salts. They were thermally, electrochemically and chemically stable, insensitive towards water or air, could work with modern electrode materials including those susceptible to HF (thus incompatible with $LiPF_6$), exhibited good transport properties (especially lithium cation transference number) and could be manufactured in the inexpensive way. This is why they are becoming popular in the field (at least 30 articles were written on them in the last 5 years by independent groups, *e.g.* Zaghib *et al.* (4), Lemordant *et al.* (5)), as dealing with them is much easier than with $LiPF_6$, as they are more stable and do not harm cathode materials, contrary to $LiPF_6$ in some instances. All those advantages resulted in introduction to the mass production in 2018 and application in consumer lithium-ion cells.

Among all salts actually used in the Li-ion cell field, LiTDI and LiPDI are the closest related and most similar to each other (even more than LiFSI and LiTFSI). Hence, they provide the unique possibility to look for the clues on electrolyte properties changes due to anion structure differences.

Such investigation, along with analysis of previously synthesized salts can provide unique information for design and tailoring of new anions for even better performance both in cells and other applications.

Results and discussion

The most important results from the theoretical and fundamental point of view is actual catching the differences in electrolyte properties between LiTDI- and LiPDI-based and explanation of their origin. Superficially, they both has almost identical electrochemical performance (such as conductivity) with individual results within the range of measurement error. However, when analyzed in detail, non-electrochemical results or change of solvent to strengthen some traits can yield bigger difference. For instance, lithium transference number in different olygoglycols will show advantage of LiTDI in more viscous systems, especially at higher salt concentrations, while LiPDI will have lower association effect when FTIR-based indirect associates are investigated (Fig. 1). Although TDI anion is smaller and thus forms less viscous solutions at the same concentration, PDI anion has a group that has slightly stronger electron-withdrawing property. Thus, the two main molecular properties, that are size/shape factor and uniform charge distribution are almost perfectly balancing each other. LiHDI on the other hand (next analog in the family of anions) is an anion that has completely different set of electrochemical parameters, as those two properties are outbalanced. Size is even bigger and shape is considerably farther from sphere-like, side chain has bigger freedom of movement, while electron withdrawing effect of the -*n*-C_3F_7 group is almost the same as the -C_2F_5 one.

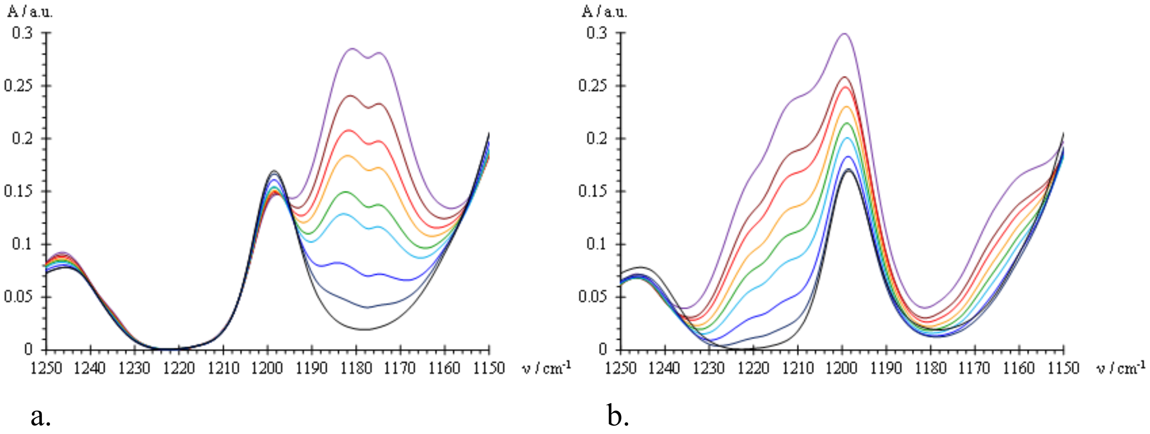

Figure 1. *FTIR spectra (zoomed in 1150-1250 cm^{-1} region) of triglyme solutions of lithium salt prepared in salt to solvent ratio of (top to bottom): 1:3 (purple line), 1:4, 1:5, 1:6, 1:8, 1:10, 1:20, 1:50 and pure triglyme (black line) a. LiTDI; b. LiPDI.*

The results come in concert with investigations of other imidazole-based double-ring anions LiTDBI (lithium 5,6-dicyano-2-trifluoromethylbenzimidazolide) published by our group - L. Niedzicki *et al*. (5) and LiTDPI (lithium 4,5-dicyano-2-trifluoromethylimidazopyrazine), also by L. Niedzicki *et al*. (6).

All abovementioned results were used to form rules for design of new anions, particularly for new generation of non-fluorine salts. First such salts are LiPCP (lithium 1,1,2,3,3-pentacyanopropenide) (7) and LiHCAP (lithium 1,1,2,4,5,5-hexacyano-3-aza-1,4-pentadienide) (8). The results for both are promising in terms both of electrochemical performance (conductivity) as well as battery cycling results.

Conclusions

Rules for design of tailored anions for application as electrolyte in lithium-ion cells are formed as a result of detailed analysis of minute differences of electrochemical properties of electrolyte based on LiTDI and LiPDI salts. Results are also backed up by results from other imidazole-derived salts. Rules are used to design new salts with tailored properties as well as they can be used for further development of anions.

Acknowledgments

This work has been supported financially by Warsaw University of Technology.

References

1. L. Niedzicki, M. Kasprzyk, K. Kuziak, G.Z. Żukowska, M. Armand, M. Bukowska, M. Marcinek, P. Szczeciński, W. Wieczorek, *J. Power Sources*, **192**, 612 (2009)
2. L. Niedzicki, G.Z. Żukowska, M. Bukowska, P. Szczeciński, S. Grugeon, S. Laruelle, M. Armand, S. Panero, B. Scrosati, M. Marcinek, W. Wieczorek, *Electrochim. Acta*, **55**, 1450 (2010).
3. S. Paillet, G. Schmidt, S. Ladouceur, J. Frechette, F. Barray, D. Clement, P. Hovington, A. Guerfi, A. Vijh, I. Cayrefourcq, K. Zaghib, *J. Power Sources*, **294**, 507 (2015).
4. C.L. Berhaut, R. Dedryvere, L. Timperman, G. Schmidt, D. Lemordant, M. Anouti, *Electrochimica Acta*, **305**, 534 (2019).
5. L. Niedzicki, P. Oledzki, A. Bitner, M. Bukowska, P. Szczecinski, *J. Power Sources*, **306**, 573 (2016).
6. L. Niedzicki, J. Korczak, A. Bitner, M. Bukowska, P. Szczecinski, *RSC Adv.*, **5**, 101917 (2015).
7. L. Niedzicki, M. Bukowska, T. Trzeciak, A. Bitner-Michalska, P. Szczeciński, M. Marcinek, W. Wieczorek, Polish Patent PL232856.
8. L. Niedzicki, T. Trzeciak, J. Niewiedział, Polish Patent PL227209.

Linking crystallographic and electrochemical properties of layered oxide cathodes

K. Fröhlich[a], I. Abrahams[b], M. Jahn[a]

[a] Center for Low-Emission Transport, AIT Austrian Institute of Technology GmbH, 1210 Vienna, Austria

[b] School of Biological and Chemical Sciences, Queen Mary University of London, London, E1 4NS, United Kingdom

The kinetics of lithium ion diffusion in electrode materials are essential for the electrochemical performance of the corresponding Li-ion battery. The electrodes' crystal structure, where lithium ions are inserted and extracted during charging and discharging, determines reaction kinetics and therefore determines the chemical diffusion coefficient. In this work, the lithium ion diffusion coefficient is calculated via the Galvanostatic Intermittent Titration Technique (GITT) measurement and linked with crystallographic analysis of $LiNi_{1/3}Mn_{1/3}Co_{1/3}O_2$ (NMC) cathodes at different lithiation states.

Introduction

For insertion electrodes such as common cathode materials for Li-ion battery systems, the crystal structure and its properties such as chemical diffusion coefficient of Li^+-ions, unit cell parameters and the voltage limitations during cycling, are principal factors to determine for existing and future material design. Galvanostatic Intermittent Titration Technique (GITT) is among the most reliable and simple tools to determine chemical diffusion coefficients in electrode materials.

In this work, the open-circuit voltage (OCV) at different lithiation states is derived from the GITT measurements and then plotted versus the fitted unit cell parameters to link crystallographic and electrochemical properties of the NMC cathode material.

Experimental

GITT measurements of half cells were performed to determine the chemical diffusion coefficients of lithium ions in the via co-precipitation route synthesized NMC cathodes over the cycling range from 3 to 4.2 V. Current pulses for 600 s at 0.1C were applied. The open-circuit voltage was directly derived from the experiment, whereas the lithium diffusion coefficient in the cathode was calculated accordingly as first described by Weppner and Huggins[1].

CV measurements were performed prior to the crystallographic analysis with scan rates of 0.1 mV s^{-1} up to 4.5 V. The measurements were stopped at different potentials to attain the desired lithiation state of the corresponding cathode, which was further crystallographically analyzed via Rietveld fitted XRD measurements.

Results & Discussion

The applied current and expected voltage profile during the GITT measurement for one pulse are schematically shown in Fig. 1 (left). The corresponding calculated chemical diffusion coefficients of lithium ions in the NMC cathode are presented in Fig. 1 (right).

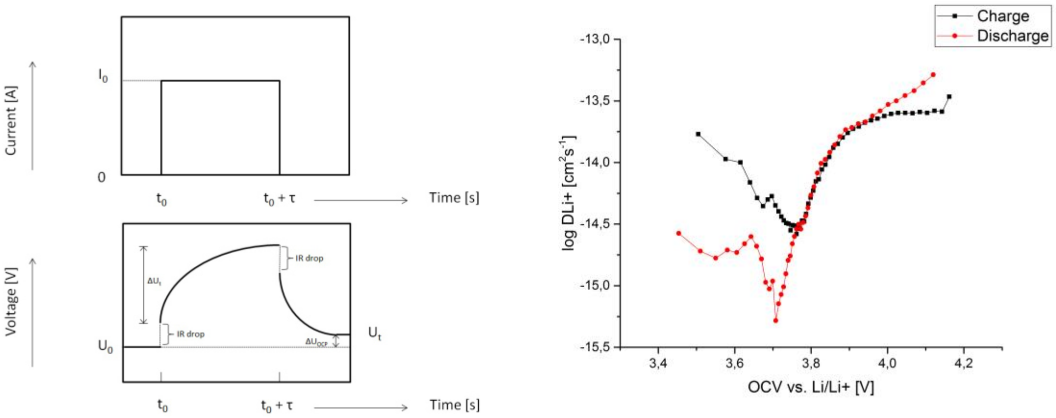

Figure 1. *Schematic current and voltage profile during the measurement (left). Chemical diffusion coefficient of lithium ions in the material in logarithmic scale at different OCV (right).*

The open-circuit voltage shows a plateau in the region of 3.7 - 3.8 V, whereas above 3.9 V, the OCV is constantly increasing. Meanwhile, up to 3.8 V, the chemical lithium ion diffusion is lower for discharging than charging case in this material. During charging, lithium ions are extracted from the cathode, whereas in the discharging case, lithium ions are inserted into the NMC structure. From 3.8 to 4.0 V, charge and discharge diffusion coefficients are increasing, exhibiting similar characteristics and values. Above this state, the chemical discharge diffusion coefficient is higher compared to charging.

Figure 2 plots the refined unit cell parameters from the Rietveld fit of the XRD pattern over the OCV versus lithium.

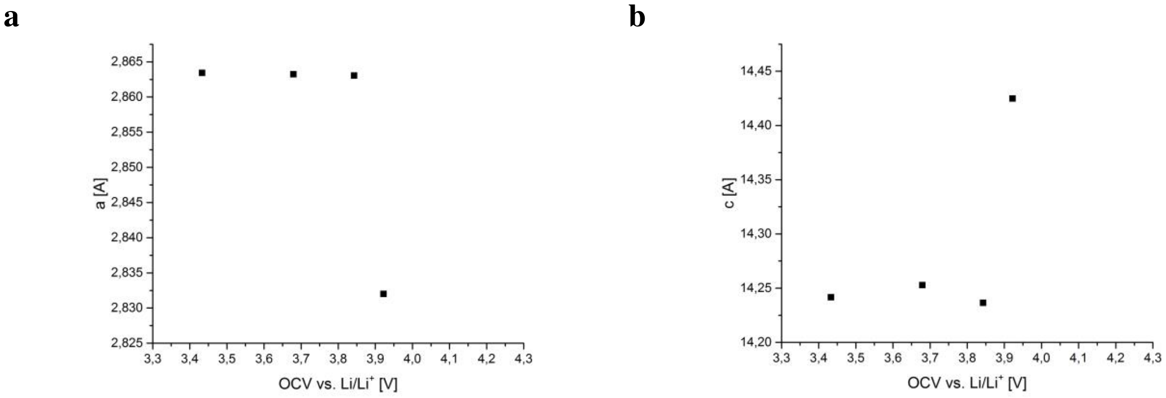

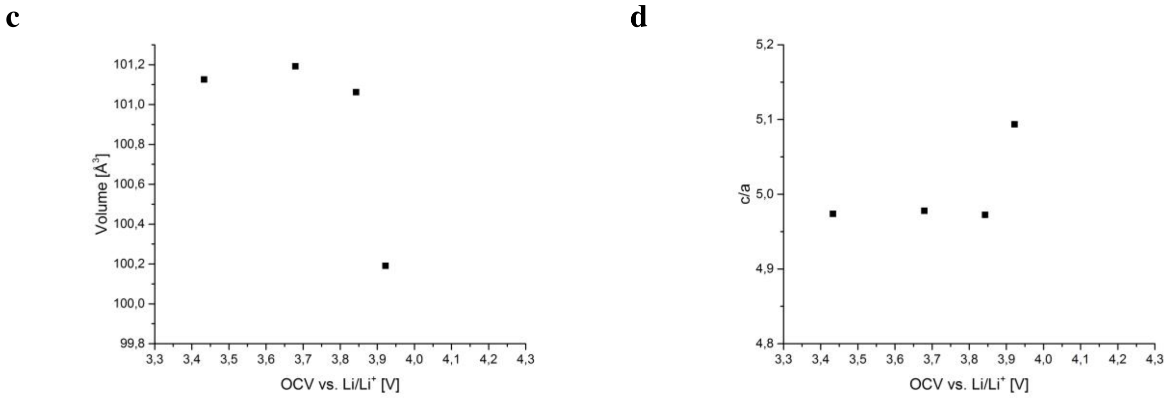

Figure 2. *Unit cell parameters of the NMC cathode over the OCV. (a) The a-parameter refers to the interslab distance in the transition metal oxide layers, whereas the (b) c-parameter represents the intraslab distance between these layers, where lithium ions are inserted/extracted during discharging/charging.*

The a-axis is decreasing in the measured OCV range, where the strongest decay was observed between 3.8 - 3.9 V. The decrease of the interslab distance (a) is linked to the ionic radii of the Ni-ions, which are responsible for charge compensation in this region[2]. Meanwhile, the c-axis of the structure is increasing with the most pronounced difference in the same OCV region. The increase of the interslab distance during extraction of Li^+ seems contradictory, but is caused by electrical repulsion between the transition metal oxide layers[3]. The unit cell volume is mainly dominated by the a-axis variation, showing an overall change of solely 1%, which is favorable during cycling to avoid particle cracking or pulverization in long term cycling. The c/a-ratio between the axes of the unit cell is linear up to 3.9 V OCV, where it is increasing due to the non-linear changes in the corresponding axes.

The presented data shows good reliability with a simple measuremental set-up, where no neutron diffraction or *in situ* cells are needed. The data can even be recorded from realistic environments and can easily be applied to standard electrochemical measurements. Considering the scientific movement towards nickel- and lithium-rich layered oxides, the presented data could help understanding phase change behaviour of novel cathode structures better.

Acknowledgments

This work was financially supported by the Austrian Federal Ministry for Transport, Innovation and Technology (bmvit).

References

1. W. Weppner and R.A. Huggins, J. Electrochem. Soc., **124**, 1569 (10 1977).
2. W.-S. Yoon, K.Y. Chung, J. McBreen, X.-Q. Yang, Elect. Comm., **8**, 1257 (2006).
3. M. Labrini, I. Saadoune, A. Almaggoussi, J. Elhaskouri, P. Amoros, Materials Research Bulletin, **47**, 1004 (2012).

Electrochemical Properties of $Li_4Ti_5O_{12}$ with Conductive Binder

S. N. Eliseeva[a], M. A. Kamenskii[a], V. V. Kondratiev[a]

[a] Institute of Chemistry, Saint Petersburg State University, Saint Petersburg, 199034, Russia

Electrochemical properties of $Li_4Ti_5O_{12}$-electrodes (LTO) with water-based combined conductive polymer poly(3,4-ethylenedioxythiophene):polystyrenesulfonate and carboxymethylcellulose (PEDOT:PSS/CMC) binder were investigated. It was shown, that LTO-electrodes with PEDOT:PSS/CMC binder has superior properties in comparison with conventional electrodes based on PVDF in term of higher specific capacity (increase up to 14%), improved C-rate capability (especially at high rates 10–30 C) and life cycle stability of battery. SEM-investigation of morphology of LTO-electrodes before and after electrochemical tests shows the good adhesion to Al substrate and good binder properties of conducting polymers. Ageing processes of LTO-electrodes during long-cycling were investigated for the two types of binders.

Introduction

Among the negative electrode materials for lithium-ion batteries (LIB), lithium titanium oxide $Li_4Ti_5O_{12}$ (LTO) is a promising anode material due to its zero lattice strain during charge-discharge and excellent safety as particular advantages (1–3) as compared with graphite. However, LTO has low electronic conductivity 10^{-13} Sm·cm^{-1} (4,5). Therefore, the nanostructuring of LTO-grains (6,7) and the introduction of conductive additives to improve high rate performance and efficient material utilization (8–10) is required. Concerning the stability issues, the LTO electrodes with PVDF binder has shown irreversible surface morphology changes resulting in capacity loss and low cycle life.(5,11)

Several approaches have been proposed to improve the electrochemical performance of LTO materials, among them surface modification of LTO by TiO_2 layers polyaniline or polythiophene layers and replacing PVDF binder by water soluble binders. Water soluble binders have received great attention for application in LIBs due to their environmental friendliness and possibly improved safety of the obtained batteries. Different types of water soluble binders improving the electrochemical performance of electrode materials have been proposed (12,13). Among water soluble binders used for LTO based electrodes are sodium carboxymethyl cellulose (CMC), sodium carboxymethyl cellulose combined with styrene butadiene rubber, poly(acrylic acid), commercial Acryl S020 binder, and sodium alginate.

Results and discussions

In this work we present a simple and cost-effective approach to fabricate $Li_4Ti_5O_{12}$-electrodes with enhanced functional properties by using eco-friendly water-based binder, which is an alternative to fluorine-containing binders. The obtained results show that the using of PEDOT:PSS/CMC binder in the fabrication of LTO-electrodes maintains the good integrity of material and adhesion to current collector. Electrochemical characterization was performed by galvanostatic charge-discharge, cyclic voltammetry and impedance spectroscopy. The LTO-electrodes with combined PEDOT:PSS/CMC binder have superior properties, in particular increased specific capacity and improved C-rate performance during charge-discharge. By using PEDOT:PSS/CMC binder instead of PVDF, the practical specific capacity was increased up to 14 %. Highest stability during long cycling was observed for $Li_4Ti_5O_{12}$-electrode with this binder at less than 1% decay after 100 cycles at 1C. The drop in specific capacity for PVDF-bound LTO-electrode after 100 cycles was 5 % (14). The kinetic parameters were obtained from analysis of the impedance spectra for electrodes (charge transfer resistance R_{ct}, resistance of the solid electrolyte layer R_{SEI}, Warburg constant σ_W and apparent diffusion coefficient D_{app}), that characterize charge transfer processes in LTO-electrodes.

Combined conductive polymer binder provides partial or complete wrapping of the LTO grains, that can more effectively inhibit the interaction of the active material with the electrolyte and side reactions, reducing the degradation of LTO-electrode in the case of PEDOT:PSS/CMC binder.

Acknowledgments

The financial support from the St Petersburg State University (grant № 26455158) is gratefully acknowledged. The authors would like to thank the Center for X-ray Diffraction Methods, the Interdisciplinary Center for Nanotechnology Research park of Saint Petersburg State University, Resource Centre of Physical methods of surface investigations of Saint-Petersburg State University, where data were obtained with support of RFBR grant № 19-03-00593-a.

References

1. M. Armand, J. M. Tarascon, *Nature*, **451**, 652 (2008)
2. K. Zaghib, M. Simoneau, M. Armand, M. Gauthier, *J. Power Sources*, **81–82**, 300 (1999)
3. J. Lu, C. Nan, Q. Peng, Y. Li, *J. Power Sources*, **202**, 246 (2012)
4. T. Yuan, X. Yu, R. Cai, Y. Zhou, Z. Shao, *J. Power Sources*, **195**, 4997 (2010)
5. C. H. Chen, J. T. Vaughey et al, *J. Electrochem. Soc.*, **148**(1), A102 (2001)
6. L. Xiao, G. Chen, J. Sun, D. Chen, H. Xu, Y. Zheng, *J Mater Chem A.*, **1**(46), 14618 (2013)
7. N. Liu, W. Li, M. Pasta, Y. Cui, *Front. Phys.*, **9**(23), 323 (2014)
8. B. Zhao, R. Ran, M. Liu, Z. Shao, *Mater Sci Eng R Reports*, **98**, 1 (2015)
9. M. Kitta, T. Akita, M. Kohyama, *J. Electrochem. Soc.*, **162**(7), A1272 (2015)
10. C. P. Sandhya, B. John, C. Gouri, *Ionics*, **20**(5), 601 (2014)
11. T. F. Yi et al, *J. Phys. Chem. Solids*, **71**(9), 1236 (2010)
12. J.-T. Li et al, *Adv. Energy Mat.,* 1701185 (2017)
13. S. L. Chou, Y. Pan, J. Z. Wang, H. K. Liu, S. X. Dou, *Phys. Chem. Chem. Phys.,* **16**(38), 20347 (2014)
14. S. N. Eliseeva et al, *Solid State Ionics,* **333**, 18 (2019)

Solid Polymer Electrolyte for Improving the Safety of Lithium-Sulfur Battery

O. V. Kolomoiets[a], E. M. Shembel[a, b], A. Straková Fedorková[c]. and M. Yu. Koltsov[a]

[a] Scientific-Research Laboratory of Chemical Power Sources, Ukrainian State University
of Chemical Technology, Dnipro, 49005, Ukraine. okolomoyets@gmail.com

[b] Eneize Corporation, Coral Springs, 33067, FL, USA. eshembel@enerize.com

[c] Pavol Jozef Safarik University, Kocice, SK-04154, Slovak Republic. andrea.fedorkova@upjs.sk

Polymer electrolytes that containing: 1) Polymer matrix Polyvinylidene fluoride (PVDF), 2) Ionic liquid / quaternary ammonium salt, 3) Lithium salt - $LiN(CF_3SO_2)_2$, 4) Plasticizer - tetraglym (G4) have been investigated using: scanning electron microscopy, impedance, cyclic voltammetry and galvanostatic studies in the lithium-sulfur system. The prospects of the polymer electrolyte use for improving the safety of lithium-sulfur batteries are shown.

Introduction

Power sources based on the lithium-sulphur system are promising, but have not yet become wide commercial. Among the many problems in operation, the Li-S system are the problems of self-discharge and stability of the cycling. Electrolyte is an important factor for solving this problem (1). The developers (2) suggest using a polymer electrolyte as a way of improving the lithium electrode properties.

Experimental

The issues with composition and properties of electrolyte for Li batteries led to the search for alternative ionic-liquid based electrolyte systems consisting exclusively of cations and anions (for example, the Quaternary Ammonium Compounds Class (QAC) on the basis of imidazoline, pyrrolidined, pyridine derivatives, etc.).

It seems perspective the research and development of some properties of solvate ionic liquids on the basis of quaternary ammonium compounds, in combination with the glyms (low molecular weight polyethers of the general structural formula CH_3-O - (- CH_2-CH_2-O-) n-CH_3 (n = 3-4), and salt of alkali metals.

It is expected that the ion conductivity of the complex at room temperature will be sufficient to maintain a high level of charge/discharge characteristics of the power source and will depend on the ratio of G4 : $LiN(CF_3SO_2)_2$. To increase the level of ionic conductivity and thermal stability of electrolyte systems such as solvate ion liquids based on [Li (G4) x] [$N(CF_3SO_2)_2$], we propose the use the benzyl-phenyl-dimethylammonium chloride or benzyl-3-methyl ammonium chloride. This is promising since it is known that imidazolinium compounds are characterized by a high level of thermal stability - up to 300°C, which depends on the structure of the cationic and anionic part of the QAC.

As a polymer matrix for promising polymer electrolytes, a copolymer of vinylidene fluoride with hexafluoropropylene SOLEF 21508 (Solvey), which has a high level of thermal and electrochemical stability, was also selected. Technology the processes of organizing the interface between the polymer electrolytes and electrode materials also have been developed during realizing presented investigations.

We develop a new solid polymer electrolyte with Ionic-liquid as the specific additive. Composition of new solid polymer electrolyte is as following:

- Polymer matrix - PVDF copolymer 21508 (Solway, Belgium);
- Ionic liquid - Quaternary ammonium compounds (QAC)
- Lithium salt - $LiN(CF_3SO_2)_2$;
- Plasticizer - tetraglym (G4)

New solid polymer electrolyte that developed has a high level of thermal stability and conductivity. Operating range of the temperature is from minus 20^0C to plus 100^0C

Scanning electron microscopy was used to study the microstructure of the surface morphology of polymer films. As is shown (Fig. 1), the films are solid, non-porous, homogeneous. The introduction of QAC changes the morphology of the surface, but the film remains solid, non-porous, homogeneous.

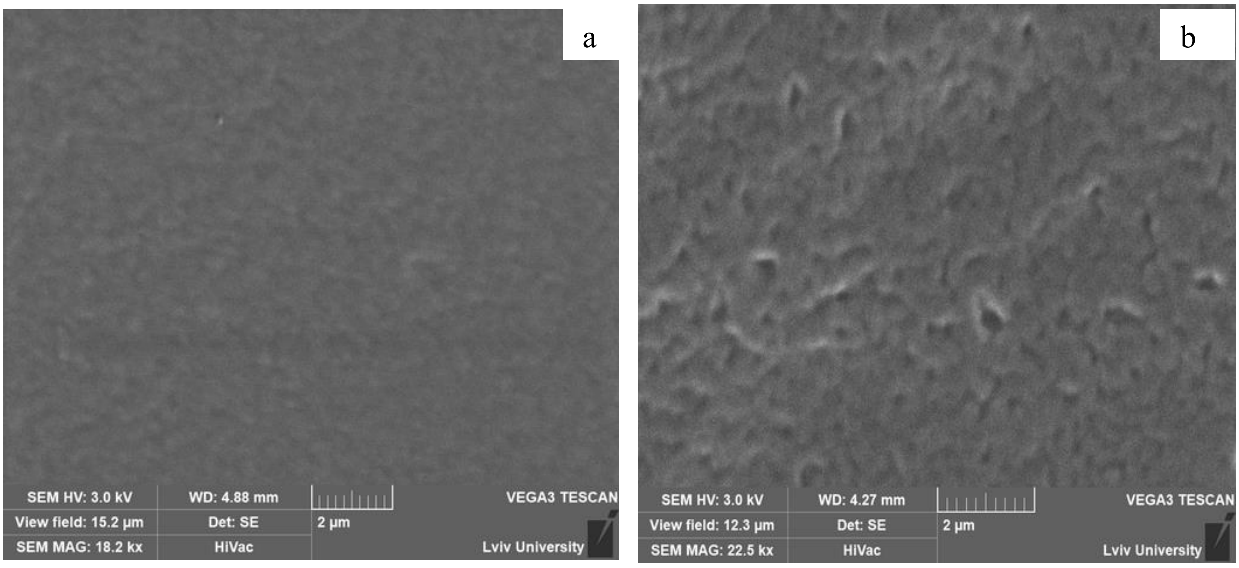

Figure 1. *SEM of solid polymer electrolytes without QAC (a) and with benzyl-phenyl-dimethyl ammonium chloride (b) in its composition*

The ionic conductivity of polymer electrolytes was measured using impedance spectroscopy in cells with nickel electrodes of 1 cm^2. Polymer electrolytes satisfy the requirements for conductivity at a level of 10^{-3} S/cm (Fig. 2). After temperature studies, the film was stored at +60°C and then at +90°C. The conductivity of the films did not change during several weeks after coating polymer on the electrode, which confirms the stability of the polymer compositions to high temperatures.

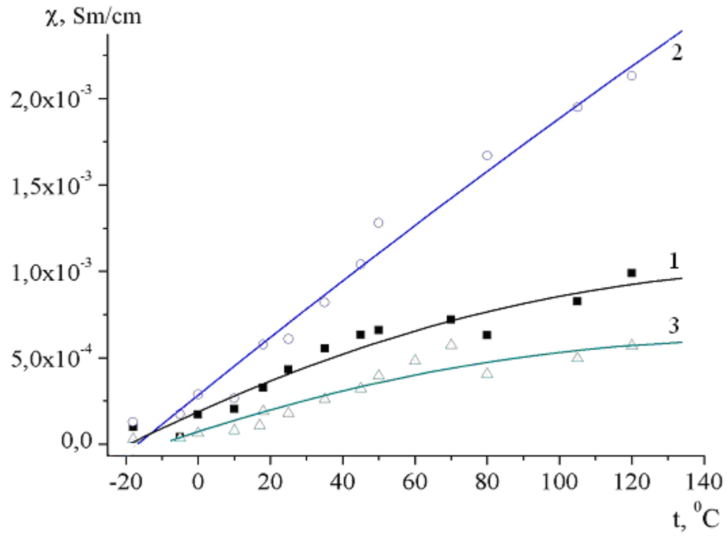

Figure 2. *The dependence of conductivity on temperature. Comparison of the electrolytes:*
1 – (PVdF-1 M $LiN(CF_3SO_2)_2$*– G4 (without QAC)),*
2 – (PVdF-1 M $LiN(CF_3SO_2)_2$ *-* $[PhCH_2NMe_3]^+Cl^-$ *– G4),*
3 – (PVdF-1 M $LiN(CF_3SO_2)_2$ *-* $[PhCH_2NMe_2Ph]^+Cl^-$ *– G4)*

In order to determine the electrochemical stability of the developed polymer electrolytes, cyclic voltammetry was carried out. It is established that electrolytes are stable in the potential range 1,5 – 4,5 V (Fig. 3), which allows us to recommend them for the lithium-sulfur system.

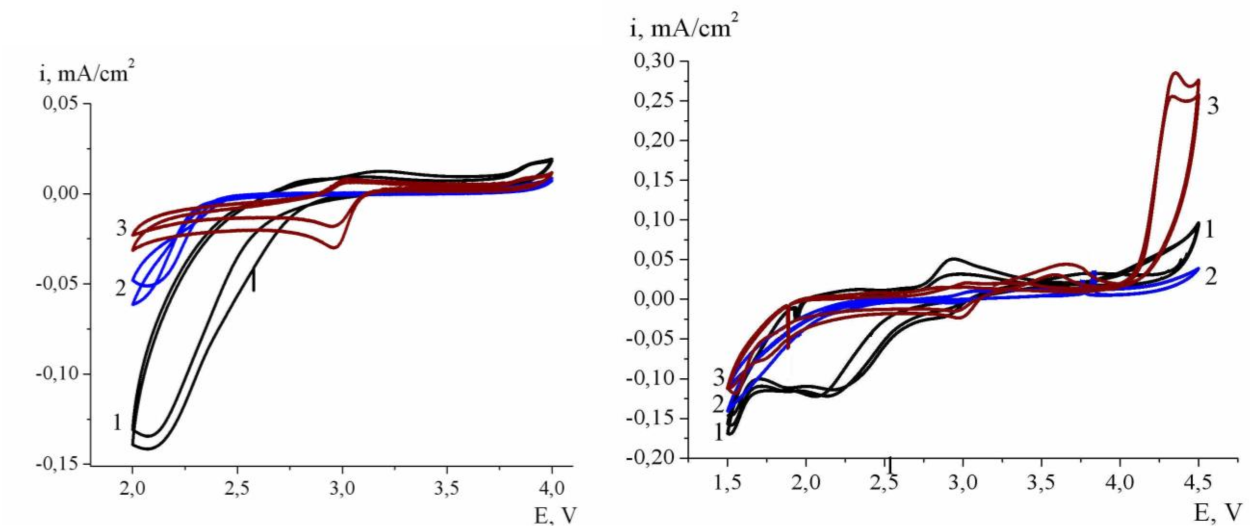

Figure 3. *Cyclic voltammetry of the Pt-Pt-Li system with polymer electrolytes:*
1 – electrolyte (PVdF-1 M LiN(CF3SO2)2– G4 (without QAC)),
2 – electrolyte (PVdF-1 M LiN(CF3SO2)2 - [PhCH2NMe3]+Cl- – G4),
3 – electrolyte (PVdF-1 M LiN(CF3SO2)2 - [PhCH2NMe2Ph]+Cl- – G4)
in the range of potentials 2,0 – 4,0 V(a) and 1,5 – 4,5 V (b)

Figure 4 demonstrates the discharge-charge characteristics of Li-S power sources with developed polymer electrolytes.

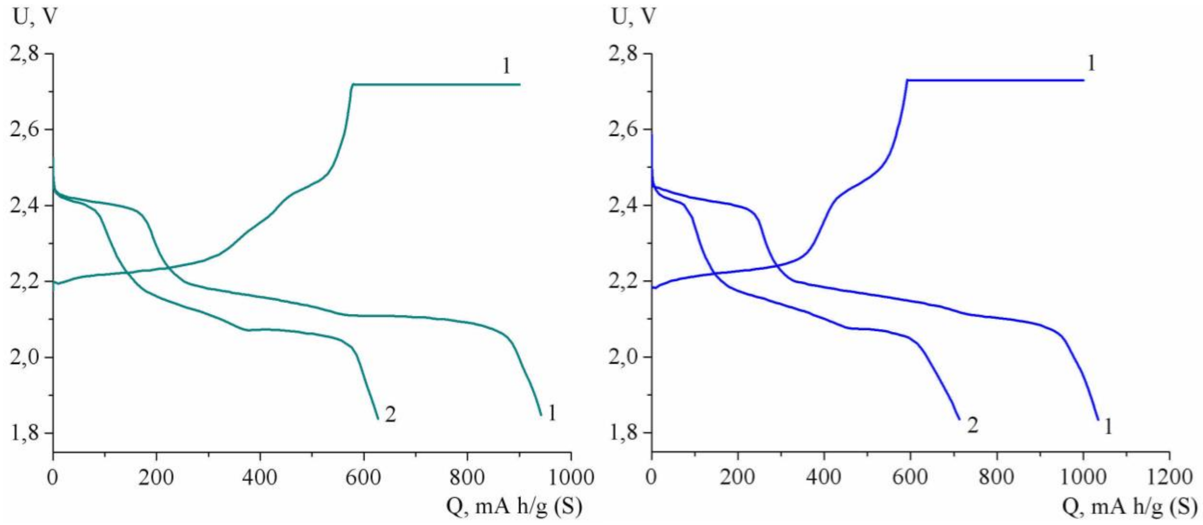

Figure 4. *Discharge – charge curves of Li-S systems with electrolytes:*
a – electrolyte (PVdF-1 M LiN(CF3SO2)2 - [PhCH2NMe3]+Cl- – G4),
b – electrolyte (PVdF-1 M LiN(CF3SO2)2 - [PhCH2NMe2Ph]+Cl- – G4)

Presented results confirm the possibility of using polymer electrolytes, which developed, in lithium-sulfur batteries.

Acknowledgments

This work has been done in the framework of NATO SPS 985148 project "Development of New Cathodes for Stable and Safer Lithium-Sulfur Batteries" / Science for Peace and Security Programme. Enerize Corporation is an industrial partner under NATO SPS 985148 project. Prof. E. Shembel is the Head of SRLCPS USUCT and Partner country-Ukraine Director of this NATO project.

References

1. N. Angulakshmi and A.M. Stephan, Frontiers in Energy Research: Energy Storage, **3**, 7 (2015).
2. X. Cheng, R. Zhang, Ch. Zhao, F. Wei, J. Zhang and Qiang Zhang, Advanced Science, **3**, (2016).

Conductivities of Powders Graphene, Graphite, Oxides, Sulfides, etc. of Electrode Materials are Critical Parameters for Efficiency Li Batteries. Non-Destructive Electromagnetic Testing. Electrochemical Properties

Vlad Redko[a], Elena Shembel[a,b], Timothy Pastushkin[a], Nellya Zaderey[b], Soheil Davaryar[c],
Yuliya Polishchuk[b] , Irina Maksyuta[b], Yurii Pustovalov[a], Alexander Redko[b]

[a] Enerize Corporation, Coral Springs, FL, 33067, USA

[b] Scientific Research Laboratory of Chemical Power Sources (SRLCPS) of Ukrainian State

University of Chemical Technology (USUCT), Dnipro, 49005, Ukraine

[c] Company Soheil Davaryar, Australia.

Correlation between conductivity the components of electrodes mass of Li batteries and electrochemical properties of these electrodes and Li batteries based on these electrodes have been investigation. The various types of the graphene and the graphite have been used as conductive additives for cathodes (positive electrodes). Various types of manganese dioxide, lithium manganese spinel, and sulfides have been used as active materials of electrodes of Li batteries. The conductivity of powder materials have been investigated using the innovating non-contact non-destructive electromagnetic method. Impedance, galvanic cycling and current-voltage characteristics of the electrodes were investigated.

Introduction

The goal of our investigation and development is the optimization the technology and efficiency of porous electrodes of Li batteries. Porous electrodes of lithium current sources are systems with distributed parameters that determine the distribution of the electrochemical process in the volume of the electrode. The efficiency of electrochemical processes in the volume of porous electrodes is determined by the ratio of the following parameters: 1) resistance of the electrochemical reaction at the boundary of the active material of the electrode & electrolyte; 2) the resistance of the electrolyte in the pores of the electrode; 3) the electronic resistance of the carbon additive, which is introduced into the electrode mass; 4) electronic & ionic resistance of the active material of the electrode; 5) resistance of the contact of the active material of the electrode and the carbon additive. For evaluation the conductivity of powdered materials the innovating method of non- destructive non-contact electromagnetic impedance method has been used.

Experimental

Non-destructive control of properties and quality of starting materials during lithium battery production is one of the most cost effective method to achieve the highest possible product quality and reliability of Lithium batteries. Below presented photo of the innovating devise for non-contact non-destructive electromagnetic evaluation of the electrical conductivity of powdered materials under wide operation range of the frequency. Equipment includes unique inductive transducer design that generates a uniform electromagnetic field. More detailed information about the operating principal of this method and parameters of this devise is presented in patents [1, 2] and will be discussed during our presentation.

Figure 1. *Device for electromagnetic evaluation the conductivity of powdered materials for electrodes of lithium batteries.*

Results and its discussion

Conductivity and density of Graphene and various types of Graphite

Below presented results of comparison the conductivities and densities of various carbon materials, including: 1) Graphene that developed and produced Mr. Soheil Davaryar, Australia; 2) Chemically modified natural graphite and side graphite from metallurgical process (CNK); method of modification are developed by company Enerize Corporation [3]; and 3) Graphite from market (BG-34).

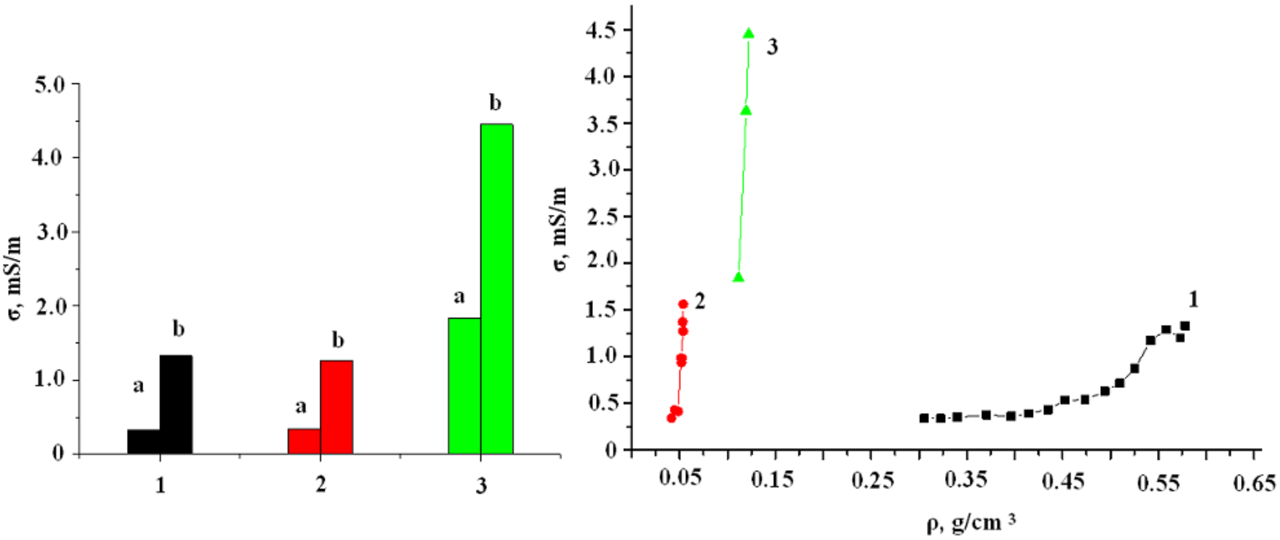

A B

Figure 2A*. Conductivity the powder of carbon materials: (a) initial; (b) after compaction*
Samples of carbon materials: 1: BG-34; 2: CNK; 3: Graphene. Electromagnetic transducer with a frequency of 20 MHz has been used
Figure 2B. *Conductivity versus density. Samples of carbon: 1: BG-34; 2: CNK; 3: Graphene. Electromagnetic transducer with a frequency of 20 MHz has been used.*

Electrochemical properties of electrode based on polymer sulfur with various types of additives: graphene and modified graphite.

Special attention has been connected with investigated the influencing the properties of carbon additives on the efficiency of positive electrodes in Li batteries. Some example of positive electrodes based on polymer sulfur for Li-S batteries are presented below.

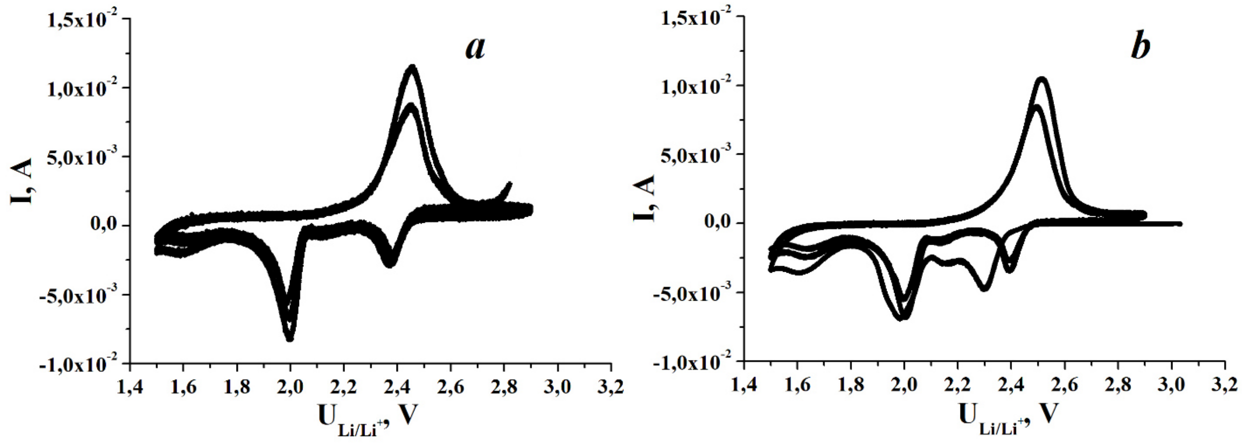

A B

Figure. 3. *CV characteristics of Sulfur based electrodes in cells with three electrodes: Li-S-Li cell. Operating range of voltage from 1.5V and up to 2.9 V. The potential scan rate is 0.5 mV/s. Electrode area 2 cm^2. Electrolyte: 0.7M LiIm, 0.25M LiNO$_3$, DME: DOL (2:1). Cathode contain: 50% polymer sulfur, 30 % carbon black, 10% PVdF, 10% Graphene (A) or 10% Graphite CNK (B)*

Results that presented on the Fig. 3A illustrate that Sulfur based electrode with additives of graphene has higher level stability during cycling as the Sulfur based electrode with additives of graphite CNK

Below presented results of the test two electrodes based on the polymer sulfur, which have two deference conductive graphite additive: BG-34 and CNK. (Fig.4) two graphite have similar conductivities (see Fig.2A). However, graphite CNK has lower density (see Fig. 2B). Presented results confirm follower: sulfur based electrode with graphite additives that has lower density (CNK) has higher electrochemical properties. This is because the graphite CNK has more evenly distributed over the porous volume of the electrode active material.

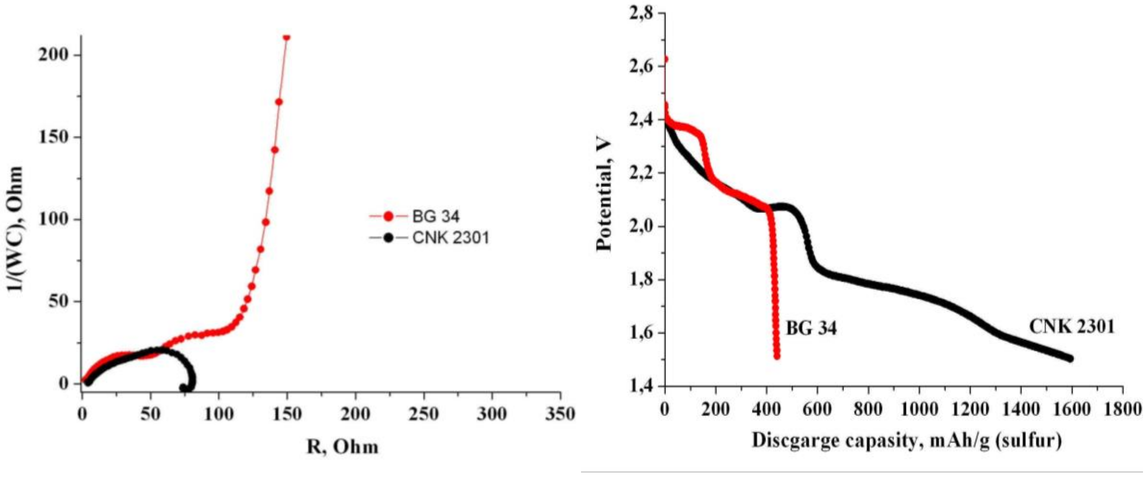

A B

Figure 4. *Electrochemical properties of two positive electrodes based on polymer sulfur with graphite additives. Electrode area 2 cm^2. Electrolyte: 1 M LiIm, DME : DOL = 1:1. Content the Polymer Sulfur in positive electrode mass is 75%. A: Impedance of these two electrodes. B: Curves of discharge. Discharge current – 0.1 mA.*

<u>Conductivity and density of lithium manganese spinel powders that synthesized based on Ukrainian manganese ores.</u>

Method synthesis of this spinel has been developed by Enerize Corporation [4]

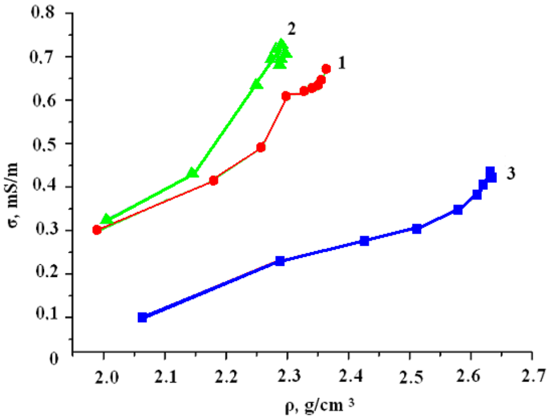

Figure 6. *Conductivity and density of different types of lithium manganese spinel: 1) 102/3; 2) Enerize; 3)76/9. Electromagnetic transducer with a frequency of 20 MHz has been used.*

Below Fig. 7 is presented.

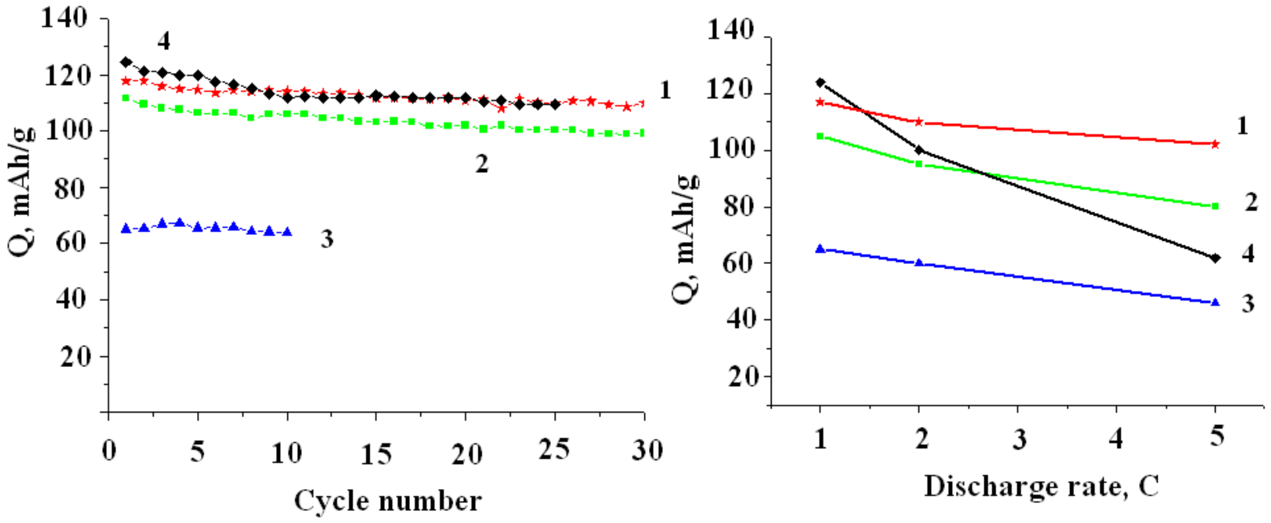

A B

Figure 7A. *Changing the discharge capacity during process of cycling the cathodes based on LiMn$_2$O$_4$. Discharge current: 1C.*
Figure 7B. *Changing the discharge capacity of cathodes based on depending on current Types of LiMn$_2$O$_4$:1) 102/3; 2) Enerize; 3) 76/9; 4) 76*

It is important to confirm that the conductivity and density of powdered materials that used in negative and positive electrodes of Li batteries generates a synergistic effect the influencing the efficiency of the electrochemical parameters of the electrodes and the current source as a whole.

Acknowledgments

This investigations have been carried out in cooperation of Company Enerize Corporation, USA, and the SRLCPS of USUCT, Ukraine. Investigation and tests have been done also under framework of NATO SPS 985148 project “Development of New Cathodes for Stable and Safer Lithium-Sulfur Batteries”/ Science for Peace and Security Programme. Enerize Corporation is industrial partner under NATO SPS 985148 project. Prof. E. Shembel is the Head of SRLCPS USUCT and Partner country-Ukraine Director of this NATO project.

References

1. V. Redko, E. Shembel, etc. *US Patent* No. 7,288,941 *Method and Apparatus for Measuring Conductivity of Powder Materials Using Eddy Currents*.
2. V. Redko, E. Shembel, T. Pastushkin, etc. *US Patent* No. 8,102,181. *Method and Device for Rapid Non - Destructive Quality Control of Powdered Materials.*
3. Y. Pustovalov. E.,Shembel, E. Vishnyakov L. etc. *US Patent application* No. 10/898631, Carbon material for electrodes of Lithium on power sources and method of production thereof
4. E. Shembel, V. Maslov, I. Maksuta etc. *US Patent Application* No. 12128,7396 *Manganese lithium spinel and method for production thereof.*

Effect of superhalogen anions on the electrochemical behavior of V_2O_5 electrodes in redox reactions with lithium in EC-DMC/Li-salt solutions

R. Apostolova*, B. Markovsky**, E. Shembel*, D. Aurbach**

*Ukrainian State University of Chemical Technology, Dnipro, 49005, Ukraine
**Bar-Ilan University, Ramat-Gan, 52900, Israel

In recent years, we observe an increased interest to vanadium pentoxide V_2O_5 as a promising cathode material for lithium-ion batteries (LIBs). This is due to the fact that lithium ions can be reversibly inserted in the free spaces of the layered crystal structure of the orthorhombic V_2O_5 with particles of the nanometer level, providing high discharge capacity which approximates to the theoretical capacity (442 mAh/g) [1]. In practical V_2O_5/Li-cells, the reversibility of the insertion of lithium ions is lost during charge-discharge cycling due to the instability of the V_2O_5 structure caused by intercalated lithium ions and other factors leading to a drop in the discharge capacity [2].

The method of electro-deposition of V_2O_5 from aqueous solutions is one in the series of proposed methods for the synthesis of V_2O_5 nano-particles. In previous publications [3-5], we have determined the composition, physical, chemical, and structural properties, kinetics parameters of the redox processes, Li^+ solid state diffusion in the host cathode and discharge-charge performance in Li batteries of V_2O_5 synthesized by electrolysis. We have established that the efficiency of the electrochemical performance of V_2O_5 in lithium batteries depends largely on the electrolyte.

In the present publication we analyze the results of cyclic voltammetry studies of electrochemically synthesized thin-layer V_2O_5 in electrolytes based on typical salts like $LiAsF_6$ or $LiPF_6$ superhalogens in a mixture of ethylene carbonate (EC) and dimethyl carbonate (DMC) solvents. The main focus of the current paper was to study the effect of these salts anions $(AsF_6)^-$, $(PF_6)^-$ on the electrochemical performance of V_2O_5 electrodes in redox reactions with lithium. The novelty of this investigation is in using theoretical calculation simulations by classical molecular dynamics – MD, and quantum chemical density functional theory – DFT, of binary EC-DMC solution structures.

V_2O_5 oxides were electrodeposited on stainless steel 18H12X9T plates under conditions of stationary electrolysis from oxovanadium sulfate solutions (0.2 mole / L, pH 1.8-2.0) [4]. For electrochemical measurements, 3-electrode cells were used with an electrolyte based on EC, DMC solvents from Merck, Li battery grade, with 1 mole / L of $LiAsF_6$ (FMC), (EC, DMC, $LiPF_6$ 1 mole / L, Merck)-solution, select pure series used as received. The water content in the electrolyte solutions with $LiAsF_6$ and $LiPF_6$ was usually around 20 ppm. For cyclic voltammogram studies, analytical radiometer VoltaLab PGZ 301 was used.

The electrochemical behavior of V_2O_5 electrodes in the redox reactions with lithium has specific features when using $LiAsF_6$ or $LiPF_6$ in the electrolyte solutions.

We have analyzed the results of cyclic voltammetry (CVA) of V_2O_5 electrodes with the loading of 1.5 mg / cm^2 on a stainless steel substrate. Initially, this was studied using 1 mole / L $LiAsF_6$, EC: DMC (1: 3 by volume) solution. Potential scan rates of 0.05; 0.10; 0.25; and 0.50 V/s were used. As it is evident from (Fig. 1 a), the intercalation/ extraction of lithium ions into/from V_2O_5 occurs in several active sites (positions) indicated as 1 – 13, in the potential range of 3.8-2.0 V.

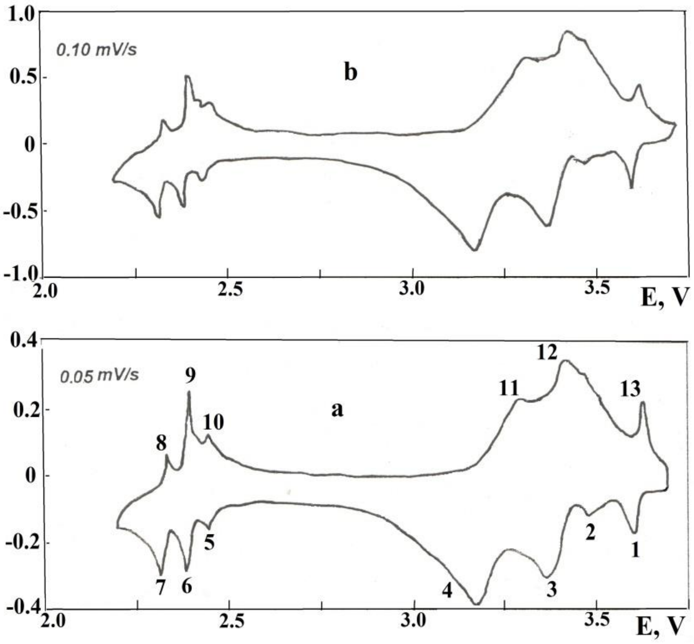

Figure 1. *CVA of V_2O_5 electrodes in EC-DMC/$LiAsF_6$ solution at potential scanning rates, V/s: 0.05 (a); 0.10 (b).*

In the Fig. 1 a, we distinguish a multistage process of reversible intercalation/deintercalation reactions of lithium ions with a number of additional sites which are absent in CVA of micrometer-sized V_2O_5. The multistage of the electrode process, shown in Fig. 1 a, is characteristic of nano-materials with a developed surface area and as a result, with excess surface energy. This facilitates the formation of additional sites during the electrode process around redox couple potentials of 2.49/2.45 V, 2.41/2.31 V, and 3.65/3.60 V. Activation of these additional sites is preceded by a period of delay. In the first cycle, they are inactive and can be detected only after 3-5 activation cycles. In accordance with the analysis of CVA, the process of intercalation is reversible in all sites, except of site with the redox couple potentials of 3.29/3.18 V. The process related to the phase transition in V_2O_5 oxide (ε-δ) [2] which can be considered as quasi-reversible.

Then, we analyzed the results of CVA of V_2O_5 electrodes in 1 mole / L $LiPF_6$, EC: DMC (1: 1 by volume) solution. We distinguish two anodic and two cathodic waves in CVA (Fig. 2) with maximal currents at redox potentials around 3.21/2.89 V and 2.77/2.48 V. Unlike the multistage electrode process of V_2O_5 oxide in the $LiAsF_6$-containing solution, in the $LiPF_6$-containing solution the number of active sites decreased to 4.

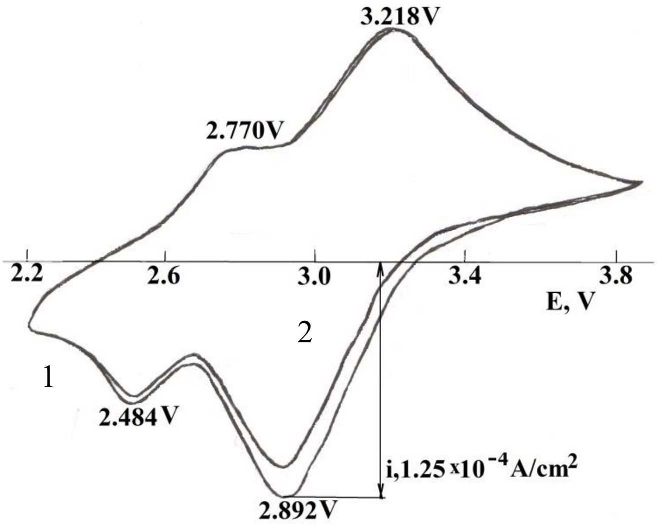

Figure 2. *CVA of V_2O_5 electrode in EC-DMC (1:1 by volume) $LiPF_6$-containing solution. υ = 0.10 mV/s.*

The possible effects of solvent composition as well as the anion effects on the V_2O_5 performance were taken into account. Non-aqueous electrolytes containing Li-salts possess complicated solvation structure. Lithium-ion battery performance is influenced by the ionic conductivity of the electrolyte, which depends on the Li ions migration-diffusion rates and relates to their solvation structure. In this work, EC and DMC solvents were used with different ratios: EC, DMC (1:1 by volume) in combination with $LiPF_6$ and EC, DMC (1:3 by volume) in combination with $LiAsF_6$. Both EC and DMC participate in solvating Li^+. The solvent can greatly affect both solvation and diffusivity of Li ions. For the analysis of the Li^+ solvation in (EC) and (DMC) and their binary EC−DMC, 1:1 molar composition, theoretical calculation simulations (classical molecular dynamics – MD, quantum chemical density functional theory – DFT, etc.) have been reviewed by us.

We present some properties of the EC/DMC, 1 mole / L salt-solutions for the comparison of their similarities and distinctions: vertical detachment energy, donor number, conductivity, capability of hydrolysis, the range of dissociation of Li-salts, mobility of anion, the radius of anion, chemical, thermal, anodic, corrosive stability of $LiAsF_6$, $LiPF_6$. On the available literature data, in AsF_6^-, EC / DMC (1:3 by volume) solution the preferred interaction of Li^+ with DMC in the first coordination sphere is, resulting in an increase of the dipole moment of the solvate complex. In this case, a more efficient solvation structure is formed compared to the one formed in the electrolyte with the ratio of 1:1 of EC: DMC.

Summary.

It was found out that the number of active sites for the insertion/extraction of lithium ions into / from the V_2O_5 structure depends on superhalogen anion and solvents. During discharge-charge cycling of V_2O_5 electrode, the unstable sites and phase transitions are identified. To increase the structural stability of phase transitions, we propose the electrochemical doping of V_2O_5 by Mn. For the acceleration of the conductivity of V_2O_5 results in opening of the additional sites for Li–ion insertion in V_2O_5 structure can be usefull electrochemical co-deposition of V_2O_5 with conducting polymer by polyaniline type.

For elucidating the difference in the electrochemical behavior of V_2O_5 in redox reactions with lithium in different F^--containing solutions used in this work, the peculiarities of lattice structure of V_2O_5, the diversity of heterogeneous vanadium-oxide compounds and the properties of the solutions were also analyzed. The lattice of V_2O_5 formed from the tunnels with the different orientations of the transfer of the guest ions. Lithium ions insert in the lattice structure forming the phase $Li_xV_2O_5$ with the domain of the homogeneity that is determined by the limited quantity of inserted ions (x) in the phase. At the excess of the limit in the phase, the new phase forms. The availability of the energetically preferable sites for the Li^+ insertion into V_2O_5 lattice and the stability of the structure of new phase at intercalation/deintercalation are the necessary conditions for the formation of the new phase and its effective performance. Such conditions hold true at the electrochemical performance of V_2O_5 electrode in the $LiAsF_6$, EC, DMC (1:3 by volume) solution. In the first 1-(3-5) cycles, the phases observed in V_2O_5 CVA such as these in CVA of practical lithium batteries with micrometer sized V_2O_5 around 3.4; 3.2; 2.3 V. The activation and accumulation of Li^+ occurs during the first 1-(3-5) cycles which results in the formation of new phases. The new phases are chemically and electrochemically stable and take part in the reversible performance of V_2O_5 electrode. Solvation structure of Li^+ in $LiAsF_6$, EC, DMC (1:3 by volume) solution with optimal ratio of the solvents facilitates opening of the additional sites, ensures reversible performance of new phases and their stability at storage during 200 days.

In contrast, the initial performance of V_2O_5 in $LiPF_6$-containing solution is observed only in 4 sites from the CV data. The qualities of the solution determined by the availability of $LiPF_6$ and Li^+ solvation structure of the solution with ratio of EC: DMC=1:1 does not provoke the positive effect of $LiAsF_6$—containing solution. One of the possible causes of the small quantities of sites in $LiPF_6$-containing solution can be the dissolution of intermediated products of the electrode reaction which provoked by most hygroscopic $LiPF_6$. The dissolution of the electrode materials in non-aqueous electrolytes with the admixture moisture is a well known fact. The structural stability of new phases can be increased by doping V_2O_5 with copper which generates the emergence of the additional sites in V_2O_5 in $LiPF_6$-containing solution along with the increasing of the electro-conductivity and structure stability of V_2O_5 [6].

Based on the analysis of the literature data about the solvation of lithium ions by alkyl carbonate solvents in combination with superhalogen anions, the assumptions have been made by us regarding the difference in the solvation of lithium ions in EC / DMC mixtures with different ratios of the solvents. We took into consideration the model of classic molecular dynamics [7] accounting more value of the first solvation shell of Li^+ than the value of radius of Li^+. In such case the ratio of EC: DMC=1:3 in $LiPF_6$-containing electrolyte is more preferential than that used in this work equals to (1:1). The ratio EC: DMC=1:3 in $LiPF_6$-containing electrolyte can improve V_2O_5 performance in redox reactions with lithium.

References

1. Yue Y., Liang H. // *Adv. Energy Mater.* ***7***, 1602545 (2017).
2. Leger C., Bach S., Soundan P., Perreira J. // *J. Electrochem. Soc.* ***152***, 236 (2005).
3. Shembel E., Apostolova R., Nagirniy V., Aurbach D., Markovsky B. // *J. Power Sources.* ***80***, 90 (1999).
4. Shembel E., Nagirniy V., Apostolova R., Chaykovskaya V. // *Journal prikladnoi khimii*. ***73***, 409 (2000). (In Russian).
5. Markovsky B., Apostolova R., Nagirniy V., Aurbach D., Shembel E. // *Voprosi khimii i khimicheskoi tekhnologii.* ***issue No 5***, 138 (2003).(In Russian).
6. Liu Peng. Vanadium-oxide-based electrode materials for Li-ion batteries. A thesis submitted for the degree of Doctor of Philosophy at The University of Queensland in 2016, School of Chemical Engineering. Australia.
7. Skarmoutsos I., Ponnuchamy V., Vetere V., Mossa S. // J. Phys. Chem. C. ***119***, 4502 (2015).

Synthesis of Ag-vanadates obtained by ion change on the base of electrochemically synthesized $V_2O_{5-x}\cdot yH_2O$ and the their behavior in the electrodes for lithium accumulator

R.D. Apostolova

Scientific Research Laboratory of Chemical Power Sources of Ukrainian State University
of Chemical Technology, Dnipro, 49005, Ukraine

It is known the effective electrochemical performance in redox reaction with lithium of xerogels, aerogels, and aerogel-liked V_2O_5 oxides which have been doped by the metals (Ag, Cu, Zn, Al, Ni, etc) [1]. The efficiency depends on the structure and morphology of doped oxides which are particularly sensitive to the preparation method. Typical layered V_2O_5 gel possesses differ inter-layered space (d) on the dependence the method of the synthesis (d=8,8 Å for xerogel, d=12,5 Å for aerogel, whereas inter-layered space of crystal a V_2O_5 d=4,4 Å). Gel structure with expanded inter-layered space acts similar as universal host for the guest lithium ions. The inclusion of lithium ions may achieve 2,0-2,5 Li/V_2O_5 in the films of the xerogels aerogels and in composite electrodes on the base of aerogel-liked doped V_2O_5 oxides.

The perfection of the preparation V_2O_5 technology with using gel solution under electrochemical deposition on the cathode gives opportunely approach its discharge capacity to the theoretical capacity [2].

Obtained electrochemically $V_2O_{5-x}\cdot y\ H_2O$ oxide is effective exchanger similarly gels, which is protonated in acid environment and can exchange with acid environment by ions. It was shown that sodium ions can be inserted in the oxide by ion-exchanging way [3]. Na^+-insertion in vanadium oxide improves its characteristics in redox reaction with lithium.

In this work, the similar ion change was realized for the insertion of Ag^+ in $V_2O_{5-x}\cdot yH_2O$ precursor in accordance with reaction (1) for the improvement of its discharge properties in the electrodes for lithium accumulator:

$$H^+(V_2O_{5-x}\cdot yH_2O)^- \leftrightarrow Ag^+(V_2O_{5-x}\cdot yH_2O)^- \tag{1}$$

The products of the electrochemical synthesis from oxovanadium sulfate solution without following annealing were used for the effective ion exchange [4].

Argentums modified vanadium oxide compounds were synthesized as the dispersed powder. Vanadium oxide precursor with black color obtained on anode-plate from stainless steel 18H12X9T with area of 10 cm^2. The conditions of depositing: cathodes – titanium VT-1 alloy; anode current – 15-20 mA / cm^2; ratio anode area to cathode area $S_{anode}:S_{cathode}=1 : (5\text{-}6)$. The electrolyte temperature was of 80-85 °C. The electrolyte composition was $VOSO_4$ – 0.2 mole / l, pH 2.0-2.2. The depositing continued during 1 hour. The electrode after each period of depositing extracted out of the electrolyzer, refined the deposit, rinsed it's by distilled water, dried in air atmosphere 20-24 hour. The synthesis product characterizes disordered structure of orthorhombic $V_2O_{5-x}\cdot yH_2O$ (x=0,4-0,6; y=1,1-1,6). The grain size of oxide equals to 1-3 μm, crystalline grain is of (13-15) nm.

The synthesized electrochemically powder $V_2O_{5-x}\cdot yH_2O$ was exposed during 15 hour in solution of 0.1mole/L $AgNO_3$ (pH 2.0). Thereafter, the powder was rinsed by the acidic distillate water (pH 2.0) and annealed at 500° C during 7 hour.

The final products of the synthesis were investigated using X-ray analysis at set DRON-2, absorption IR spectroscopy (Specord-75 IR). The electrochemical behavior of synthesized products was investigated in redox reaction with lithium in galvanostatic mode using software-based test device.

For this, the electrodes were made by applying the active mass on the stainless steel mesh 18H12X9T, size of 1×1 cm. The active mass contains the mixture of argentum-modified vanadium oxide (80% mass), acetylene black (10% mass), binding agent F4-D (10% mass) in ethyl alcohol. The electrodes were dried at 250 °C (5-7 h). The study of the electrodes was provided in the glass cell with lithium counter electrode in the electrolyte 1 mole/L $LiClO_4$ (Iodobrom), propylene carbonate (Sigma-Aldrich), dimetoxyethane (ALFA-AESAR). The operations of the cell assembly were provided in gloving box with dry argon atmosphere.

X-ray patterns of $V_2O_{5-x}\cdot y\ H_2O$ powder exposed in $AgNO_3$ solution indicate on the availability argentums vanadates: α-$AgVO_3$ [PCPDF WIN № 19-1151]; AgV_7O_{18} [PCPDF WIN № 19-1164]; $Ag_4V_2O_7$ [PCPDF WIN № 19-1166]; $Ag_2V_2O_{11}$ (Fig. 1). The $Ag_2V_2O_{11}$ shows maximum intensity of the reflexes of diffraction repulse.

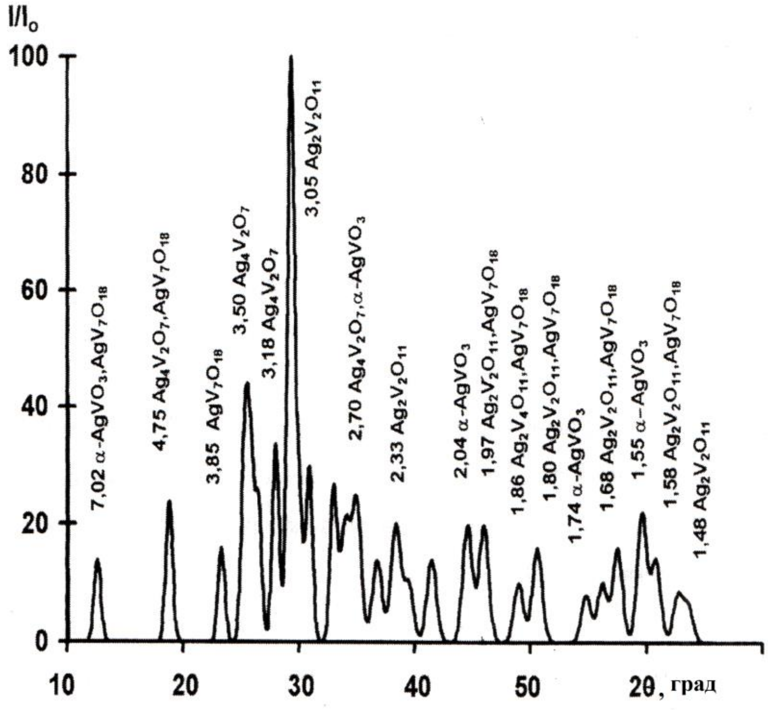

Figure 1. *X-ray patterns of a* $V_2O_{5-x}\cdot y\ H_2O$ *oxide exposed in an* $AgNO_3$ *solution.*

The vanadates α-$AgVO_3$, AgV_7O_{18}, $Ag_4V_2O_7$, $Ag_2V_2O_{11}$ are known as effective cathode materials in lithium batteries for the implantable devices [4].

Synthesized silver vanadates showed the ability to be repeatedly converted into redox reactions with lithium over the course of 26 discharge-charge cycles with getting 220 mAh /g.

The article was prepared in the research laboratory of chemical current sources, headed by prof. E.M. Shembel with the support of the Ministry of Education and Science of Ukraine.

References

1. Coustier F., Hill J., Owens B.B., Passerini S., Smyrl W.H. // *J. Electrochem. Soc.* **146**, 1355 (1999).
2. Liu Y., Clark M., Zhang Q., Yu D., Liu D., Liu J., Cao G. // *Adv. Energy Mater.* 1, 194 (2011).
3. Apostolova R., Shembel E., Nagirny V., Aurbach D., Markovsky B., Langzam Ja. // *Electrokhimija.* **37**, 1205 (2000). (In Russian).
4. Schembel E., Nagirny V., Apostolova R., Chaikovskaya V. // *J. Appl. Chem.* **73,** 409 (2000). (In Russian).
5. Zhou J., Liang Q., Pan A., Zhang X., Zhu Q., Liang S., Cao G. **//** ***Mater. Chem. A.*** 2**,** 11029 (2014).

Effect of Carbon Materials for Electrochemical Properties for Lithium-Sulfur Batteries

D. Capková[a], T. Kazda[b], A. Straková Fedorková[a], R. Oriňaková[a]

[a] Department of Physical Chemistry, Faculty of Sciences, Pavol Jozef Šafárik University in Košice, Moyzesova 11, 04154, Košice, Slovak Republic

[b] Department of Electrical and Electronic Technology, Faculty of Electrical Engineering and Communication, Brno University of Technology, Technická 10, 616 00, Brno, Czech Republic

Development of advanced energy-storage batteries for portable electronic devices and electric vehicles must accomplish several requirements: safety, low-cost, nature-friendly, long lifecycle, high energy density, and high theoretical capacity. Lithium-sulfur batteries can execute these requirements. However, the practical application of lithium-sulfur battery is hindered by several major disabilities, such as the volumetric expansion of sulfur, structural instability, high self-discharging, poor electronic conductivity of sulfur, and low cycle life. This article deals with different types of carbons as additives in the cathode for the lithium-sulfur battery.

Introduction

Lithium-sulfur (Li-S) batteries are considered to be the most promising energy-storage solution for a rapidly growing demand for energy [1]. Theoretical capacity of sulfur is 1672 mAh/g that is five times higher compared to the commercial lithium-ion battery. Thanks to high theoretical capacity, the gravimetric energy density of Li-S batteries is more than 2500 Wh/kg. Abundance and nontoxicity of sulfur make Li-S batteries environmentally friendly and low-cost system for energy storage. Thanks to these qualities, Li-S batteries are attractive for stationary storage or renewable energies (solar and wind), if we can achieve long lifecycle and high efficiency [2].

The main barrier that blocks the commercialization of Li-S batteries is the low electrochemical utilization of sulfur and decrease of the capacity [3]. This type of accumulator is not based on intercalation process of lithium ions during cycling but rather on the conversion of elements. The reaction between lithium and sulfur results in lower (Li_2S, Li_2S_2) and higher (Li_2S_4, Li_2S_6, Li_2S_8) polysulfides. The higher polysulfides, which are soluble in the organic electrolyte, migrate freely between electrodes and deposit on the surface of metallic lithium anode. This process is leading to the shuttle effect during the cycle process. The consequence of the shuttle effect is an irreversible loss of the capacity, instability of electrode structure and passivation of the lithium anode [4, 5]. Both, sulfur and discharge product Li_2S are electronically and ionically insulating. The solution for insulating characteristic of sulfur is the incorporation of sulfur into a conductive matrix (in our case the carbon). This process forbids the long-term cycling stability [3, 6]. The volumetric expansion of sulfur during cycling is about 80 %. This volume change leads to the destruction of the integrity of the cathode structure and isolation of active materials in the cathode. The consequence of this process is the fast decay of capacity [7].

Experimental

Different sulfur-carbon composites with 60 wt.% of sulfur were prepared. Two types of carbon black have been used: Super P and Ketjen black (KJB). PVDF (Polyvinylidene fluoride) was used as a binder. The composition of electrodes were: 60 wt.% of sulfur + 30 wt.% Super P + 10 wt.% PVDF and 60 wt.% S + 33 wt.% KJB + 7 wt.% PVDF 5130. The electrodes were dried and pressed using the pressure of 325 kg/cm^2. Pure lithium was used as the anode and the electrolyte was a mixture of DME (1,2-Dimethoxyethane):DOL (1,3-Dioxolane) 2:1 with 0.7 M LiTFSI (Lithium bis(trifluoromethanesulfonyl)imide) + 0.25 M $LiNO_3$ (Lithium nitrate). The electrolyte was impregnated into glass fiber separator. The electrodes were cut out with the diameter of 18 mm and inserted into the electrochemical test cell (El-Cell®). The whole assembly was done in the argon-filled glove box. Electrode with Super P had sulfur loading 0.99 mg/cm^2 and electrode with KJB had 1.20 mg/cm^2.

Figure 1 presents the comparison of cyclic voltammograms for the S+Super P+PVDF electrode and the S+KJB+PVDF electrode at a slow scan rate of 0.1 mV/s. The current axis is related to 1 gram of sulfur. We can see oxidation and reduction peaks for both electrodes. First cathodic peaks are at 2.35 V and second cathodic peaks can be observed around 2.0 V. Positions of this peaks related to the reduction of the elemental sulfur to higher polysulfides and then their reduction to lower polysulfides in both electrodes. We can also see anodic peaks at 2.32 V. The electrode with carbon Super P has two narrow peaks and electrode with KJB has wide peak and the second peak is hardly seen. The current per square centimeter of the electrode reached higher values in the case of carbon Super P than the current for the electrode with KJB.

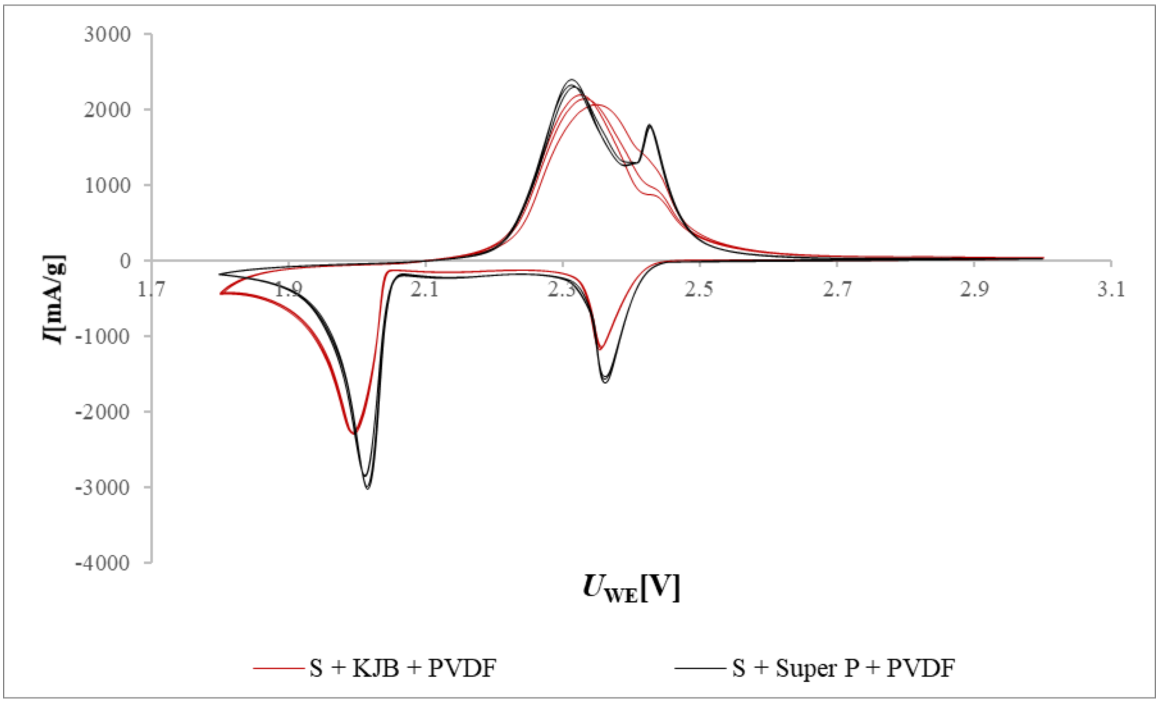

Figure 1. *The comparison of cyclic voltammograms at scan rate 0.1 mV/s of S+Super P+PVDF and S+KJB+PVDF between 1.8 V to 3.0 V*

Conclusions

Significant effects of carbon type on properties of S-C composite have been shown in this study. We have demonstrated a carbon Super P and Ketjen black as a cathode conductive matrix for Li-S batteries. Ketjen black has a higher surface area, sulfur loading, but the smaller size of pores then carbon Super P. Cyclic voltammograms show that electrode with carbon Super P has higher intensity, narrow peaks and it indicates better reaction kinetics.

Acknowledgments

This research was sponsored by the NATO Science for Peace and Security Programme under grant 985148. The authors gratefully acknowledge the financial support from the Ministry of Education, Youth and Sports of the Slovak Republic under project VEGA 1/0074/17 and research project VVGS 2019-1048.

References

1. Ch. Zhang, H. Bin Wu, Ch. Yuan, Z. Guo, X. Wen Lou, *Angewandte Chemie International Edition*, **51** (38), 9592-9595 (2012).
2. Y.-X. Yin, Y.-G. Guo, L.-J. Wan, *Angewandte Chemie International Edition*, **52** (50), 13186-13200 (2013).
3. A. Manthiram, S.-H. Chung, Ch. Zu, *Advanced materials*, **27** (12), 1980-2006 (2015).
4. T. Kazda, P. Čudek, J. Vondrák, M. Sedlaříková, J. Tichý, M. Slávik, G. Fafilek, O. Čech, *Journal of Solid State Electrochemistry*, **22**, 537–546 (2018).
5. N. Jayaprakash, J. Shen, S. S. Moganty, A. Corona, L. A. Archer, *Angewandte Chemie International Edition*, **50** (26), 5904-5908 (2011).
6. A. Straková Fedorková, T. Kazda and K. Gavalierová, *Int. J. Electrochem. Sci.*, **13**, 551-562 (2018).
7. K. Chen, Z. Sun, R. Fang, Y. Shi, H.-M. Cheng, F. Li., *Advanced functional materials*, **28** (38), 1707592 (2018).

Graphite Electrode: Influence of Binders on Electrochemical Properties

Michal Fíbek[a], A. Zsigmond[a] and J. Libich[a]

[a]Department of Electrical and Electronic Technology, Faculty of Electrical Engineering and Communication, Brno University of Technology, 616 00 Brno, Czech Republic

At the present time, the lithium-ion batterie is the leading kind of rechargeable electrochemical cells. The battery capacity production growing annually, this year the whole world factory capacity hit 300 GWh. This growth is especially powered by the electric vehicle makers and renewable energy sources demands. This growth is connected with technology development that aims to decrease costs and environmental impact. Into this field belong the research and development of new materials for lithium-ion batteries. This work deals with various types of binders used in the negative electrode material of lithium-ion batteries. The materials used as binders were Polyvinylidene fluoride (PVDF), Styrene-butadiene rubber (SBR) and Polyimide P84. Some of those binders are water-base thus more environmentally friendly and bring some advantages like lower drying temperature, non-toxic vapours etc. The influence of those binders on electrochemical properties of negative electrode in lithium-ion cell based on graphite are investigated and evaluated.

Introduction

In the production of lithium ion battery electrodes, the binder plays an important role. It not only binds the active materials and the conductive additive to the current collectors, but also strongly affects the electrode processing and the electrochemical performance of the laminate. Polyvinylidene fluoride (PVDF) is the generally used binder, which requires the use of the volatile, organic compound N-methyl pyrrolidone in its application. Recently, sodium salt of carboxymethyl cellulose (CMC) and styrenebutadiene rubber (SBR) have been introduced as a suitable replacement in the manufacture of lithium ion anodes. The use of the water soluble binder system leads to a cheaper and greener electrode processing.

Experiments and Results

In our experiments, the different binders were chosen and compared from technology and electrochemical point of view.

The Polyvinylidene fluoride (PVDF) is a highly non-reactive and pure thermoplastic fluoripolymer. It is produced by the polymerization of vinylidene difluoride and is used in applications requiring the highest purity, strength, and resistance to solvents, acids, bases and heat. Compared to other fluoropolymers, it has a lower melting point, around 177 °C, also a lower density (1.78 g/cm3). It is available as piping products, sheet, tubing, films, plate and an insulator for premium wire. It can be injected, molded or welded and is commonly used in the chemical, semiconductor, medical and defense industries, as well as in lithium ion batteries.

The Styrene-butadiene or styrene-butadiene rubber (SBR) is derived from styrene and butadiene, a type of synthetic rubber. These materials have good abrasion resistance and good aging stability when protected by additives. SBR is not to be confused with athermoplastic elastomer made from the same monomers, styrene-butadiene block copolymer. Latex (emulsion) SBR is extensively used in coated papers, being one of the

cheapest resins to bind pigmented coatings. It is also used in building applications, as a sealing and binding agent behind renders, an alternative to PVA. SBR can be used to "tank" damp rooms or surfaces, a process in which the rubber is painted onto the entire surface (sometimes both the walls, floor and ceiling) forming a continuous, seamless damp-proof liner; a typical example would be a basement. It is also used by speaker driver manufacturers as the material for Low Damping Rubber Surrounds. Additionally, it is used in some rubber cutting boards. A possible way of using SBR as a binder is to use it together with carboxymethyl cellulose (CMC). The active material would be mixed with approximately 2 % CMC aqueous solution, additionally with a 4 % of SBR.

The Polyimide P84 an be produced in different forms. The base material for P84 fibers is composed of aromatic backbone units. Despite the non melting aromatic, halogen free structure it is classified as non-flammable. P84 fibers are used as filter media for high temperature filtration, protective clothing, sealing materials for space craft and high temperature applications such as thermal insulation. Another form is a solution of P84, a fully imidized polyimide. It is used for coatings in the electric and electronics industry, due to its low dielectric constant or high dielectric strength. Available solvents are dimethylformamide (DMF) or N-methyl pyrrolidon (NMP) or N-ethyl pyrrolidon (NEP). The third form of P84 is polyimide powder. This powder shows typical properties of polyimide, high temperature stability up to 350 °C, chemical resistance, high mechanical strength, a low friction coefficient and minimal abrasion. It can be used in industrial applications, such as automotive industry, aerospace applications and office machines.

Conclusion

The results (see TABLE I) received during these experiments showed that every binder works to a certain extent. A possible way to continue this thesis would be to determine the exact amount of P84 and SBR binders needed. A series of rate capability measurements would also indicate the effect of the binders. Also the use of the above mentioned lithiation process, or the use of treated natural graphite (smaller particle-grains, enhanced specific surface etc.) should provide better results, it is worth exploring.

***TABLE I**. Summarization of obtained results for all binders.*

Weight rato [wt. %]	Binder	Capacity @10th cycle [mAh]	Irreversible capacity at first cycle [%]	Coulomb efficiency in first cycle [%]
10	PVDF	130.	8.3	91.7
6	PVDF	238	11.4	88.6
3	PVDF	262	2.9	97.1
10	Polyimide P84	4	82.1	17.9
6	Polyimide P84	49	59.2	40.8
3	Polyimide P84	258	2.2	97.8
6	SBR	63	21.3	78.7
4	SBR	13	88.5	11.5
2	SBR	38	80.0	20.0

Acknowledgments

This work was supported by the project of specific research: Materiály a technologie pro elektrotechniku III, reg. no. FEKT-S-17-4595

References

1. Y. Imai, A.Watanabe , *Journal of Alloys and Compounds* **439** (2007).
2. J. Ni, W. Liu, J. Liu, L. Gao, J. Chen, I, *Electrochemistry Communications*, **35** (2013).
3. Ch. Lin, B. Ding, Y. Xin, F. Cheng, M. O. Lai, L. Lu, H. Zhou, *Journal of Power Sources*, **248** (2014).
4. M. B. Dines, *Materials Research Bulletin*, **10** (4), (1975).
5. A. Hofmann, M. Schulz, S. Indris, R. Heinzmann, T.s Hanemann, *Electrochimica Acta*, **147**(20), (2014).
6. M. L. Lee, Y. H. Li, S. Ch. Liao, J. M. Chen, J. W. Yeh, H. C. *Shih, Electrochimica Acta*, **112** (2013).
7. N. Takami, H. Inagaki, Y. Tatebayashi, H. Saruwatari, K. Honda, S. Egusa, *Journal of Power Sources,* **244** (2013).
8. G. Guigay, J. Eliasson, D. Gojkovic, L. G. Bengtsson, *Fire Technology*, **45** (2009).
9. H. Jin, G. Pan, S. J. Xue, and F. P. Wang, *ECS Transaction,* **58**(48) (2014).
10. J. Libich, J. Máca, J. Vondrák, O. Čech, M. Sedlaříková, *J. of Energy Storage*, **17**(3) (2018).
11. J. Libich, J. Vondrak, M. Sedlarikova, J. Maca and O. Cech, *Surface Engineering and Applied Electrochemistry* **53**(6) (2017).
12. C. Lei, F. Markoulidis, Z. Ashitaka, C. Lekakou, Electrochimica Acta, **92**(2013) 183-187.
13. J. Sun et al., Materials Today Energy, **5**(2017) 1-14.
14. N. Takami, H. Inagaki, Y. Tatebayashi, H. Saruwatari, K. Honda, S. Egusa, Journal of Power Sources, **244** (2013).
15. G. Guigay, J. Eliasson, D. Gojkovic, L. G. Bengtsson, Fire Technology, **45** (2009).
16. H. Jin, G. Pan, S. J. Xue, and F. P. Wang, ECS Transaction, **58**(48) (2014).
17. S. Suzuki, M.Yano, M. Miyayama, ECS Transaction, **16**(29) (2009).
18. T. Oguni, at al., ECS Transaction, **50**(26) (2013).
19. J. Zhang, B. Wu, J. Huang, J. of Power Sources, **259**(1), (2014).
20. W. Jiang, T. Tran, X. Song, K. Kinoshita, J. of Power Sources, **85**(2), (2000).
21. B, Kang, K. Honda, T. Aki, T. Omasa, H. Ohtake, D. Warren and J. M. Woodall, Thermochimica Acta, **517**(12), (2011).

Effect of Ambient Environment on Different Types of Li-Ion Cathode Materials

K. Karmazínová[a], T. Kazda[a], O. Čech[a]

[a] Department of Electrical and Electronic Technology, Faculty of Electrical Engineering and Communication, Brno University of Technology, Technická 10, 616 00 Brno, Czech Republic

The research considers the influence of ambient atmosphere on different types of lithium-ion accumulators within a time period. For recycling process was chosen method of the solvent extraction. The results show a comparison of two the most common used cathode materials for lithium-ion accumulators – $LiCoO_2$ and $LiMn_{1/3}Ni_{1/3}Co_{1/3}O_2$. At the forefront is the time period from disassembly the lithium-ion accumulator to extract cathode active material without structure changes due to the effect of the air atmosphere.

Introduction

The lithium-ion batteries are currently the most used source of electric energy for portable electronic devices, electric vehicles or energy smart storage systems. Hand in hand with rising consumption of lithium-ion batteries goes issue of emerged waste which contain substances hazardous to health but also highly valuated heavy metals (as Nickel, Cobalt, Manganese). Commercial methods for recycling lithium-ion accumulators are based on pyrometallurgical process. During this process, the disassembled battery is subjected to high-temperature smelting procedures to recover cobalt and nickel as alloys, but this process does not lead to the recovery of lithium active material from the battery. (1) However, for absolute recycling, we also have to focus on active material and separation of lithium from this type of accumulators. Due to the different materials used and the complexity of the traction batteries, the development of recycling processes is a complex task that requires the interaction of different disciplines. Combination of mechanical, fluid process enginering and hydrometallurgical methods are used to achieve the highest possible recovery rates. (2)

Solvent extraction

Dominated processes for recycling accumulators include the process of solvent extraction also known as liquid-liquid extraction, which increases the efficiency of metals recovery ratio. The process consists of the weakening of adhesive bonds of binder which are used to attach active material of electrodes to the current collector. During this process is necessary to choose the right organic solvent which is able to decompose binder as polyvinylidene fluoride or polytetrafluoroethylene. (3)

For that application was chosen environment-friendly agent dimethyl sulfoxide (DMSO). Dimethyl sulfoxide is an apolar protic solvent that is generally used as a reaction medium and reagent in organic reactions. DMSO is well-nigh non-toxic and affordably priced in comparison with other commonly used solvents NMP (N-Methyl-2-pyrrolidone). The process has to be fully controlled because each binder or each type of cathode has a different time to break down the adhesive bonds between aluminum foil and cathode material.

The influence of ambient atmosphere to extracted material

Obtained material from solvent extraction was dried overnight, pulverized in a ball mill and left in the ambient atmosphere. The prepared cathode material was separated into several samples that were continuously analyzed by XRD. For this research was used two types of cathode material for Li-ion accumulators. The influence of ambient atmosphere to degradation of active cathode material was investigated during measurements of samples for research recycling process of $LiCoO_2$ cathode material. It led to thinking if other types of commonly used lithium-ion cathode materials undergo the same range of degradation in the ambient atmosphere.

$LiCoO_2$ cathode material

The $LiCoO_2$ active material was extracted from prismatic Li-ion accumulator. The XRD analysis was carried out within 24 hours and 4 weeks from accumulator disassembly. As shown in the following figure it was observed the material degradation. In time 24 hours after disassembly, the active material consists of pure $LiCoO_2$. The remeasure was performed after 4 weeks. The results (Figure 1) compare the XRD results. There are changes in the high and the positions of peaks. After 4 weeks was detected 91.02 % $Li_{0.35}CoO_2$ and 9.0 % Co_3O_4.

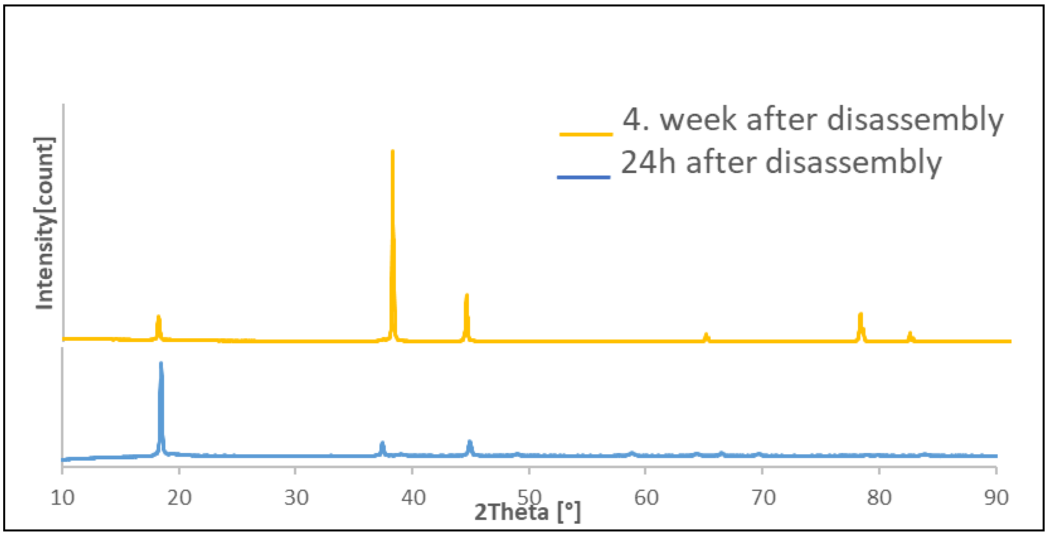

Figure 1. *$LiCoO_2$ active material XRD analyze within 24 h. and after 4 weeks after extraction.*

$LiMn_{1/3}Ni_{1/3}Co_{1/3}O_2$

This is the currently most used type of active material in Li-ion accumulators. The $LiMn_{1/3}Ni_{1/3}Co_{1/3}O_2$ active material was extracted from cylindric Li-ion accumulator Panasonic NCR18650B.

The XRD analyze was performed within time period from 24 hours, to 20 days after disassembly. As is shown on figure, in comparison with $LiCoO_2$, the active material is not so influenced by the environment. During 20 days, when the material was exposed to the ambient environment and after remeasure, the composition of the material was not changed.

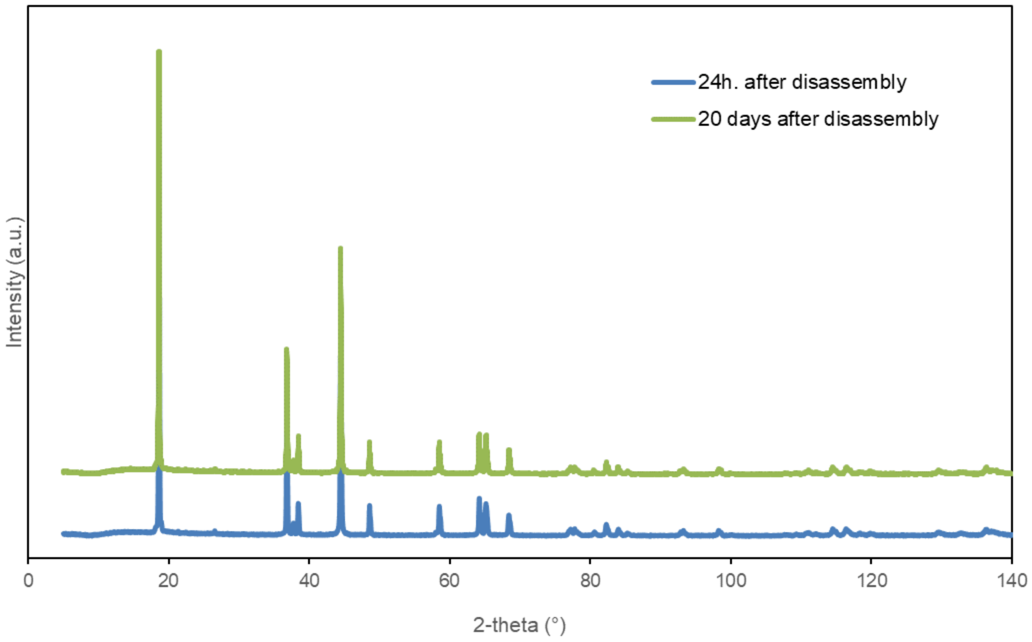

Figure 2. *Comparison of XRD of active material* $LiMn_{1/3}Ni_{1/3}Co_{1/3}O_2$ *within time period*

Conclusion

From the research we can conclude that different type of cathode active material could be affected by the ambient atmosphere and other type is more stable in the surrounding environment. Until now the $LiCoO_2$ and $LiMn_{1/3}Ni_{1/3}Co_{1/3}O_2$ active cathode materials were tested within the time period to influence of the ambient atmosphere. $LiCoO_2$ undergo degradation in the environment. The origin chemical composition has changed with realizing the amount of Co_3O_4. Instead of this, the $LiMn_{1/3}Ni_{1/3}Co_{1/3}O_2$ active cathode material does not change the chemical composition within 20 days after disassembly, so the process of next recovery can lead to better quality recycled cathodes. According to observed results is for finding comprehensive recycling process for lithium-ion accumulators necessary to know the exact battery composition and optimize the process of active material extraction.

Acknowledgments

Authors gratefully acknowledge the financial support from BUT specific research programme (project No. FEKT-S-17-4595).

References

1. A. M Bernardes, D. Crocce Romano Espinosa, and JA Soares Tenório. *Recycling of batteries: a review of current processes and technologies.* Journal of Power Sources 130.1-2 (2004): 291-298.
2. Georgi-Maschler, Tim, et al., *Development of a recycling process for Li-ion batteries.* Journal of power sources 207 (2012): 173-182.
3. D.b.Todd, *Solvent Extraction. Fermentation and Biochemical Engineering Handbook: Principles, Process Design, and Equipment* [online]. Elsevier, (2014), 225-238.

An Analytical Solution for Lithium-Ion Batteries Cooling

Seyed Saeed Madani

Department of Energy Technology, Aalborg University, Aalborg, DK-9220, Denmark

Cooling of the lithium-Ion batteries is an important issue in electric vehicles industries. This paper introduces a simple analytical solution for the battery cooling by considering different parameters that affect the air and liquid cooling of lithium-Ion batteries. It was assumed that the cell dimension is 204mm*129mm.

Introduction

Environmental problems such as air pollution, lack of energy sources, carbon dioxide emissions are increasing and destructive effects of fossil fuels on climate change is noticeable. Electric Vehicles (EVs) and Hybrid Electric Vehicles (HEVs) could be a beneficial solution to these problems. EVs, which employ batteries as their principal power source, produce no pollutions and are independent on oil and gas. Because of these advantages, EVs are considered as powerful candidates for the future of transportation systems.

These batteries have so many advantages compared to other battery chemistries such as competitive cost and high-energy storage density. Notwithstanding, these batteries produce considerable heat during high power discharge and charge. Therefore, cooling of the Li-ion batteries has been the center of attention of automotive manufacturers and researchers in the past few years as a main issue for the expansion of EVs.

An extreme local temperature increase in Li-ion batteries is a principal issue in the thermal management correlated to Lithium-ion batteries, which causes a decrease of cycle life and may result in thermal runaway of an individual cell or entire battery pack.

Between different approaches for thermal management of the Li-ion batteries such as air-cooling, liquid cooling, pipes cooling and using phase change materials air-cooling has attracted more considerations among researchers owing to its simplicity, design flexibility, low cost and compactness.

Lithium-ion batteries are the main source of energy for the electric vehicles. During discharge and charge processes, heat is generated inside lithium-Ion batteries that leads to rise their temperatures.

Temperature is one of the most important parameters of a lithium ion battery that needs to be attentively controlled, owing to the optimal working condition is generally limited between 20 and 65 °C [1,2]. Additionally, the battery's functioning temperature remarkably influences the battery's lifetime, cell degradation and efficiency. To achieve this goal many researchers are investigating to find new procedures for maintaining the temperature of lithium-Ion batteries in an appropriate functioning temperature range.

Evolution of the surface temperature of the battery cell was investigated [3]. In addition, cooling simulation of the battery cell was investigated. The outcomes demonstrate that to attain an optimum power consumption for the battery cell cooling, a lowest amount of average heat transfer coefficient could be picked [4].

Results

An analytical solution for heat transferred per unit width of a lithium-Ion battery cell with air-cooling and liquid-cooling was investigated.in the following parts these methods are described.

1. Estimate the heat transferred per unit width of the battery with air-cooling:

It is assumed that air at a temperature of 0 °C and 6 kPa pressure with a velocity of 10 m/s flow over the battery. It is supposed that the heat transferred to the surrounding is able to maintain the average surface temperature of the battery at 25 °C. The battery is 0.204m long as shown.

Conclusion

Heat transferred per unit width of the battery was estimated by using both air-cooling and liquid cooling. It was concluded that heat transfer per unit width liquid cooling is more than air-cooling. Consequently, liquid cooling is able to provide a faster and stronger cooling. A liquid velocity equal to 3m/s is able to provide a heat dissipation equal to 1000 W/m but this heat dissipation for the battery cell which cooled by air is about 10 W/m.

References

1. Abdul-Quadir Y, Heikkila P, Lehmuspelto T,Karppinen J, Laurila T, Paulasto-Krockel M. Thermal investigation of a battery module for work machines.In Thermal, Mechanical and Multi-Physics Simulation and Experiments in Microelectronics and Microsystems Conference (EuroSimE). IEEEXplore Digital Library:Palais Kaufmannischer Verein, Linz, Austria, 2011; 1–6.
2. Baronti F, Fantechi G, Leonardi E, Roncella R, Saletti R. Effective modeling of temperature effects on lithium polymer cells. In International Conference on Electronics, Circuits, and Systems (ICECS), Vol. 17. IEEEXplore Digital Library: Athens, Greece, 2010;990–993.
3. S. S. Madani, M. J. Swierczynski, and S. K. Kær, "Evolution of surface temperature of a 13 amp hour Nano Lithium-Titanate battery cell under fast charging," in *ECS Transactions*, 2017, vol. 81, no. 1.
4. S. S. Madani, M. J. Swierczynski, and S. K. Kær, "Cooling simulation and thermal abuse modeling of lithium-ion batteries using the Newman, Tiedemann, Gu, and Kim (NTGK) model," in *ECS Transactions*, 2017, vol. 81, no. 1.

Thermal Analysis of an Indirect Liquid Cooling with Different Geometries for a Lithium-ion Battery

S.S.Madani[a]

[a]Department of Energy Technology, Aalborg University, Aalborg, DK-9220, Denmark

E-mail: ssm@et.aau.dk

A new method for simulating and modeling thermal behavior of the battery was developed. A big temperature heterogeneousness was seen in surface of the battery cell particularly at big current rates. This occurrence might be expressed by big amount of heat loss owing to bigger temperature gradient. Moreover, the amount of surface temperature of the battery cell which was estimated by the model was compared with the experimental data. It was observed that it is in good agreement with the data from the model. bigger temperature heterogeneousness was observed at the battery cell surfaces because of bigger current rate. Correspondingly, construct of a suitable thermal management system particularly during big current rates discharging and charging could play an essential role in stopping big temperature growing of the battery cell. The simulation approach, which was indicated in this research could cooperate to the advancement of a battery thermal management system, that facilitates the temperature development of lithium-ion batteries as an interdependent of time to be more exactly determined. Moreover, it could contribute to forecast the evolution of the electrical, thermal and chemical processes.

Introduction

With quickly developing energy requirements, there is a big growth in need for further renewable and efficient energy resources. Many applications depend on fossil fuels for furthermost of their energy requirements. Combustion of fossil fuels causes the release of greenhouse gases in the direction of through to the atmosphere. Global warming is a straightforward outcome of the aggregation of greenhouse gases. Internal combustion engines are a significant supply of carbon monoxide release and consequently substitute energy supplies for automotive propulsion utilizations is one of the beginning motivations of research throughout the world.

The renewable supplies such as wind energy and solar energy are green supplies of energy. Nevertheless, these are periodic sources. Especially for a continuing application, storage of energy is essential.

Li ion batteries are electrochemical storage appliances via which energy could be saved in the configuration of chemical potential diversity and utilize it on every occasion it is required. With many utilizations in portable electronics including laptops, mobile phones, and other electronic appliances and potential implementations for automobile goal.

lithium ion batteries have acquired a lot of consideration from researchers worldwide. Purely electric vehicles, hybrid electric vehicles, plug in hybrid vehicles advancements have been the attention of the research activities of furthermost of the automotive companies.

For the automotive implementations lithium ion batteries are restricted by gravimetric and volumetric energy density, accompanied by cycle life. With superior construction of the electrode magnitude, mechanical and shape properties, there are lots of opportunities for advancement.

Attributable to their big power and energy densities, lithium-ion batteries are a considerably essential element of electric vehicles. Their application has enhanced noticeably in the last few years.

One of the important issues of employing lithium ion batteries in electric and hybrid vehicles is appropriate thermal management. Designing thermal management is essential with the intention of controlling degradation at a satisfactory rate when optimizing the performance of the lithium-ion batteries. In addition, it is important to decrease the risk of thermal runaway.

It is usually appropriately comprehended that enhancing the working temperature of a lithium ion battery tends to raise the rate of degradation. Notwithstanding, there is insufficient comprehension regarding the advantageous technique in which to thermally control the lithium-ion battery cells in a battery pack. In addition, the influences of temperature gradients among battery cells in a battery pack are not well understood.

Whilst thermal management of the lithium-ion battery is a considerably complicated problem. The solution for thermal management will be dissimilar for dissimilar pack topologies, battery cells, and different applications.

The investigation which is represented in this Ph.D. thesis demonstrates a considerable scientific advancement and improvement in the comprehension of thermal management in lithium ion battery cells.

A comprehensive experiential laboratory characterization experiment method was established and exerted to different lithium-ion batteries. Consequently, the batteries' power, open circuit voltage, capacity, capability, internal resistance,

and signal AC impedance were determined for different load currents and over an extensive temperature range.

According to these performance outcomes, battery models which were capable of predicting the dynamic behavior of the lithium-ion batteries were improved and experimentally validated under different operating conditions.

Various experimental research has been accomplished on the thermal and electrical performances of lithium-ion batteries. Experimental investigations were restricted to surface temperatures integrated with the thermal or analytical modeling of heat dissipation with the intention of achieving battery temperatures and to determine the battery cell total heat loss.

Improved Electrochemical Performance of NCM Cathode Materials Based on the Modification of the Salt Content in the Electrolyte

M. G. Ortiz[a,b,c], O. Čech[c], and M. Sedlaříková[c]

[a] Instituto de Investigaciones Fisicoquímicas Teóricas y Aplicadas (INIFTA), Facultad de Ciencias Exactas, UNLP, CCT La Plata-CONICET, 1900, La Plata, Argentina

[b] Centro de Investigación y Desarrollo en Ciencia y Tecnología de Materiales (CITEMA), Universidad Tecnológica Nacional - CICPBA, 60 y 124, 1923, Berisso, Argentina

[c] Department of Electrical and Electronic Technology, Faculty of Electrical Engineering and Communication, Brno University of Technology, Technická 10, 61600, Brno, Czech Republic

In this work, NCM cathode materials, for Li-ion batteries, were synthesized via a solid-state reaction routine, in which manganese (IV) dioxide, nickel (II) oxide, cobalt (II) hydroxide and lithium hydroxide monohydrate were employed as metal precursors with different calcination temperature. The prepared materials were used as a cathode material for lithium-ion batteries and the electrochemical performance was studied by galvanostatic charge-discharge cycling, cyclic voltammetry, electrochemical impedance spectroscopy and rate capability, in which as electrolyte, 1M and 1.5M $LiPF_6$ in a mixture of ethylene carbonate and dimethyl carbonate (EC:DMC- 1:1 w/w) were employed.

Introduction

Lithium-ion batteries (LIBs) with enhanced energy density are now pursued as the most viable power sources for portable electronics, electric and hybrid vehicles, and even for grid-scale power storage applications (1). The current LIBs technology is based on insertion-reaction electrodes and organic liquid electrolytes. With an aim to increase the energy density or optimize the other performance parameters, new electrode materials (2) and electrolytes (3) are being intensively pursued. For the cathode, within the three existing choices, the layered $LiMO_2$ (M = Mn, Co, and Ni denoted as NCM), have been extensively studied and considered to be a promising candidate of cathode material for future LIBs because of their high theoretical capacity, low cost, safety, high cycling stability and low toxicity (4). However, it is considered that the need to continue with these studies, to be able to improve their electrochemical behavior (especially with respect to its low initial coulomb efficiency and poor rate capability (4)), is still present. To reach this goal, various strategies including optimized particle morphology (5), size (5), and composition (6), using the cation doping in the bulk phase (7), and surface coating (8) have been developed.

Experimental

The NCM materials were synthesized through a solid state reaction routine. The precursor powders were prepared via a ball milling. In a typical process, raw materials employed in the experiment were nickel oxide (99.8%), cobalt hydroxide (95%), manganese oxide (95%) and lithium hydroxide monohydrate (98.9%). All the starting raw materials, with the certain molar ratio

Li: Ni: Co: Mn=1: 0.33: 0.33: 0.333, were milled for 1h. Afterwards, the mixture was heated in two temperature steps, first at 450 °C for 5h and then, at different temperatures (800/850/900/950 °C) for 12 h.

The working electrodes were prepared by casting the slurry of the active material (NCM-800/850/900/950) (80%), Super P (10%) and polyvinylidene fluoride (PVDF) (10%) dissolved in the appropriate amount N-methyl-2-pyrrolidone (NMP) on an aluminum foil. Electrochemical experiments were carried out with the cell ECC-STD (El-Cell©), which were assembled inside an Ar-filled glove box, using the prepared working electrodes as cathode and Li metal foil as counter as well as reference electrodes. As electrolyte, 1M and 1.5 M $LiPF_6$ in a mixture of ethylene carbonate and dimethyl carbonate (EC:DMC- 1:1 w/w) was employed.

Cyclic voltammetry was done in the potential window from 2 to 4.9 V vs. Li/Li^+ and the scan rate was set to 0.1 mV/s. vs. The cells were cycled in the potential range 2 - 4.8V vs. Li/Li^+, using a VMP-2Z multi-channel galvonostat-potentiostat (Bio-Logic). Electrochemical impedance spectroscopy (EIS) measurements were performed using similar equipment with an AC voltage amplitude of 5 mV in the frequency range of 0.1- 100.000 Hz. All electrochemical tests were performed at room temperature.

Fig. 1 (A) and (B) presents the cyclic voltammograms of NCM samples with 1M and 1.5M $LiPF_6$ in the electrolyte. As shown in the figures, for both concentrations, the CV peaks corresponding to a redox process can be seen better defined, with a higher current associated with these peaks and a better reversibility related to the redox process is observed in the NCM-800 and NCM-850 electrodes. The cycling behavior of working electrodes is presented in Fig. 1 (C) and (D), NCM-900 exhibit the highest initial discharge specific capacities, however this decreases in cycling. The NCM-850 electrodes delivered a specific discharge capacity of 105 mAh g^{-1} and 127 mAh g^{-1} for the concentration of 1 M and 1.5 M $LiPF_6$ respectively, after 75 cycles.

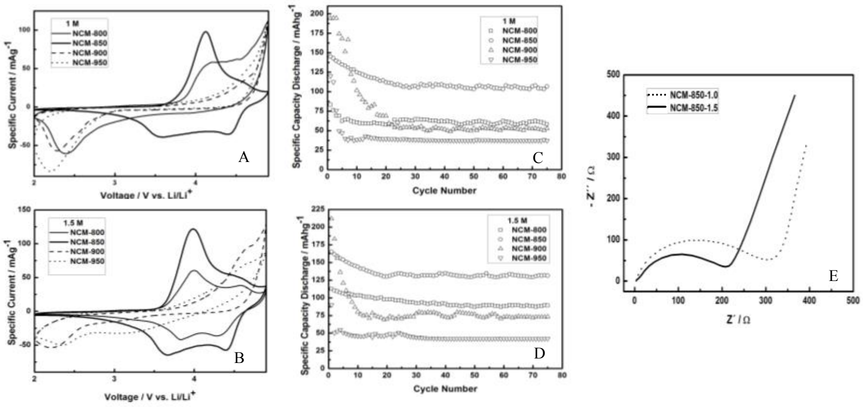

Figure 1. *Cyclic voltammograms of NCM electrodes with A) 1M $LiPF_6$, B) 1.5M $LiPF_6$, Cyclic performance of NCM electrodes with C) 1M $LiPF_6$, D) 1.5M $LiPF_6$, and E) Nysquist´s diagrams.*

Nyquist diagrams at 50% of charge, corresponding to NCM-850 working electrode, are presented in Fig. 1 (E). In the high frequency domain, a distorted semicircle is observed, which can be associated with the overlapping of the SEI formation/ decomposition resistance along with the charge transfer process (resistance) in the cathode/electrolyte interface. In the low frequency region, a Warburg-type impedance was observed, that is related to the Li ion diffusion in the solid active material. The smaller high-frequency semicircle observed in the impedance spectra of the NCM-850-1.5 electrode - it could be attributed to the resistive reaction layer.

Conclusion

Results indicate that the NMC materials annealed at 850 ºC (NCM-850) exhibit an improvement of their electrochemical performance compared with that obtained with others temperatures. These improvements include better specific capacity, cycling stability and lower impedance modulus.

Acknowledgments

Authors gratefully acknowledge the financial support from the European Union, European Structural and Investment Funds Operational Program Research, Development and Education, and Ministry of Education, Youth and Sports of the Czech Republic under BUT specific research program (project N°. CZ.02.2.69/0.0/0.0/16_027/0008371).

References

1. Q. Wanga, B. Mao, S. I. Stoliarov, J. Sun, *Progress in Energy and Combustion Science*, **73**, 95 (2019).
2. A. Mishra, A. Mehta, S. Basu, S. J. Malode, N. P.Shetti, S. S. Shukla, M. N. Nadagouda, T. M. Aminabhavi, *Materials Science for Energy Technologies*, **1**, 2, 182 (2018).
3. Q. Wang, L. Jiang, Y. Yu, J. Sun, *Nano Energy*, **55**, 93 (2019).
4. N. Nitta, F. Wu, J. T. Lee and G. Yushin, *Materials Today*, **18**, 5, 252 (2015).
5. M-J. Uddin, P. K. Alaboina, S-J. Cho, *Materials Today Energy*, **5**, 138 (2017).
6. Y. Xi, Y. Liu, D. Zhang, S. Jin, R. Zhang, M. Jin, *Solid State Ionics*, **327**, 27 (2018).
7. D. Liu, X. Fan, Z. Li, T. Liu, M. Sun, C. Qian, M Ling, Y. Liu, C. Liang, *Nano Energy,* **58**, 786 (2019).
8. D. Zuo, G. Tian, X. Li, D. Chen, K. Shu, *Journal of Alloys and Compounds*, **706**, 24 (2017).

Gel Polymer Electrolytes Based on Methyl Methacrylate Modified Flame Retardants

I. Veselkova[a], M. Sedlaříková[a] and G. Fafilek[b]

[a] Department of Electrical and Electronic Technology, Brno University of Technology, Technická 10, 616 00 Brno, Czech Republic

[b] Vienna University of Technology, Getreidemarkt 9, 1060 Vienna, Austria

This article deals with preparation of gel polymer electrolytes modified by flame retardants. Two methods of preparation of gel polymer electrolyte were tested for the comparison of electrochemical and thermal properties of gel electrolytes. This work is focused on measuring electrical conductivity and potential window of gel electrolytes. The main goal is increasing thermal, electrical and electrochemical properties of gel polymer electrolytes.

Introduction

Rechargeable lithium ion batteries are one of the most promising power sources due to their high energy density. However, there are still potential safety issues in the commercial lithium ion batteries arising from leakage and combustion of organic electrolytes [3].

Among the various secondary batteries, lithium-ion batteries are most promising during their high energy and power densities. Many electronic devices used these batteries. However, in lithium-ion batteries, liquid electrolyte is used as electrolyte. This type of electrolyte has a high conductivity, but can leak from the battery, which is not safe. Gel polymer electrolytes were introduced to provide both cohesive properties of solid electrolyte and diffusive properties of liquid electrolyte. Gel polymer electrolytes consist of a large quantity of liquid electrolyte and polymer network, which are completely compatible with each other to form a stable gel [1].

Today, gel polymer electrolytes are the most perspective materials, which have many advantages. They have a lower lithium-ion transference number, higher viscosity, lower ionic conductivity, and slower kinetics than liquid electrolytes.

Subsequent research has focused on increasing electrical conductivity, improving electrical and thermal stability of gel polymer electrolyte with selected flame retardants.

Chemical composition

Chemical composition of gel polymer electrolyte can be divided into two components: conductive component and polymer component. The conductive component consists of a salt lithium hexafluorophosphate ($LiPF_6$), which dissolved in an organic solvent ethylene carbonate : diethyl carbonate (EC:DEC in weight 1:1). The polymer component consists of a monomer methyl methacrylate (MMA) in concentration 20 mol% in the conductive component, a cross-linking agent ethylene glycol dimethacrylate (EDMA) in concentration 3.5 mol% in the monomer and initiator of UV polymerization benzoin ethyl ether (BEE) in concentration 1 mol% in the monomer.

As flame retardants were chosen triethyl phosphate (TEP), trimethyl phosphate (TMP), tributyl phosphate (TBP), triphenyl phosphate (TPP) and dimethyl methylphosphonate (DMMP) [2].

Experiment

This work describes two different experiments. These experiments included the preparation of gel polymer electrolytes modified by flame retardants.

First experiment was focused on preparation of gel samples with different amount of one type of flame retardant. The amount of flame retardant in the chemical composition was changed from 10% to 100%. The concentration of lithium salt was 0.5 mol/l in solvent. Figure 1 shows values of conductivity, which were measured in the first experiment.

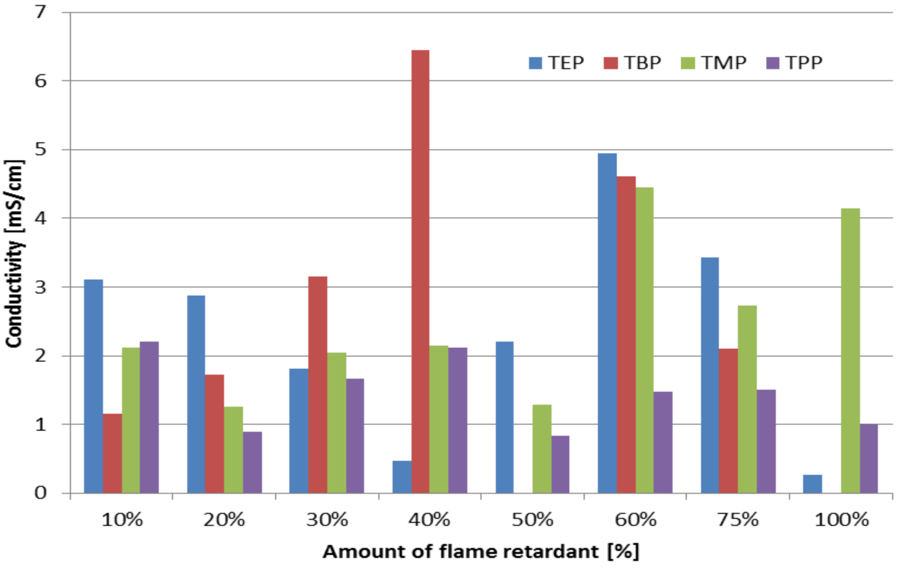

Figure 1. *Conductivity of gel polymer electrolytes with flame retardant as modifier*

Second experiment was focused on the preparation of gel samples without any solvent. Flame retardants were added to gel electrolytes not only as modifiers, but also as solvent. In this experiment, the concentrations of lithium salt were changed from 0.25 mol/l to 1.5 mol/l [2]. The salt was dissolved in the same amount of flame retardant. Figure 2 shows the values of conductivity of gel samples, which were measured in the second experiment.

Gel samples prepared in glove box JACOMEX with argon atmosphere. Polymerization process took place in chamber with UV-light for 60 minutes. Thickness of the samples was 0.9 mm with diameter 16 mm [2].

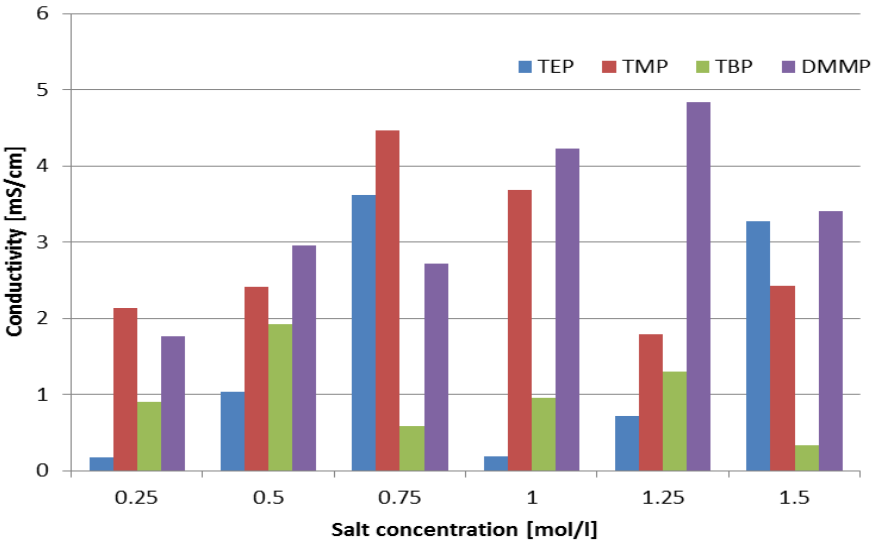

Figure 2. *Conductivity of gel polymer electrolyte with flame retardant as solvent*

Conclusion

Current development is focused on improving the following parameters of gel polymer electrolytes: ionic conductivity, potential window, long-term electrochemical and thermal stability of the polymer and solvent. For increasing thermal stability with conductivity. gel polymer electrolytes with selected flame retardants were prepared. Two different method of preparation of this type of electrolytes were tested.

From obtained results, gel samples with high conductivity were chosen, which will be testing by TGA and DTA analysis.

Acknowledgments

This work was supported by the grant FEKT-S-17-4595 "Materiály a technologie pro elektrotechniku III" and also sponsored by the NATO Science for Peace and Security Programme under grant 985148. Authors gratefully acknowledge financial support from grant AKTION “Gel polymer electrolytes with ionic liquids” (83p2).

References

1. B. C. F. Wong, A. Ahmad, S. A. Hanifah and N. H. Hassan, Effects of ethyleneglycol dimethacrylate as cross-linker in ionic liquid gel polymer electrolyte based on poly(glycidyl methacrylate), **21** (2), (2016).
2. I. Veselkova, M. Jahn, M. Sedlaříková and J. Vondrák, Electrochemical properties of gel polymer electrolytes with flame retardant using as solvent, (2018).
3. S. Thayumanasundaram, V. Sh. Rangasamy, J. W. Seo and J.-P. Locquet, Lithium polymer electrolytes based on sulfonated poly(ether ether ketone) for lithium polymer batteries, **32**, (2015).

Using Copolymers in Gel Polymer Electrolytes

I. Veselkova[a], S. Peterová[a] and M. Sedlaříková[a]

[a] Department of Electrical and Electronic Technology, Brno University of Technology,
Technická 10, 612 00 Brno, Czech Republic

Gel polymer electrolytes are more perspective materials, which can replace liquid electrolytes in lithium ion batteries. This article deals with the preparation of gel polymer electrolytes based on copolymer. Copolymer is used in gel polymer electrolyte like monomer, which consists of two different methacrylate chemicals. The main goal of this experiment was to find a gel electrolyte with higher conductivity and higher electrical stability. Impedance spectroscopy and linear voltammetry were used for the measurement of these properties.

Introduction

Liquid electrolytes are used in different electronic devices for several decades due to their high ionic conductivity and good contact with electrodes. However, the use of liquid electrolyte is not safe, because of the risk of leakage and even combustion of organic electrolytes.

Gel polymer electrolytes are perspective materials, which can replace liquid electrolytes in lithium ion batteries. This type of electrolytes has many advantages over liquid electrolytes such as elimination of the risk of electrolyte spillage, high safety (no organic solvents with toxins are used), low density, high shape flexibility, resistance to mechanical stress and high temperatures, low reactivity due to the solid gel component and other [1]. Due to the workability of polymers, the gel polymer electrolytes can render the energy storage devices with adjustable shapes and high flexibility, which is promising for burgeoning portable and wearable electronics. Gel polymer electrolytes have become one of the most desirable alternatives among various electrolytes for electrochemical devices, and significant progress has been made in lithium ion batteries, supercapacitors and the other kinds of electrochemical energy storage devices. In order to meet the requirements of wearable devices for flexibility and deformability, more special gel polymer electrolytes with tough, stretchable and compressible functionalities have been developed as well [4].

Chemical composition

Chemical composition of gel polymer electrolyte can be divided into two main components: a conductive component and a polymer component. Conductive component consists primarily of a salt and an organic solvent. This component determines the conductivity of gel polymer electrolyte. Polymer component consists of a monomer, a cross-linking agent and an initiator of polymerization. This component determines a gel structure, which is achieved by polymerization process.

Lithium hexafluorophosphate 98% (LiPF6), ethylene carbonate (EC), diethyl carbonate (DEC), ethylene glycol dimethacrylate (EDMA), benzoin ethyl ether (BEE), methyl methacrylate (MMA), ethyl methacrylate (EMA), lauryl methacrylate (LMA), trimethoxysilylpropyl methacrylate (TSPMA), ethoxyethyl methacrylate (EOEMA), butyl methacrylate (BMA) and isobutyl methacrylate (IBMA) were chosen for the preparation of gel polymer electrolytes [2].

Table I. shows chemical properties of selected monomers.

***TABLE I.** Chemical properties of selected monomers*

Monomer	**Molecular weight [g/mol]**	**Density [g/cm^3]**	**Melting point [°C]**	**Boiling point [°C]**	**Flash point [°C]**
MMA	100.121	0.94	-48	101	10
EMA	114.14	0.917	-75	117	20
LMA	254.41	0.868	-7	142	107
TSPMA	248.35	1.045	-	190	92
EOEMA	158.19	0.96	-	185	69.5
BMA	142.20	0.894	-75	162-165	54
IBMA	142.20	0.886	-61	155	42

Experiment

All gel samples were prepared in glove box JACOMEX with argon atmosphere. Polymerization was made in chamber with UV-light for 60 minutes. A gel sample means a circle gel polymer electrolyte with diameter of 16 mm and with a thickness of 0.9 mm [3].

Table II. shows conductivity of gel polymer electrolytes based on copolymer. The molar ratio is a ratio of monomers, which are in the table II. The molar ratios of MMA calculated from molar ratio of another monomer in copolymer.

***TABLE II.** Conductivity of gel polymer electrolytes based on copolymer*

Conductivity γ [mS/cm]						
Molar ratio [%]	**Monomer**					
	EMA	**LMA**	**TSPMA**	**EOEMA**	**BMA**	**IBMA**
5	3.32	3.51	2.47	2.18	2.67	2.83
10	3.52	2.79	2.17	3.21	2.10	2.23
20	3.23	1.20	1.71	3.37	1.60	2.56
30	3.92	0.58	1.53	2.44	3.67	2.18
40	3.30	0.47	1.70	2.01	3.91	2.17
50	2.20	-	2.00	1.94	3.17	2.56
60	4.53	-	1.44	1.59	2.04	3.01
70	3.06	-	1.87	1.49	2.69	1.67
80	-	-	1.09	1.58	0.41	0.66
90	-	-	1.42	1.48	0.10	0.99
95	-	-	1.50	1.33	0.008	0.017

The concentration of $LiPF_6$ was 0.5 mol/l in solvent. Mixed EC:DEC in weight 1:1 were used as solvents. The concentration of EDMA was 3.5 mol% in copolymer. The concentration of BEE was 1 mol% in copolymer. The concentration of copolymer was 20 mol% in solvent.

Copolymer was mixed from two monomers: MMA and another monomer. The molar ratio of monomers that was made of a copolymer was changed from 5 mol% to 95 mol%. The total amount of copolymer was 100 mol%.

Gel samples with MMA and LMA had bad mechanical properties. When molar ratio of MMA was growing up, mechanical properties of gel samples got worse. From table II can be seen, that conductivity of these samples was growing with higher molar ratio of LMA.

Conclusion

Current development is focused on improving electrochemical parameters of gel polymer electrolytes: increasing conductivity, extending potential window and improving long-term chemical and electrochemical stability of the polymer and solvent. Using a copolymer in gel polymer electrolyte can change the structure of polymer in gel, it can improve the observed parameters. Further research will be focused on improving thermal stability of gel electrolytes. The best gel samples will be testing in lithium cells.

Acknowledgments

This work was supported by the grant FEKT-S-17-4595 "Materiály a technologie pro elektrotechniku III" and also sponsored by the NATO Science for Peace and Security Programme under grant 985148.

References

1. Emad M. Masoud, *Citrated porous gel copolymer electrolyte composite for lithium ion batteries application: an investigation of ionic conduction in an optimized crystalline and porous structure*, **651**, (2015).
2. M. Jahn, I. Veselkova, M. Sedlaříková, K. Bartušek and M. Zatloukal, *Gel polymer electrolytes modified nanoparticles or copolymers and polymerized in magnetic and electric fields*, **1**, (2018).
3. M. Jahn, S. Peterová, M. Sedlaříková, J. Vondrák and I. Veselkova, *Gel polymer electrolytes for lithium cell based on various methacrylates*, **1**, (2018).
4. X. Cheng, J. Pan, Y. Zhao, M. Liao and H. Peng, *Gel polymer electrolytes for electrochemical energy storage*, **8**, (2018).

Electrochemical Supercapacitor with Thiourea-based Aqueous Electrolyte

G. Lota, M. Graś, Ł. Kolanowski, J. Wojciechowski

Institute of Chemistry and Technical Electrochemistry, Poznan University of Technology,
Berdychowo 4, 60-965 Poznan, POLAND

The capacitance of electrochemical capacitors may be improved by providing additional charge originating from faradaic reactions. The application of a novel type of electrolyte (1 mol dm^{-3} of Na_2SO_4 aqueous electrolyte with thiourea addition) with a broad voltage window is considered, but the stability of this new generation of electrolyte during long term cycling of capacitors is not yet confirmed.

Introduction

Electrochemical capacitors (ECs) are able to store the electric charge by reversible electrostatic adsorption of ions in the electric double layer. ECs are characterized by high power rates, excellent cyclability and the ability to quickly charge and discharge. Unfortunately, the electrochemical capacitors have some drawbacks – low energy density in comparison with other power sources and high self-discharge [1,2].

Since the energy density of the capacitor strongly depends on the operating voltage window and capacitance values, electrolytes with wide electrochemical stability are the main challenge. Electrochemical capacitors operating in aqueous medium demonstrate several interesting features [3,4]. They are environmentally friendly, safe and have a relatively low price. Moreover, the cell assembling process does not require an inert atmosphere.

The increase of capacitance could be realized by the so-called pseudocapacitance effect. The pseudocapacitance effects can originate from the quick faradaic reactions at the electrode/electrolyte interface. The pH of the electrolyte has a significant influence on the possible redox mechanisms, involving proton and electron transfer [5]. Usually, potassium iodine [6], bromide [7], hydroquinones [8] and other benzene derivatives [9] are applied.

Experimental

All experiments were carried out at ambient conditions in the two and three-electrode Swagelok® cells made of polytetrafluoroethylene with 316 L stainless steel current collectors. The commercial activated carbon with BET surface area of 2364 $m^2\ g^{-1}$ was used as the active material of composite electrodes.

Different concentrations of thiourea solution (80, 160, 240,320 mmol dm^{-3}) with the supporting electrolyte (1 mol dm^{-3} of Na_2SO_4) served as the electrolytes. It is well known that the addition of thiourea into an aqueous solution may inhibit H_2 evolution, therefore all measurements were carried out in the voltage range of 0 – 1.6 V.

The capacitance properties (expressed per mass of a single electrode) were examined by galvanostatic charge/discharge, cyclic voltammetry and electrochemical impedance spectroscopy. After electrochemical measurements electrodes were subjected to XPS analysis.

Results and discussion

The presented studies show that thiourea is suitable for the enhancement of capacitance of carbon/carbon capacitors in aqueous media by inducing pseudocapacitive effects. The electrochemical reactions which are considered, concern the oxidation of thiourea (TU) to formamidine disulfide (FDS) and the reduction of FDS which is formed during the anodic oxidation according to the following reaction:

$$2\,H_2NC(S)NH_2 \leftrightarrow HN = C(NH_2)S - SC = NH(NH_2) + 2e^- + 2H^+ \qquad (1)$$

An increase in capacitance depends on the electrolyte composition. For the optimal value of thiourea (160 mmol dm^{-3}), the enhancement of capacitance is observed for high values of scan rate and high current densities. XPS measurements proved that carbon electrodes working in thiourea solutions contain oxygen, nitrogen and sulphur functional groups. It should be noted that samples working in thiourea solutions are characterized with a higher content of oxygen in the comparison with sample working in pure Na_2SO_4 electrolyte [10].

Acknowledgments

The authors acknowledge the financial support from the National Science Centre of Poland, grant No DEC-2013/10/E/ST5/00719.

References

1. R. Kotz, M. Carlen, *Electrochim. Acta*, **45**, 2483 (2000).
2. F. Béguin, V. Presser, A. Balducci, E. Frackowiak, *Adv. Mater.*, **26**, 2216 (2014).
3. J. M. Miller, A. Burke, *Electrochem. Soc. Interface*, **17,** 53 (2008).
4. P. Simon, Y. Gogotsi, *Nat. Mater.,* **7,** 845 (2008).
5. Q. Abbas, P. Ratajczak, P. Babuchowska, A. Le Comte, D. Bélanger, T. Brousse, F. Béguin, *J. Electrochem. Soc.*, **162** A5148 (2015).
6. G. Lota, E. Frąckowiak, *Electrochem. Commun.,* **11**, 87 (2009).
7. S. Yamazaki, T. Ito, M. Yamagata, M. Ishikawa, *Electrochim. Acta,* **86,** 294 (2012).
8. S. Sathyamoorthi, V. Suryanarayanan, D. Velayutham, *J. Power Sources,* **274** 1135 (2015).
9. Y. Tian, R. Xue, X. Zhou, Z. Liu, L. Huang, *Electrochim. Acta,* **152,** 135 (2015).
10. M. Graś, Ł. Kolanowski, J. Wojciechowski, G. Lota, *Electrochem. Commun.,* **97**, 32 (2018).

Chitosan as a Precursor for N-reached Carbon Electrode Materials in Electrochemical Capacitor Application

K. Lota[a], I. Acznik[a], A. Sierczynska[a], L. Kolanowski[a] and G. Lota[b]

[a] Division in Poznan, Łukasiewicz Research Network - Institute of Non-Ferrous Metals
Central Laboratory of Batteries and Cells, 61-362 Poznan, Poland

[b] Institute of Chemistry and Technical Electrochemistry, Poznan University of Technology,
60-965 Poznan, Poland

Activated carbons with the developed surface area are generally used as electrode materials for electric double-layer capacitors. One of the methods to enhance their electrochemical performance is to enrich them with heteroatoms such as nitrogen. Chitosan, like the one of the most popular natural polymer, is obtained as a derivative of chitin and can be used as a precursor of nitrogen-doped porous carbons. In this work, nitrogen-doped carbon materials were prepared via one-step, the simple method with chitosan as the source and potassium citrate as the activator. Additionally, porous carbons were prepared through KOH activation, using different temperature of activation. The prepared materials were characterized by SEM, BET and elemental analysis for their morphology, specific surface area and elemental composition, respectively. As an electrode material, prepared activated carbons delivered the high specific capacitance, excellent rate capability and cyclability in 1 M H_2SO_4 solution.

Introduction

Excellent properties of electrochemical capacitors such as high power density, fast charge and discharge capabilities and good cycle performance influence on their increasing applications (1,2). The charge storage for such devices is realised mainly by ions adsorption at the electrode/electrolyte interface. As electrode materials are generally used activated carbons, due to their many advantages such as low cost, chemical stability, conductivity and developed the specific surface area (3,4). Functional groups or heteroatoms such as nitrogen can increase the charge-exchange characteristics of carbon, leading to enhancement of electrochemical capacitance. There are different ways to incorporate nitrogen, e.g. by doping process using nitrogen-reached compounds or using nitrogen-reached precursor-like chitosan (5,6). In this work, we proposed to apply chitosan-based activated carbons as electrode materials for electrochemical capacitors with superior electrochemical performances.

Experimental

The activated carbons were prepared using chitosan (Aldrich®) as a carbon precursor.

Two methods of chemical activation were applied. The first method used KOH as an activator. The ratio of C:KOH was established as 1:4 and different temperatures in the range of 750–850 °C was applied. The activation process was proceeded by pyrolysis of chitosan. The second one as an activator potassium citrate adopted and different temperatures in the range of 500–850 °C was applied.

The physicochemical properties of activated carbons were estimated using scanning electron microscopy, nitrogen adsorption/desorption measurements and elemental analysis. The carbon materials were tested in 1 M H_2SO_4 electrolyte in two-electrode Swagelok® system. The methods: cycling voltammetry, galvanostatic charge/discharge and electrochemical impedance spectroscopy were used to estimate electrochemical properties of prepared materials.

Results and Discussion

The BET surface area of prepared carbons ranges from several hundred m^2/g up to 2800 m^2/g depending on method preparation and applied temperature. The prepared carbons contain heteroatoms and functional groups and as the temperature of activation grows the percentage of carbon increases, while nitrogen decreases. Surface morphologies of the initial chitosan and after activation processes were characterized using scanning electron microscopy. SEM images of prepared carbons are shown in Fig. 1. The two-stage process of KOH activation (Fig.1b) causes that carbon particles have smallest and more irregular shapes, while after process with potassium citrate chitosan grains covered by nanoflakes are well visible in Fig. 1c.

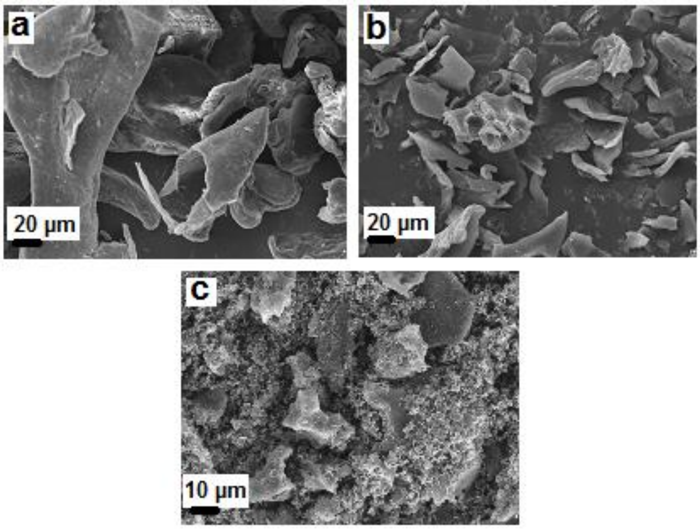

Figure 1. *SEM figures of a) chitosan b) KOH activated carbon from chitosan at 750 ^{0}C and c) $K_3C_6H_5O_7$ activated chitosan at 750 ^{o}C*

Electrochemical properties of prepared activated carbons were examined in acidic electrolyte. Galvanostatic charging/discharging with increasing current load for carbon materials activated with potassium citrate are shown in Fig. 2. When the current load rises, the most visible drop of capacitance is observed for carbons with a higher amount of nitrogen, which were prepared at lower temperatures. It can be observed that materials with higher amount of nitrogen (with pseudocapacitance properties) cannot keep up fast charging/discharging measurements, although the highest value of capacitance is recorded with moderate regimes. In the case of KOH activation, the most stable and highest capacitance values were obtained for activated chitosan at 750^{o}C.

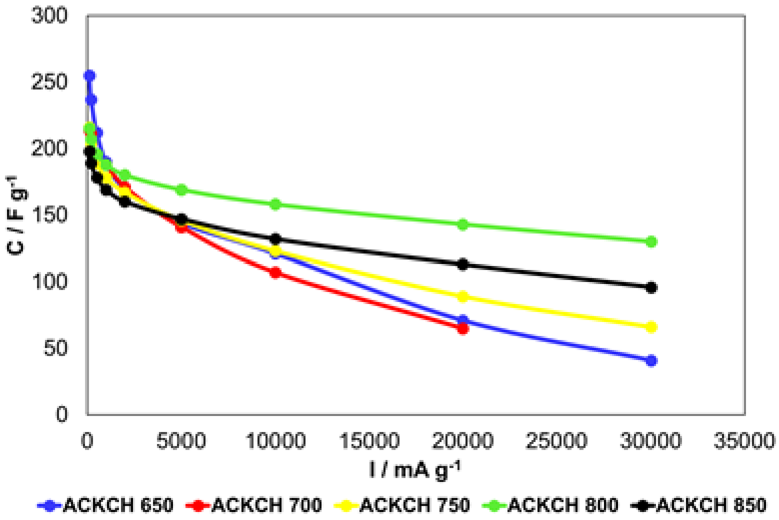

Figure 2. *Capacitances values versus current load for carbons activated with potassium citrate*

Conclusion

Chitosan can be successfully used as a precursor of nitrogen-doped porous carbons. The porosity and surface area, as well as nitrogen content, strongly depend on the temperature of activation. The highest value of capacitance was obtained for carbon materials with developed surface area, which enhances the efficient use of the electrode surface and influence on the capacitance properties of the material. Even though activated carbons with several percent contents of nitrogen show good electrochemical properties, the loss of capacitance with increasing scan rate and current regimes is observed. However, the application of a suitable activation method ensures chitosan-based carbon materials with good charge propagation and excellent cycling stability.

Acknowledgments

The authors acknowledge the financial support from the Ministry of Science and Education (Poland) – subvention 2019.

References

1. P. Sharma, TS. Bhatti, *Energy Conversion and Management* **51**, 2901 (2010).
2. W. Raza, F. Ali, N. Raza, Y. Luo, K. Kim, J. Yang, S. Kumar, A. Mehmood, E.E. Kwon, *Nano Energy*, **52,** 441 (2018).
3. K. Fic, A. Platek, J. Piwek, E. Frackowiak, *Materials Today*, **21** (4), 437 (2018).
4. J. Lee, Y.A. Lee, Ch. Yoo, J.J. Yoo, R. Gwak, W.K. Cho, B. Kim, H. Yoon, *Microporous and Mesoporous Materials,* **261**, 119 (2018).
5. L. Wang, Q. Zhu, J. Zhao, Y. Guan, J. Liu, Z. An, B. Xu, *Microporous and Mesoporous Materials,* **279**, 439 (2019).
6. K. Lota, I. Acznik, A. Sierczynska, G. Lota, *Materials Letters,* **173**, 72 (2016).

The Influence of the Modification of Current Collectors on the Electrochemical Capacitor Parameters

J. Wojciechowski[a], Ł. Kolanowski[a], M. Graś[a], K. Szubert[b], A. Bund[c], K. Fic[a] and G. Lota[a]

[a] Institute of Chemistry and Technical Electrochemistry, Poznan University of Technology, Berdychowo 4, 60-965 Poznan, Poland

[b] Faculty of Chemistry, Adam Mickiewicz University, Umultowska 89b, 61-614 Poznan, Poland

[c] Electrochemistry and Electroplating Group, Technische Universität Ilmenau, Gustav-Kirchhoff-Straße 6, 98693 Ilmenau, Germany

This paper discusses the effect of corrosion of steel current collectors on the performance of an electrochemical capacitor and a possible way of protecting these collectors from the destructive phenomena, through the use of a hydrophobic siloxane coating. The presented results of electrochemical techniques, mainly the potentiostatic technique (voltage-holding tests) confirm the fact that the current collector, being one of the elements of positive electrode, on which during charging, oxidation reactions occur, after 200 hours in the charged state undergoes tremendous degradation. In the case of a current collector with a siloxane coating, subjected to an identical test regime, there was no deterioration of the performance of the electrochemical capacitor.

Introduction

The energy storage phenomena in the electrochemical capacitors is performed on the basis of the formation of the electrical double layer at the electrode/electrolyte interface. These systems are built of two activated carbon electrodes separated by a separator. Both, electrodes and separator are soaked with organic or aqueous electrolyte. Active electrode material is applied on the metal or steel current collector surface. Those current collectors are exposed to corrosive electrolytes [1]. Thus, they are subjected to corrosion processes [2-5]. This phenomena deteriorates working parameters of whole device. Protection of metals and steels against corrosion consist among others of application of organic coatings [2-5]. Promising candidates are organofunctional silanes which contain in its structure silicone atom [6-8]. Thus, they are organic-inorganic hybrids that combine features of both organic and inorganic compounds which makes them capable to form covalent bonds also with inorganic substrates such as metals and steels. Due to the presence of hydrophobic aliphatic chain, bonded to silicon atom, coatings composed of organofunctional silanes fulfil their anti-corrosive properties.

Materials and methods

In this study we present a new approach to silane coatings deposited on the surface of 316L stainless steel current collectors subsequently used in electrochemical capacitors. The so-modified steel current collectors were placed in a two- and three-electrode Swagelok® type systems, containing also two electrodes (carbon material), separator and aqueous electrolyte (1 M Na_2SO_4).

On the end, electrochemical measurements (linear polarization, cyclic voltammetry, galvanostatic charge/discharge and electrochemical impedance spectroscopy) were performed. Additionally, as well as electrochemical, spectroscopic and surface analysis methods were engaged to characterize the deposited coatings structures.

Results and discussion

On the basis of the obtained results it is concluded that corrosion and oxygen evolution potentials of 316L stainless steel samples treated with siloxane coatings were shifted toward more positive (more noble) values. There is a creation of metal-O-Si covalent bonds prevalent on the stainless steel surfaces and Si-O-Si covalent bonds within the coating structure. This allow to enhance the surfaces hydrophobicity. Additionally, on the atomic force microscopy images it could be seen gel coatings covering stainless steel surfaces. Moreover, in case of electrochemical capacitor measurements, this phenomenon inhibits corrosion processes of steel current collectors and influenced electrochemical capacitor working parameters. The results obtained by applying electrochemical ageing protocols (voltage-holding tests) confirm that the current collector, during 200 hours in the charged state, undergoes tremendous degradation. In order to prevent the detrimental impact of the corrosion, a hydrophobic siloxane coating has been successfully implemented. In the case of siloxane-protected current collectors, subjected to an identical ageing protocol, no significant deterioration in the electrochemical capacitor performance was observed.

Acknowledgments

This work was financially supported by the National Science Centre of Poland on the basis of grants numbers DEC-2013/10/E/ST5/00719 and 2016/23/N/ST8/03766.

References

1. J. Wojciechowski, L. Kolanowski, A. Bund, G. Lota, *J. Power Sources*, **368**, 18 (2017).
2. R.W. Revie, H.H. Uhlig, *Corrosion and Corrosion Control*, fourth ed., John Wiley & Sons, New Jersey (2008).
3. E. R.W. Revie, *Uhlig's Corrosion Handbook*, third ed., John Wiley & Sons, New Jersey (2011).
4. E. McCafferty, *Introduction to Corrosion Science*, Springer, New York (2010).
5. A. Groysman, *Corrosion for Everybody*, Springer, New York (2010).
6. K. Szubert, J. Wojciechowski, J. Karasiewicz, H. Maciejewski, G. Lota, *Int. J. Electrochem. Sci.*, **11**, 8256 (2016).
7. J. Wojciechowski, K. Szubert, R. Peipmann, M. Fritz, U. Schmidt, A. Bund, G. Lota, *Electrochim. Acta*, **220**, 1 (2016).
8. K. Szubert, J. Wojciechowski, J. Karasiewicz, H. Maciejewski, G. Lota, *Prog. Org. Coat.*, **123**, 374 (2018).

Effect of electrode processing and cell assembly on the performance of supercapacitor in prototype pouch cell format

Dhrubajyotı Bhattacharjya[1*], Aitor Villaverde[1], Jon Ajuria[1], Daniel Carriazo[1]

[1]CIC energiGUNE, Albert Einstein 48, 01510 Vitoria-Gasteiz (Basque Country), Spain

dbhattacharjya@cicenergigune.com

Supercapacitors are a key technology for future renewable energy storage due to their high-power density, long cycle life, low maintenance cost and better safety compared to rechargeable batteries.[1] Although the commercial manufacturers mostly prefer the cylindrical cell design for fabrication of large supercapacitors, the alternative pouch cell design are extensively being adopted for a range of applications due to many advantages such as smaller dead volumes both in the cell and on the module level, lower component requirement, lightweight and higher degrees of design freedom.[2] On the other hand, the laboratory scale testing and validation of the different supercapacitor components are mostly carried out using very small quantity of materials assembled in Swagelok cell or coin cell set up. At this level, many parameters related to electrode processing and cell assembly such as electrode thickness, calendering conditions, current collector surface, electrode composition and mass loading are given less emphasis. However, these parameters significant affect the overall electrochemical performance in terms of capacity, durability, power and energy density in a commercially viable cylindrical or pouch cell.

This work demonstrates that an impressive performance of a supercapacitor in small lab scale testing does not always prove successful during the scaling-up effort to commercially viable device level. Herein, through a meticulous optimization of several slurry and electrode fabrication processes parameters, it was possible to study their impact on the performance during a prototyping effort of supercapacitor from 1.12 cm^2 Swagelok cell to a 20.25 cm^2 pouch cell prototype using state of the art electrodes in standard organic electrolyte. At each step, the fabricated electrode was electrochemically evaluated and compared to the industrially manufactured electrode to identify scalability problems and to solve them in the following step through modification of the fabrication process or electrode component. Finally, once the optimum performance was reached, further scale up to a multilayer pouch cell with 25 F capacitance was carried out, which outperformed a comparable 25 F cylindrical cell in terms of specific energy.

References

1. A.Gonález et. al, Renew. Sust. Energ Rev., 58 1189 (2016).
2. B.K. Kim et. Al, Handbook of Clean Energy Systems, (2015)

Acknowledgments

Spanish Ministry of Economy and Competitiveness (MINECO/FEDER) (MAT2015-64617-C2-2-R) and the Basque Government (CICe Elkartek 2018) are acknowledged for the financial support of this work.

Electroactive Materials Doped by Heteroatoms for Energy Storage and Conversion

Ł. Kolanowski[a], J. Wojciechowski[a], M. Graś[a], K. Szwabińska[a], P. Krawczyk[a], K. Lota[b], G. Lota[a]

[a] Institute of Chemistry and Technical Electrochemistry, Poznan University of Technology, Berdychowo 4, Poznan 60-965, POLAND
[b] Łukasiewicz Research Network, Institute of Non-ferrous Metals Division in Poznan, Central Laboratory of Batteries and Cells, Forteczna 12, Poznan 61-362, POLAND

lukasz.m.kolanowski@doctorate.put.poznan.pl

The purpose of this research is to find the relationships between physicochemical and electrochemical properties of carbon materials rich in heteroatoms. In this work, new carbon materials with oxygen and nitrogen functional groups for electrochemical application were obtained. Broad electrochemical analysis proved that obtained carbon materials are desirable for electrochemical capacitors as well as electrodes for the oxygen reduction reaction.

Introduction

Organic substances which are rich in elemental carbon can be used as organic precursors for the production of activated carbon (AC). Activated carbon precursors currently used on an industrial scale include for example: fossil fuels, wood or coconut shells. Moreover, biomass-derived from industrial or agricultural waste can also be used for AC production. Carbon materials due to interesting properties (high surface area, conductivity, sorption properties) are widely used in industry, environmental protection, for energy storage and conversion. Moreover, carbon materials can be produced in the forms of powders, granulates, fibres, fabrics and felts (1).

The rapid development of civilization and strong demand for portable electronic devices has led to significant development of different chemical power sources. The really close attention has paid to lithium-ion batteries, alkaline batteries, photovoltaic cells, fuel cells and electrochemical capacitors. Electrochemical capacitors are characterized by high power density, quick charge/discharge time and long cycling stability. Despite their many advantages, it is desirable to increase the energy density of this system. The increase in energy can be realised by appropriate modification of the electrode material to develop the functional groups rich in heteroatoms (2,3).

On the other hand, fuel cells are characterised by high energy density by their production is still expensive. Taking into account the cost of the fuel cells due to the presence of platinum as an electrode material, it is desirable to construct efficient electrode materials. It should be noted that carbon materials can catalyse the oxygen reduction reaction on the cathode (ORR), and it could be used to produce electrode material. Broad research and development are needed to determine the mechanism and kinetics of ORR on carbon materials of different structures/morphology (4).

Experimental

Activated carbons have been obtained by the carbonization process of lignocellulosic waste materials. The activation process has been conducted by using potassium hydroxide in the tube furnace at 750°C. Moreover, commercial activated carbon was modified in order to introduce oxygen and nitrogen, functional groups. The modified and unmodified activated carbons were used as electrode materials of an electrochemical capacitor and to study the oxygen reduction reaction. The broad physicochemical and electrochemical analysis were performed to determine the processes occurring at the electrode/electrolyte interface. The performance of the electrochemical capacitor were measured in two- and three-electrode cells assembled in a Swagelok® system in aqueous electrolytes. The capacitance properties were examined by galvanostatic charge/discharge, cyclic voltammetry and electrochemical impedance spectroscopy. The oxygen reduction processes have been investigated by cyclic voltammetry (CV) and linear sweep voltammetry (LSV) with rotating disc electrode measurements (RDE). The glassy carbon, as well as modified glassy carbon, were used as the working electrodes (0.07 cm^2), platinum wire and saturated calomel electrode were used as counter and the reference electrode, respectively.

Summary and Conclusions

The presented study shows that all obtained materials are suitable for the construction of electrochemical capacitors. Materials, after being carbonized and activated, are rich in functional groups responsible for the pseudocapacitive effect. Pseudocapacitive effect contributes to the overall capacitance due to quick and reversible redox reactions. The process of modification proved that the excess of oxygen content disrupts surface conjugation of carbon material. Electrochemical measurements proved that the negative electrode was characterized by the higher capacitance than the positive one. Moreover, the obtained confirmed that carbon materials rich in oxygen functional groups catalyse the oxygen reduction reactions. The calculated numbers of electrons exchanged during this process indicate many intermediates during this reaction.

Acknowledgments

The authors acknowledge the financial support from the National Science Centre (Poland) - Grant no DEC-2013/10/E/ST5/00719.

References

1. F. Béguin and E. Frackowiak (Ed.), *Supercapacitors: Materials, Systems and Applications*, Wiley-VCH, Weinheim (2013).
2. G. Lota, P. Krawczyk, K. Lota, A. Sierczyńska, Ł. Kolanowski, M. Baraniak, T. Buchwald, *J. Solid State Electrochem.*, **20**, 2857 (2016).
3. Ł. Kolanowski, M. Graś, M. Bartkowiak, B. Doczekalska, G. Lota, *Waste Biomass Valori.*, Article in press, doi: 10.1007/s12649-019-00598-w (2019).
4. J. Stacy, Y. N. Regmi, B. Leonard, M. Fan, *Renew. Sust. Energ. Rev.*, **69**, 401 (2017).

The Impact of Thiourea Addition on the Borohydride Hydrolysis Reaction

M. Graś[a], J. Wojciechowski[a], Ł. Kolanowski[a], K. Lota[b], G. Lota[a]

[a]Institute of Chemistry and Technical Electrochemistry, Poznan University of Technology,
Berdychowo 4, 60-965 Poznan, POLAND

[b]Lukasiewicz Research Network-Institute of Non-ferrous Metals Division in Poznan Central
Laboratory of Batteries and Cells, Forteczna 12, 61-362 Poznan, POLAND

By the addition of thiourea to the borohydride fuel, it is expected an improvement of the coulombic efficiency of DBFC by inhibiting the H_2 evolution reaction. However, thiourea is an organic sulphur compound, and it is well known that the sulphur species are poisons for the metallic catalysts. This is why this paper discusses its direct use in borohydride fuel.

Introduction

Humans consume more energy than ever before in history. There are predictions that in the 2035 year, the demand for electricity will increase almost twice than in the year 2008 [1]. The direct borohydride fuel cell (DBFC) seems to be an optimistic alternative to the existing and well-known fuel cells. Sodium borohydride offers a large specific energy density (9.3 Wh/kg) owing to its high hydrogen content (10.8 wt.%) [2]. Borohydrides (MBH_4, M = Na, K, Li) are attractive chemical compounds because they are chemically stable and not flammable [3]. Furthermore, metal hydride compressors make it possible to replace the liquid or compressed hydrogen fuel tanks by a solid fuel tank [4]. Because the borohydride oxidation reaction competes with hydrogen evolution reaction, not only the nature of electrocatalyst but also its structure play a significant role in the final efficiency improvement [5]. The most commonly used anodic materials are expensive noble metals [6]. It is, therefore, necessary to find solutions that will reduce the cost of fuel cell production, as well as improve its efficiency. Unfortunately, highly active borohydride oxidation catalysts are also highly active toward the borohydride hydrolysis. When AB_5-alloy based electrode is used as the anode catalyst for borohydride oxidation in alkaline solution, the hydrogen produced may be stored in the form of a metal hydride or released in the form of gas bubbles, when the rate of hydrolysis reaction is higher than the hydride absorption rate [7]:

$$BH_4^- + 2\,H_2O + 8\,M \leftrightarrow BO_2{}^- + 8\,MH_{ads} \tag{1}$$

$$MH_{ads} \leftrightarrow MH_{abs} \tag{2}$$

$$MH_{ads} \leftrightarrow 1/2\ H_2 + M \tag{3}$$

It is also well known that the addition of thiourea into an aqueous solution may inhibit H_2 evolution [8]. Therefore, the main purpose of our study is to raise the question about the risk of poisoning of metallic anode catalysts by the sulphur present in thiourea.

Experimental

To prepare the working electrode, the commercial AB_5 – type alloy of formula $LaMnNi_{3.55}Al_{0.30}Mn_{0.40}Co_{0.75}$ was used. The alloy was mixed with nickel carbonyl and carbon materials. A three-electrode measurement system was built of the working electrode, the counter electrode made of the nickel foam and the Hg/HgO electrode as the reference one. All the electrochemical tests were carried out in a 6 mol dm^{-3} KOH solution containing 0.5 mol dm^{-3} of $NaBH_4$ with different concentrations of thiourea.

Results and discussion

Although the OCP of all types of fuel solutions were less negative than the theoretical BH_4^- /BO_2^- equilibrium potential, they were significantly lower than the potential of hydrogen electrode in alkaline medium, confirming the activity of hydrogen storage alloy based electrode for the borohydride oxidation reaction. The simultaneous use of materials with physicochemical properties favouring hydrogen sorption processes with an effective inhibitor of fuel hydrolysis significantly improved the working conditions of DBFC.

Acknowledgments

The authors acknowledge the financial support from the National Science Centre of Poland, grant No DEC-2017/27/N/ST8/02916.

References

1. Y. Liang, Y. Li, H. Wang, H. Dai, *J. Am. Chem. Soc.*, **135**, 2013 (2013).
2. I. Merino-Jiménez, C. Ponce de León, A.A. Shah, F.C. Walsh, *J. Power Sources,***219**, 339 (2012).
3. R. Valiollahi, R. Ojani, J.B. Raoof, *Electrochim.Acta,***191**, 230 (2016).
4. D.M.F. Santos, C.A.C. Sequeira, *Renew.Sust.Ener.Rev.,***15**, 3980 (2011).
5. G. Lota, A. Sierczyńska, I. Acznik, K. Lota, *Int. J. Electrochem. Sci.*, **9**, 659 (2014).
6. K. Wang, K. Jiang, J. Lu, L. Zhuang, C. Cha, X. Hu, G. Z. Chen, *J. Power Sources*, **185**, 892 (2008).
7. W. J Paschoalino, E. A. Ticianelli, *Int. J. Hydrog. Energy,* **38**, 7344 (2013).

Hydrogen evolution reaction on iridium-modified nickel foam surfaces

Mateusz Łuba, Tomasz Mikolajczyk, Boguslaw Pierozynski

University of Warmia and Mazury in Olsztyn, Department of Chemistry

Present poster reports on a.c. impedance examinations of hydrogen evolution reaction (HER), at Nickel foam (Ni foam) and Ir-modified Ni foam tow materials. The HER was studied in 0.1 M NaOH solution for surface-activated Ni foam and deposited Ir on Ni foam tow materials. The deposition of the Ir on the surface of Ni foam was made by means of spontaneous deposition (30 sec at 40 °C and 5 minutes at 40 °C) and by means of electrodeposition (5.2 mA/10 min). Kinetics of the hydrogen evolution reaction were examined at room temperature, over the cathodic overpotential range: -100 to -400 mV vs. RHE. Corresponding values of the exchange current-density, the charge-transfer resistance for the HER and other electrochemical parameters for examined catalyst materials were obtained.

Keywords: Nickel foam; Ni Foam; Ir-modified CF; HER; impedance spectroscopy

Electrochemical Synthesis Partially Unzipped Multi-Walled Carbon Nanotubes as Electrode Materials for Fuel Cells

M.O. Danilov[a], I.A. Rusetskii[a], G.I. Dovbeshko[b], S.S. Fomanyuk[a], G.Ya. Kolbasov[a]

[a]V.I.Vernadskiy Institute of General and Inorganic Chemistry of the NAS of Ukraine, 32/34
Palladin Avenue, Kyiv, 03142, Ukraine

[b]Institute of Physics of the NAS of Ukraine, 46 Nauky avenue, Kyiv, 03039, Ukraine

Results of electrochemical anodic oxidation of multi-walled carbon nanotubes in 80% sulfuric acid are presented. Using X-ray diffraction analysis, electron microscopy, and Raman spectra, it has been proven that, as a result of anodic oxidation, partially unzipped multi-walled carbon nanotubes were obtained by anodic oxidation. It is shown that the degree of unzipping multi-walled carbon nanotubes depends on the time of electrochemical oxidation of these materials. Using the oxygen electrode as testing electrodes was shown the dependence of the electrochemical characteristics of these materials of the degree of unzipping the multi-walled carbon nanotubes. It is suggested that the controlled synthesis of partially unzipping nanotubes is possible. It is also suggested that it is possible to estimate the degree of unzipping the nanotube based on the study of the electrochemical characteristics of oxygen electrodes. By the electrochemical method obtained partially unzipped multi-walled carbon nanotubes which are promising electrode materials.

Introduction

Multi-walled carbon nanotubes (MWCNTs) consist of several graphene layers rolled into a seamless tube. By applying any oxidative effect, MWCNT can be unzipped longitudinally. At the same time, by stopping the process of nanotube unzipping, multi-walled carbon nanotubes with a defective structure can be obtained (1) or, as they are also called, partially unzipped multi-walled carbon nanotubes (PUMWNT) (2). The literature describes various methods of unzipping nanotubes, which differ in the method of the acting on multi-walled carbon nanotubes leading to a partial unzipping of nanotubes or the creation of a defective hybrid structure in nanotubes. They can be classified as chemical (3), mechanical (4), physical (5), electrochemical (6), and physicochemical methods (7). The resulting structures of carbon nanotubes can be called etched, partially unzipped, and completely unzipped nanotubes with further exposure can be obtained agglomerated nanocomposite fragments of graphene nanoplates. The most promising is electrochemical method. Under the influence of voltage, current and time of process, it is possible to control the process of unzipping graphene structures and obtain materials with predetermined parameters and, accordingly, electrocatalytic properties. Due to the presence of a tubular mesoporous carbon structure and low bulk density, it is possible to expand the triple contact electrode-electrolyte-oxygen zone, in which the process of generating current in the oxygen electrodes of fuel cell takes place. Applications of such hybrid materials are fuel cell electrodes (8), sensors (9), lithium-ion batteries (10). It is known that the electrocatalytic properties of oxygen electrodes depend on the structure and specific surface of the electrode material, and the increasing the imperfection and specific surface of the material, increase the working current density of the oxygen electrode at the same potential. Studying the electrocatalytic characteristics of oxygen electrodes from such materials on the increasing current density we can draw conclusions about the increase in specific surface and structure imperfection, which may indicate the degree of the unzipping the multiwall carbon nanotubes.

The aim of our work was to check the possibility of controlled unzipping of multi-walled carbon nanotubes under the influence of electrochemical anodic oxidation for the obtaining electrode materials with given electrocatalytic parameters.

Experimental part

MWCNT were subjected to electrochemical anodic oxidation. Anodic oxidation of carbon nanotubes was carried out in 80% solution of sulfuric acid. Double-layer oxygen electrodes were prepared by the pressing. The hydrophobic layer contained acetylene black and the active layer contained material from partially unzipped carbon nanotubes. Studies were performed on a fuel cell mock-up, with a zinc electrode being used as the anode in solution of 6M KOH. Samples of the partially unzipped carbon nanotubes were examined using electron microscope, X-ray phase analysis and Raman spectra.

Results and discussion

On Figures 1 shows electron micrographs of partially unzipped carbon nanotubes obtained by us. The Raman spectra, X-ray phase analysis and electron microscopy confirm that with anodic oxidation of MWCNT, etched (Figure 1 b), partially unzipped nanotubes (Figure 1 c), and fully unzipped multi-walled carbon nanotubes (Figure 1 d) are obtained. These materials were obtained by changing the time of anodic oxidation of the studied materials.

The dependences of the electrochemical characteristics of oxygen electrodes on the time of MWCNT oxidation were obtained. It was found that with an increase in the time of anodic oxidation up to 4 hours, the electrochemical characteristics of oxygen electrodes (current density at the same potential) increase. This indicates a change in the structure and specific surface of the studied materials. The resulting dependence of the current density on the potential can be explained by the fact that first the etched nanotubes (Figure 1 b) are obtained; with a further increase in the oxidation time ($\leq$ 2 hours), partially unzipped carbon nanotubes are produced (Figure 1 c). With a subsequent increase in the time of anodic oxidation, fully unzipped multi-walled nanotubes are obtained (Figure 1 d). This pattern confirms the fact of the gradual unzipping of carbon nanotubes depending on the applied oxidative effect. By controlling the processing, we obtained unzipped carbon nanotubes with a controlled level of unzipping of multi-walled carbon nanotubes, with a modified surface, the number of defects and functional groups on the surface. Oxygen electrodes, based on electrochemically prepared samples, were stable in galvanostatic mode at current densities of 200 mA / cm^2 for the six months. Thus, by oxidizing multi-walled carbon nanotubes at different oxidation times, we can get controlled unzipping of multi-walled carbon nanotubes. The resulting materials are a

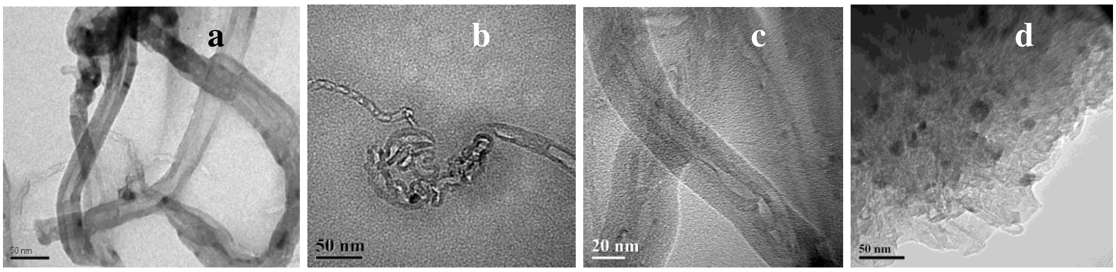

Figure 1. *Electron micrograph of the initial MWCNT (a), etched (b), partially unzipped (c), fully unzipped (d).*

promising catalyst carrier for electrodes of power sources. By deposition various catalysts on them, it is possible to obtain hybrid nanocomposites with predetermined characteristics.

Conclusion

By anodic electrochemical oxidation of multi-walled carbon nanotubes, partially unzipped multi-walled carbon nanotubes were synthesized in an acidic medium. Using electron microscopy, X-ray phase analysis, and Raman spectra, it has been established that partially unzipped multi-walled carbon nanotubes can be obtained by this method.

It is shown that the study of the electrochemical characteristics of oxygen electrodes can be one of the methods for estimating the degree of unzipping of the multi-walled carbon nanotubes. As a result of electrochemical studies, it was established that the obtained samples of partially unzipped multi-walled carbon nanotubes are promising materials as a carrier of catalysts for oxygen electrodes of fuel cells.

References

1. D. Torres, J. L. Pinilla, R. Moliner, I. Suelves, *Carbon*, **81,** 405 (2015).
2. C. Tang, W. Guo, C. Chen, *Phys. Rev. B*, **83,** 075410 (2011).
3. B. Huang, Y. -W. Son, G. Kim, W. Duan, J. Ihm, *J. Am. Chem. Soc*., **131,** 17919 (2009).
4. H. Hu, Y. Song, M. Feng, H. Zhan, *Electrochim. Acta*, **190,** 40 (2016).
5. A. A. Silva, R. A. Pinheiro, A. C. Rodrigues, M. R. Baldan, V. J. Trava-Airoldi, E. J. Corat, *Appl. Surf. Sci.,* **446,** 201 (2018)/
6. M. O. Danilov, I. A. Rusetskii, I. A. Slobodyanyuk, G. I. Dovbeshko, O. Y. Khyzhun, V. V. Strelchuk, G. Ya. Kolbasov, *Fuel cells*, **19,** 202 (2019).
7. D. Long, W. Li, W. Qiao, J. Miyawaki, S.-H. Yoon, I. Mochida, L. Ling, *Chem. Commun*., **47**, 9429 (2011).
8. P. Chandran, S. Ramaprabhu, *Int. J. Hydrog. Energy*., **43,** 18477 (2018).
9. S. Chen, Q. Chen, D. Cai, H. Zhan, *J. Alloys Compd*., **709,** 304 (2017).
10. B. Xiao, X. Li, X. Li, B. Wang, C. Langford, R. Li, X. Sun, *J. Phys. Chem.* C, **118,** 881 (2014).

New Hybrid Polysiloxane Membranes for Fuel Cells

M. Mika[a], D. I. Oren, and J. Michal

[a] Department of Glass and Ceramics, University of Chemistry and Technology, Prague, 16628,
Czech Republic

Currently, the low operating temperatures of commercial proton conducting polymer membranes and their humidity requirements for achieving sufficiently high proton conductivity add high complexity to fuel cell systems, which impacts their cost and durability. In our research, we focused on the development of new cost-effective polymer nanocomposite membranes with better medium-temperature performance.

Introduction

For the production of cost-effective medium-temperature fuel cells, it is necessary to develop a new type of membrane able to achieve sufficiently high proton conductivity in a dry atmosphere. To meet these criteria, a high concentration of relatively stable hydroxyl groups is required in the structure of the membrane. When such groups are close to each other, they form diffusion pathways suitable for fast proton migration even in a dry atmosphere above 100 °C. Therefore, we developed a nanocomposite membrane based on a hybrid inorganic-organic polymer with a polydimethylsiloxane backbone containing phosphorous heteroatoms.

Experimental

Our first-generation hybrid inorganic-organic polymer membranes was based on a polydimethylsiloxane backbone containing phosphorous heteroatoms (1). The desired structure of the membrane was formed by the reaction of dimethyldichlorosilane and tetraethoxysilane in molten orthophosphoric acid. For the improved second-generation of our membranes, the first-generation polymers were filled with spherical SiO_2 nanoparticles (5 to 20 nm, specific surface of 200 $m^2 \cdot g^{-1}$) covered with -OH functional groups (2). Moreover, the structure of the membranes was reinforced with microwires and nanowires based on SiO_2. The membrane proton conductivity was precisely measured using electrochemical impedance spectroscopy in a temperature range of 25—200 °C. The impedance data were recorded with an Autolab PGSTAT30 potentiostat in a frequency range of 10 mHz—1 MHz. The resulting impedance spectra were analyzed in Bode and complex Nyquist plane diagrams using the equivalent circuit approach.

Results and Discussion

The proton conductivity of the first-generation membranes calculated from the circuit parameters was promising. Therefore, using based on them simulations, we optimize the composition and structure of the second-generation membranes. Their proton conductivity was further enhanced when the polymers were filled with spherical SiO_2 nanoparticles covered with -OH functional groups and their structure was more reinforced by incorporating microwires and nanowires based on SiO_2.This resulted in membranes with an improved mechanical strength and elasticity with higher conductivity of about 9 $S \cdot m^{-1}$ at 150 °C in a dry atmosphere. Next, we tested the performance of the membranes in a laboratory H_2/O_2 fuel cell in the range from 20 to 180 °C using dry H_2 and O_2 input gases. The fuel cell was equipped with standard electrodes made of carbon paper with a Pt/C catalyst; the surface area of the electrodes was 5 cm^2. The performance of the fuel cell significantly improved as the temperature increased. Power density maxima increased and moved to higher current densities and current/voltage characteristics became less steep. Following these tests, the membranes were characterized using other analytical tools, including optical and electron microscopy, differential thermal analysis, thermal gravimetric analysis, infrared and Raman spectroscopy, and nuclear magnetic resonance. The collected data were used for the simulations to optimize our furthermore advanced polysiloxane membranes.

Conclusion

Collectively, our results indicate that the developed hybrid polymer membranes containing nanoparticles, microwires and/or nanowires are promising for the construction of H_2/O_2 fuel cells operating at elevated temperatures in a dry atmosphere.

Acknowledgments

We acknowledge our colleagues M. Paidar, B. Klapste, P. Hron, M. Masinova for their help in the development of our hybrid polysiloxane membranes.

References

1. M. Mika, J. Michal, B. Klapste, P. Hron, *Patent*, **303939** (July 3, 2013).
2. M. Mika, J. Michal, B. Klapste, P. Hron, *Patent*, **304129** (September 25, 2013).

Impact of Morphological And Structural Changes On Performance Of Solid Oxide Cells

Michal Carda, Daniel Budáč, Martin Paidar, Karel Bouzek

University of Chemistry and Technology, Prague,
Technická 5, Prague 6 Dejvice, 166 28, The Czech Republic

cardam@vscht.cz

Renewable energy sources with an unstable power output over time such as wind and solar energy require efficient technology for intermittent energy storage. Currently one of the best technologies for storage of electric energy is a conversion of electricity to easily storable chemical energy of hydrogen molecule – the so-called hydrogen economy concept. Hydrogen economy consists of a water electrolysis device for hydrogen production and hydrogen utilizing device mainly fuel cell. The combination of fuel cell and water electrolyser in one device is desired for space utilization. But in low temperature e.g. PEM systems it brings several troubles in operation. On the other hand, due to the high operating temperature of the solid oxide cells (SOCs), this technology offers a possibility to produce hydrogen and later utilize it within a single device keeping high efficiency of both processes. This is one of many significant advantages that make the technology of SOCs essential within the whole concept of the hydrogen economy. Importance of SOCs is mainly the consequence of high operating temperature (700 – 900 °C), which leads to fast electrodes kinetics and lower energetic demand for water splitting without the need of PGM catalyst. Despite these benefits, there remain obstacles to introducing the large scale application of SOCs. The degradation processes occurring during SOCs operation are the most significant. Only insufficient reliable data exists regarding morphological and structural changes occurring during the operation of SOCs. Despite these changes may have a significant impact on the performance of SOCs.

Within SOCs operation morphological and structural changes of electrode and electrolyte materials have to be considered. The most important are changes at the interface contact of electron and ion conductive phases. The impact of different operating conditions and set-ups on these changes is still not sufficiently described in the literature. Materials intended for SOCs must have suitable mechanical and chemical stability, and thermal expansion similar to each other. Today state of art material used for SOCs fabrication is ZrO_2 – 8 mol.% Y_2O_3 (YSZ) as ion conductive material of electrolyte. $(La_{0.8}Sr_{0.2})_{0.95}MnO_{3-x}$ (LSM) in mixture with YSZ is used as electron conductive material for oxygen electrodes. Fuel (hydrogen) electrodes usually consist of Ni-YSZ. Accordingly, a number of SOCs based on commercially available materials were prepared. YSZ electrolytes were prepared by coaxial moulding of powder and subsequent sintering. Electrodes were deposited by a screen printing method on YSZ button electrolyte. These in-house fabricated cells were examined in different working conditions (temperature, operation mode, feed gases partial pressure). Two different assemblies were used. Symmetrical cells in oxygen pump mode having only oxygen electrodes on both sides: LSM-YSZ|YSZ|LSM-YSZ and asymmetrical cells having one hydrogen and one oxygen electrode: Ni-YSZ|YSZ|LSM-YSZ. Cells were examined by various electrochemical methods (cyclic voltammetry, potential pulse, electrochemical impedance spectroscopy) and morphological and structural changes were examined by post-mortem SEM and XRD analysis. The asymmetric cells were operated as fuel cell and afterward switched to the water electrolysis mode. Oxygen electrodes in symmetric cells were studied in fuel cell mode (oxygen reduction reaction) as well as water electrolysis mode (oxygen evolution reaction).

Results indicate that during the operation of SOCs most structural changes occur at fuel electrode. Particles of fuel electrode (Ni) sinter and agglomerate to bigger particles which lead on one hand to higher porosity which supporting better mass transport, but on the other hand it causes a loss of active boundary between ion and electron conductive phases. It leads to the decrease of cell current density and overall performance. SEM analysis of oxygen electrode-electrolyte interface suggested no visible morphological changes at the interface regardless of operating mode or length of the experiment. Despite this finding the decrease of cell performance was observed. Therefore, XRD analysis was used to clarify potential changes of this particular interface. XRD analysis showed the development of a new nonconductive phase at the interface probably developing at a lower partial pressure of oxygen regardless of polarization. This new nonconductive phase caused a significant increment in ohmic resistance of cells. Formation of this phase is known in literature but only at much higher temperatures than 1000 °C. It is significantly higher than the maximum operating temperature used in this work (800°C).

Identification of critical operating conditions promoting described degradation phenomena will enable significant prolongation of SOCs lifetime.

This work was supported by Czech Science Foundation (GACR), contract No: 19-142-44-J and specific university research (MSMT No 21-SVV/2019).

Factors Affecting the Performance of Negative Electrode for Ni-MH Cell

Ł. Kolanowski[a], K. Lota[a], P. Swoboda[a], I. Acznik[a], A. Sierczyńska[a], R. Mańczak[a], G. Lota[a,b]

[a] Division in Poznan, Łukasiewicz Research Network - Institute of Non-Ferrous Metals Central Laboratory of Batteries and Cells, Forteczna 12, Poznan 61-362, POLAND

[b] Institute of Chemistry and Technical Electrochemistry, Poznan University of Technology, Berdychowo 4, Poznan 60-965, POLAND

lukasz.kolanowski@claio.poznan.pl

The aim of this research is to determine the factors affecting the performance of negative electrode for Ni-MH batteries. In this study two different hydrogen-storage alloys (AB_5 and AB_2-type) were used. Moreover, the influence of different amounts of nickel in electrode composition was determined. In order to increase the conductivity and hydrogen sorption properties the carbon materials have been used as additive for negative electrode.

Introduction

There is an increasing production of tools, portable electronics and electric vehicles in which rechargeable batteries plays an important role as a power sources. In such a case, the large demand for batteries of high power/energy density accelerated the development of new electrode materials for electrochemical power sources. Several types of rechargeable batteries have attracted great attention like: lithium-ion batteries, lead acid batteries, nickel cadmium and nikel-metal hydride batteries (1).

The nickel-cadmium accumulators consists of cadmium as negative electrode and nickel oxide hydroxide as positive one. This kind of electrochemical cell is characterized by stable work in broad range of temperatures (from -20°C to 50°C) and high efficiency in low temperatures. Taking ito account the toxicity of cadmium this cell have been replaced by Ni-MH batteries (2).

The structure of electrodes in Ni-MH cells are very similar to Ni-Cd batteries. Instead of cadmium, the negative electrode consists of hydrogen absorbing alloys. Nickel metal-hydride batteries are characterized by higher energy density than Ni-Cd. Moreover, Ni-MH cells posses low internal resistance thus are able to deliver constant voltage dutring the discharge. The most often used multicomponent alloys are AB_5 and AB_2-type alloys. The first one is based on the nickel and rare earth elements while AB_2-type alloy is a mixture of nickel and titanium, zircnonium or vanadium (3-4).

Nowadays, more attention is paid to research and development of new electrode materials in order to construct cheap and efficient power sources which can be characterized by not only high power density but also energy density and low self-discharge. In this work the modification of negative electrode material for Ni-MH cell was performed.

Experimental

Two types of hydrogen absorbing alloys (AB_5-type and AB_2-type) were prepared in arc furnace by using metals of analytical grade. For electrode preparation, all alloys were mixed with 10 wt.% of nickel carbonyl and 3% of poly(vinyl alcohol) (PVA) aqueous solution as a binder. Apart from PVA the poly(vinylidene fluoride) (PVDF) was also used as a binder in order to determine the best performance of electrode materials. Moreover, the metal alloy was also mixed with different amount of carbonyl nickel in the amount from 0% to 20 wt.% of the electrode active mass.

The composites of metal alloys with the addition of carbon materials were prepared by chemical polymerization of monomers (aniline, pyrrole, 3,4-ethylenedioxythiophene). After the polymerization all samples were subjected to carbonization process in a tube furnace at 500°C for 10 min under the flow of nitrogen.

The resulting mixtures of all electrode materials were spread into a 1 cm^2 of nickel current collector. Then, electrodes were subjected to drying for 24 h at 50°C and were pressed under 10 MPa. All electrochemical measurements were conducted in three-electrode cell configuration by selected AC/DC techniques (i.e. cyclic voltammetry, galvanostatic charge/discharge, electrochemical impedance spectroscopy) All measurements were conducted at ambient condition in 6 M KOH electrolyte.

Summary and Conclusions

The presented study shows that electrode composition and its method of preparation strongly incluence the performance and efficiency of negative electrode of Ni-MH cell. The best performance was determined for the electrode based on the AB_5- type alloy ($MmNi_{3.55}Al_{0.3}Mn_{0.4}Co_{0.75}$) with 3% of poly(vinyl alcohol) aqueous solution as a binder. This kind of binder provide proper dispersion and good homogeneity and connection of all components. The addition of 10 wt.% nickel to the electrode facilitated the diffusion of hydrogen and thus the current density. Moreover, the presence of carbon material in negative electrode participated in its capacity by sorption properties in micropores. Taking into account that carbon materials coated the alloy particles, their addition could not only prevent the corrosion properties in alkaline solution but also increased the conductivity between alloy particles.

Acknowledgments

The authors acknowledge the financial support from the National Science Centre (Poland) - Grant no DEC-2013/09/N/ST5/00910.

References

1. F. Beck, P. Rüetschi, *Electrochim. Acta*, **45**, 2467 (2000).
2. C. A. Vincent, B. Scrosati, *Modern batteries. An introduction to electrochemical power sources,* Butterworth-Heinemann, Oxford, 1997.
3. A.K. Shukla, S. Venugopalan, B. Hariprakash, *J. Power Sources*, **100**, 125 (2001)
4. W.H. Zhu, Y. Zhu, Z. Davis, B.J. Tatarchuk, *Appl. Energ.*, **106**, 307 (2013).

In situ and ex situ measurements of lead acid battery cell by PEIS

Petr Křivík[1], Sebastian Vaculík[1], Petr Bača[1], Jiří Kazelle[1]

[1] Department of Electrotechnology, Faculty of Electrical Engineering and Communication, Brno University of Technology, Technická 10, 616 00 Brno, Czech Republic

The paper compares changes of important parameters of lead acid battery cell during discharge and charge by potential electrochemical impedance spectroscopy (PEIS) method measured in situ and ex situ. Nyquist diagrams were used for determination of ohmic and charge transfer resistance of lead acid battery cell.

Introduction

The electrochemical impedance of a battery characterizes its dynamic behaviour - response to an excitation of small amplitude [1, 2]. Impedance diagrams are often plotted in the Nyquist diagram (imaginary part of the impedance vs. real part).

In Nyquist diagram of a battery cell is included a high frequency ohmic resistance due to the connections, the separator, the electrolyte resistivity and the surface coverage of the electrodes by crystallized lead sulphate.

Size of capacitive loop, corresponds to charge transfer resistance. Charge-transfer reaction has a certain speed and depends on the temperature, the concentration of the reaction products, and the potential. Double layer capacitance is determined by space charge distribution in the electrochemical double layers.

Second loop at low frequencies is controlled by mass transport of Pb^{2+} ions and depends on the sulphatation reaction on the electrodes. Warburg impedance is caused by ionic diffusion in the electrolyte and in the pores of the electrodes [3, 4].

Experiment

For the experiment exploring changes of impedance in the lead acid battery cell during charge and discharge, a sealed lead acid cell was used, with spiral construction, containing AGM separator with a capacity of 2.5 Ah, nominal voltage 2V and internal resistance about 5 mΩ [5].

The cell was inserted in temperature chamber with constant temperature of 25 °C.

In situ measurement comprised discharge with current 0.4 A to end of discharge 1.6 V. After attaining of limiting voltage, charging continued with a charge current 0.4 A with a 2.4 V voltage limitation. In the course of discharge and charge, the potential electrochemical impedance spectroscopy (PEIS) was measured. Amplitude of PEIS was 5 mV, frequency interval was from 6 kHz to 50 mHz, with 6 measured points per decade.

Ex situ measurement comprised an intermittent discharge. Discharge current was 0.4 A for 1 hour, followed by period of current off state for 2 hours. End of discharge was determined by reaching of voltage 1.6 Volts. Then intermittent charge continued with a charge current 0.4 A with a 2.4 V voltage limitation for 1 hour, followed by current off state for 2 hours. Twelve charging intervals were performed in total. During this cycling, a potential electrochemical impedance spectroscopy (PEIS) were measured at the end of current off intervals.

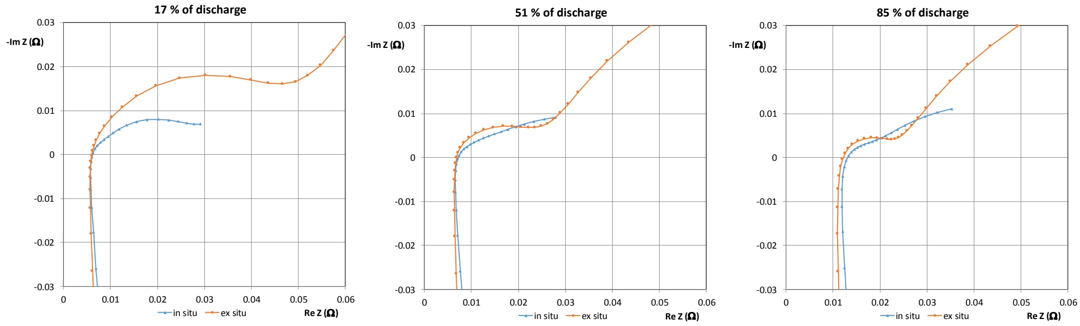

Figure 1. *Comparison of Nyquist diagrams of the cell during discharge (DoD = 17%, 51% and 85%) in situ and ex situ measured by PEIS.*

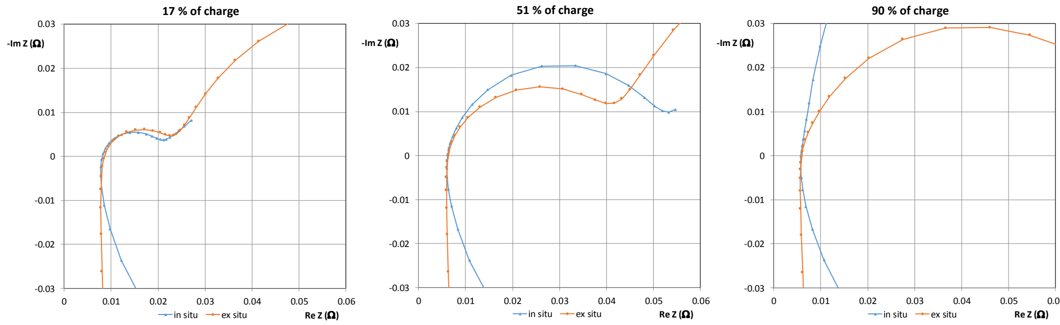

Figure 2. *Comparison of Nyquist diagrams of the cell during charge (SoC = 17%, 51% and 90%) in situ and ex situ measured by PEIS.*

Figure 1 compares Nyquist diagrams of the cell during discharge in situ and ex situ measured by PEIS.

Ohmic resistance, which is visible at the intersection with x-axis, grows during discharge both at in situ and ex situ measurements. At the end of discharge, the internal resistance for in situ measurement is higher than for ex situ measurement. After intermission of the discharge, the cell relaxes and the sulphate ions are partially dissolved to the electrolyte. This results in a decrease of resistance.

Charge transfer resistance corresponds to size of capacitive loop. It is higher at the beginning of discharge for ex situ measurement, and decreases during discharge at both measurements.

Second loop at low frequencies, controlled by mass transport of Pb^{2+} ions, is more visible in ex situ measurements. For in situ measurements, the transition between first and second loop is not so visible and is affected by the discharge - the cell is not in the steady state.

Figure 2 compares Nyquist diagrams of the cell during charge in situ and ex situ measured by PEIS.

Ohmic resistance decreases during charging for both measurements. For in situ and ex situ measurements, the value of the internal resistance is the same, only at the beginning of charging is slightly higher at ex situ measurement.

Charge transfer resistance increases during charging for both measurements, while at in situ measurement significantly higher than at ex situ measurement. With current load, the charge transfer resistance increases during charging, the relaxation during current off interval decreases this resistance. This is manifested by a lower radius of the capacitive loop. At the end of charging, the charge transfer resistance is high, the charging reactions cannot proceed, and the charge current is consumed for parasitic reactions such as gassing, corrosion, and cell heating.

The second loop is only visible at the beginning of charging in both measurements. With the increase of charge transfer resistance, the second loop gradually disappears, at in situ measurement earlier than at ex situ measurement.

Conclusions

Important cell parameters such as ohmic resistance, charge transfer resistance, and Warburg impedance are influenced by mode of the measurement (in situ / ex situ). Nyquist diagrams of the cell measured by PEIS reflect changes of these important parameters.

Acknowledgements

This work was supported by by the specific research of the Brno University of Technology No. FEKT–S–17–4595.

References

1. S. Rodrigues, N. Munichandraiah, A.K. Shukla, A review of state-of-charge indication of batteries by means of ac impedance measurements, J. Power Sources 87 (2000) 12.
2. H. Blanke et all, Impedance measurements on lead–acid batteries for state-of-charge, state-of-health and cranking capability prognosis in electric and hybrid electric vehicles, J. Power Sources 144 (2005) 418.
3. E. Barsoukov, J. Macdonald, Impedance Spectroscopy: Theory, Experiment, and Applications, Wiley (2005).
4. Ch. Fleischer et all, On-line adaptive battery impedance parameter and state estimation considering physical principles in reduced order equivalent circuit battery models, J. Power Sources 260 (2014) 276.
5. P. Křivík, S. Vaculík, P. Bača, J. Kazelle, In Situ Measurement of PEIS of Lead Acid Battery Cell, ECS Transactions, 87 (1) (2018) 307.

Ultrasound Assisted Mixing of Zinc Active Mass with Conductive Ceramic Additives for Ni-Zn Battery

V. Petrova[a], A. Stoyanova-Ivanova[a], P. Lilov[a], O. Petkov[a], G. Ivanova[b], B. Karamanova[b], A. Stoyanova[b], V. Mikli[c]

[a]Georgi Nadjakov Institute of Solid State Physics, Bulgarian Academy of Sciences, 72 Tzarigradsko Chaussee Blvd., 1784 Sofia, Bulgaria.

[b]Institute of Electrochemistry and Energy Systems "Academician Evgeni Budevski", Acad. Georgi Bonchev Str, Block 10, 1113 Sofia, Bulgaria.

[c]Insitute of Materials and Environmental technology, Tallinn University of Technology, Ehitajate Str., 19086 Tallinn, Estonia

Three zinc electrodes with carbon additive were prepared through ultrasound treatment. Two of them were mixed with conductive ceramic additives from the Bi-Sr-Ca-Cu-O (BSCCO) system with nominal chemical composition $Bi_{1.7}Pb_{0.3}Sr_2CuO_x$ (B(Pb)SCCO 2201) and $Bi_{1.7}Pb_{0.3}Sr_2CaCu_2O_x$ (B(Pb)SCCO 2212). The phase composition and morphology of the as-prepared samples were characterized by scanning electron microscopy (SEM) and energy-dispersive X-ray spectroscopy (EDX). The EDX specters suggest that the composition of the active mass does not change during the ultrasound treatment. The micrographs show that the active mass with carbon and 2201 additive has superior particle distribution compared to the other two samples.

Introduction

Ni-Zn batteries are a rechargeable system with high energy and power densities, high working potential and wide working temperature range. They have considerable advantages like low toxicity, low cost and abundant resources stable in aqueous electrolyte and has a low equilibrium potential (1,2). Along with the listed advantages, the main disadvantage of this type rechargeable batteries is the rather poor electrical conductivity of ZnO, limited life, expressed in cycles, which is mainly due to the zinc electrode (3,4). Several approaches have been used to solve the existing problem, and a modern solution is to introduce conductive ceramic powder additives to the zinc active mass of the nickel-zinc battery which will lead to its stabilization and consequently to the improvement of the performance of the system under consideration (5,6). The preparation method of the active mass has a significant effect on the electrochemical properties of the electrode. Homogeneous particle distribution of zinc oxide and ceramics, as well the binder agents are very important for the robust operation of the electrode.

During the 1980s the discipline sonochemistry has undergone rapid development with the release of generators of high-intensity ultrasound. The ultrasonic irradiation during solid-liquid reaction ball milling has yielded excellent results in the synthesis of high-quality homogenous ZnO nanoparticles (7,8). The use of ultrasound during the synthesis process seems to be a future-proof way of acquiring metal oxides (9,10).

These ultrasonic properties have wide application and provoke our interest to apply this method in preparation on the Zn- electrode mass. The aim of this work is the characterization of zinc active mass with conducting additives, obtained by ultrasound assisted mixing. The obtained results can be applied in the further electrochemical studies of the Zn electrode in the Ni/ Zn cell.

Materials and methods

One electrode was composed by powder ZnO (67 %), acetylene black (14 %) and binding agents – polytetrafluorethylene (PTFE, 5 %) and carboxymethylcellulose (CMC, 14 %). The other two were prepared with acetylene black (7 %), additives – conducting ceramic powder B(Pb)SCCO 2201 and B(Pb)SCCO 2212, synthesized by solid-state reaction (7 %) and the same binding agents. For better mixing, the active mass was homogenized in an ultrasonic bath with frequency 42 kHz for 3 hours at room temperature (23 °C) using Ultrasonic cleaner, model CD-3800A. The pasted zinc electrodes prepared by inserting the zinc paste on the matrix of cooper foam (successively covered with tin and zinc) with dimensions 5,0 x 3,0 cm (thickness 0,15 cm)are used for current collector and carrier of the zinc mass. The pasted electrode is dried at 700 ^{o}C for 2 hours and then pressed under 30 MPa for 2 min.

The microstructure of the electrode was studied by means of Zeiss EVO MA-15 scanning electron microscope (SEM) with LaB_6 cathode on the polished cross-section of the samples. The chemical composition was determined by X-ray microanalysis using the energy dispersive spectroscopy (EDS) method and Oxford Instruments INCA Energy system. The qualitative and quantitative analyses were carried out at accelerating voltage 20 kV.

Results and discussion

In Fig. 1 the micrographs of ZnO with carbon additive, ZnO with carbon and B(Pb)SCCO 2201 additive and ZnO with carbon and B(Pb)SCCO 2212 additive are shown. The ultrasound assisted mixing of the active mass leads to superior particle distribution, as seen on the SEM images. This is most noticeable on Fig. 1b.

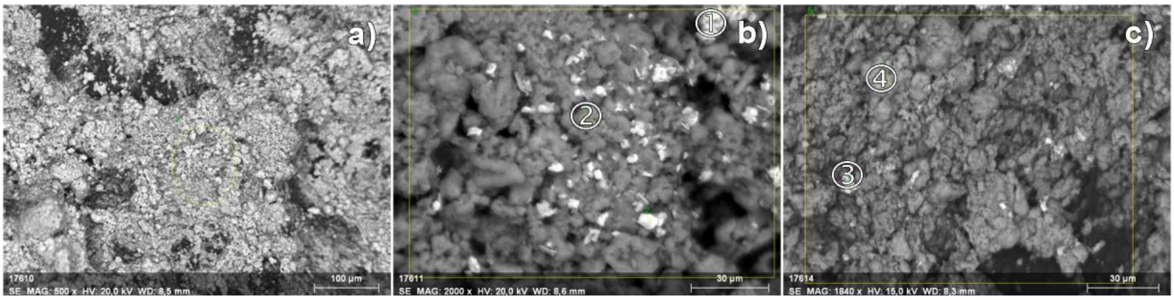

Figure 1. *SEM images of ZnO with carbon additive (a), ZnO with carbon and B(Pb)SCCO 2201 additive and ZnO (b) with carbon and B(Pb)SCCO 2212 additive (c) with EDX analysis.*

In Table I average values of EDX results are presented. It is seen that the composition did not change during the ultrasound mixing.

TABLE I. *EDX analysis results for ZnO with carbon additive (Sample A), ZnO with carbon and 2201 additive and ZnO (Sample B) with carbon and 2212 additive (Sample C).*

Samples	**Elemental content, [at. %]**							
	Zn	**C**	**Bi**	**Pb**	**Sr**	**Ca**	**Cu**	**O**
Sample A	18.27	21.81						59.91
Sample B								
Spectrum 1	4.25		6.57	1.34	7.04		3.74	77.07
Spectrum 2	25.33						0.36	74.31
Sample C								
Spectrum 3	5.20		6.41	0.76	6.19	5.35	7.57	68.52
Spectrum 4	46.76							53.24

Conclusions

To improve the homogenization of the additives and the ZnO, an ultrasound assisted mixing method was used. The micrographs show that the active mass with carbon and B(Pb)SCCO 2201 additive has superior particle distribution compared to the other two samples. The composition of the active mass is preserved during the ultrasound treatment.

The influence of the B(Pb)SCCO additives, physically mixed with active zinc mass for Ni-Zn battery has already been proven in our past investigations. That is why we believe that the better homogenization through ultrasonic irradiation of the additives with the ZnO may improve the conductivity, the stability and prolong the life of the battery even further. The results of this research give us basis for future investigations of the newly prepared Zn electrodes in a Ni-Zn electrochemical cell.

Acknowledgments

This work was funded by the Bulgarian National Scientific Fund under project № КП-06-М29/3 as well as a part of a bilateral project between the Bulgarian Academy of Sciences and Estonian Academy of Science, Tallinn University of Technology (Estonian projects TK 141 IUT 19-28).

References

1. Zhang L., H. Huang, W. K. Zhang, Y. P. Gan, C. T. Wang, *Electrochim. Acta*, **53**, 5386 (2008).
2. Zhao T., E. Shangguan, Y. Li, J. Li, Z. Chang, Q. Li, X. Yuan, H. Wang, *Electrochim. Acta*, **182**, 173 (2015).
3. M. Ma, J.P.Tu, Y F Yuan, X. L. Wang, K.F.Li, F.Mao, Z.Y.Zeng, *J. Power Sources,* **179**, 395 (2008).
4. W. Long, Z. Yang, X. Fan, B. Yang, Z. Zhao, J. Jing, *Electrochim. Acta*, 40 (2013).
5. G. Ivanova, A. Stoyanova-Ivanova, D. Kovacheva, A. Stoyanova, *Bulg. Chem. Comm.*, **51**(1), 66 (2019).
6. L. Stoyanov. S. Terzieva. A. Stoyanova. A. Stoyanova-Ivanova. M. Mladenov. D. Kovacheva. R. Raicheff, *J of Progr. Res. in Chem.*, **2,** 83 (2015).
7. D. Chen and T. Xiao, *J of the Am. Ceram. Society*, **93**(9), 2675 (2010).

8. K.D. Bhatte, S.I. Fujita, M. Arai, A.B. Pandit, B.M. Bhanage, *Ultrason. Sonochem.*, **18**, (2011).
9. D. Chen, H.-Y. Liu, *Mater. Lett.*, **72**, 95 (2012).
10. D. Chen, H.Y. Liu, S.R. Xia, *Ceram. Int.*, **38,** 821 (2012).

Combined Effect Of Fiberglass And TiO In Negative Active Mass Of Lead-acid Accumulator

J. Zimáková[a], P. Bača[a], M. Bouška[a]

[a] Brno University of Technology, Technická 10, 616 00 Brno, Czech Republic

The aim of the work was in situ observation of the negative lead electrode surface in various modes of operation using AFM. A total of two measurement procedures were chosen, which mainly differed during the charging / discharging cycles. Lead plate was used as a negative electrode. Glass fibers and barium sulphate were built into its surface.

Introduction

Today's environmental problems and ever-decreasing fossil fuel reserves are leading to research in the field of hybrid electric vehicles and electric vehicles. The main component of these types of vehicles include is an accumulator that stores the electrical energy. This energy is, if necessary, converted to another type of energy, typically mechanical. Examined secondary cells, that might be suitable for these types of vehicles, includes lead accumulator. The trend of recent years has been the investigation of lead accumulator electrodes, resp. composition of active mass. Special attention is turned to negative active mass because of its properties are also associated with so-called sulphation, which causes a reduction in the capacity of the battery. To improve the properties of the negative electrode, there are added various additives into its active mass. Observation of the electrode surface of the lead-acid accumulator using an AFM atomic force microscope is not a very explored technique. This microscope, used to study the surface material, can process with atomic resolution and in terms of electrochemistry is essential that the surface can be observed even though the electrode is flooded with electrolyte. Thanks to these properties, it is suitable for a detailed understanding of the reactions on the negative electrode.

Experiment

Lead sheet with thickness of 0.7 mm was at first cleaned with ethanol and distilled water using a glass fiber separator. Subsequently, it was homogenized on the roller to obtain a flat and uniform surface of 0.2 mm thickness. The sheet was cut to approx. 25x35 mm. Since the sheet was cleaned by an AGM separator, some fibers were added into the sheet surface. This is why the glass fibers will always be used as one of the electrode additives. In order to ensure a higher occurrence of glass fibers on the surface, the fibers are further prepared from a non-woven fabric and pressed into the surface with a defined downforce of 80 N / cm 2. The press was pre-cleaned to avoid contamination of the sample. Subsequently, an additional additive, in this case barium sulfate, of an approximate weight of 7 mg, was added

Figure 1 shows used electrochemical cell and configuration of electrodes. A polished lead electrode was used as a working electrode (size 20 x 20 mm). A pure lead wire was used as counter electrode and as a referent electrode was used cadmium wire. Sulfuric acid solution (density 1.28 g/ml) was injected from side ports of electrochemical cell.

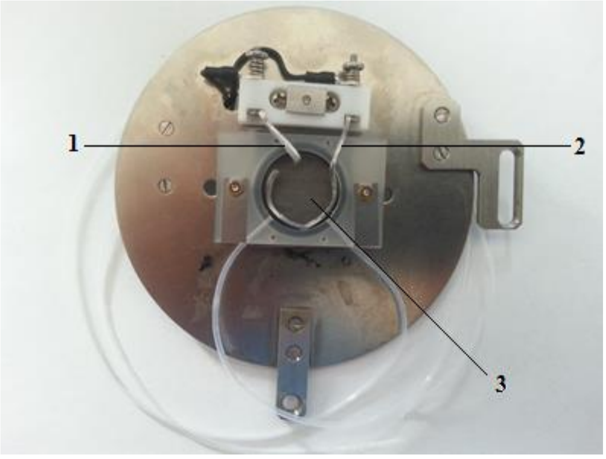

Figure 1. *Electrochemical cell: 1 – referent Cd electrode, 2 – counter electrode, 3 – working electrode*

Measuring instruments

The Agilent 5500 SPM Scanning Probe Microscope (SPM), which is located in the anti-vibration chamber. The scanning window contains 128 lines and has a size of 5x20 µm. One line is rendered in 1 second, which means that one image is rendered in about 2 minutes and 10 seconds. Measuring tip (manufacturer NANOSENSORS ™; type designation: PPP-CONT-50) is made of SiC and has the following characteristics: thickness 2.0 ± 1 µm, length 450 ± 10 µm and width 50 ± 7.5 µm.

Figure 2. *Agilent 5500 SPM located in the anti-vibration chamber*

It is measured in the AFM contact mode as this ensures good surface response in the case of electrochemistry (due to electrolyte).

All measurement procedures are provided by the VSP potentiometer / galvanostat and EC-Lab software from Bio-Logic Science Instruments.

Measuring procedures

Before the work procedure was created, cyclic voltammetry measurements were made to determine the working potentials of the electrode during charging / discharging.

Procedure I:

1. The first step is OCV (open circuit voltage). The time to stabilize the potential of the cadmium electrode is selects according to the conditions during AFM setting, usually about 10 minutes.
2. When the reference electrode potential has stabilized, the negative electrode is charged - connected to -43 mV potential (vs. reference el.), which lasts 10 minutes. Once the process is completed, the electrode starts to discharge (connection to potential 235 mV) for 30s. The charge / discharge cycle is repeated in a total of 5 times.
3. After the last cycle, the electrode charged for 30 minutes. After this time electrode is discharged at 50% of the capacity measured at the end of discharge in the last cycle of the previous step.
4. The last step is again OCV, where spontaneous changes are monitored on electrode surface. This part usually takes 1 hour.

The cycling results show differences between charging and discharging. Because the discharging lasted only 30 seconds, it was possible to observe this action on a part of one AFM frame, because each frame contains 128 lines, one line is rendered in 1 second. This makes it possible to observe changes in the surface morphology of the negative electrode when switching between charging and discharging. For example, figure 2, which show the transition between charging and discharging. If these AFM images are always compared to the previous and next image, it is clear that the to the growth of lead sulphate crystals and to dissolve when discharged.

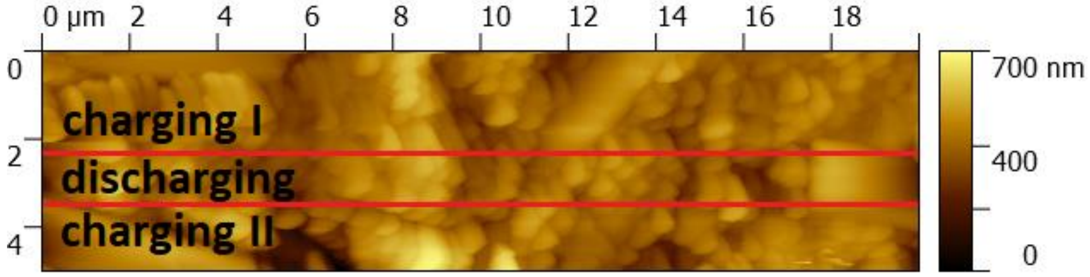

Figure 3. *transition between charging and discharging*

Procedure II

1. 1.The first step is to sense the cadmium electrode (OCV) voltage response for approximately 10 minutes.
2. Charging with current -0.2 mA, while once the potential limit of -43 mV at the working electrode is reached, the current is limited and charged at a constant potential of -43 mV. The charging process takes 24 minutes.
3. Discharging at 0.2 mA with a potential limit of 235 mV. When the limit value is reached, the current is limited and the negative electrode is discharged at a constant potential of 235 mV. The whole process takes 15 minutes.

4. Charging and discharging is repeated four times. In total, there will be 5 charge / discharge cycles.
5. The last step is again the OCV for about 1 hour.

During charging II, progressive dissolution of lead sulfate crystals can be observed, with the electrode surface becoming smoother. During discharging II is not apparent, at first look, significant change in the morphology of the electrode surface. The formation of sulfate crystals is evident after comparison details changes in the same places in the images. During discharging, a gradual exposure of the metal lead surface, formed from previous charging, can be seen.

From the time dependence of the potential of the negative electrode, the charge received (or removed) and the current between the negative electrode and the positive electrode shows that no voltage limitation has been achieved in any of the cycles. This implies that the current and charge waveforms are identical in all cycles.

Acknowledgements

This work was supported by the specific graduate research of the Brno University of Technology No. FEKT-S-14-2293.

References

1. D. Adrienko, *Cyclic voltametry,* (2008)
2. P. E. West, *Introduction to Atomic Force Microscopy, theory, practice, aplications*, (2006).
3. M. Shiota, J. Power Sources, vol **113**, 277-280 (2003).
4. Agilent Technologies 5500 Scanning Probe Microscope: User’s Guide, *The Characterization Facility, University of Minnesota* [online]. [cit. 2018-10-06].
5. Y. Yamaguchi, J. Power Sources, vol 85, 22-28 (2000)
6. Y. Yamaguchi, J. Power Sources, vol 93, 104-111 (2001)
7. H. Vermesan, J. Power Sources, vol. 133, 52-58 (2003)

Synergy in Lanthanide stabilized Ru and Ir Pyrchlores as Electrocatalysts for the Oxygen Evolution Reaction (OER)

Rebecca Pittkowski[1], Daniel F. Abbott[2], Ivano E. Castelli[3], Thomas J. Schmidt[2], Petr Krtil[1]

[1]J. Heyrovsky Institute of Physical Chemistry, Dolejškova 3, 18223 Prague, Czech Republic

[2]Electrochemistry Laboratory, Paul Scherrer Institut, 5232 Villigen, Switzerland

[3]DTU Energy, Technical University of Denmark, 2800 Kgs. Lyngby, Denmark

Rebecca.pittkowski@jh-inst.cas.cz

Efficient energy storage solutions are of vital importance to enable the replacing of fossil fuels with renewable electricity sources.[1] Hydrogen is deemed as suitable for large-scale energy storage and energy conversion using electrochemical devices such as electrolyzers.[2] The technology is, however, limited by the sluggish kinetics of the electrocatalytic oxygen evolution reaction (OER).[3] To improve the current state-of-the-art catalyst's feasibility, one may either aim at maximizing the number of active surface sites or at reducing the costly catalyst components. Here, the latter approach is outlined on the benchmark oxygen evolving systems for acid media, based on rutile structured RuO_2 and IrO_2. A decrease of noble metal content can conveniently be achieved if one moves from binary to ternary phases. Cubic pyrochlores of the $A_2B_2O_7$ type have been studied as promising catalysts to replace conventional Ir and Ru OER catalysts. For the catalytically active Ru or Ir occupying B-sites of the flexible pyrochlore structure, the A-sites can be occupied by many lanthanides. These rare earth elements are subject to the effect of lanthanide contraction, differing in ionic radius. Hence, different lanthanide cations change the unit cell parameter and, consequently, the metal-to-metal distance between the transition metal cations. This again influences the position of the catalyst's d-band center.[4]

This work presents the synthesis and characterization of a new set of rare earth pyrochlore catalysts of the general structure $Ln_2(Ru_xIr_{1-x})_2O_7$ (Ln = Yb, Gd, Nd), introducing different ratios of iridium and ruthenium as B-site cations (x_{Ru}=0, 0.2, 0.4, 0.6, 0.8, 1). The motive for cation mixing is the beneficial effect of the Ir/Ru coexistence on the catalyst's performance in mixed rutile type oxides: Iridium is well-known to stabilize RuO_2 in mixed oxide electrodes.[5,6] However, by introducing iridium into the ruthenium oxide, the catalytic activity in OER is slightly lessened.

The catalysts presented were synthesized *via* the spray-freeze freeze-dry approach and the obtained materials were characterized by XRD, SEM, and EDX. The new catalyst reported herein employing cation mixing all exhibit an unprecedented improvement of OER activity compared to the catalysts without mixing of Ru/Ir, as well as the benchmark IrO_2. The local structure of the materials was analyzed using X-ray absorption fine structure (EXAFS) analysis and related to the observed improved catalytic activity.

References:

1. Carmo, M.; Fritz, D. L.; Mergel, J.; Stolten, D. *Int. J. Hydrogen Energy* 2013, *38*, 4901.
2. Bockris, J. O. *Int. J. Hydrogen Energy* 2008, *33*, 2129.
3. Dau, H.; Limberg, C.; Reier, T.; Risch, M.; Roggan, S.; Strasser, P. *ChemCatChem* 2010, *2*, 724.
4. Norskov, J. K.; Abild-Pedersen, F.; Studt, F.; Bligaard, T. *PNAS* 2011, *108*, 937.
5. Kasian, O.; et al. *Electrochem. Soc.* 2016, *163*, F3099.
6. Escudero-Escribano, M. M.; et aI. *J. Phys. Chem. B* 2018, 122, 947.

Nanosized $NaNi_{0.5}Mn_{0.3}Co_{0.2}O_2$ as a cathode material for sodium-ion batteries

A. V. Potapenko[a,b], S. A. Kirillov[a], M. Wu[b]

[a] Joint Department of Electrochemical Energy Systems, Kyiv, 03680, Ukraine

[b] University of Electronic Science and Technology of China, Chengdu, 611731, P.R. China

Numerous cathode materials for sodium-ion batteries are direct analogues of those used in lithium-ion batteries. Moreover, some of them seem particularly attractive because their lithium-containing counterparts appear much successful in applications and are commercialized. This is especially true for layered single, binary and ternary oxides of nickel, manganese and cobalt, which are widely employed in lithium-ion batteries readily available on the market. In this paper, we present the data on synthesis, characterization and electrochemical testing of nanosized $NaNi_{0.5}Mn_{0.3}Co_{0.2}O_2$ and prove that this material is prospective for applications, being able to deliver the specific capacity of 156 mAh/g at low current loads, sustain currents of 2370 mA/g and withstand long-term cycling by 105 cycles.

Introduction

Despite the growing number of publications and reviews on cathode materials for sodium-ion batteries (SIBs), see, for example, references [1-4] to mention only a few of them, the solution of the problem remains far from being solved. Numerous cathode materials for SIBs are direct analogues of those used in lithium-ion batteries. Moreover, some of them seem particularly attractive, because their lithium-containing analogues are very successful in application and commercialization. This is especially true for layered single, binary and ternary oxides of nickel, manganese and cobalt, which are widely used in lithium-ion batteries available on today market.

The main difficulty in working with sodium-containing layered oxides is that, unlike their lithium counterparts, they represent a wide variety of structures and easily pass from one structure to another. Depending on the location of sodium ions and the boundary separation of MO_6 octahedral units, where M is a transition metal, these structures can form prismatic (P) or octahedral (O) Na^+ coordination. In addition, MO_6 layers can be packed into a unit cell in a variety of ways. Therefore, it is necessary to consider the so-called P2, O2, P3 and O3 structures, where the numerical values correspond to the number of layers with different oxygen environment of transition metal ions.

A lot of triple oxides of nickel, manganese and cobalt of P2 and O3 types are investigated in sodium-ion cells. Compared with the samples free from Co, the addition of cobalt is believed to greatly improve high-rate capability and cycle performance [5]. In other words, P2 structures appear to contribute to high performance, since in these structures Na^+ can easily migrate between two trigonal prismatic sites in Na layers [6].

In this paper, we present the data on synthesis, characterization and electrochemical testing of $NaNi_{0.5}Mn_{0.3}Co_{0.2}O_2$ and prove that this material is prospective for applications, being able to deliver the specific capacity of 156 mAh/g at low current loads, sustain currents of 2370 mA/g and withstand long-term cycling.

Experimental Section

Transition metal oxides (NiO, MnO, CoO), lithium carbonate (Li_2CO_3), and citric acid were used as starting materials for precursor preparation. The preheat treatment temperatures for the sample were 450 and 560 ºC. Final annealing procedure was carried out at 600 and 700 ºC during 10 h. Multistage sample treatment strategy was chosen for perfect crystal formation, as will be shown further.

Electrochemical measurements were performed in CR2032 coin cells on a PARSTAT 4000A electrochemical workstation using galvanostatic charge/discharge cycling method. Cells with a sodium metal anode serving as a counter and reference electrode, a cathode made of the material in question, a Celgard 2500 separator membrane, and 1 mol/L solution of $NaPF_6$ in a mixture of EC/DMC/DEC with a mass ratio of 1:1:1 were assembled in a dry glove box. The working electrodes were made of 81% of the material under consideration, 11% of a conducting additive and 8% of a poly (vinilidene difluoride) binder. After the removal of the solvent under an IR radiator, the quantity of the material in a dried remainder was 1.7-2.7 $mg \cdot cm^{-2}$.

Galvanostatic studies were performed in a range of potentials of 2.65-4.5V *vs.* Na/Na^+ varying charge/discharge currents from 11.85 $mA \cdot g^{-1}$ (0.05C) to 2370 $mA \cdot g^{-1}$ (10C). Parameters of discharge were expressed in C [$mA \cdot g^{-1}$] units, which were calculated based on the value of the theoretical discharge capacity of $NaNi_{0.5}Mn_{0.3}Co_{0.2}O_2$ of 237 $mA \cdot g^{-1}$.

Results and Discussion.

Fig. 1 shows X-ray diffraction (XRD) patterns of the products obtained at different calcination temperatures. As has been shown, the low temperature is not enough for necessary phase formation. The patterns can be indexed in the rhombohedral Na_xCoO_2 structure (PDF 01-070-2030). When the precursor is calcined at 850 °C for 10 h, strong characteristic diffraction peaks of rhombohedral structure are observed. The lattice parameters of $NaNi_{0.5}Co_{0.2}Mn_{0.3}O_2$ obtained at 850 °C are calculated by the Unit cell software [7] as $a = b = 0.3027$ nm, $c = 1.5864$ nm, $\alpha = \beta = 90°$, $\gamma = 120°$, which are larger than those of $NaCoO_2$ ($a = b = 0.2888$ nm, $c = 1.5606$ nm).

It is found that increasing a temperature is advantageous for the formation of more perfect crystal structure. This observation and nanosized nature of the materials are confirmed by scanning electron microscopy (SEM) (Fig.1).

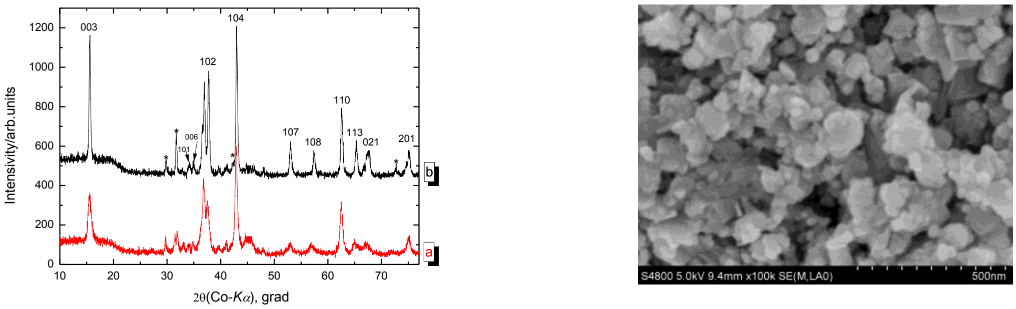

Figure 1. *X-ray diffraction data for* $NaNi_{0.5}Mn_{0.3}Co_{0.2}O_2$ *samples obtained at 400 °C (a) and 850 °C (b) (left-hand side) and the SEM image of the sample obtained at 850 °C (right-hand side).*

The electrochemical tests of electrodes consisting $NaNi_{0.5}Mn_{0.3}Co_{0.2}O_2$ demonstrate reversible discharge capacities changing from 158 mAh·g^{-1} to 156 mAh·g^{-1} at 0.05C on 1-10-th cycles and the coulombic efficiency values rising from 89 to 98%, respectively. The power tests demonstrate the ability of the electrode material to endure the maximal current load equal to 10C; at this current load, the discharge capacity value is 71 mAh·g^{-1}. We would like to point out that at 4C, the capacity value for electrodes is the half of theoretical value and equals to 117 mAh·g^{-1}.

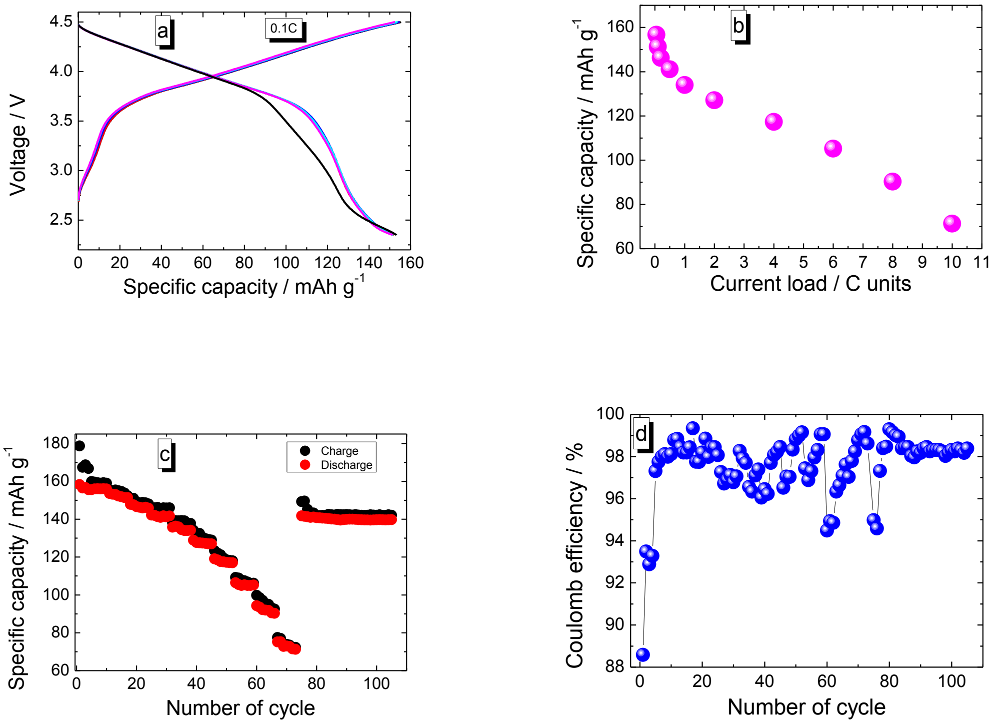

Figure 2. *Electrochemical parameters of* $NaNi_{0.5}Mn_{0.3}Co_{0.2}O_2$ *obtained at 850 °C: charge-discharge curves for stationary cycles at 0.1C (a); dependence of the capacity on the current load (b); dependence of the capacity on the number of cycle (c); dependence of the coulombic efficiency on the number of cycle (d).*

References

1. N. Yabuuchi, K. Kubota, M. Dahbi, S. Komaba, *Chem. Rev.* **114** (23), 11636-11682 (2014).
2. N. Ortiz-Vitoriano, N.E. Drewett, E. Gonzalo, T. Rojo, *Energy Environ. Sci.* **10** (1), 1051-1074 (2017).
3. J.-Y. Hwang, S.-T. Myung, Y.-K. Sun, *Chem. Soc. Rev.* **46** (12), 3529–3614 (2017).
4. P.-F. Wang, Y. You, Y.-X. Yin, Y.-G. Guo, *Adv. Energy Mater.* **8** (8), 1701912-1701934 (2017).
5. Z.-Y. Li, J. Zhang, R. Gao, H. Zhang, Z. Hu, X. Liu, *ACS Appl. Mater. Interfaces* **8** (24), 15439-15448 (2016).
6. J. Zheng, P. Yan, W.H. Kan, C. Wang, A. Manthiram, *J. Electrochem. Soc.* **163** (3) A584-A591.
7. T. J. B Holland, S. A. T. Redfern, *Mineralog. Mag.* **61** (1), 65-77 (1997).

Optimization of felt compression for high performance VRFB stack

J. Charvát[a], P. Mazúr[a], J. Dundálek[a], J. Pocedič[b], J. Mrlík[a], J.Vrána[b], J. Kosek[a,b]

[a] Department of Chemical Engineering, University of Chemical Technology Prague, Technická 3,
166 28 Praha 6, Czech Republic tel.
[b] New Technologies – Research Center, University of West Bohemia, Univerzitní 8, 306 14 Plzeň,
Czech Republic

Vanadium redox flow battery is one of the most developed type of stationary energy storage technology and excels among other due to its decoupled power (kW) and capacity (kWh), long lifetime and high efficiency. Carbon felt electrode is a key component of the battery and significantly contributes to the battery stack polarization through the charge transfer, ohmic, mass transport and conversion resistances. There are several possibilities as to how to modify the electrode and enhance the efficiency of the battery.

This work deals with the effect of felt compression on the performance of the battery cell.

The electrode compression can significantly reduce stack polarization, however, at the cost of increased pump consumption due to reduced felt porosity. The following properties were measured under different felt compression rates: a) electrical and mechanical properties of the felt, b) pressure drop through the felt for vanadium electrolyte comprising vanadium of 1.6 mol dm^{-3} H_2SO_4 of 2 mol dm^{-3} and 0.3 % of H_3PO_4 in state of charge of -50 %, c) performance in lab-scale single-cell (Ohmic and charge transfer resistance of the cell were determined from electrochemical impedance spectra. The cell resistance under current load at 50 % state of charge was evaluated from charging and discharging load curves and efficiency of VRFB single-cell was characterized by charge/discharge cycles.)

The optimal compression was found strongly dependent on material and inner structure. The trade-off between stack polarization and pumping losses was found around 30 % for polyacrylonitrile based felt and 60 % for rayon based felt.

With optimized felt compression, effect of the flow rate of the electrolyte and temperature on the performance of the battery for different state of charge was studied. The optimized system resulted in high maximal discharge power over 1.1 W cm^{-2} for 40 °C and for state of charge of 90 %.

Lithium Intercalation Thermodynamics: Do We Think that We Understand Graphite?

M. Mercer[a,b], A. Zülke[a,b], E.P.M. Leiva[c], D. Kramer[b,d], H. E. Hoster[a,b]

[a] Energy Lancaster, Lancaster University, Lancaster LA1 4YB, UK;
ALISTORE European Research Institute, CNRS FR 3104, 80039, Amiens, France

[b] The Faraday Institution, Didcot OX11 0RA, UK

[c] Departamento de Química Teóretica y Computacional, Facultad de Ciencias Químicas, INFIQC-CONICET, Universidad Nacional de Córdoba, Córdoba, Argentina

[d] Engineering Sciences, University of Southampton, Southampton, SO17 1BJ, UK

The intercalation of Li into graphite electrodes undergoes a few stages. Those stages involve different ordered distributions of the Li atoms and of the graphite layers. The stages are apparent in the voltage profiles during charge/discharge and also in entropy profiles. Entropy profiles can be recorded if the temperature is systematically and repeatedly varied during charge or discharge. We will illustrate the atomic scale patterns and processes that are behind the visible features in voltage and entropy profiles. Our findings are based on high-precision laboratory experiments in combination with thermodynamic atomic-scale modelling. We will explain how a rapid change of the Li-carbon interaction at low Li content (as recently predicted in *ab-initio* calculations) influences voltage and entropy profiles. Last but not least, we will demonstrate how these findings relate to the measurable behaviour of commercial Li ion batteries.

Experiment meets Modelling

Understanding the performance and degradation of Li-ion batteries (LIBs) requires uniting the current scales gap between atomistic, continuum and cell level models. This requires physically informed and experimentally validated parameters for the open circuit voltage (OCV), E_{OCV} and its derivative with respect to temperature dE_{OCV}/dT. The latter, related to configurational entropy of Li/vacancy arrangements in the electrode materials [1-4], has been proposed to diagnose structural changes caused by aging.

Phase transitions and what is behind them

Here, we model phase transitions of lithium insertion in graphite. Our model results in a commonly observed but poorly understood feature (P3) shown in Figure 1. In particular, we describe and experimentally validate the OCV, enthalpy and entropy change of the Stage I – Stage II transition in graphite (two large peaks in Figure 1 d and f). We extend our previous methodology (3,5) based on a two-level mean field model.

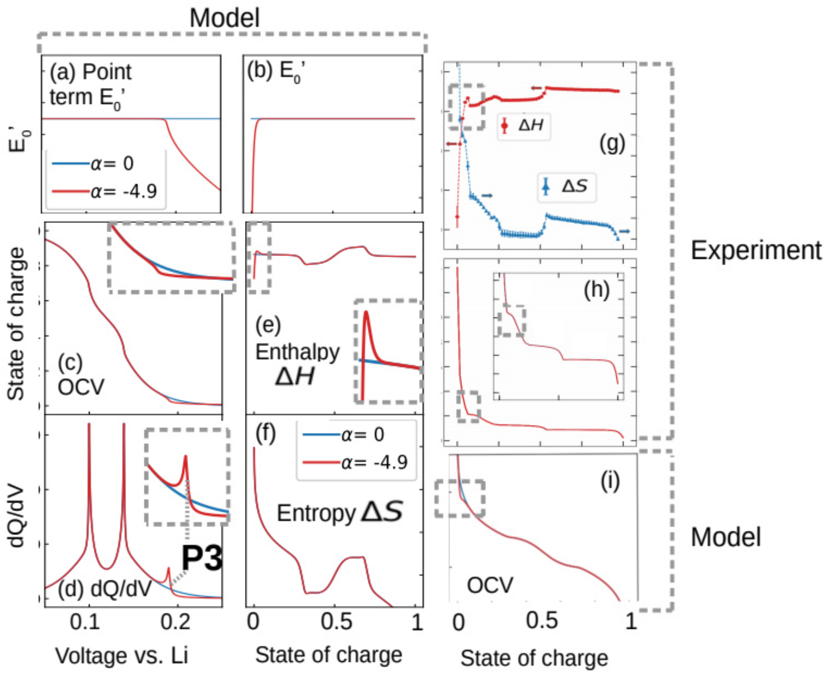

Figure 1. *(a-f) simulated profiles as indicated. As indicated in the legend of (a), α causes a change in the point term, E_0', with occupation (a,b), in contrast with the usually assumed case, α = 0. This results in additional features (peak P3, as shown in grey dashed boxes) in the simulated observables (c) OCV, (d) dQ/dV, (e) enthalpy change ΔH, but not in (f) entropy change ΔS, indicating the highlighted features are not from Li-Li interactions. Experimental data for (g) partial molar enthalpy and entropy and (h) OCV show good agreement with the simulations in the highlighted features (dashed boxes).*

<u>Interactions that drive the phase transitions.</u> The model includes interactions between the Li atoms, and a dynamically varying Li-C interaction (α term) based on physical arguments presented in earlier work (6,7). The varying interaction term results in experimentally observed peak P3. We assign the peak P3, highlighted in Figure 1d, to a rapid change in the interaction between Li and the C lattice with respect to the occupation of Li during the early stages of lithiation (Figure 1 a-b).

This model is supported by a recent DFT study of Li binding on graphene (7), which suggested a similar change in interaction energy at low Li occupation. Earlier work by Dahn et al. (6) highlighted that the movement of the Fermi level through a gap in the density of states, as in a semimetal like graphite, can result in a non-fixed interaction between Li and the host lattice (contrary to usual assumptions in lattice gas models). We can therefore model this effect alongside the staging transitions and hence consistently describe changes in the whole OCV profile (i.e. Figure 1 h-i). Our model is a physically informed approximation with a thermodynamic basis. The highlighted feature in Figure 1 e was predicted by us and subsequently validated by experiment (Figure 1 g).

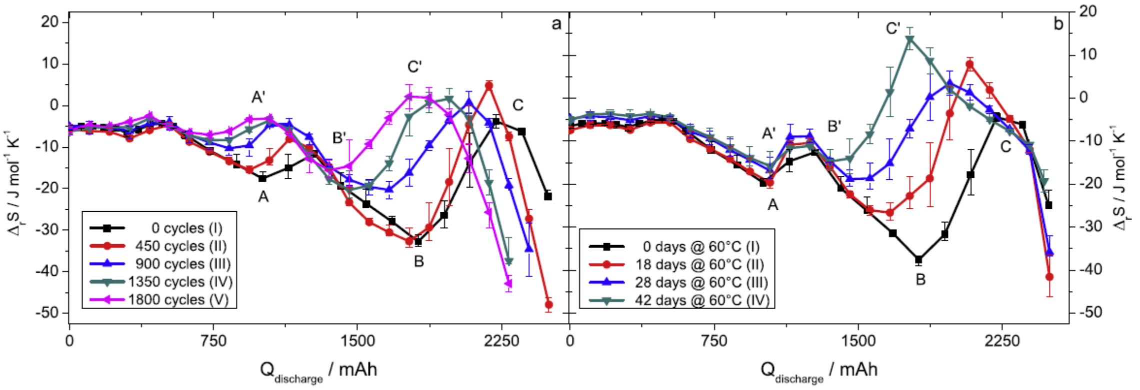

Figure 2. *Influence of cycle and calendar ageing on entropy profiles of commercial 18650 LIB cells with NMC-based cathodes. (a) after cycling at 25° C with 1C and (b) after several days of storage at 100% SOC at 60°C. From ref. 2.*

Observations in technical LIB cells. As illustrated in Figure 2, entropy profiles of technical LIB cells carry two signature features related to the graphite anode. One is the order/disorder transition marked as A/A', and the other is the steep decrease in entropy change towards the end of discharge, which is the regime of low Li content in graphite. Depending on the ageing process, these features change in amplitude and/or drift "horizontally" on the state-of-charge scale. The former can be related to an increasing density of defects and/or a less homogeneous local state-of-charge (3,4). The latter is the result of loss of lithium inventory or active material at the cathode or anode (8).

In summary, atomic scale thermodynamic models give an improved understanding of the processes behind the voltage and entropy profiles that can be easily measured at the external tabs of lithium ion batteries. Those insights are not only relevant from an academic point of view, but will be the basis for the next generation of battery models which will be stronger in considering the physics and chemistry within the electrodes.

Acknowledgments

We thank the Faraday Institution (faraday.ac.uk; EP/S003053/1), grant number FIRG003, for funding. MPM would like to thank the Royal Society of Chemistry for a Researcher Mobility Grant. EPML acknowledges grants PIP CONICET 11220150100624CO, FONCYT PICT-2015-1605 and SECyT of the Universidad Nacional de Cordoba. Support by CCAD-UNC and GPGPU Computing Group, Y-TEC and an IPAC grant from SNCAD-MinCyT, Argentina, are also gratefully acknowledged.

References

1. Y. Reynier *et al.*, *Phys. Rev. B* **70** (2004) 174304.
2. P. J. Osswald *et al.*, *Electrochim. Acta* **177** (2015) 270-276.
3. S. Schlueter *et al.*, PCCP **20** (2018) 21417.
4. M.P. Mercer et al., *Electrochim. Acta* **241** (2017) 141-152.
5. M. Otero *et al.*, *Electrochim. Acta* **245** (2017) 569-574.
6. J. Dahn et al., *Phys. Rev. B* **45** (1992) 3773-3777.
7. A.M. Garay-Tapia et al., *J. Chem. Theory Comput.* **8** (2012) 1064–1071.
8. Y. Li *et al., Renewable and Sustainable Energy Reviews* **113** (2019) 109254

Evaluation of internal and external sensor measurements for determining the state-of-charge and state-of-health of Li-ion pouch cells

B. Kossl[a,b], H. Popp[a], K. Froehlich[a], G. Fafilek[b], M. Jahn[a]

[a] Center for Low-Emission Transport, AIT Austrian Institute of Technology GmbH, 1210 Vienna, Austria

[b] Institute of Chemical Technologies and Analytics, Technical University of Vienna, 1040 Vienna, Austria

Owing to the construction, Li-ion cells can cause dangerous situations if they are not operated properly. Therefore, battery management systems must obtain the state of the battery as accurately and fast as possible. Temperature and pressure sensors can help to determine the state of health and the state of charge of the cell and detect over temperatures and over pressures immediately. The change of stiffness of the anode and cathode material during charging and discharging can be derived by measuring the time of flight of vibrations that are sent through the battery. In this work, several methods to determine the state of charge and state of health are analyzed and their accuracy and feasibility are discussed.

Introduction

For a secure and efficient operation of Li-ion pouch cells exact knowledge of the state of charge (SOC) and state of health (SOH) of the battery is vital. High temperatures can cause the destruction of the cell or initiate the thermal run away which can lead to dangerous situations for the people using those batteries. Side reactions can cause the formation of gases, which can indicate the SOC during the operation of the battery. By determining the state of charge and state of health of a cell, the battery management system can adjust the charging and discharging properties to extend the life of batteries.

In this work, the correlation between the temperature, pressure and stiffness of a pouch cell and its SOC and SOH is analyzed.

Experimental

The cells used for the experiments are self-manufactured NMC622 (BASF, Germany) / Graphite (Jiangxi Zichen, China) pouch cells with 2 Ah (170 mA/cm^2) consisting of 6 cathodes and 7 anodes. The length of the cells is 100 mm, the length 70 mm and height 3 mm.

Temperature Measurement

Thermocouples type K have been used as temperature sensors. The inner sensor was inserted centered at the core anode of the stack during the assembling of the pouch cell and the outer sensor was attached centered at the outside of the cell with Kapton.

During the experiment the fully charged cell was overcharged with a rate of 2C till either the double maximal cell voltage or 200 % SOC was reached.

Pressure Measurement

The cell together with a sheet of foamed plastic was clamped between two plates of phenolic paper, the strain gauge was placed between the battery and the foamed plastic and the conductance was measured with a non-inverting amplifier. The cell was cycled with the constant current/constant voltage (CCCV) method at different charging and discharging rates.

Time of Flight Measurement

Piezo-electric disc beeper have been used as actuator and sensor to measure the time of flight (TOF) of a vibration sent through the cell. The beepers were glued to the outside of the pouch cell with epoxy resin at a distance of 8 cm from each other. Via a function generator a triangle signal was modulated with a high frequency sinus signal and fed to the actuator beeper and the generated voltage signal of the sensor beeper was measured and the time of flight was calculated[1].

Results

Temperature Measurement

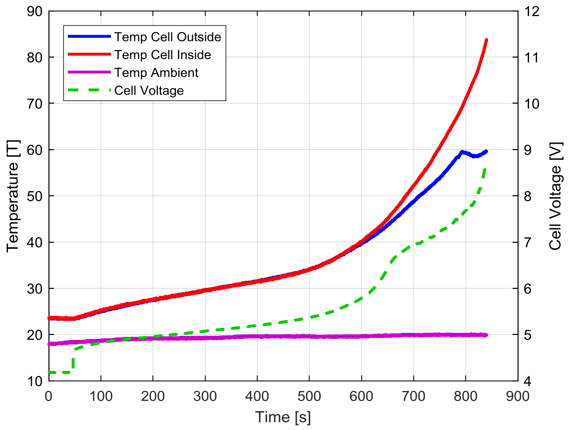

Figure 1. *Temperature and voltage measurement during overcharge test*

For an intact cell the difference between the inside and outside temperature measurement during the normal operation are only marginal but deforming of the cell or the formation of gases inside the cell can lead to a significant error for the outer sensor. In the test shown in **Figure 1** both sensors are measuring similar temperatures up to a cell voltage of about 5.7V, then gases were formed in the cell which lead the outer sensor to be lifted from the electrode stack and caused a temperature drop. At the end of the overcharge test the difference between inner and outer measurements raised to about 25°C, which is in good agreement with findings of other papers[2].

Pressure Measurement

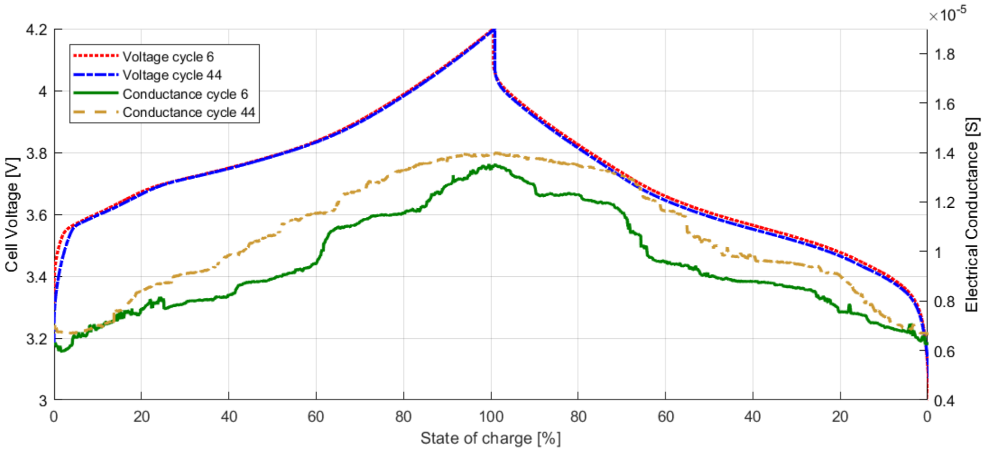

Figure 2. *Conductance of a strain gauge used to measure the pressure change during charging and discharging; the conductance is directly proportional to the pressure;*

The measurement shows a repeatable difference between a charged and an uncharged cell, which is in accordance with past findings[3].

Figure 2 depicts a slight drop in pressure at the begin of charging which is followed by a linear increase up to a SOC of about 75 %. For discharging a less linear relationship between pressure and SOC can be observed, the pressure drops similar to the charging process until a SOC of about 65% is reached but is then followed by a plateau until a SOC of 25 %. The start and end value of the pressure is not changing much for higher cycles, but the curve is becoming smoother. The pressure variation is related to gas evolution inside the cell, side film formation and/or other side reactions. The continuous variation after several cycles indicates a reversible nature of these reactions.

Time of Flight Measurement

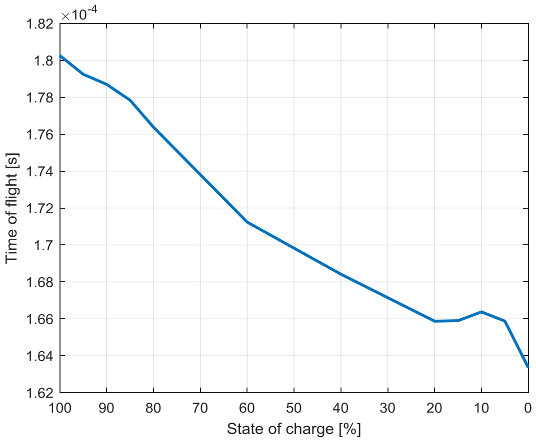

Figure 3. *TOF of a wave through the cell over SOC during discharging*

The stiffness variation of mainly the anode but also cathode materials cause the decreasing of the time of flight when the cell is discharged. As shown in Figure 3 From 100 % until 20 % state of charge the decrease is linear which shows the possibility to use this measurement for determining the state of charge.

Acknowledgments

This work was financially supported by the Austrian Federal Ministry for Transport, Innovation and Technology (bmvit).

References

1. P. Ladpil, F.Kopsaftopoulos, F. Chang, *Estimating state of charge and health of lithium-ion batteries with guided waves using built-in piezoelectric sensors/actuators,* ScienceDirect
2. X. Zhu, Z. Wang, Y. Wang, H. Wang, C. Wang, L. Tong, M. Yi, *Overcharge investigation of large format lithium-ion pouch cells with Li(Ni0.6Co0.2Mn0.2)O2 cathode for electric vehicles: Thermal runaway features and safety management method,* ScienceDirect
3. A.J. Louli, L.D.Ellis, J.R.Dahn, *Operando Pressure Measurements Reveal Solid Electrolyte Interphase Growth to Rank Li-Ion Cell Performance,* Joule (2018).

Anatase as Anode for Sodium-Ion Cells

O. Čech[a], P. Benešová[a], P. Čudek[a], T. Kazda[a]

[a] Department of Electrical and Electronic Technology, Faculty of Electrical Engineering and Communication, Brno University of Technology, Technická 10, 616 00, Brno, Czech Republic

In the proposed work, we used conventional TiO_2 anatase powder consisting of submicron particles as anode material for sodium-ion cells. In our experiment, we demonstrate that this material is stable during cycling, reveals strong formation effect and we discuss the electrochemical performance and structural properties.

Introduction

Sodium, a highly abundant element with almost inexhaustible supplies and much lower cost than lithium, is one of the candidates for use in the areas of electromobility and non-portable power storage for large-scale applications. Although the knowledge gained by studying materials for lithium-ion batteries can be assumed to some extent, there are still a number of obstacles preventing the commercial expansion of sodium-ion technology. A large number of suitable cathode materials are currently being explored, such as layered oxide structures, polyanionic compounds, etc. However, little has been found in anode materials with the desired properties and it is, therefore, necessary to continue their research. Carbon materials, especially hard carbon, and titanium dioxide TiO_2 materials are currently the most promising. Titanium dioxide as the anode material for sodium-ion batteries excels in price, good stability, low volumetric expansion, non-toxicity, and availability. Of the known titanium dioxide polymorphs, anatase, which can theoretically accommodate the highest amount of sodium ions, offers a working potential of 0.8V vs Na^+/Na, but suffers from low electron and ionic conductivity, which is usually compensated by its nanostructuring, composite preparation or by applying surface layers, eg Al_2O_3 [1; 2].

Also, the use of suitable electrolytes, which greatly affect the thickness and stability of the SEI layer, is a widely discussed topic. An article by Xu et al. compares the use of ethers-based solvents (DEGDME, DME) and carbonates (EC / DEC, EC / PC).

Experimental

The negative electrode of the sodium ion battery was prepared by the conventional method of applying an electrode paste to the copper foil. The electroactive material studied was nanostructured anatase from Sigma-Aldrich. The electrode composite was prepared in a manner common to testing lithium-ion battery electrode materials, where anatase was mixed with Super P carbon black (Timcal) and polyvinylidene fluoride (PVDF) polymer binder, which was dissolved in N-methyl pyrrolidone (NMP). The ratio of dry components in the composite was 80% anatase, 10% Super P and 10% PVDF. The electrode paste was coated with a Spiral Bar Coater (Neurtek) on a copper foil, dried, and 18 mm disks were cut from the electrode and subsequently used in an electrochemical cell. The battery was sealed in El-Cell-Std in a glove box.

Structural analysis

Figure 1 shows TiO_2 anatase images from a scanning electron microscope showing that the material consists of submicron spherical particles (dimensions in the range of 200-800 nm), but which are partially sintered and interconnected. During the mixing of the electrode paste, it was evident that the material was well dispersed, but it was unlikely that the mass was completely separated and dispersed at the submicron level.

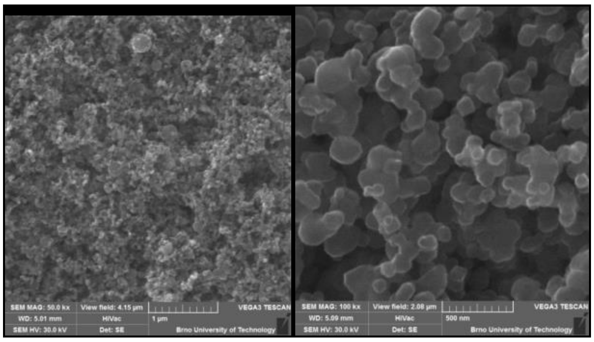

Figure. 1. *Images of used TiO_2 anatase from electron scanning microscope, view field 4.15 and 2.08 µm*

The X-ray diffraction spectroscopy in Figure 2 confirmed that the material obtained is pure anatase. It is a tetragonal lattice where a = b = 3.7842 Å c = 9.5146 Å.

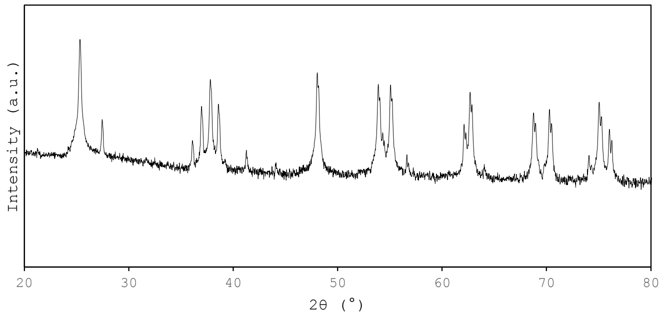

Figure. 2. *X-ray diffraction spectroscopy of TiO_2 anatase used for the sodium-ion battery anode. The intensity is plotted on a logarithmic scale.*

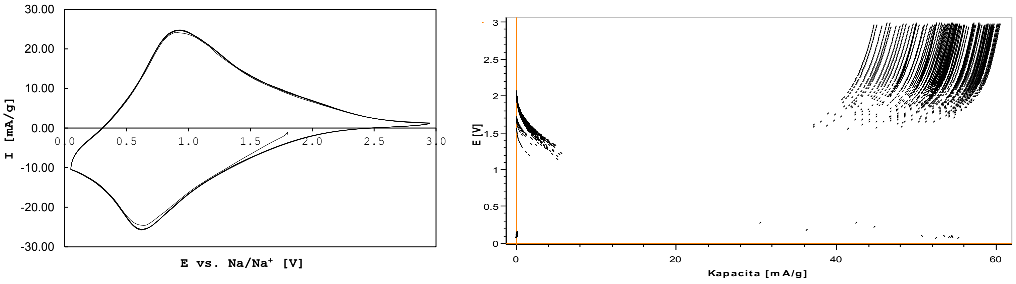

Figure. 3. *Cyclic voltammetry (left) and discharging characteristics (right) of anatase in the sodium-ion cell. Cyclic voltammetry was performed at a sweep rate of 0.1 mV / s, discharge characteristics measured by a specific current of 0.5C (80 µA / cm^2).*

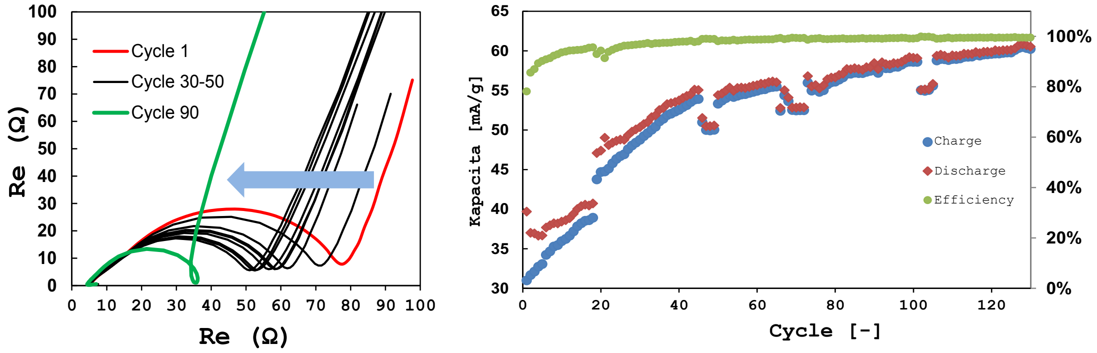

Figure. 3. *Impedance spectra measured during molding cycling (measurement every ten cycles) and the course of forming anode with anatase by galvanostatic cycling with a specific current of 0.5C.*

Results and discussion

From the measured electrochemical characteristics, it can be seen that the mechanism of the reaction of sodium with TiO_2-anatase is different from the commonly mentioned intercalation in the case of lithium ions. The shape of the cyclic voltammetry curve is rather pseudocapacitive in its large area and shape without a sharp transition. The impedance spectroscopy in Figure. 3, which has been inserted after each tenth cycle of galvanostatic cycling, supports the idea of phase-transition forming. The usual tendency is that, based on the formation and eventual growth of the SEI layer, the Rct resistance gradually increases. It can be seen here that with each subsequent cycle it gradually decreases, which would correspond to the fact that a new form of material is preferred for the sodium reaction by cycling. Galvanostatic cycling clearly shows how the gradual formation of a new phase leads to the formation of an electrode. At the beginning of cycling, the efficiency is approx. 80%, but very quickly reaches the threshold of 100%, while capacity grows slowly linearly. It can, therefore, be assumed that at the beginning it is the formation of an SEI layer, which is soon formed and is no longer promoted. The initial anatase specific capacity was 30 mAh / g and doubled in 130 cycles. We attribute local sinks to temperature changes in the measurement room, always a few cycles in succession, which have a lower capacity and do not match the trend.

Acknowledgments

This work was supported by a specific research grant at BUT (No. FEKT-S-17-4595). Authors gratefully acknowledge the financial support from the Ministry of Education, Youth and Sports of the Czech Republic under project No. LTT19001, BUT specific research programme (project No. FEKT-S-17-4595).

References

Complete citations should appear at the end of the text. Use the reference style that is shown below for all references.

1. J. Doe and R. Hill, *J. Electrochem. Soc.*, **152**, H1902 (2005).
2. R. Smith, *Electrochem. Solid-State Lett.*, **10**, A1 (2007).
3. E. Gaura and R. M. Newman, *ECS Trans.*, **4**(1), 3 (2006).

Electrolytes for sodium-ion batteries

N. I. Globa, V. A. Sirosh, Yu. V. Shmatok

Joint Department of Electrochemical Energy Systems,

38A Vernadsky Ave., 03680 Kyiv, Ukraine

This paper is devoted to investigation of electrolytes for sodium-ion batteries. The results of studies of electrical conductivity and electrochemical stability of a number of electrolyte systems are presented.

The main requirements for electrolytes for sodium-ion batteries are high specific conductivity in a wide temperature range, wide electrochemical stability window, chemical inertness and compatibility with sodium anode. Compliance with these conditions allows for minimizing the influence of side processes during cycling and providing high level of specific capacity and cycling efficiency.

Conductivity of electrolytes is determined by the salts and solvents properties. The choice of the optimal salt and solvent composition allows to obtain high values of specific conductivity. Depending on the dielectric constant, solvents are arranged in the following sequence: EC > FEC > PC > Triglyme > DME > DMC > DEC. It is assumed that depending on the dissociation degree, sodium salts can be arranged approximately in the same sequence as lithium salts, i.e. $LiBPh_4$ > LiBETI, LiTFSI, $LiSbF_6$ > $LiAsF_6$> $LiPF_6$ > $LiClO_4$ > LiI > $LiBF_4$ > $LiCF_3SO_3$ > LiBr > $LiNO_3$ > $LiCF_3CO_2$ [1], but their solubility and conductivity of electrolytes differ from similar lithium systems. The electrolyte solutions based on sodium salts have higher conductivity than the similar solutions of lithium salts. The authors [2] showed that transition from Li to Na reduces dissociation energy of the ion pair by about 15-20 %, which provides higher conductivity of the sodium salt contained electrolytes.

The following solvents and salts were used to prepare electrolytes: propylene carbonate, ethylene carbonate, dimethyle carbonate, diglyme, triglyme and tetraglyme (all Sigma-Aldrich, ≥98%), fluoroethylene carbonate (Alfa Aesar, 98%), recrystallized sodium perchlorate (Chemlaborreactiv, 98%) and sodium tetrafluoroborate (Sigma-Aldrich, 98%). Electrolyte solutions were prepared in a dry glove box.

Conductivity of the electrolytes was measured in hermetically sealed two-electrode cells with plane-parallel platinum electrodes in the temperature range from –10 to +50°C with a Z-2000 impedance meter (Elins, Russia). The cell constant was determined with a 0.1N KCl solution.

Compositions of the investigated electrolyte solutions and their conductivities at the temperature of 25°C are presented in Table 1.

Table 1. *Composition and conductivity of electrolytes.*

	Solvents composition	**Salt concentration**	**Conductivity (25°C), mSm/cm**
$NaClO_4$			
1	PC	1M	6.13
2	Diglyme	1M	5.76
3	Tetraglyme	1M	1.9
4	EC:DMC (30:70; v:v)	1M	8.07
5	EC:DMC (50:50; v:v)	1M	10.09
6	EC:DMC (70:30; v:v)	1M	10.01
7	EC:DMC (90:10; v:v)	1M	9.82
8	FEC:DMC (30:70; v:v)	1M	6.54
9	EC:DMC:FEC (45:50:5; v:v:v)	1M	9.8
10	EC:DMC:FEC (40:50:10; v:v:v)	1M	9.23
11	EC:DMC:FEC (30:50:20; v:v:v)	1M	8.33
12	EC:DMC:FEC (20:50:30; v:v:v)	1M	8.16
$NaBF_4$			
13	Diglyme	1M	4.04
14	Triglyme	1M	2.13
15	Tetraglyme	1M	1.39

It is shown that the electrochemical stability of the FEC contained electrolytes is higher by about 200 mV then for the EC-DMC based electrolytes.

References

1. W. A. Henderson, *Macromolecules*, **40**(14), 4963 (2007).
2. E. Jonsson, P. Johansson, *Phys. Chem. Chem. Phys.*, **14**(30) 10774 (2012).

Sodium Titanate Material for Sodium-Ion battery

J. Libich[a], M. Sedlaříková[a], J. Vondrák[a], J. Máca[a], P. Čudek[a] , Michal Fíbek[a] and Andrey Chekannikov[b], Werner Artner[c] and Guenter Fafilek[c]

[a]Department of Electrical and Electronic Technology, Faculty of Electrical Engineering and Communication, Brno University of Technology, 616 00 Brno, Czech Republic

[b]Skolkovo Institute of Science and Technology, 143026 Moscow, Russian Federation

[c]Vienna University of Technology, Getreidemarkt 9, 1060 Vienna, Austria

The current top leading electrochemical system for energy storage is lithium-ion battery. This kind of battery become commercially available in year 1991, it is almost 30 years ago. The technology and human society evolution of that time was different form the technology of the contemporary world. New applications like off or on grid stationary energy storage systems with power in orders of megawatts. These new applications totally differ from the original intention for using of lithium-ion batteries in smart portable devices like camera. These applications have specific requirements as low cost, sustainable environmentally friendly energy storages. The lithium-ion batteries are adapted for these applications, but the economic and environment point of view mirror the fact that we need another electrochemical system for these applications that will better respect their requirements. In case of energy storage for renewable energy sources, as the most promising seems to be a sodium-ion battery.

Introduction

Fast growth and demand for renewable energy, that should be used worldwide in the mass scale, tends to origin of new systems, technology and processes. These factors are strongly responsible for effective utilization of electric energy produced by renewable energy sources. Wind and solar energy are great opportunities to help reduce carbon footprint that we make. These renewable energy sources have one basic and irremovable disadvantage, both are non-dispatchable. It means that they cannot be turned on or off in order to meet the society electricity needs. It is the opposite of dispatchable sources, like for example hydroelectric power, of electricity which are very flexible, being able to change their output quickly in order to fulfil instant electricity demands. Non-dispatchable electricity sources are often highly intermittent, which means that they are not continuously available due to factors that cannot be controlled. The non-dispatchable renewable energy power sources need for their proper integration to the distribution grid the electric energy storage. The pumped hydroelectric power plant can be good energy storage system. Unfortunately this system is not suitable for small range applications due to its cost, geographic and geologic requirements. As only viable solution of energy storage for renewable energy sources is the electrochemical energy storage system, i.e. the battery. The lithium-ion batteries are widely used in these applications, but the limitations especially lithium ore deposits and its abundant in the earth crust need us to seek for next generation batterie so-called post-lithium systems. Among most promising battery successor of lithium-ion batteries, in renewable energy storage application range, seems to be sodium-ion batteries.

The sodium-ion battery technology is very similar to lithium-ion battery. Among main advantages of sodium-ion batteries relative to the lithium-ion are economy and environmental aspects. Sodium is abundant, 6th most abundant elements in the earth crust (lithium occupies 33th position), it reaches year production over 225 M tonnes (lithium just around 0.043 M tonnes). Sodium-ion batteries work on the same principles as the well-known and described lithium-ion batteries, they use same technology most of them use aprotic electrolytes DMC (dimethyl carbonate), EC (ethylene carbonate), PC (propylene carbonate) with salts as $NaClO_4$ (sodium perchlorate) or $NaPF_6$ (sodium hexafluorophosphate). Cathode materials for sodium-ion batteries, analogy to convention stable cathode materials for lithium-ion batteries. Cathode material $NaCoO_2$ (sodium cobalt oxide) or $NaNi_{1/2}Mn_{1/2}O_2$ (sodium nickel manganese oxide).

Experiments and Results

Anode materials are issue, Lithium-Ion batteries use manly graphite as active electrode materials for negative electrode (anode), in case of sodium ion it is not possible to use graphite, because sodium ion having large diameter and cannot be inserted among graphite sheets. This work is focused on electrochemical analysis of sodium titanite ($Na_2Ti_3O_7$) as negative electrode material in sodium-ion cell.

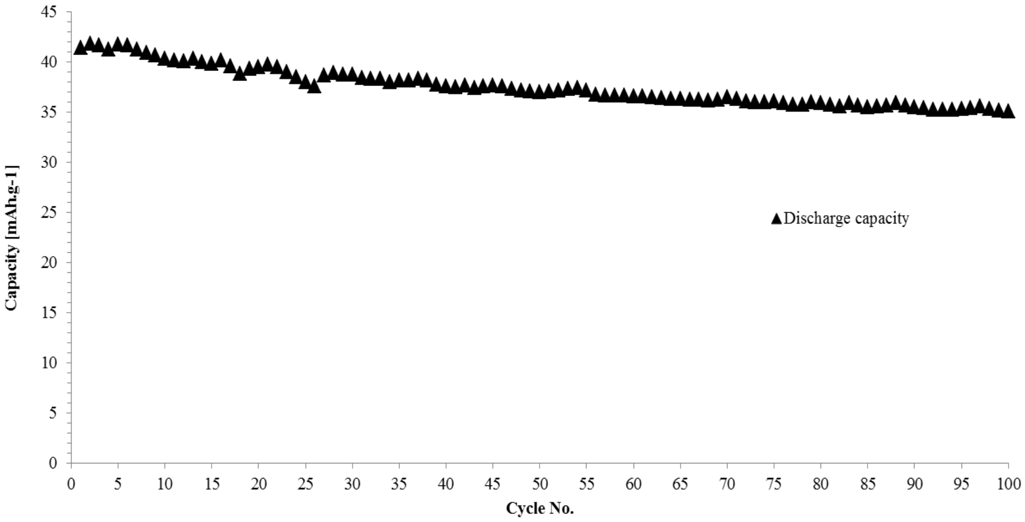

***Figure 1.** Galvanostatic cycling of $Na_2Ti_3O_7$ at rate 0.2 C.*

Acknowledgments

This work was supported by the project of specific research: Materially a technologie pro elektrotechniku III, reg. no. FEKT-S-17-4595

References

1. T. L. Kulova, Y. O. Kudryashova, A. A. Kuzmina, A. M. Skundin, I. A. Stenina, A. A. Chekannikov, A. B. Yaroslavtsev and J. Libich, *Journal of Solid State Electrochemistry*, **23**(2) (2019).

2. J.-H. Kim, M.-J. Jung, M. J. Kim, Y.S. Lee, *Journal of Industrial* and *Engineering Chemistry* **61** (2018).
3. L. P.Wang, L. Yu, X. Wang, M. Srinivasan, Z. J. Xu, ournal of Materials Chemistry A, **3** (2015).
4. Y.Wang1, X. Yu, S. Xu, J. Bai, R. Xiao, Y.S. Hu, H. Li, X. Q. Yang, L. C. and X. Huang, *Nature communications*, **4** (2013).
5. K. Kubota, S. Komaba, *Journal of The Electrochemical Society*, **162**(14) (2015).
6. M. E. Arroyo-De Dompablo, *Functional Materials Letters*, **7**(6) (2014).
7. M.D. Fang, T.H. Ho, J. P. Yen, Y. R. Lin, J.L. Hong, S. H. Wu, J.J. Jow, *Materials* **8** (2015).
8. N. Loeffler, D. Bresser, S. Passerini, M. Copley, *Johnson matthey technology review*, **59** (1) 2015.
9. J.-H. Kim, M.J. Jung, M.J. Kim, Y.S. Lee, *Journal of Industrial and Engineering*
10. *Chemistry* **61** (2018)..
11. Y.Pana, Y. Zhang, B. S. Parimalam, C. C. Nguyen, G. Wang, B. L. Lucht, *Journal of Electroanalytical Chemistry* **799** (2017).
12. D. Kumar, S. K. Rajouria, S. B. Kuhar, and D. K. Kanchan, *Solid State Ionics*, **312**, 8-16 (2017).
13. C. Ding, T. Nohira, and R. Hagiwara, *Journal of Power Sources*, **354**, 10-15 (2017).
14. L. Zhu, Y. Li, J. Wang, and X. Zhu, *Solid State Ionics*, **327**, 129-135 (2018).
15. R. Bi et al., *Electrochimica Acta*, **284**, 287-293 (2018).
16. S. Guo et al., *Science Bulletin*, **63**, 376-384 (2018).
17. C. del M. Saavedra Rios, V. Simone, L. Simonin, S. Martinet, and C. Dupont, *Biomass and Bioenergy*, **117**, 32-37 (2018).
18. J. -H. Kim, M. -J. Jung, M. -J. Kim, and Y. -S. Lee, *Journal of Industrial and Engineering Chemistry*, **61**, 368-380 (2018).
19. D. Wu, K. Luo, S. Du, and X. Hu, *Journal of Power Sources*, **398**, 99-105 (2018).
20. X. Pan, A. Chojnacka, P. Jeżowski, and F. Béguin, *Energy Storage Materials*, **2019**, 10 (2019).
21. S. Kaushik, K. Matsumoto, Y. Sato, and R. Hagiwara, *Electrochemistry Communications*, **102**, 46-51 (2019).
22. S. Wheeler, K. Hurlbutt, and M. Pasta, *Chem*, **4**, 666-668 (2018).
23. C. Guhl et al., *Electrochimica Acta*, **268**, 226-233 (2018).
24. S. Chen, F. Feng, Y. Yin, X. Lizo, and Z. Ma, *Energy Storage Materials*, **28**, 10 (2018).
25. X. Jiang et al., *IScience*, **10**, 114-122 (2018).
26. J. Rodríguez-García, I. Cameán, A. Ramos, E. Rodríguez, and A. B. García, *Electrochimica Acta*, **270**, 236-244 (2018).
27. H. Gao, S. Xin, L. Xue, and J. B. Goodenough, *Chem*, **4**, 833-844 (2018).
28. X. Song et al., *Electrochimica Acta*, **281**, 370-377 (2018).
29. J. I. Kim, K. Y. Chung, and J. H. Park, *Journal of Membrane Science*, **566**, 122-128 (2018).
30. W. Hou et al., *Nano Energy*, **52**, 279-291 (2018).
31. Y. Lu, L. Li, Q. Zhang, Z. Niu, and J. Chen, *Joule*, **2**, 1747-1770 (2018).
32. S. Brutti et al., *Electrochimica Acta*, **306**, 317-326 (2019).
33. Y. Wang et al., *Nano Materials Science*, **1**, 91-100 (2019).
34. A. Eftekhari and D. -W. Kim, *Journal of Power Sources*, **2018**, 336–348 (2018).
35. J. -Y. Hwang, S. -T. Myung, and Y. -K. Sun, *Chemical Society Reviews*, **46**, 87 (2017).

Optimalization of Negative Electrode for Sodium Ion Accumulators

J. Maca, M. Sedlarikova, J. Libich, T. Kazda and K. Jasso

Brno University of Technology, Technická 10, Brno, 616 00, Czech Republic

Energetics is one of the main areas which the humanity is deal with. The mobility development brought the accumulators as a power source for them. To the most common used accumulators belong lead acid accumulators which can be found in almost all cars. The second used type is lithium ion accumulators. Lithium ion accumulators are used in many applications such as stationary storages, power supply for small mobile devices like phones, laptops, small power tools and also as energy sources in electro cars. The main disadvantages of lithium are high price and relatively rarity in earth's crust. This paper, focus on composition optimization of negative electrode material for sodium ion accumulators. The sodium metatitanate is used as base electrode material and the ratio of conductive components is changed. The optimal composition for best material performance was established.

Introduction

The social pressure on lowering of greenhouse gases is forcing us to leave the fossil fuels and substitute them with renewable power sources like solar or wind power plants. The developing of these technologies brought a need of effective electric energy storage systems, because renewable power sources do not produce electricity continuously but in narrative ways. Big development in storage system is connected mostly with lithium ion accumulators[1]. Lithium is rare and its deposits are located only in few parts or the World. On the other hand sodium is common and basically everywhere.

The principle of operation of sodium ion accumulators is based on the knowledge of lithium ion accumulators. It is known, that lithium is easy intercalating and deintercalating into different cathode and anode materials. The positive electrode materials are usually based on lithium metal oxides and the negative materials mainly graphite based materials, lithium titan ceramic (LTO) or silicon. Unfortunately sodium do not intercalate or not even react with these materials (silicon). It is caused by larger size of sodium ions and lower mobility. From these reasons new material need to be found. To the tested negative electrode materials belong hard carbon in with the reversible capacity of 300 mAh/g was observed or tin phosphides based materials[2,3]. The usage of tin have similar disadvantage like lithium and that is its rarity. Experiments of using fullerene as material for negative electrode were done. The capacity 325 mAh/g was achieved, bud it have large capacity drop during cycling. Another possibility is sodium titan ceramic based materials like sodium metatitanate[4,5].

Experimental

The electrode material was made from sodium metatitanate ($Na_2Ti_3O_7$), PVDF binder (10 wt%) and conductive component Super P. The ratio of Super P was changed in two steps 10 and 20 wt% from the whole weight of the electrode material. The mixture was applied to a cupper current collector. The thickness of electrode material was 150 μm. The application of the film on current collector was carried out by coating bar. After drying out the electrodes were pressed by 2000 kg/cm^2 pressure.

The measurement was made by help of electrochemical cells type El-Cell. The cycling was carried out in the voltage range 0.01V to 2.5V. The charging and discharging current was calculated and set to 0.1C. Ten cycles were made on Biologic potentiostat.

Results

In fallowing figure 1 is shown the capacity dependence of electrode compound from 10 wt% Super P, 10 wt% PVDF and 80 wt% $Na_2Ti_3O_7$ on cycle number (star). It is visible that the capacity decrease with the cycle number from initial 136 mAh/g to 93 mAh/g in the tenth cycle. The capacity dependence of electrode two compound from 20 wt% Super P, 10 wt% PVDF and 70 wt% $Na_2Ti_3O_7$ on cycle number is figured by cross symbols. The capacity is higher than in the first case and started on 158 mAh/g in first cycle and finish with 107 mAh/g in last cycle.

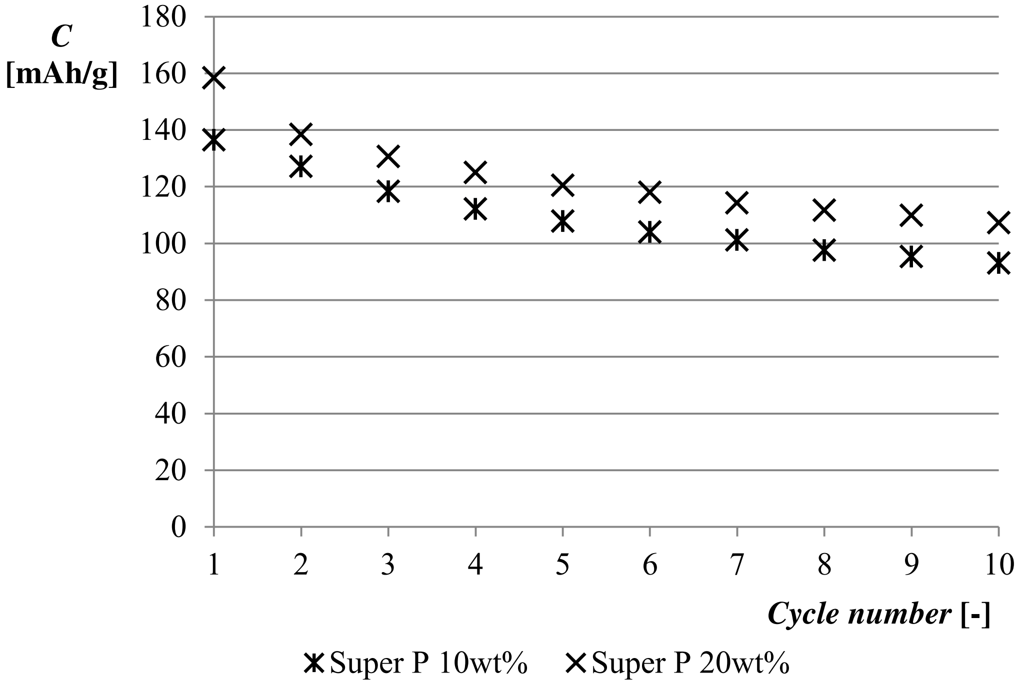

Figure 1. *Capacity of electrode $Na_2Ti_3O_7$: 10 wt% Super P (star) and 20 wt% Super P (cross)*

Discussion

From the result mentioned above is clear that higher among of conductivity compound Super P increase the capacity of the electrode material. The conductivity of the sodium metatitane is lower than in the LTO. The higher among of conductive compound causes better coverage and connections between each ceramic grain. This causes that more of the electrode material is actually used and increased the capacity of the electrode material. Due the low conductivity of the sodium metatitanate, low charging and discharging current was applied. In this case only 0.1C of reached capacity was used.

Conclusion

Two ratios of conductive compound in negative electrode for sodium accumulators were tested. The 10 wt% and 20 wt% of Super P were tested. The highest obtained capacity was 158 mAh/g and that with use of 20 wt% of Super P. Another investigation and optimization of negative electrode will be needed before commercial application of sodium ion accumulators.

Acknowledgement

Authors gratefully acknowledge the financial support from the Ministry of Education, Youth and Sports of the Czech Republic under project No. LTT19001 and BUT specific research programme (project No. FEKT-S-17-4595).

References

1. QI, Shihan, Daxiong WU, Yan DONG, et al., 2019. Cobalt-based electrode materials for sodium-ion batteries. *Chemical Engineering Journal*. **370**, 185-207.
2. DAHBI, Mouad, Takeshi NAKANO, Naoaki YABUUCHI, et al., 2014. Sodium carboxymethyl cellulose as a potential binder for hard-carbon negative electrodes in sodium-ion batteries. *Electrochemistry Communications*. **44**, 66-69.
3. USUI, Hiroyuki, Yasuhiro DOMI, Ryota YAMAGAMI a Hiroki SAKAGUCHI, 2019. *Degradation mechanism of tin phosphide as Na-ion battery negative electrode*. **4**(2).
4. PONTIROLI, Daniele, Silvio SCARAVONATI, Michele SIDOLI, Giacomo MAGNANI, Laura FORNASINI, Chiara MILANESE a Mauro RICCÒ, 2019. Fullerene mixtures as negative electrodes in innovative Na-ion batteries. *Chemical Physics Letters*. **731.**
5. ZHANG, Ruie, Ying CUI, Wei FAN, Guang HE a Xizheng LIU, 2019. Ambient stable Na0.76Mn0.48Ti0.44O2 as anode for Na-ion battery. *Electrochimica Acta*. **295**, 181-186.

Lithium Manganese Spinels as Cathode Materials for Sodium-Ion Batteries

N. I. Globa, Yu. V. Shmatok, V. A. Sirosh, S. A. Kirillov

Joint Department of Electrochemical Energy Systems,
38A Vernadsky Ave., 03680 Kyiv, Ukraine

Lithium manganese spinel is an effective cathode material for lithium-ion batteries, so its investigation as a possible cathode material for sodium-ion system is promising. Based on this, six different $LiMn_2O_4$ samples have been studied as cathodes in a sodium system. The processes occurring during cycling of the $LiMn_2O_4$ samples in sodium cells are discussed.

Lithium manganese spinel ($LiMn_2O_4$) is an effective cathode material of lithium-ion batteries. Its advantages include high specific capacity (148 mAh/g) and discharge voltage (~4 V), as well as good cycling reversibility. Besides, existing synthesis methods allow for obtaining $LiMn_2O_4$ materials with different particle size and morphology that define their electrochemical characteristics, especially under the high current loads and during long cycling.

The use of the lithium-containing materials in sodium-ion batteries, i.e. electrochemical substitution of lithium ions for sodium ions during charge/discharge process in a cell with sodium anode is tempting for obtaining sodium-containing cathode materials. The main processes affecting electrochemical exchange are accumulation of lithium ions in the near-electrode layer and the thermodynamic stability of the new sodium-containing phase formed. It is known that sodium manganese spinel is thermodynamically unstable and cannot be obtained in direct syntheses. That’s why the use of $LiMn_2O_4$ in sodium cells may have good prospects.

This paper presents the results of investigation of six different samples of $LiMn_2O_4$. Morphology and particle size of $LiMn_2O_4$ samples have been studied by means of scanning electron microscopy and their structural characteristics have been obtained by XRD method. Specific capacity, cycling stability and discharge rate parameters of $LiMn_2O_4$ in lithium and sodium electrochemical systems were analyzed and discussed.

In lithium cells, electrochemical properties of $LiMn_2O_4$ are shown to strongly depend on the particle size, which, in turn, is determined by the synthesis method and the nature of the raw materials (Figure 1). The values of specific capacity of $LiMn_2O_4$ samples are from 80 mAh/g to 125 mAh/g in the voltage range of 3-4.3 V vs. Li/Li^+.

In sodium cells, lithium ions in the initial $LiMn_2O_4$ structure are electrochemically substituted by sodium ions, which can be reversibly intercalated during further cycling. Gradual substitution of lithium ions is shown to cause structural transformations reflecting on the shape of charge/discharge curves. Specific capacity obtained ranges from 150 mAh/g to 205 mAh/g at the cycling voltages of 2-4.05 V vs Na/Na^+ (Figure 2).

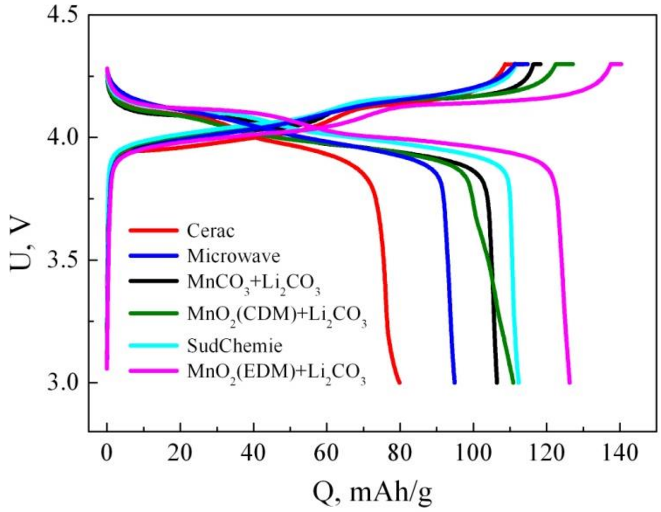

Figure 1. *Charge/discharge curves of the first cycle at the current density of 0.1 mA/cm^2 for $LiMn_2O_4$ samples in lithium cells. The order of samples corresponds to the growth of the discharge capacity.*

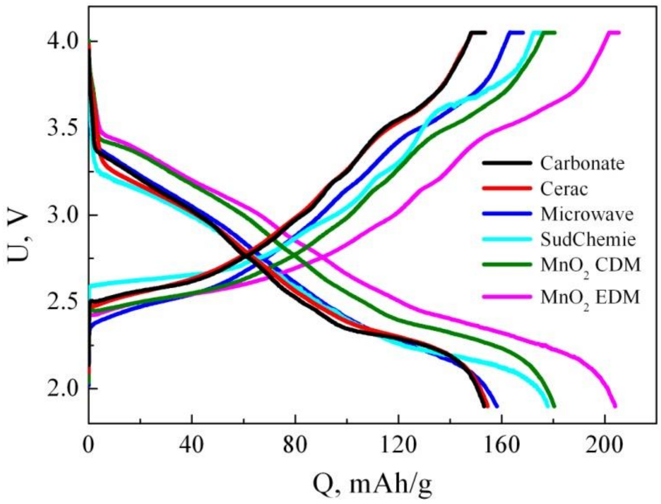

Figure 2. *Typical charge/discharge curves at the current density of 0.05 mA/cm^2 for $LiMn_2O_4$ samples in sodium cells. The order of samples corresponds to the growth of the discharge capacity.*

Influence of particle size of $LiMn_2O_4$ on the structural transformation rate from the initial cubic spinel to the layered oxide phase Na_xMnO_2 is determined. It is shown that spinel particles undergo significant changes associated the structural reorganization and leading even to their breakdown.

Based on the results obtained one can conclude that lithium manganese spinels can be used as cathode materials for sodium-ion system. The effectiveness of their work in the sodium system is largely determined by the initial process of replacing lithium with sodium in the original spinel and the stability of the new sodium-containing phase formed.

Sodium rhodizonate as cathode material for sodium-ion batteries

N. I. Globa, V. A. Sirosh, Yu. V. Shmatok, S. A. Kirillov

Joint Department of Electrochemical Energy Systems,
38A Vernadsky Ave., 03680 Kyiv, Ukraine

Investigation of sodium rhodizonate ($Na_2C_6O_6$) as an active material of the positive electrode of sodium-ion batteries has been carried out. Electrochemical characteristics of the $Na_2C_6O_6$ cathodes in the sodium cells have been determined. It has been shown that the stability of specific capacity depends on the method of manufacturing a positive electrode and on electrolyte composition.

Introduction

Sodium-ion electrochemical systems are considered as an alternative to lithium-ion batteries, the demand for which is constantly growing. However, the development of sodium-ion systems is hampered by the low specific characteristics of cathode and anode materials. Among cathode materials, transition metal oxides are the most widely investigated. On the other hand, depending on the electrolyte composition and electrode manufacturing technique, sodium rhodizonate $Na_2C_6O_6$ is able to provide high specific capacity close to theoretical value of 501 mAh/g [1,2] and can be considered as an alternative to the oxide cathodes. In this work, the results of galvanostatic investigation of $Na_2C_6O_6$ supplied by a local producer (Synbias, Ukraine) are presented.

Experimental

Electrodes based on $Na_2C_6O_6$ were made with two types of binders, such as poly(vinylidene difluoride) (PVdF, Solef-6020, Solvay Chemicals, Belgium) and polytetrafluoroethylene binder (F4D, Makrokhim, Ukraine). Super P carbon black (Timcal, Switzerland) was used as a conductive additive. The mass ratio of components in the cathode mass (active material, conductive additive and binder) was 2:2:1. Depending on the type of binder and manufacturing method, the active material loading was 1–1.5 mg/cm^2 in the case of PVdF use and 3–4 mg/cm^2 in the case of F4D. Electrode tests were carried out in 2016 coin type cell with the sodium metal anode at the constant temperature of 25±1°C. 1M solutions of $NaBF_4$ in diglyme and $NaClO_4$ in tetraglyme were used as electrolytes. The separator was a polypropylene film Celgard 2400.

Results and Discussion

Some properties of the electrolytes used in this work are shown in Table I. These depend on the anion of the salt and solvent and are acceptable for use in metal-ion batteries.

TABLE I. *Properties of the electrolytes used.*

Electrolyte composition	**Ionic conductivity (25°C), mSm/cm**	**Activation energy, kJ/mol**
1M $NaClO_4$ in tetraglyme	1.9	19,3
1M $NaBF_4$ in diglyme	4.0	7.1

Electrochemical stability potential ranges of electrolytes determined by cyclic voltammetry with aluminum work electrode are 0.1–4.8 V and 0.1–4.3 V versus Na/Na^+ for 1M solution of $NaClO_4$ in tetraglyme and 1M solutions of $NaBF_4$ in diglyme, respectively.

Charge and discharge capacities of $Na_2C_6O_6$ differ depending on the manufacturing method of electrodes and electrolyte composition. Fig. 1*a* shows charge/discharge curves of the first cycle for the $Na_2C_6O_6$ cathodes based on the PVdF binder. The discharge specific capacities were 212 mAh/g using 1M $NaBF_4$ in diglyme and 244 mAh/g in case of 1M $NaClO_4$ in tetraglyme. It corresponds to the intercalation of 1.7 and 1.95 mole of sodium, respectively. The discharge capacities in the case of the F4D binder are practically independent of electrolyte composition and equal to ~160 mAh/g thus corresponding to the intercalation of 1.3 mole of sodium (Fig. 1*b*).

Character of the charge/discharge curves changes upon cycling. It is connected with differences due to changes between the initial and subsequent processes of saturation with sodium [1].

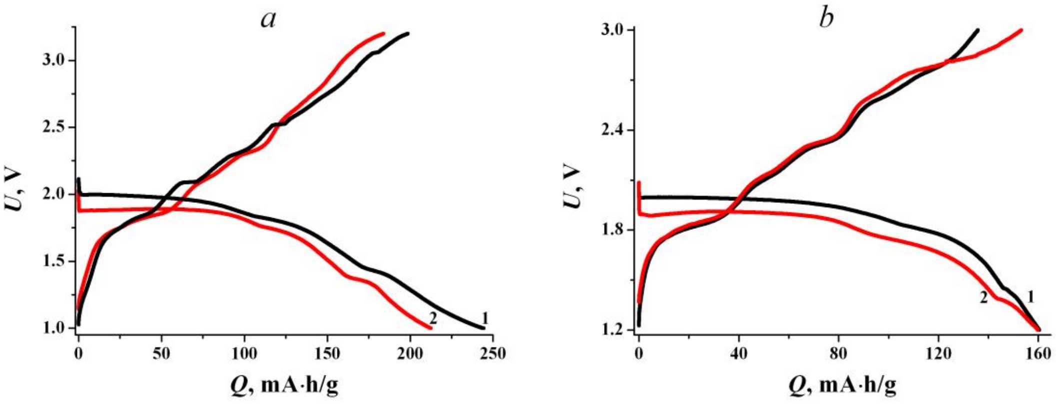

Figure 1. *Charge/discharge curves of the $Na_2C_6O_6$ cathodes on the first cycles depending on the type of binder: a – PVdF, b – F4D. Electrolyte compositions: 1 – 1M $NaClO_4$ in tetraglyme, 2 – 1M $NaBF_4$ in diglyme. Current density – 50 $\mu A/cm^2$.*

Fig. 2 demonstrates the dependences of specific capacity on cycle number. Specific capacity of the $Na_2C_6O_6$ electrode based on PVdF binder after the first 20 cycles noticeably decreases and on the 80 cycle is 132 mAh/g. In the case of the F4D based cathode, the specific capacity of $Na_2C_6O_6$ remains stable.

The results obtained are promising the further studies of sodium rhodizonate as a cathode material for sodium-ion batteries. They demonstrate that enhancing the specific capacity and cycling stability of the $Na_2C_6O_6$ cathodes can be reached by improving the cathode preparation method, selecting the optimal electrolyte composition and choosing proper operating conditions.

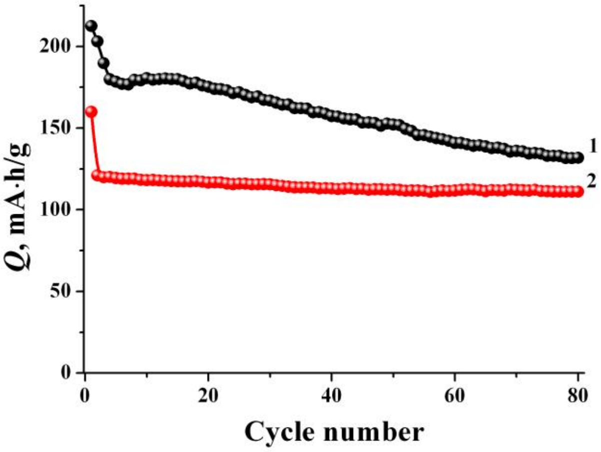

Figure 2. *Cycling performance of the $Na_2C_6O_6$ cathodes manufactured with the use of different binders: 1 – PVdF, 2 – F4D. Electrolyte – 1M $NaBF_4$ in diglyme. Current density – 50 μA/cm^2.*

References

1. M. Lee, J. Hong, J. Lopez, Y. Sun, D. Feng, K. Lim, W. C. Chueh, M. F. Toney, Y. Cui and Z. Bao, *Nat. Energy*, **2**(11), 861 (2017).
2. Y. Wang, Y. Ding, L. Pan, Y. Shi, Z. Yue, Y. Shi and G. Yu, *Nano Lett.*, **16**(5), 3329 (2016).

Effect of replacing a faulty module with a different power module to the total PV power rating

J. Vanek[1], and P. Maule[2]

[1] Centrum výzkumu a vyžití obnovitelných zdrojů energie, Vysoké učení technické v Brně, Technická 10, 612 00 Brno

[2] Fakulta elektrotechniky a komunikačních technologií, Vysoké učení technické v Brně, Technická 10, 612 00 Brno

Introduction

At present, any small or larger repair of the power plant, its source or its components, is a nightmare of all decentralized renewable energy sources operating in the Czech Republic. Although this is not a small number of sources of energy (sun, wind, water) and is increasing, legislators have not had time to adopt and define legal or sub-statutory measures, explaining, supplementing or regulating this area of small energy. In the past, the Energy Regulatory Office proceeded very hard, incorrectly, and interpreted the repair of the plant according to what the client said about the repair. Decision making was at odds with operators' expectations.

Repair power plant due to common defects, wear and tear, damage, natural disasters could not be canceled, so their practical solutions almost always ended up unofficially, without accounting documents in the repair accounts, fearing loss of entitlement to operating financial support. This is very unfavorable in the increased annual profits of the power plants, which pay more taxes than they would have and achieve a better economic return than they should actually achieve.

In November 2018, a draft amendment to the Energy Act and the Act on Supported Energy Sources was issued for interdepartmental comment procedure. Unfortunately, the prepared proposals are not constructively prepared (in the light of the practice) and final adoption is expected by 2020 at the earliest, with effect from 2021. Meanwhile, electricity generators are aging and cannot rely on any legislative adjustment. One of the most frequently discussed repairing is replacing a malfunctioning, damaged, or otherwise unsuitable module.

After more than 15 months' postponement of its issuance (the original date was promised in autumn 2017), the Energy Regulatory Office clarified the conditions under which it is possible to carry out repair or maintenance at the electricity production plant by its interpretative opinion No.10 / 2018 of 18.12.2018. In the final summary, ERO informs that it is possible to carry out the repair by replacement in the case of module or other defect of the module, natural or harmful event or termination of the service life, but the installed capacity of the production plant must not be exceeded, at the same time that the technological and ecological level of the production must not be increased up to the level of the newly established plants.

Goal of work

For reasons of legislative disagreement, it is important to find out how the module replacement is influenced by the module replacement for a module with a higher output. This is one of the most frequent interventions (in the form of repair in exchange) into a non-functional part of the production plant, where a certain part of the plant is totally or partially non-functional - with a reason for a physical or mechanical failure of the module, which in time becomes a production defect or a consequence of natural or other elements.

In 99.999% of the plants, the modules are connected in series strings, so our goal was to find out if the exchange of the photovoltaic module involved in the string (string) affects the subsequent positive or negative electrical power of the chain, respectively. nominal system performance and, as a result, the total annual energy yield.

Problems of Serially Connected Modules

The photovoltaic modules have a very limited voltage and current output range. The applications where we can use the power of the standalone module are mostly determined by the maximum voltage size, which makes its use for charging purposes for 12 V or 24 V batteries, which was most apparent at the very beginning of the photovoltaics. Today, for most applications, it is necessary to increase the voltage to a certain minimum level, so it is advisable to connect the modules in series to electrically larger units, so-called strings.

Identical PV cells and modules connected to the string

The criterion for connecting modules into string is the energy aspect of losses. In the case of an increase in the total string voltage to twice, the current is then equivalently halved (assuming a constant power), and the total losses in the PV wiring fall according to the relationship:

$$P = R\,I^2$$

to their quarter. This is why most of the world's module and inverter producers push the maximum voltage of string from today's 1000 V to 1500 V.

The serial connection of the three modules and cells in series is shown in Figures 1 and 2.

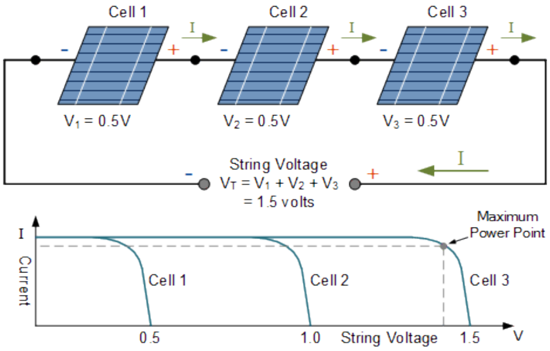

Figure 1. *Serial connection of three photovoltaic cells [1]*

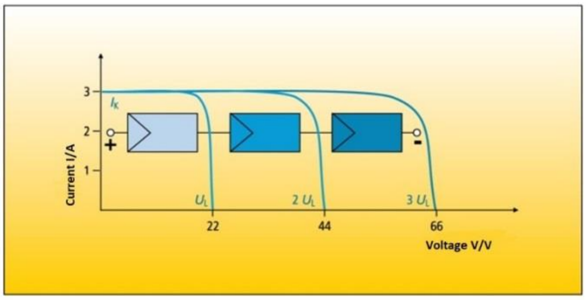

Figure. 2. *Serial connection of three photovoltaic modules by 36 cells in module [2]*

Figure 1 shows the total voltage and current parameters in a series of three completely identical photovoltaic cells. Volt-ampere characteristic of one module due to connecting in series is graphically added according to voltage. The result is a sum of open-circuit voltages while leaving the short-circuit current. The result of the serial connection and the resulting behavior is therefore identical for the cell and the module as shown in Fig. 2.

From the above it can be deduced that if the measurements and subsequent computer simulation are carried out principally on the modules, the detected character of the serial behavior of the modules will also be applicable to the behavior of the series connected cells and vice versa.

Graphical simulation

Based on the measured values of the PV modules, a simulation of the graphical sum of the volt-ampere characteristics for the modules connected in series was compiled. The necessary sums of currents, based on the selected set of voltages, were created in Microsoft Office Excel by the sum of currents of individual modules and the result is shown in Figure 3.

***Table 1. Simulation** result of three series-connected modules*

Module no.	Nominal Output Power [W]	Real Output Power [W]	Combinated output power (1+2+3) [W]	Combinated output power per module [W]	Nominal Performance deviation[%]	Real Performance deviation
1	85	82.16	138.96	46.32	45.51	43.62
2	50	44.69		46.32	7.36	-3.64
3	50	42.57		46.32	7.36	-8.81

The maximum power point was found with a simulation of 138.96 W, converted to three modules, representing 46.32 W per module. When the nominal power is increased from 50 W to 85 W, which is 70%, the highest deviation from the measured power was recorded by an increase of 8.81% (causing an increase in performance) but due to the nominal power the deviation is 7.36% (reserve to real power is 3.68 W).

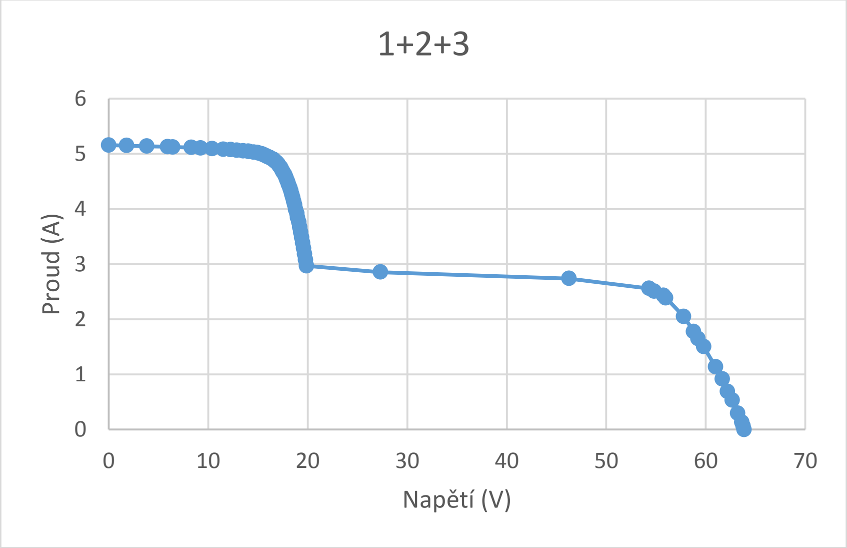

***Figure 3.** VA simulation of three series-connected modules*

The photovoltaic modules under consideration are about 10 years old, with various experiments being carried out on them, and therefore there is a noticeable difference between nominal and actual measured (real) power. Therefore, the maximum nominal power is not exceeded.

Table 2. *Dependence of power deviation on number of modules no.*

	Quantity of module no. 2								
	1	2	3	4	5	10	15	20	40
Deviation [%]	-11,04	-7,04	-5,03	-3,83	-3,03	-1,43	-0,98	-0,75	-0,38

If only two modules are connected (number = 1), the maximum rated power increases by 11% relative to module 2. The nominal power will always increase if module 1 is larger than module 2. If string contain sixteen modules (1 + 15), the total nominal power increase will be up to 1% against module no. 2.

Conclusion

The aim of this work was to find out by measuring that the replacement of the old, damaged or otherwise inoperative module in the connected module chain can be done by replacing the module with the higher peak power, which does not increase the overall rated power of the system. The replaced module has a peak power exceeding the original peak power of the old module, but by plugging it into a modular string the power of the string is result of serial combination influenced by the output current of the weakest module. This was confirmed by both computer and graphical simulation and will be verified by measurement.

Acknowledgments

The publication was created with the financial support of a specific research project at VUT FEKT-S-17-4626.

References

1. Bypass Diode for Solar Panel Protection,(2019) Online: http://www.alternative-energy-tutorials.com/energy-articles/bypass-diode.html
2. Haselhuhn R., Maule P.: Fotovoltaické systémy. Energetická příručka. 1. vydání, 803 stran, Česká fotovoltaická asociace, Plzeň, 2017, ISBN: 978-80-906281-5-1

Integrated Circuits for Charging Batteries from the Photovoltaic Panel

D. Benda, P. Vorel

Department of Power Electrical and Electronic Engineering, Faculty of Electrical Engineering and Communication, Brno University of Technology, Brno, Czech Republic

This paper deals with the comparing currently available integrated circuits (IC) for charging batteries from the photovoltaic panel. The paper focus on the ICs for higher power applications, e.g. photovoltaic power plants, small uninterruptible power supplies, etc. The paper does not deal with the IC for the smaller power applications, typically wearable electronics. At the end of the paper is presented battery charger based on the LT8490 circuits for the lead acid battery.

Integrated Circuits for Chargers

In two subparagraphs below will be presented parameters of ICs for the battery charger powered from the photovoltaic panel and some types of ICs from producers.

Basic Parameters for the Selection the Right Integrated Circuit for the Charger

At the beginning is necessary to specify basic parameters which will be critical for the IC selection. The first parameter is the mode of the charger power part. It can work in linear or switching mode. In general, the switching mode is more efficient than the linear mode so the vast majority of the IC contains drivers for the switching mode. Some chargers require the higher output voltage than output voltage of photovoltaic panel (input voltage to charger). With the linear mode is impossible to achieve the higher output voltage than the input voltage. The second parameter is the energy harvesting function. This function covers maximum power point tracking (MPPT) algorithms [1], which tracking current output power from photovoltaic panel with the respect to e.g. changing solar irradiance, temperature and load. The chargers include the switching power part and suitable MPPT algorithm are proper for the most battery applications. Others parameters, e.g. input/output voltage and current, type of used MPPT algorithm, topology of the power part, telemetry functions, size, cost and type of the supported battery (charging profile) depends on the application.

Integrated Circuits for the Charger Overview

In this paragraph will be presented typical ICs from two producers. ICs with critical parameters are mentioned below in TABLE I. All ICs in the TABLE I include MPPT function. However, ICs from Analog Devices (formerly Linear Technology) are cover range of higher power (at least 10 A charge current) with many types of ICs for chargers. Another companies produce chargers ICs too, but without MPPT functions or for the lower voltage or the lower current (for wearable electronics). Typical producers of mentioned ICs are e.g. Maxim Integration, Microchip, Renesas, STMicroelectronics.

TABLE I. *Battery charger ICs.*

Part	**Producer**	**Battery type**	**Input voltage [V]**	**Maximum output voltage [V]**	**Maximum charge current [A]**	**Telemetry**
LTC4013	Analog Devices	Lead Acid, LiFePO4,Li-Ion, Li-Polymer, NiCd, NiMH	4.5 – 60	60	20	No
LT8490	Analog Devices	Lead Acid, LiFePO4,Li-Ion, Li-Polymer	6 - 80	80	10	Yes
LTC4015	Analog Devices	Lead Acid, LiFePO4, Li-Ion, Li-Polymer	4.5 – 35	35	20	Yes
bq24650	Texas Instrument	Lead Acid, LiFePO4, Li-Ion, Li-Polymer,	5 - 28	26	10	No

The Charger for Lead Acid Batteries with the LT8490 controller

The LT8490 [1], [2] controller from Analog Devices (formerly Linear Technology) was selected for the experimental charger powered from the photovoltaic panel for the charging lead acid battery. The LT8490 is based on the buck/boost topology with external switchers what is very useful, because the output voltage can be lower or higher than the input voltage (the output voltage of the photovoltaic panel).

The charger with LT8490 was designed for the powering from the one photovoltaic panel with 250 W output power and 24 V nominal output voltage. The experimental charger charging one lead acid battery with 12 V nominal voltage. The LT8490 contains profile for charging lead acid batteries based on constant current - constant voltage (CC/CV) algorithm. The experimental charger uses telemetry based on the UART bus for higher supervising. The MPPT algorithm used in the LT8490 is based on the “Perturb and Observe” method.

The charger contains many interlocks for increase the safety and long life of the charged battery (e.g. the undervoltage of battery, the checking of temperature battery, the overcurrent protection…). The maximal charge current is limited to 20 A. The entire charger is presented below in Figure 1. The charger efficiency is better than 96 %. The dimensions of the charger board are 70x100 mm (four layers).

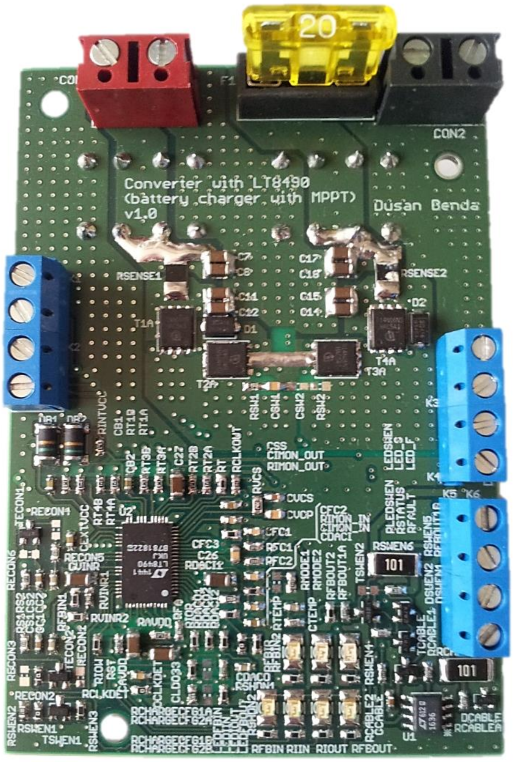

Figure 1. *The experimental charger with LT8490.*

Acknowledgments

This research work has been carried out in the Centre for Research and Utilization of Renewable Energy (CVVOZE). Authors gratefully acknowledge financial support from the Ministry of Education, Youth and Sports of the Czech Republic under NPU I programme (project No. LO1210) and BUT specific research programme (project No. FEKT-S-17-4374).

References

1. D. S. Morales, Maximum Power Point Tracking Algorithms for Photovoltaic Applications *Maximum Power Point Tracking Algorithms for Photovoltaic Applications*, thesis, Aalto University (2010)
2. Linear Technology, *LT8490: High Voltage, High Current Buck-Boost Battery Charge Controller with Maximum Power Point Tracking (MPPT).*, Milpitas (2015).
3. Linear Technology, *LT Journal of Analog Innovation V24N1 - April 2014 - 80V Buck-Boost Lead-Acid and Lithium Battery Charging Controller Actively Finds True Maximum Power Point in Solar Power Applications.*, Milpitas (2014).

Tests of the HK-1 module of the mobile mining machine

Bartosz Polnik

The paper discusses laboratory tests of the HK-1 module dedicate for a roadheading mining machine, developed as part of the project on the acronym HYDKOM 75 co-financed by the National Center for Research and Development. The research was aimed at verifying the adopted technical assumptions and functionality of the developed solution, taking into account the possibility of using the HK-1 module in the potentially explosive atmospheres. The HK-1 module was designed and developed based on the lithium battery, increasing the mobility of the designed machine. In addition, after the battery has been discharged, the HK-1 module allows to operate machine on the line power from the mine network at the same time the battery are being charged. Thanks to such a solution, the mobile mining machine can be operated practically without interruption.

Tests of the electrical equipment.

Electrical equipment has been set up at the laboratory tests stand located at the KOMAG Institute of Mining Technology (fig. 1). The breaking motor was coupled with a three-phase electric mining motor, which corresponded to the electrical parameters of the target motor of the roadheading mining machine. The electric motor was powered from lithium cell batteries via a power electronic converter.

Figure 1. *Tests stand*

Through appropriate control system of the breaking motor, it was possible to test the power supply and control system of the HK-1 module in a wide range of load changes of the electric motor - conditions simulating the real scope of the operation of the roadheading mining machine. The tests were carried out during battery charging and discharging. The battery charging process was realized using a dedicated charger powered from a three-phase electrical network with a voltage of 3 x 500 V AC. The charging process was controlled by the master controller, communicating with the charger and the battery cell monitoring system (BMS) via the CAN bus. For the tests carried out, the charging process ended when the voltage on the single cell of the battery reached the maximum value of 3.65 V. Fig. 2 shows an exemplary course of voltage Udc, current Idc and power Pdc registered during the charging process.

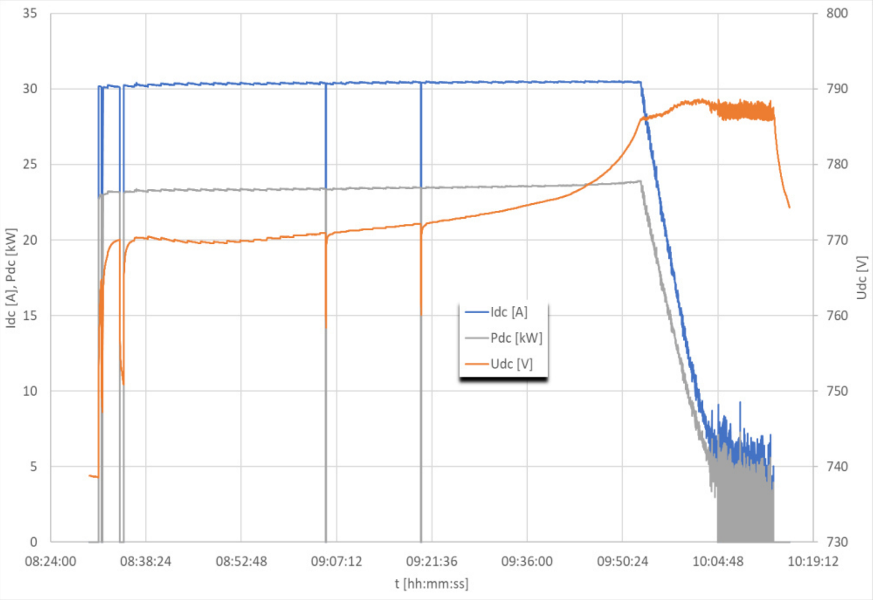

Figure 2. *Exemplary time curve of voltage, current and power registered during the charging process*

The discharging process was started after the battery was charged. Operation of the converter and the battery (BMS system) was controlled by the master controller. For the tests carried out, the discharging process ended when the voltage on a single battery cell reached the minimum value 2.65 V. Fig. 3 shows the course of voltage Udc, current Idc and power Pdc registered during the discharging process.

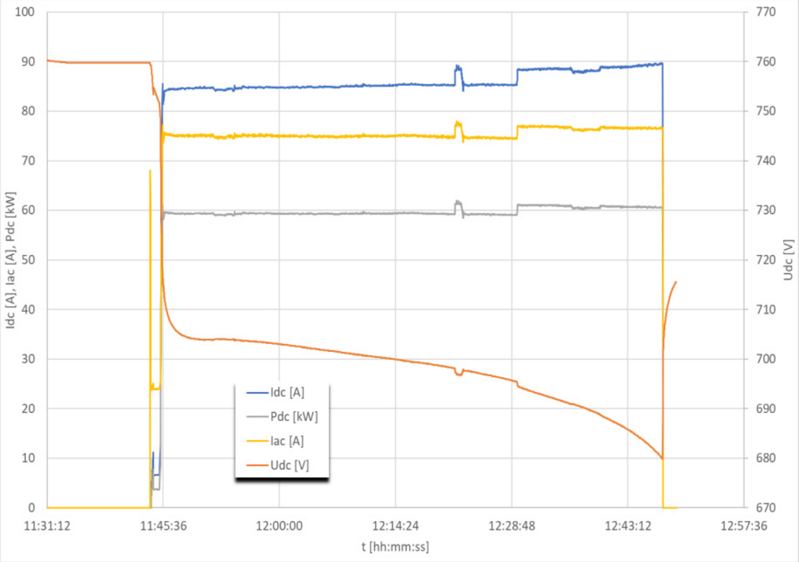

Figure 3. *Exemplary time curve of voltage, current and power registered during the discharging process*

Tests of the flameproof enclosure.

The tested object was a two-chamber flameproof enclosure for the power supply and control system HK-1 module (Fig. 4). During the tests, chambers were filled with elements simulating the inside electrical equipment.

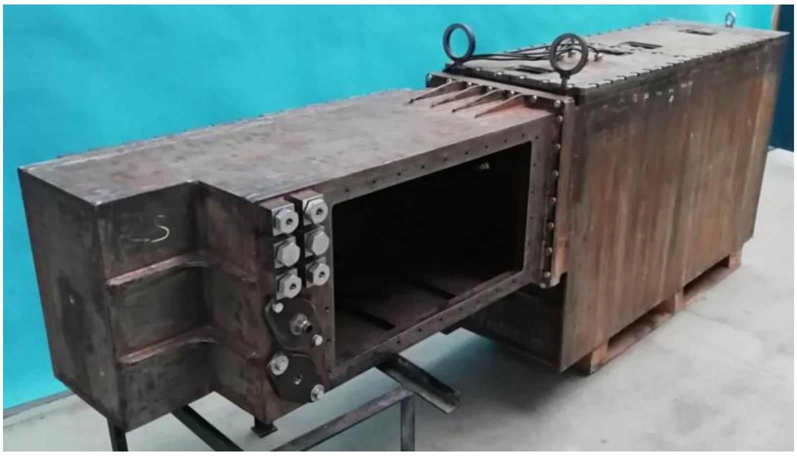

Figure 4. *Tested object*

The scope of the tests included the following measurements and checks:

- mechanical resistance to impact,
- degree of protection IP 54,
- flameproof joints,
- reference pressure,
- overpressure tests,
- non-transmission of an internal ignition.

The overpressure test consisted in evoking within the test chamber a pressure of 1.5 times the reference pressure. The test was carried out using the static method. The battery chamber pressure course from the test is shown in Fig. 5.

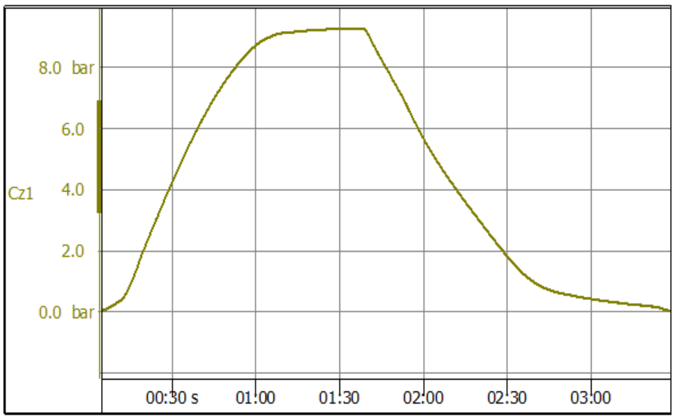

Figure 5. *The pressure curve registered under battery chamber overpressure test*

The non-transmission of an internal ignition tests were carried out in accordance with standard, using (12.5 ± 0.5)% of the mixture of hydrogen methane [(58 ± 1)% methane and (42 ± 1)% hydrogen] with air. Clearances and the length of flameproof joints were prepared before testing in accordance with the requirements of the standard. The test results are shown in Table 1.

Table 1. *Non-transmission of an internal ignition test results*

Lp.	*Chamber*	*Tests number*	*Transmission number*
1	**Battery chamber**	**10**	**0**
2	**Electrical equipment chamber**	**5**	**0**

Summary

The article discusses selected tests of the HK-1 module of the innovative mining roadheading machine BH3000B HYDKOM 75. The research concerned electrical and mechanical equipment (explosion proof housing). The scope of research, the research object and the test stand was presented. The course of individual tests and the results obtained from the tests were discussed in turn. As a result of the tests, HK-1 module design and construction assumptions regarding technical and functional parameters were confirmed.

Modelling of Cyclic Voltammetry

M. Mačák[a], P. Vyroubal[a]

[a] Department of Electrical and Electronic Technology, Brno University of Technology, Brno 616 00, Czech Republic

This article describes a numerical approach to the cyclic voltammetry. A custom model was implemented into Ansys Fluent. An analysis of a general one-electron reaction was carried out, which was in agreement with theoretical assumptions. The model was also adjusted for coupling between electrochemical and volumetric reactions.

Introduction

A cyclic voltammetry is an electroanalytical method used for analysing the behaviour of reduction and oxidation processes of molecular species. The method is based on the measurement of the resulting current as a function of an applied voltage. This paper describes a numerical approach to the cyclic voltammetry, which can be used as an alternative to experimental measurements. While the experimental measurements are not difficult nor expensive, numerical methods are beneficial as they can capture a broader range of information. For example, the time evolution of chemical species or individual reaction rates are difficult to obtain experimentally, but numerical results are easy to acquire. Numerical simulations can be also used for comparison, so potential inaccuracies could be discovered and fixed. (1, 2, 3)

Numerical model

A custom model, based on User-Defined Scalars, was created and implemented into Ansys Fluent. The model is based on the Nernst-Planck equation (4):

$$\frac{\partial c_i}{\partial t} + \nabla \cdot \left(c_i \boldsymbol{u} - D_i \nabla c_i - \frac{z_i F D_i}{RT} c_i \nabla \varphi \right) = 0 \qquad [1]$$

Where c_i is the molar concentration, t is the time, $\boldsymbol{v}$ is the velocity, D_i is the diffusion coefficient, φ is the electric potential, z is the charge number, F is the Faraday's constant, R is the molar gas constant and T is the thermodynamic temperature.

Cyclic voltammetry experiments use an abundant amount of an inert supporting electrolyte, which results in minimal ohmic losses in the electrolyte and so the migration term can be neglected (1, 2). This means that the diffusion is the only acting force on the ions:

$$\partial c_i / \partial t - \nabla \cdot (D_i \nabla c_i) = 0 \qquad [2]$$

The kinetics of reactions is defined by the Frumkin-Butler-Volmer equation (5):

$$j_{far} = j_0 \left[\frac{c_A}{c_{ref}} \exp\left(\frac{z \cdot F \cdot \alpha_A}{RT} \eta \right) - \frac{c_B}{c_{ref}} \exp\left(-\frac{z \cdot F \cdot \alpha_C}{RT} \eta \right) \right] \qquad [3]$$

Where j_0 is the exchange current density, η is the overpotential and $\alpha_{A,}\ \alpha_C$ are charge transfer coefficients.

The overpotential is calculated as a potential difference at the electrode-electrolyte interface. As described earlier, the ohmic losses in the electrolyte are minimal and so the electrolyte potential is set to zero and doesn't have to be resolved. The amount of reduced or oxidized species at the interface is calculated through the Faraday's law of electrolysis.

Results and discussion

A general one-electron electrochemical reaction was considered:

$$B + e^- \leftrightarrow A \qquad [4]$$

Then a cyclic voltammetry of four sweeps, with a scan rate of 0.1 V/s and an overpotential range of -0.5 V to 0.5 V, was carried out. The diffusion coefficient of the reactant and the product was set to $1 \cdot 10^{-9}$ m^2/s. Fig. 1. shows the resulting voltammogram. There is a minimal difference between individual sweeps as the properties of species are the same. The voltage difference between peaks was 60 mV which corresponds with a theoretical value of 59 mV for a one-electron reaction.

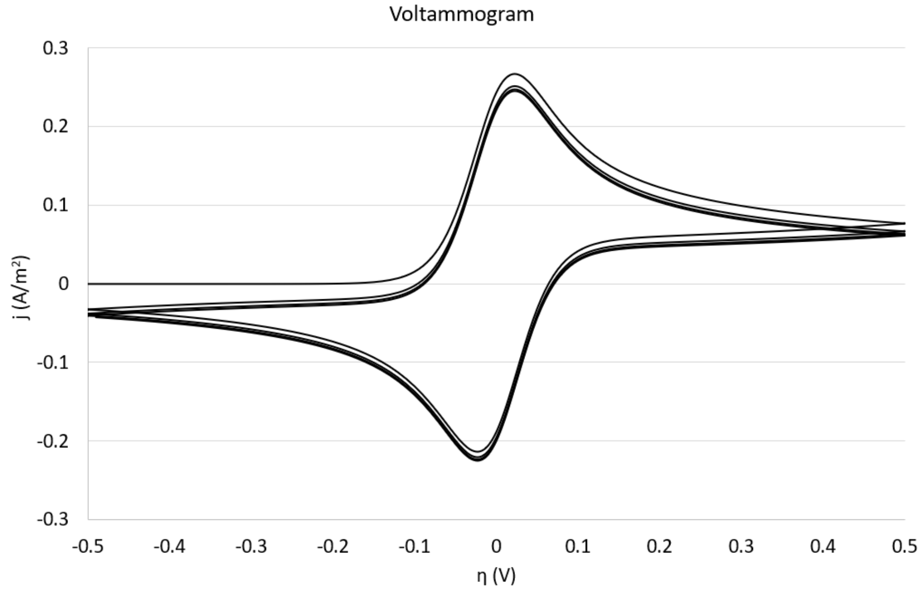

Figure 1. *Voltammogram of a general one-electron reaction*

The presented model can be also conveniently coupled with volumetric reactions. Fig. 2 describes a case similar to the previous one, but in this case, the product is transformed into an electrochemically inactive species by a chemical reaction. This results in a gradual decrease of the amplitude of the reduction and the oxidation peak.

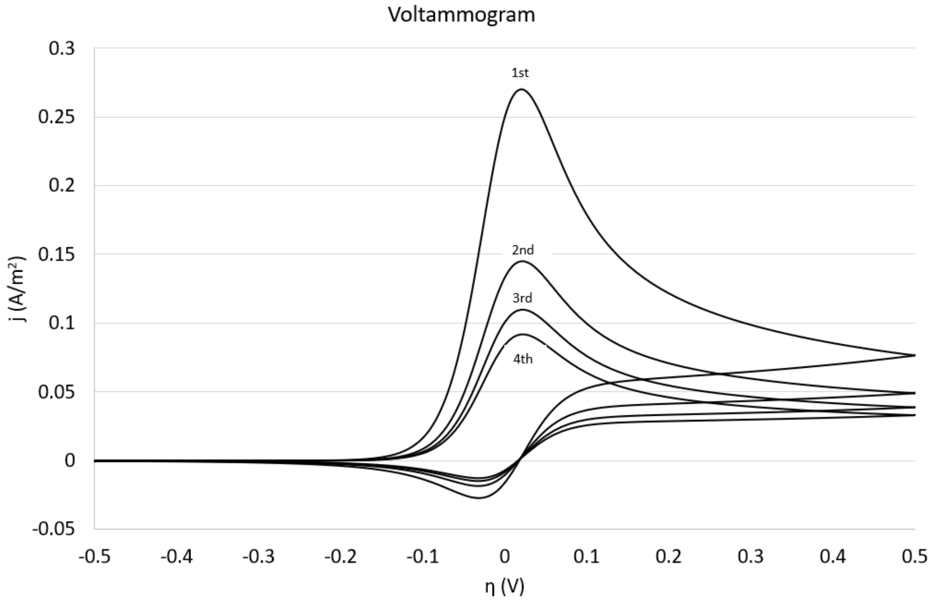

Figure 2. *Voltammogram of a one-electron reaction coupled with a volumetric reaction*

Acknowledgments

This work was supported by the BUT specific research programme (project No. FEKT-S-17-4595).

References

1. N. Elgrishi, K. J. Rountree, B. D. McCarthy, E. S. Rountree, T. T. Eisenhart, and J. L. Dempsey. *Journal of Chemical Education*, **95**(2), p. 197-206 (2017).
2. A. Eswari and L. Rajendran. *Russian Journal of Electrochemistry*. **47**(2), 181-190 (2011).
3. H. Wang, A. Thiele, and L. Pilon. *The Journal of Physical Chemistry C*, **117** (36), p. 18286-18297 (2013).
4. A. Lavacchi, U. Bardi, C. Borri, S. Caporali, A. Fossati, and I. Perissi. *Journal of Applied Electrochemistry*, **39**(11), p. 2159-2163 (2009).
5. A. V. Sokirko and F. H. Bark. *Electrochimica Acta*, **40**(12), p. 1983-1996 (1995).

Pragolab and Bio-Logic SAS: General Company Presentation

Pavel Janderka

Bio-Logic Science Instruments SAS is a French designer and manufacturer of high performance laboratory research instruments and software. The headquarters are based in Seysinnet-Pariset, France (close to Grenoble in the French Alps).

Founded in 1983 by a CNRS researcher Yves Dupont and an industrial partner, Bio-Logic SAS is currently headed by François GOY.

Bio-Logic SAS has designed instruments for a variety of domains and applications:

- Electrochemistry
- Rapid-Kinetics, Spectroscopy & Photosynthesis, including Circular dichroism
- Battery & energy devices testing
- Materials testing
- Electrochemical Scanning systems
- Electrophysiology

And wide range of tools and accessories, including Quartz crystal microbalances, rotating electrodes, spectroelectrochemistry, etc. Software EC-Lab® is a common platform for controlling all Bio-Logic potentiostats/galvanostats, be it single channel or multichannel systems and across all our hardware technologies. It is Windows based, compatible with either 64-bit or 32-bit operating systems.

Bio-Logic is a rapidly growing global company with affiliate offices in USA (**Bio-Logic USA**) and India (**Bio-Logic India**), and has a large and growing network of worldwide distributors (with representatives in most large and developing countries).

In 2012 **Bio-Logic acquired Uniscan Ltd**., a British specialist manufacturer of electrochemistry scanning instruments, expanding its product range in order to satisfy the expanding market of scanning electrochemical applications.

Our **GOALS**:

Developing high performance products with unmatched value and providing a high level support to our customers. Together with exclusive Czech and Slovak distributor Pragolab s.r.o., Biologic SAS guaranties the best quality of electrochemical instruments and their support on Czech and Slovak market.

Figure 1. *SECM150, new small footprint Scanning ElectroChemical Microscope, Fast scanning, <10 nm scanning resolution, fA current resolution*

Active balancing system of lithium cell batteries used in drive units of mining machinery

Sławomir Bartoszek, Jerzy Jura, Krzysztof Stankiewicz

Institute of Mining Technology KOMAG

The article presents the problem of active balancing of lithium cell batteries used in mining machines. The BMS, developed in ITG KOMAG, which supports high capacity lithium cells used in electric drives of mining machines were presented. The structure of the system with the description of the applied active balancing methods and algorithms of operation of individual modules, of which the system is composed, was described. The issue of proper communication and balancing in case of high capacity batteries, consisting of many cells divided into packets, is presented. Experiences from the implementation of the system on the battery of 8 cells with capacity of 40Ah, as well as from the cooperation with the battery composed of 224 cells with capacity of 100Ah were also presented.

Introduction

The latest electric batteries used in mining machines, developed by the Institute of Mining Technology KOMAG, are built from lithium cell batteries. It is connected with the necessity to use BMS (Battery Management System) to supervise their work, because improper use of this type of battery may endanger both the machine and employees. The BMS system not only ensures safety of use and reliability of work, but also extends the life of cells.

The article describes the BMS system of lithium cell batteries developed in ITG KOMAG, realizing active balancing of accumulated energy. Most of the currently used cell battery management systems use a passive balancing method based on the principle of dissipating excess energy in the form of heat. The active method described in the article works on the principle of receiving energy from overcharged cells and returning it to other, undercharged cells. This reduces, to a large extent, the adverse temperature phenomenon associated with energy dissipation, provides electricity savings and creates optimal working conditions for cells, resulting in extended battery life.

Structure of BMS

The structure of the system was described together with an indication of the applied balancing methods. In a single cell pack, the system uses the Cell to Pack method, which is based on transferring energy from an overcharged cell to the terminals of the entire battery or cell pack. In the case of large batteries consisting of multiple cell packs, a combined method of cell balancing is implemented, i.e. in addition to balancing a single cell packet, there is a charge equalisation between the packets.

The presented system is built of BMS-S modules assigned to each cell, measuring its parameters and carrying out the balancing process. In the case of large batteries, BMS-S modules are built on an additional board installed on each package, which has circuits related to communication and exchange of energy between packets. All modules are managed by a master control system BMS-M.

This chapter explains how the algorithms controlling the operation of BMS-S and BMS-M modules work. Fig. 1 illustrates the current distribution in the balancing circuits in different modes of operation.

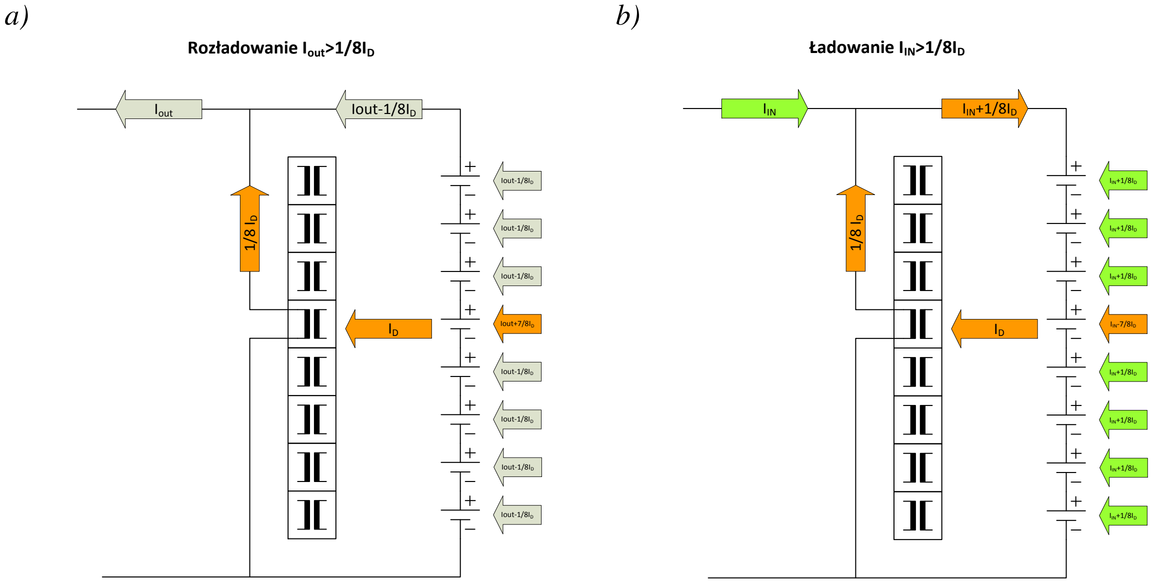

Figure 1. Method of transferring energy between cells in different battery modes: a) during discharge, b) during charging

The next part of the chapter presents the method of inter-packet balancing (Fig. 2).

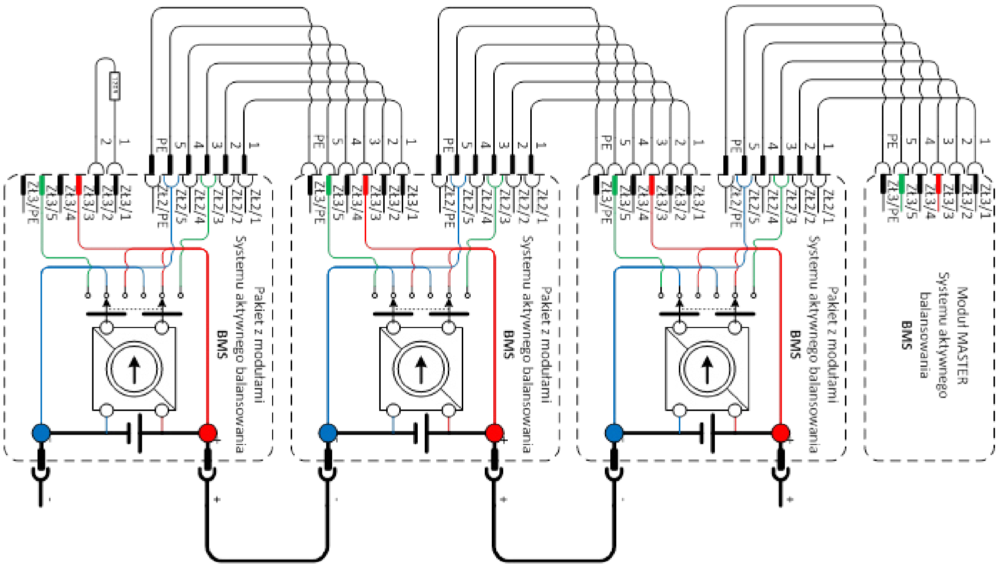

Figure 2. Connection diagram between packets with marked energy transmission paths

Implementation of BMS and results of tests

The last chapter describes experiences with the implementation of the developed circuit on a battery of 8 cells with a capacity of 40Ah (Fig. 3a), as well as with a battery of 224 cells with a rated voltage of 716.8 V, and the stored energy is 72 kWh. The single package of this battery is shown in Figure 3b. At the end, the results of the tests were described.

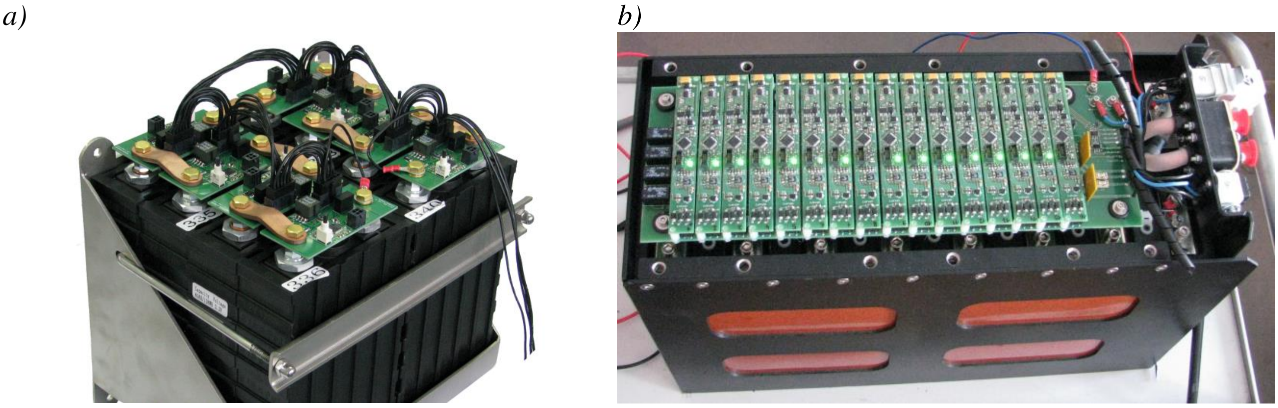

Figure 3. *Active BMS installed on: a) a battery containing 8 cells, b) a single package of 16 cells.*

Estimation of SOC of Li-ion Batteries

R. Cipin, M. Toman, P. Prochazka, and I. Pazdera

Department of Power Electrical and Electronic Engineering, Brno University of Technology, Brno, Technicka 12, 616 00, Czech Republic

This paper deals with problems with the estimation of the state of charge of Li-ion batteries. There are shown and disused two basic methods for estimation of the state of charge. There are discussed essential problems with an estimation based on so-called coulomb counting method and based on an equivalent circuit of Li-ion battery.

Introduction

The knowledge of battery state at any condition is important for battery lifetime. With maintaining battery limits, i.e., voltage current, temperature, the battery lifetime can be prolonged. In most situation, the limits parameters are minimal and maximal voltage and maximal loading current. For our study is chosen battery PANASONIC NCR18650A with parameters: minimal voltage 2.5 V, maximal voltage 4.2 V, nominal voltage 3.6 V, nominal capacity 3 A·h, and maximal current 6 A.

Estimation of SOC Based on Measured Battery Current

The state of charge (SOC) of battery is defined as a ratio of available capacity and battery rated capacity. Estimation of SOC is carried on with the following assumptions:

- Temperature influence of battery is neglected for estimation of SOC. The battery temperature strongly influences battery parameters, e.g., battery internal resistance, battery capacity, and so on, but all further mentioned methods for SOC estimation are generally valid.
- Voltage hysteresis during charging and discharging is omitted. This can be done for SOC greater than thirty percent with reasonable accuracy.
- Efficiency of battery charging, and discharging is neglected.

The simplest way to calculate SOC is by using a so-called coulomb counting method

$$z = z(t_0) - \frac{1}{Q}\int_{t_0}^{t} i_{\mathrm{bat}}(\tau)\mathrm{d}\tau, \qquad [1]$$

where z is the state of charge, Q is the battery rated capacity, i_{bat} is the battery current and t is the time. In this equation, discharging current has a positive sign and charging current has a negative sign.

In our case, a measurement error of current is about 17 mA, which corresponds to error about 0.57 % of battery nominal current. Based on this measurement error it can be easily calculated the maximal difference between estimated total battery capacity and real battery capacity as 0.034 A·h. This is a relatively small difference, but it is important to realize that is the error in only one cycle. And in only ten consequent cycles maximal error is about 10 % of battery nominal capacity. So, this method for estimation of battery capacity and also SOC is very dependent on the accuracy of the current measurement. Another drawback is that the final value of battery capacity is influenced by the efficiency of battery charging and discharging, i.e., by joule's losses transformed into heat during battery operation.

Another issue of SOC calculating based on [1] is that the initial value of the state of charge z(t0) is usually unknown or known only with limited accuracy. Actual value of SOC can be only measured with one full charging-discharging cycle, which is in common battery applications very problematic issue.

Estimation of SOC Based on Equivalent Circuit of Li-ion Battery

Previously mentioned way of SOC estimation has its limitation and it is enough only for very rough SOC estimation. The second approach for SOC estimation is based on an equivalent circuit of Li-ion battery. Figure 1 shows the simplest equivalent circuit of Li-ion battery, where R_i is the battery internal resistance, OCV is the open circuit voltage and v_bat is the battery terminal voltage.

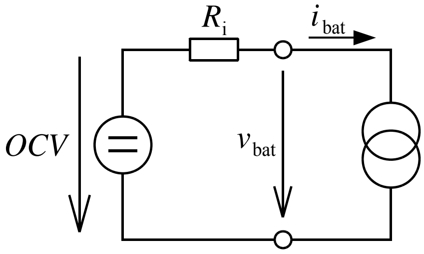

Figure 1. *Equivalent circuit of Li-ion battery – variation I.*

A battery voltage v_bat at the steady state is called an open circuit voltage (OCV), i.e., v_bat = OCV if and only if $t \to \infty$ and a battery current $i_\mathrm{bat} = 0$. At any transient state or during the charging/discharging even with a continuous current this statement is not valid. Usually, the steady state is reached after a time of the order of 24 h, see (1).

The battery OCV is dependent on the state of charge generally as $OCV = f(z)$ or in simplest way OCV(z). There is not any general function which can be used for approximation of OCV dependence on SOC, see (2). For many applications, it is most sufficient to use a lookup table with measured dependencies of OCV on SOC.

Based on Figure 1, it can be derived battery voltage as a function of battery current and SOC as follows

$$\mathrm{v_{bat}} = \mathrm{OCV(z)} - \mathrm{i_{bat}\,R_i}. \qquad [2]$$

From known (measured) values of actual battery voltage and current and known dependency of OCV on SOC, the actual value of the state of charge can be calculated from [2] as follows

$$\mathrm{z} = \mathrm{OCV^{-1}(v_{bat} + i_{bat}\,R_i)}. \qquad [3]$$

The advantage of computation of SOC by this way is that the value of SOC is estimated directly from measured values of battery voltage and current, and it isn't dependent on previous battery state as in case of SOC calculation based on [1].

The value of estimated SOC is highly dependent on the accuracy of measured voltage and current, and also on the precise knowledge of the battery inner resistance and dependence of SOC on OCV. Unfortunately, there is always present some error in measured quantities. The most practical way for SOC estimation can be by using filtered measured data but this solution doesn't bring any corrections against wrongly determined battery resistance or dependence of SOC on OCV.

The only accurate and practically usable solution can by using Kalman filters, see (3) and (4), or another optimal estimator algorithms, see (5) and (6), which use simultaneously equations [1] and [3] for estimation of SOC and also it filters all measured data.

Conclusion

The paper deals with the estimation of the state of charge of Li-ion batteries. There are shown two different approaches. The first one relies on accurate measurement of battery current during charging and discharging and SOC is estimated based on its value. The second approach is based on a simple equivalent circuit of the Li-ion battery where SOC is estimated based on actual values of battery voltage and battery current. Accurate knowledge of battery internal resistance and dependence of the open-circuit voltage on the state of charge is needed for this method.

Acknowledgments

This research work has been carried out in the Centre for Research and Utilization of Renewable Energy (CVVOZE). Authors gratefully acknowledge financial support from the Ministry of Education, Youth and Sports of the Czech Republic under NPU I programme (project No. LO1210).

References

1. S. Abu-Sharkh and D. Doerffel, *J. Power Sources*, **130**, 1-2 (2004).
2. I. Baccouche, S. Jemmali, B. Manai, N. Omar, and N. E. B.Amara, *Energies*, **10**, 6 (2017)
3. G. L. Plett, *Battery Management Systems, Volume I: Battery Modeling*, p. 346, Artech House Publishers (2015)
4. G. L. Plett, *Battery Management Systems, Volume II: Equivalent-Circuit Methods*, p. 336, Artech House Publishers (2015)
5. L. Ljung, System Identification: Theory for the User, p. 640, Prentice Hall (1999)
6. D. Simon, Optimal State Estimation: Kalman, H Infinity, and Nonlinear Approaches, p. 552, Wiley-Interscience (2006)

Protective and control systems of lithium-ion cells

Przemysław Deja, Wojciech Kurpiel

In the article the methods of balancing battery cells, made in the lithium-ion (Li-Ion) technology, used at the KOMAG research projects, are presented in the article. The most important advantages of the Li-Ion cells include quick charging, a big energy and power density as well as a broader scope of operation temperatures. However, these cells require an application of protective and control system of the cell battery (BMS), mainly due to a need of increasing operational safety. One of the most important functions of this system is an equalization (balancing) of the stored energy among the cells and the packets of cells. The active BMS system and the method of active balancing, developed of the KOMAG Institute, are presented in the article. The tests, comparing an operation of the lithium cells battery with a connected BMS system and of the battery operating without the protective-control system, are described.

Introduction

Batteries, built of lithium cells, appeared in a commercial applications at the beginning of the nineties and since then they have started to be more and more commonly used. At present different types of lithium batteries are available and their implementation possibilities increase. They are commonly used in mobile phones, tablets, laptops, cameras, electrotools, electric and hybrid cars, aviation and also in the mining industry, where they start to eliminate lead-acid batteries which have been used for years.

Lithium batteries offer the biggest energy density among all the batteries available on the market. However, they require special attention because both their overcharging as well as excessive discharging may lead to durable damage. That is why it is needed to apply appropriate protections, mainly electronic ones, and also a special housing protecting against overheating, humidity, vibrations and mechanical damages to avoid such damages.

Differences in the amount of energy stored in cells of the battery system, are very significant as regards the battery life, because without balancing system, the voltages of individual cells can differ considerably after some time. The capacity of the whole packet can also decrease quickly during its operation which causes a loss of the total battery system capability to continue its operation.

An effective diagnostics of cell battery packets is required for their functioning as reliable and stable electric energy sources as long as possible, being characterized by a high power efficiency and a high safety level. An efficient protection of cells is usually realized by an application of special electronic systems, determined by the BMS initialism (Battery Management System), which are made for the determined battery structure. In particular, it concerns a number, type and method of connecting cells.

The BMS system often performs a few tasks such as: voltage, current and temperature measurements, charge level of cells, protection of cells, temperature management, checking of charging/discharging procedures, obtaining data, communication with internal and external modules, monitoring and storage od earlier data and voltage equalizing of the battery cells, called balancing of cells.

Tests of lithium cells

The tests of lithium-ferric-phosphate ($LiFePO_4$) batteries of 10 Ah capacity are described. Two BMS systems were used for tests: passive and active. The tests were conducted at the KOMAG Institute, using a test rig prepared for this purpose. The test rig for testing lithium cell batteries is shown in Fig.1.

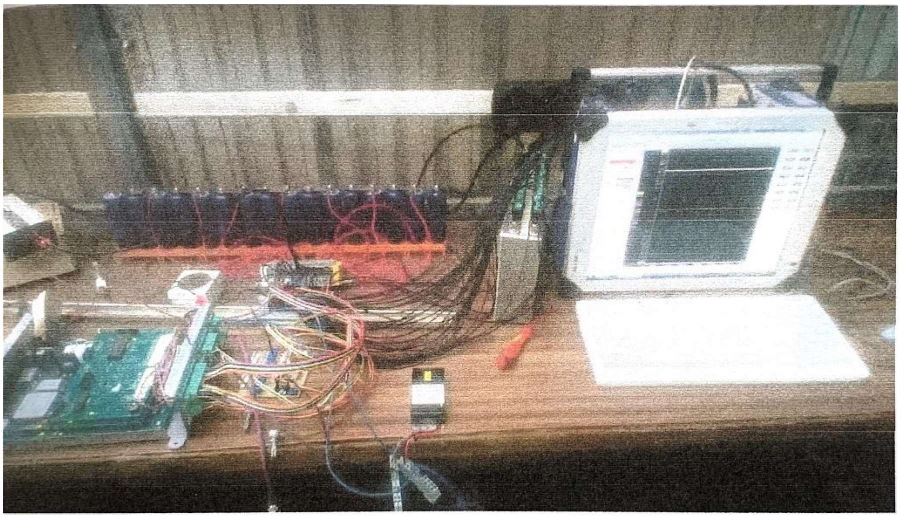

Figure 1. *Test rig for lithium cell batteries*

The tests consisted in discharging and charging od 16 cells to limit values given by the producer, and in measurements of the whole cycle lasting time (charging and discharging). An exemplary graph, presenting a process of discharging cells, is shown in Fig.2. Series of comparative tests in different configurations were conducted:

- only with a controller of cells without balancing,
- with a controller of cells and with passive balancing,
- with a controller of cells and with active balancing.

Next the results of testing lithium cells in different configurations were compared. In all the cases the same regularity was observed. During the discharge of cells the first extreme cell from the negative end side discharged faster than the other ones. This effect occurred in each cycle of testing cells

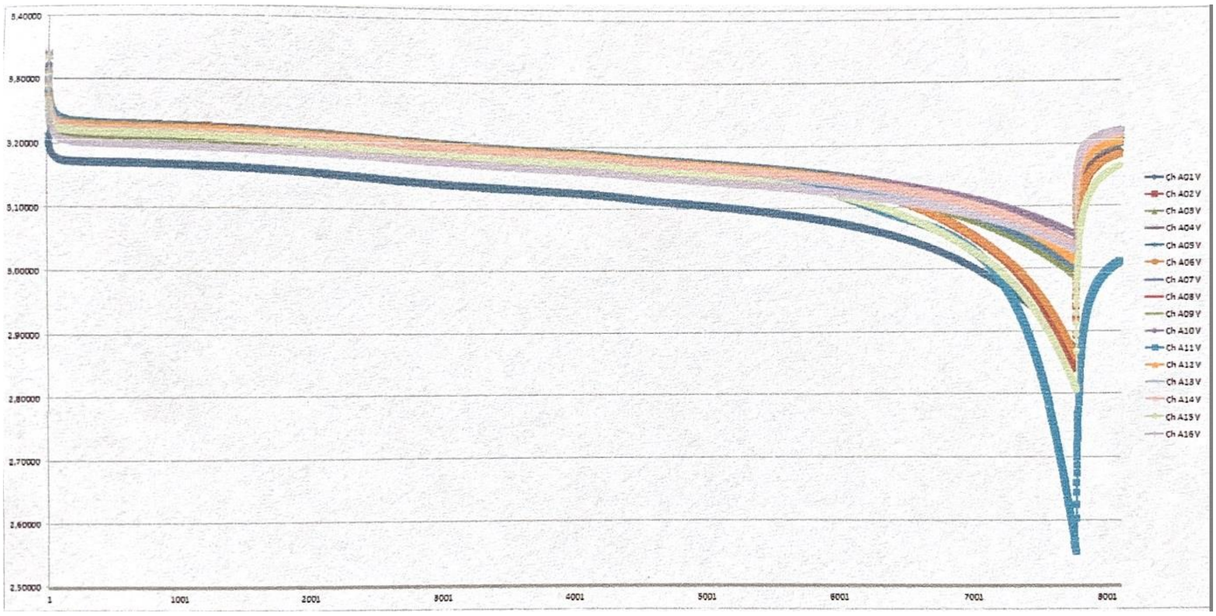

Figure 2. *Exemplary graph of discharging cells of lithium batteries*

Summary

Detailed information on testing Li-Ion cells, used in the systems developed at the KOMAG Institute, will be presented in the article. The test results obtained for an application of different balancing methods will be described. The issues related to the biggest wear of the cells connected to the battery negative end will be discussed. Some development trends in this scope will be presented and the directions of further research will be indicated.

Surface Structure Evaluation of Functional Surfaces after Plasma Nitriding

D. Dobrocký [a], Z. Pokorný [a], Z. Joska [a], Petr Dostál [b], Nela Poláková [b]

[a] Department of Mechanical Engineering, University of Defence in Brno, Kounicova 65, 602 00 Brno, Czech Republic

[b] Department of Technology and Automobile Transport, Mendel University in Brno, Zemědělská 1, 613 00 Brno, Czech Republic

With increasing demands on the functional properties of machine parts, the demands on the quality of their surfaces are increasing. Any technological method used to realize the surface of functional surfaces leaves unevenness, which is essential for the function of these surfaces. The increase of the functional properties of functional surfaces can be realized by using the plasma nitriding method. However, the used diffusion technology also changes the surface structure of the components. The presented paper deals with evaluation of the change of the structure of the ground functional surfaces of steel 42CrMo4 after plasma nitriding. Furthermore, the change in surface hardness and friction and wear coefficient, which have a direct effect on the functional properties, was analysed. The surface structure deteriorates and the friction coefficient is slightly increased after plasma nitriding. However, the wear coefficient reaches lower values, which, together with an increase in surface hardness, result in the use of this technology for exposed components.

Effect of Cycling Ageing on Impedance Spectra of $LiMn_2O_4$-electrodes

M. A. Kamenskii[a], S. N. Eliseeva[a], V. V. Kondratiev[a]

[a] Institute of Chemistry, Saint Petersburg State University, Saint Petersburg, 199034, Russia

Electrochemical properties and kinetic parameters of LMO electrodes with two different binders were investigated. It was shown that long-cycling ageing has influence on the charge transfer resistance. Additional film resistance (mainly due to solid electrolyte interface layer) is appeared after long-term cycling.

Introduction

$LiMn_2O_4$ (LMO) is one of promising and commercial materials for lithium-ion batteries. However, it undergoes slightly decreasing of the electrochemical properties that connected with some internal changes in the cell and called ageing of material or battery. There are two kind mechanisms of ageing: cycle-ageing and calendar-ageing (1). And it is important to know how the electrochemical properties of LMO will be changed during cycle-ageing or long cycling and how to increase the cycle lifetime of material. One of the ways is creating a protective coating on the surface of the grains. So, in (2) it was observed that using the binder based on conductive polymer poly(3,4-ethylenedioxythiophene):polystyrenesulfonate/carboxymethylcellulose (PEDOT:PSS/CMC) leads to increasing of functional characteristics of electrodes such as practical capacity and stability during long-term cycling in comparison with electrodes in which polyvinylidene fluoride (PVDF) is used. Furthermore, decrease of charge transfer resistance (R_{ct}) and increase of conductivity was also observed. Therefore, there is a question in the reasons of these effects which appears after long-term cycling.

In this study two types of LMO-electrodes with different binders were investigated. Ratio of components is given in table I. Viscous slurry was cast on Al foil by Dr.Blade applicator (300 μm) and then dried under vacuum for 6 hours. LMO-electrodes were investigated by cyclic voltammetry, galvanostatic charge/discharge and electrochemical impedance spectroscopy (EIS).

TABLE I. *Composition and average mass of LMO-electrodes.*

Sample	LMO, wt %	C, wt%	PEDOT:PSS, wt%	CMC, wt%	PVDF, wt%	m_{LMO} , mg
LMO_{PVDF}	80	10	–	–	10	16.0
LMO_{comb}	86	10	2	2	–	15.7

The goal of this work

To establish the difference in the kinetics of lithium intercalation/deintercalation during long charge-discharge process, LMO-electrodes were investigated by electrochemical impedance spectroscopy before and after 100 cycles of charge-discharge (at 1 C current) in coin-cells using commercial electrolyte TC-E 918 (1 M $LiPF_6$ in 1:1 EC/DEC) and Li foil as counter and reference electrode. Impedance measurements were carried out at E = 4.3 V vs Li/Li^+ after duration 2 hours.

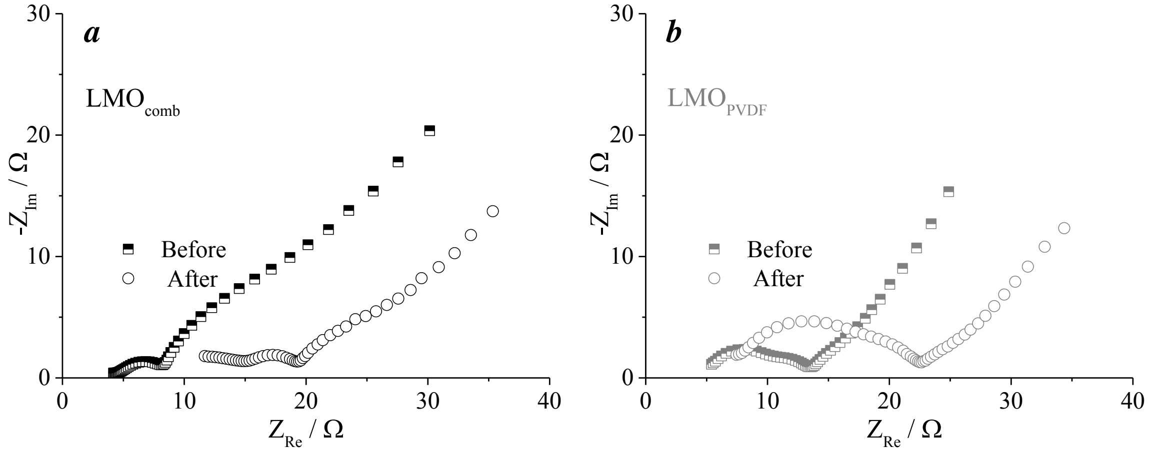

Figure 1. *EIS of LMO-electrodes with two different binders before and after long-term cycling (100 cycles) at E = 4.3 V; a) LMO_{comb}; b) LMO_{PVDF}.*

Results and discussion

From these data it could be seen that shape of electrochemical impedance spectra is dependent on the state of cycle lifetime of material. For LMO_{comb} before long cycling one semicircle is observed, and it increases after long-term cycling (Fig.1,*a*). Two semicircles on EIS of LMO_{PVDF}-electrode are observed before and after long cycling (Fig.1,*b*). One of them is associated with charge transfer on the interphase grain LMO/electrolyte (R_{ct}) and depressed part of another semicircle exists at high frequencies. After long-term cycling both semicircles are increasing. After long-term charge-discharge cycling on EIS of both electrodes in high frequencies region an additional part of semicircle appears and develops which could be linked with solid electrolyte interface layer on the surface of the electrode (3). R_{ct} values are about in 2 times higher for LMO_{PVDF} than for LMO_{comb}. Using R_{ct} values, exchange current density were evaluated. Values are presented in table II.

Using the equation below, from Z_{Re}, $-Z_{im} - \omega^{-1/2}$ curves apparent diffusion coefficients were calculated. The data are given in table II.

$$D_{\text{app}} = \frac{R^2T^2}{2A^2n^4F^4c^2\sigma_W^2} \qquad [1]$$

where *R* – universal gas constant, *T* – temperature (K), *F* – Faraday constant, *n* – number of electrons (0.5), σ_w – the Warburg constant, *A* – real surface area (cm^2).

TABLE II. *Kinetic parameters of LMO-electrodes in before and after long cycling*

Sample	State	R_{ct}, Ohm	$\sigma_{W, Ohm\cdot s^{-1/2}}$	D_{app}, $cm^2\cdot s^{-1}$	i_0, $A\cdot cm^2$
LMO_{PVDF}	Before	9	13.7	$1.2\cdot10^{-15}$	$9.1\cdot10^{-5}$
	After	15.2	9.3	$2.7\cdot10^{-15}$	$5.4\cdot10^{-5}$
LMO_{comb}	Before	5.2	16.1	$9.7\cdot10^{-16}$	$1.5\cdot10^{-4}$
	After	9.6	10.1	$2.5\cdot10^{-15}$	$8.1\cdot10^{-5}$

It observed that the values of diffusion coefficients are similar after long cycling for both type of electrodes. It is an expected outcome because diffusion coefficient is related to electroactive grain and not included the binder influence. Thus, it could be concluded that increasing of specific capacity and stability of LMO_{comb}-electrodes during 100 cycles at 300 µm thickness layer are explained by more dense electric contact between electroactive grains and between grains and Al foil. It is seen that R_{ct} values for LMO_{comb} is lower almost in 2 times than for LMO_{PVDF} at the same mass loading and values of exchange current density show the similar trend.

Acknowledgments

The financial support from the St Petersburg State University (grant № 26455158) is gratefully acknowledged. The authors would like to thank the Interdisciplinary Center for Nanotechnology Research park of Saint Petersburg State University.

References

1. P. Svens et al, *J. Power Sources*, **270**, 131 (2014)
2. K. Vorobeva et al, *J. Alloys Compd.* **766**, 33 (2018)
3. D. Aurbach et al, *J. Electrochem. Soc.,* **147**, 1322 (1998)

Corrosion resistance of plasma nitrided ferritic steels X12Cr13 and X6Cr17

P. Faltejsek, D. Kusmič[a], O. Čech[b]

[a] University of Defence, Department of Mechanical Engineering, Brno, Czech Republic, EU

[b] Brno University of Technology, Department of Electrical and Electronic Technology, Brno, Czech Republic, EU, ondra.cech@seznam.cz

The ferritic stainless steels X12Cr13 and X6Cr17 were subjected to plasma nitriding at temperature of 400°C and 550 °C, 24 h in 3H2:1N2 (l/h) and 1H2:3N2 (l/h) nitriding gas ratio and compared to untreated one. The microstructure and microhardness of the untreated and nitrided stainless steel were evaluated. The corrosion properties of the untreated and plasma nitrided steel samples were evaluated using the anodic potentiodynamic polarization tests in neutral 2.5% NaCl deaerated solution. The phase analysis of nitrided steels samples was compared to untreated one. The results showed that plasma nitriding process on the X12Cr13 and X6Cr17 steels produced a nitride case with iron carbides Fe3C and iron nitrides Fe4N at lower temperature and above that chromium nitrides Cr4N4 and chromium iron carbide Cr15Fe7C6 at higher temperature of plasma nitriding process. Plasma nitriding process significantly increased the surface hardness of the martensitic stainless steels. The pitting was evaluated, and the pitting coefficient was calculated. During electrochemical corrosion tests, the untreated X12Cr13 and X6Cr17 stainless steels showed mostly slightly higher corrosion rates compared to plasma nitrided steel at lower temperature and extremely lower corrosion rate compared to plasma nitrided steel at higher temperature of plasma nitriding process.

Comparative analysis of inserted temperature probe in the differentially pumped chamber.

P. Hlavatá[a], J. Maxa[a], P. Vyroubal[a]

[a] Department of Electrical and Electronic Technology, Brno University of Technology,
Technická 10, 616 00 Brno, Czech Republic

This article deals with the experimental chamber preparation, on which stagnation and static temperature (besides others) will be measured. The results obtained from measurement will be compared with the results from mathematical – physics analysis of Ansys Fluent system and in this system, the temperature running and expected ratios for planned experimental measuring also will be mapped in the supersonic flow in the experimental chambers.

Introduction

At the department of electrical and electronic technology FEEC BUT with the cooperation of the Institute of scientific instrument CAS, we prepare the production of the experimental chamber. This experimental chamber consists of a specimen chamber and a differentially pumped chamber (1). Both chambers are separated by a small aperture with a diameter of 0.5 mm. The aperture separates the area of the specimen chamber with the pressure of 2000 Pa from the differentially pumped chamber with the pressure of 40 Pa as is usual in an environmental scanning electron microscope (2, 3). The calculation was made as 2D axisymmetric with the boundary conditions shown in fig. 1.

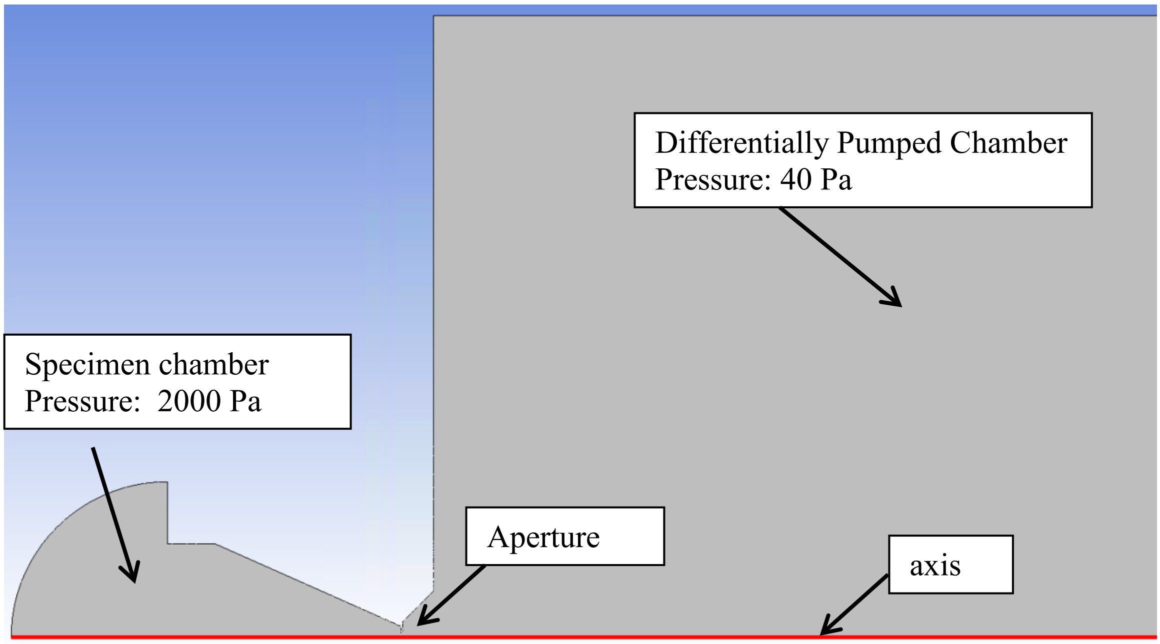

Figure 1. *2D axisymmetric profile with boundary condition*

The velocity running in the axis of the flow above the aperture will be measured (besides others) in the experimental chamber, see fig. 2A. Also, the static temperature will be captured on the path of the distance of 5mm above the aperture (4,5). The state of the inserted probe with a diameter of 0.5 mm put to the distance of 1.5 mm from the aperture is shown in fig 2B. Due to temperature measuring in the supersonic flow it was necessary to realize mathematical – physics analysis because of the measuring probe, which won't be measuring static temperature (in fig. 2B the blue and purple line) but it will measure stagnation temperature on the probe head in the braked flow (fig. 2B the green line).

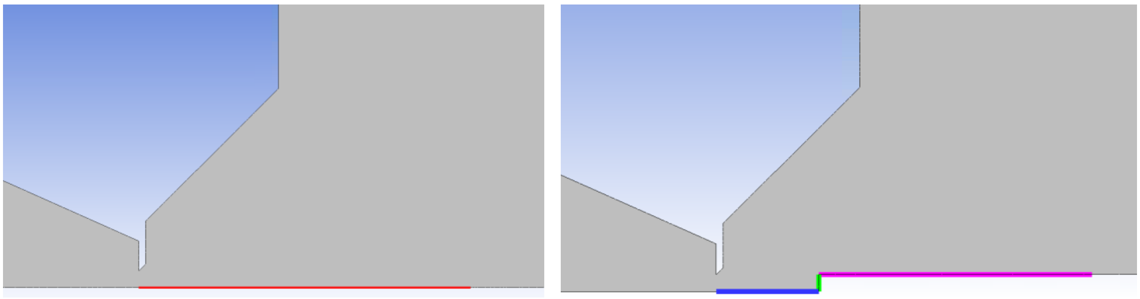

Figure 2. *Observed line: without inserted probe (A), with inserted probe (B)*

Temperature measuring in supersonic flow

In the supersonic flow, stagnation temperature is known as total air temperature and is measured by a temperature probe mounted against the direction of the measured flow. As the air is brought to rest, kinetic energy is converted to internal energy. The air is compressed and experiences an adiabatic increase in temperature. Therefore, total air temperature is higher than the static (or ambient) air temperature (6).

Total air temperature is an essential input to an air data computer to enable the computation of static air temperature and hence true airspeed.

The relationship between static and total air temperatures is given by:

$$\frac{T_{stagnation}}{T_{static}} = 1 + \frac{\mu - 1}{2} M^2 \qquad [1]$$

where: μ - Poisson constant for the air = 1,4, M – Mach number from the calculation for given state = 2,76 (Fig.6).

Results and discussions

From the results obtained using mathematical – physics analysis for the flow without the inserted probe, the temperature running of the static temperature in the distance of 1.5 mm from the edge of the aperture is 123 K (see fig 3A and 5) and the Mach number is 2,76 (see fig 4A and 6). With the inserted probe, the stagnation temperature is 315.5 K, which is situated on the head of the probe. Using the given relationship for the stagnation and static temperature ratio, the theoretical static temperature for the given place is 125 K.

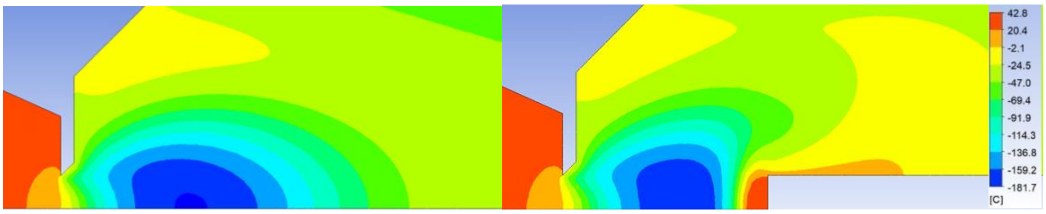

Figure 3. *Static temperature layout for variant without probe (A) and with inserted probe (B)*

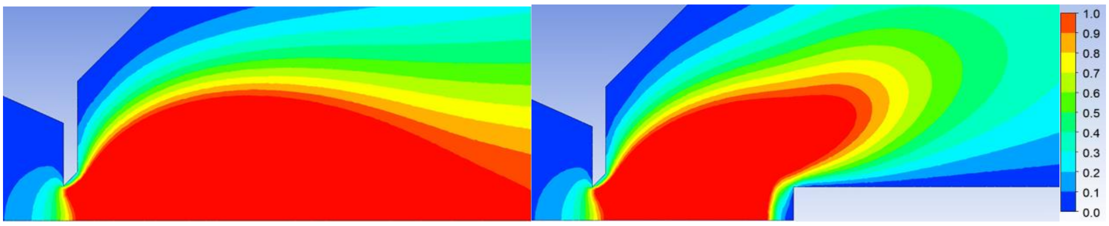

Figure 4. *Mach number layout for variant without probe (A) and with inserted probe (B)*

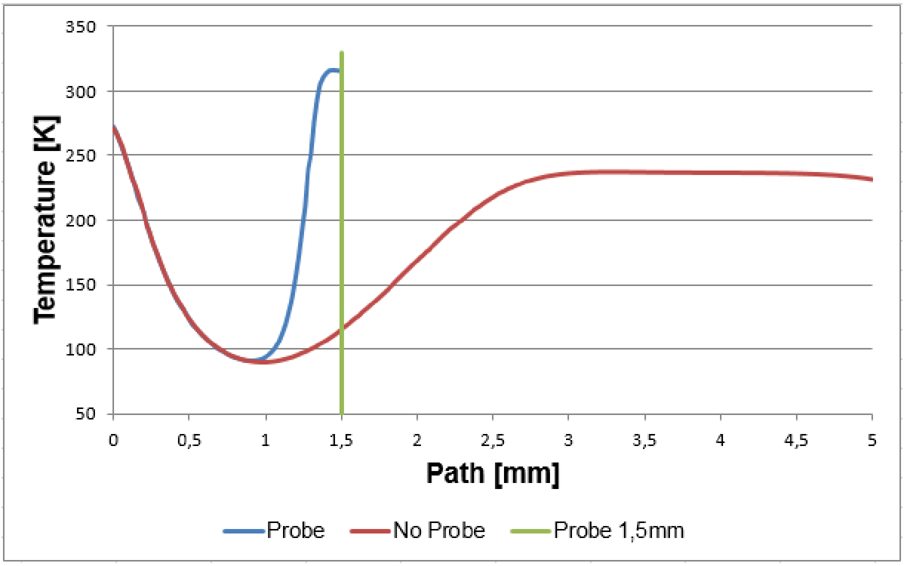

Figure 5. *Temperature running on path with and without probe*

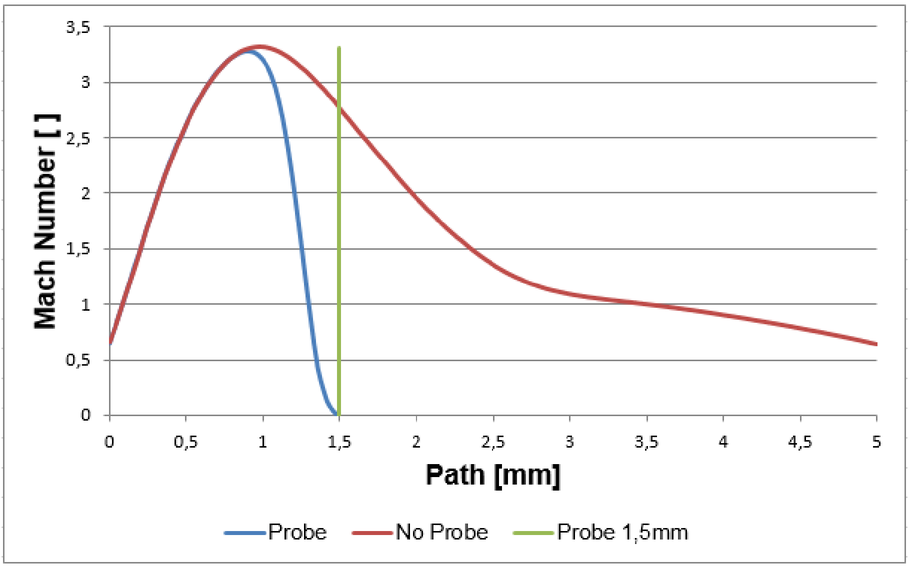

Figure 6. *Mach number running on path with and without probe*

Listed analysis mapped the temperature running and expected ratios for planned experimental measuring in the supersonic flow in the experimental chambers.

Acknowledgments

This research has been carried out in BUT specific research programme (project No. FEKT-S-17-4595).

References

1. J. Maxa; M. Bílek; P. Hlavatá; P. Vyroubal and K. Lepltová, Comparisons Using Methods of Continuum Mechanics and Monte Carlo at Differentially Pumped Chamber. Advances in Military Technology, vol. 11, no. **2**, p. 143-150. ISSN: 1802-2308. (2016).
2. P. Vyroubal; J. Maxa; V. Neděla; J. Jirák and K. Hladká, Apertures with Laval Nozzle and Circular Orifice in Secondary Electron Detector for Environmental Scanning Electron Microscope, Advances in Military Technology, vol. 8, no. **1**, p. 59-69, (2013).
3. J. Maxa and V. Neděla, The Impact of Critical Flow on the Primary Electron Beam Passage through Differentially Pumped Chamber. Advances in Military Technology, , vol. 6, no. **1**, p. 39-46. ISSN 1802-2308, (2011).
4. J. Maxa; V. Neděla; J. Jirák; P. Vyroubal and K. Hladká, Analysis of gas flow in a secondary electron scintillation detector for ESEM with a new system of pressure limiting apertures. Advances in Military Technology, vol. 7, no.**2**, p.39-44, (2012).
5. M. Řehák, Popis stavového chování plynu, p.273, ZU, Plzeň (2013).
6. V. Uruba, Metody analýzy signálů při studio nestacionárních jevů v proudících tekutinách, p. 58, ČVUT, Praha (2006)

Comparison of the solver setting in Ansys Fluent system.

A. Maxová[a], P. Hlavatá[b], J. Maxa[b]

[a] The St. Cyril and Methodius Comprehensive School and Pedagogical High School Brno

[b] Department of Electrical and Electronic Technology, Brno University of Technology, Technická 10, 616 00 Brno, Czech Republic

The article deals with the comparison of each solver variants and its discretization of Ansys Fluent system. Each variant is more suitable for different type of flow calculation. Because of this reason, we calculated the same type of flow with each solver and discretization variant. From the results it was chosen the most optimal variant.

Introduction

A flow in apertures has a special property so-called critical flow. This phenomenon is characteristic with sharp pressure and temperature gradients behind the aperture which has big claims on the computational solution. For this reason, a comparison study of the solver scheme and discretization set was made in the Ansys Fluent system (Fig. 1) (1).

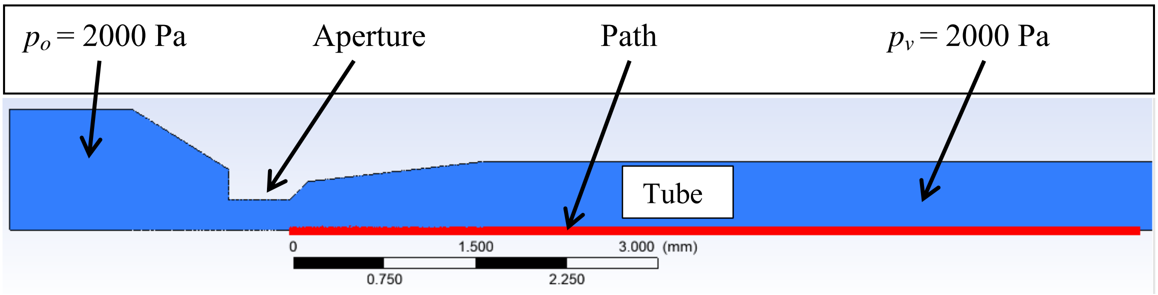

Figure 1. *Boundary conditions*

Solver setting in Ansys Fluent

Ansys Fluent enables to set of two types of the solver setting: Pressure-Based a Density-Based in which are other possibilities of a more detailed setting.

From the momentum transport equations, in Pressure Based Segregated method, first is determined medium velocity (component of the pressure gradient is ignored), using pressure equation the pressure field is determined, which is used for the adjustment of the velocity (simple deviations of the pressure field are determined) and then the energy equation is solved. In the Pressure Based Coupled method, the pressure and the velocity are solved in parallel. In the Density Based method, the pressure, velocity, and energy are solved concurrently (2,3).

These methods were examined in combination with the solver discretization: First-order upwind, where it is assumed that the value on the wall is equal to the value in the center of the cell laying on the left side in front of the flow (Fig. 2) (4).

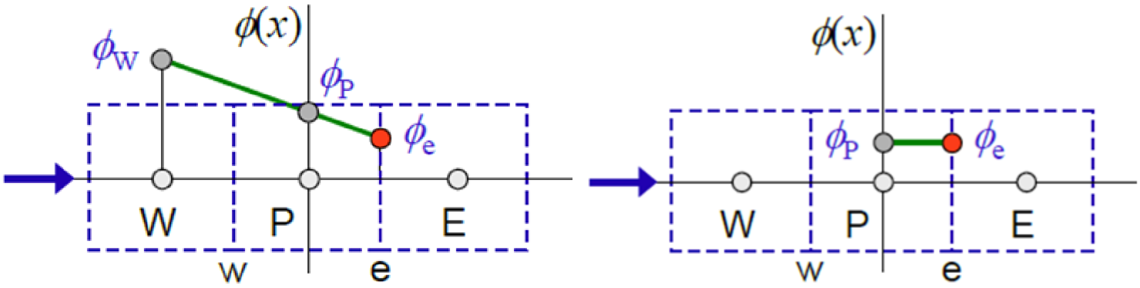

Figure 2. *First Order discretization (A), Second Order discretization (B)*

For the options, the scheme and discretization variants were chosen: Pressure Based Segregated First Order (PBS-F) (fig. 2A), Pressure Based Segregated Second Order (PBS-S) (fig. 2B), Pressure Based Coupled Second Order (PBC-S) (fig. 2B), Density Based Second Order (DB-S) (fig. 2B).

The aperture which separates both chambers was chosen according to the most using diameter of 0.5 mm in an electron microscope (fig. 1) and the diameter of the tube behind the aperture was chosen as so-called computational cross section for the supersonic cone according to the physical flow patterns for isoentropic flow, where it applies:

$$\frac{v_v}{v_{kr}}=\left[\frac{(\chi+1)M^2}{2+(\chi-1)M^2}\right]^{\frac{1}{2}} \quad [1]$$

$$\frac{v_v}{v_o}=\left[\frac{2}{2+(\chi-1)M^2}\right]^{\frac{1}{2}} \quad [2]$$

$$\frac{T_v}{T_o}=\frac{2}{2+(\chi-1)M^2} \quad [3]$$

$$\frac{p_v}{p_o}=\left[\frac{2}{2+(\chi-1)M^2}\right]^{\frac{\chi}{\chi-1}} \quad [4]$$

$$\frac{\rho_v}{\rho_o}=\left[\frac{2}{2+(\chi-1)M^2}\right]^{\frac{1}{\chi-1}} \quad [5]$$

$$\frac{\rho_v}{\rho_{kr}}=\frac{A_{kr}}{A}=M\left[\frac{\chi+1}{2+(\chi-1)M^2}\right]^{\frac{1\chi+1}{2\chi-1}} \quad [6]$$

Kde: M – Mach Number, v_v – output velocity, v_{kr} – critical velocity, v_o – input velocity, T_v – output temperature, To – input temperature, pv – output pressure, po – input pressure, ρ_v – output density, ρ_o – input density, ρ_{kr} – critical density. A – computational cross section, A_{kr} – critical cross section, χ – Gas constant.

Of given relationships the computational cross section of the supersonic flow was calculated for given Boundary Conditions which arises behind the critical cross section of 1.13 mm what ensures undisturbed supersonic flow in which the objective evaluation of chosen variant will be made (5,6).

Results and discussions

The comparison of each variant produced expected results. Variants Pressure Based segregated with First and Second Order, where the velocity is subordinate, during the calculation, to the pressure results, could not be able to capture sharp gradient which the supersonic flow brings (Fig. 3 and 4). On the contrary up to the velocity of 2 Mach, which occurs behind the aperture, the solver Pressure Based Coupled was able to give comparable results to the Density Based, which is more demanding to the convergence.

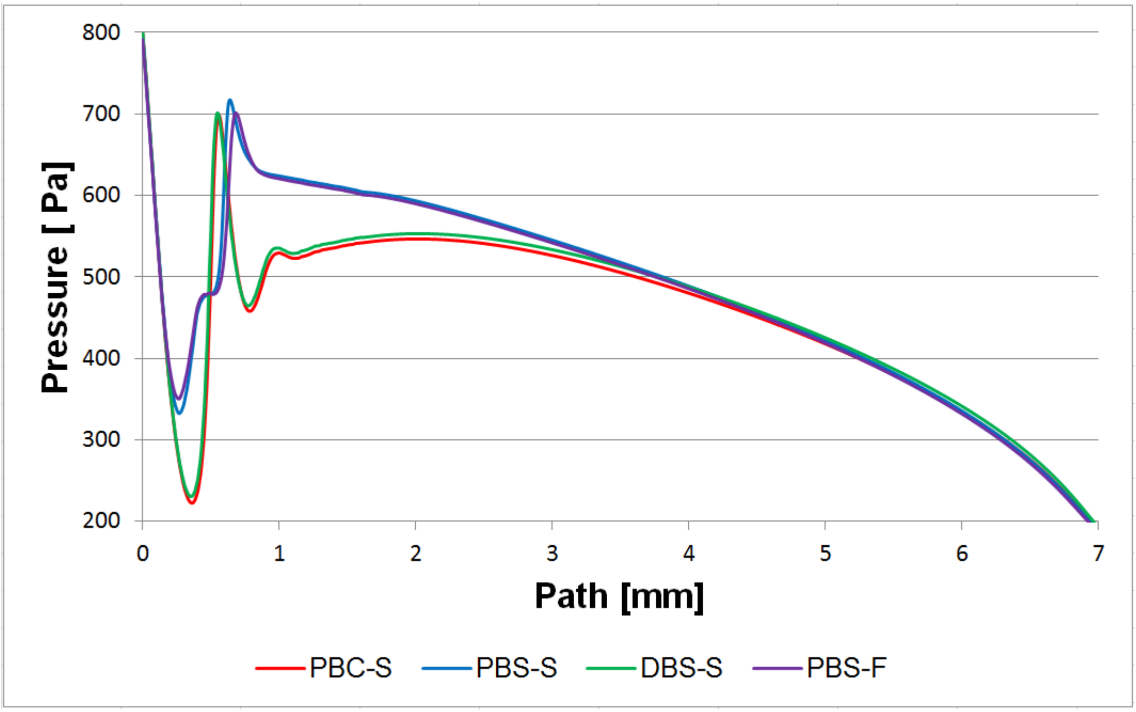

Figure 3. *Pressure running on path above aperture*

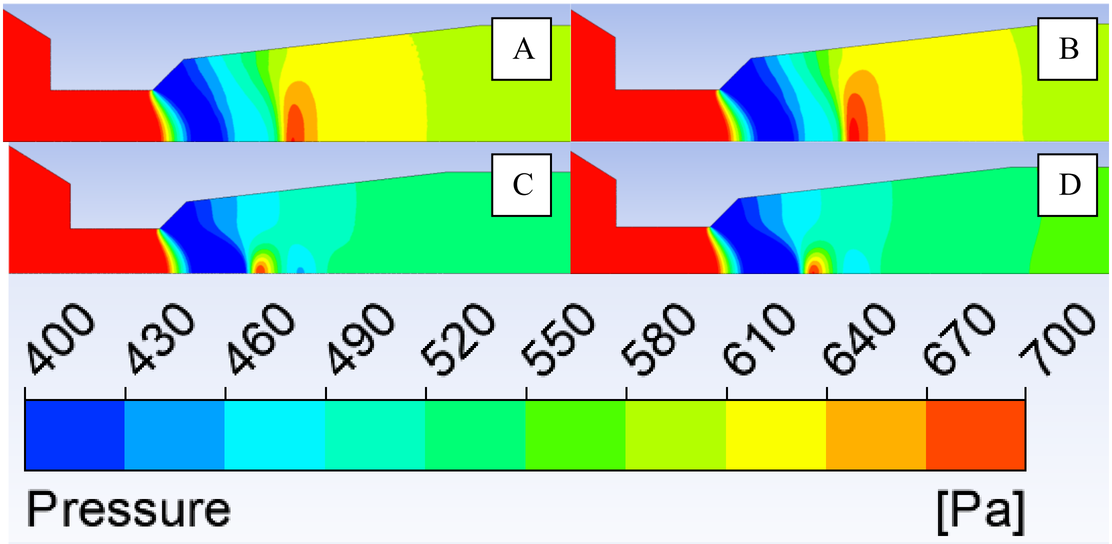

Figure 4. *Pressure layout of each variant A: PBS-F, B: PBS-S, C: PDC-S, D: DB-S.*

Acknowledgments

This research has been carried out in BUT specific research programme (project No. FEKT-S-17-4595).

References

1. J. Maxa; M. Bílek; P. Hlavatá; P. Vyroubal and K. Lepltová, Comparisons Using Methods of Continuum Mechanics and Monte Carlo at Differentially Pumped Chamber. Advances in Military Technology, vol. 11, no. **2**, p. 143-150. ISSN: 1802-2308. (2016).
2. P. Vyroubal; J. Maxa; V. Neděla; J. Jirák and K. Hladká, Apertures with Laval Nozzle and Circular Orifice in Secondary Electron Detector for Environmental Scanning Electron Microscope, Advances in Military Technology, vol. 8, no. **1**, p. 59-69, (2013).
3. J. Maxa and V. Neděla, The Impact of Critical Flow on the Primary Electron Beam Passage through Differentially Pumped Chamber. Advances in Military Technology, , vol. 6, no. **1**, p. 39-46. ISSN 1802-2308, (2011).
4. J. Maxa; V. Neděla; J. Jirák; P. Vyroubal and K. Hladká, Analysis of gas flow in a secondary electron scintillation detector for ESEM with a new system of pressure limiting apertures. Advances in Military Technology, vol. 7, no.**2**, p.39-44, (2012).
5. V. Neděla; E. Tihlaříková; J. Runštuk; J. Hudec, High-efficiency detector of secondary and backscattered electrons for low-dose imaging in the ESEM. Ultramicroscopy, p. 1-11. ISSN 0304-3991, (2018).
6. M. Daněk, Aerodynamika a mechanika letu, p. 83, VVLŠ SNP, Košice (1990).

Design of the proper shape of the aperture for optic measuring methods in experimental chamber.

R. Bayer[a], P. Hlavatá[a], P. Vyroubal[a]

[a] Department of Electrical and Electronic Technology, Brno University of Technology, Technická 10, 616 00 Brno, Czech Republic

This article deals with the experimental chamber preparation, on which shockwaves, besides other measurements, will be observed using the Schlieren optic method. Because of this reason, the replaceable aperture will be used, which will be placed against the center of the observation window. The design of the optimal aperture shape was solved using mathematical – physics analysis in the Ansys Fluent system and the results will be compared with the results obtained from the experimental measurements.

Introduction

At the department of electrical and electronic technology FEEC BUT with the cooperation of the Institute of scientific instrument CAS, we prepare the production of the experimental chamber, on which we will (besides others) evaluate shockwaves using the Schlieren optic method. For this reason, one of the replaceable apertures will be used, so its end will be placed against the center of the observation window. This article deals with the results obtained using mathematical – physics analysis in Ansys Fluent system with the expected pressure, density, velocity and temperature running (1).

Conic aperture

The 2D axisymmetric profile of the preparing experimental chamber with the cone aperture variant is shown in the fig. 1. This shape of the aperture is suitable for good observation of the shockwave using optic methods (2, 3). Due to the shockwave which arises with the pumping of the differentially pumped chamber behind the aperture, is the effort to capture this shockwave the best is possible. For this reason, it has been designed several aperture shapes. The conic aperture is customized so the supersonic flow, which arises behind the aperture, was placed against the observation window.

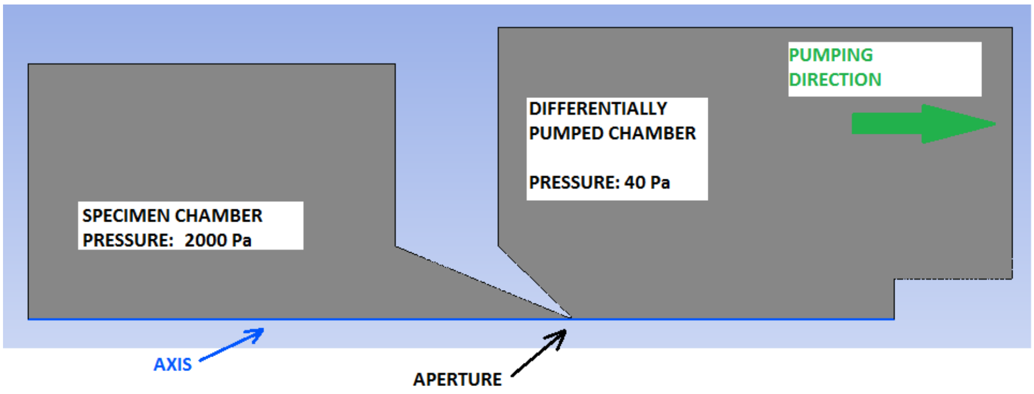

Figure 1. *2D experimental chamber profile*

Results and discussions

The mathematical – physics models were calculated for given aperture shape and suitable pressure ratios (4). The pressure and velocity layouts above the aperture which come out from the mathematical – physics analysis and will be experimentally verified (besides others) with the optic methods are shown in fig. 2 and fig. 3.

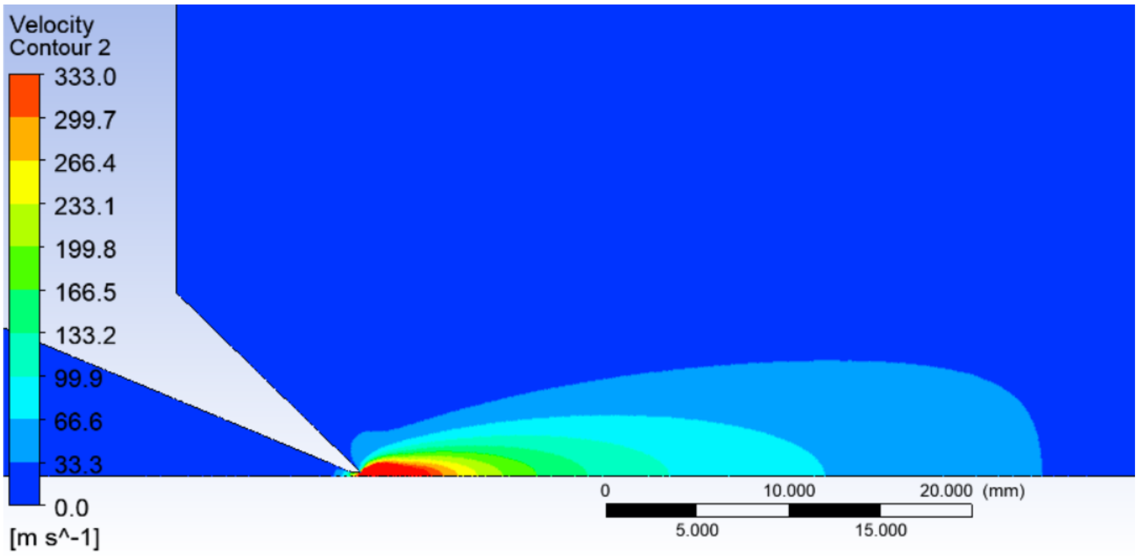

Figure 2. *Velocity layout for variant of 2000 Pa in the specimen chamber*

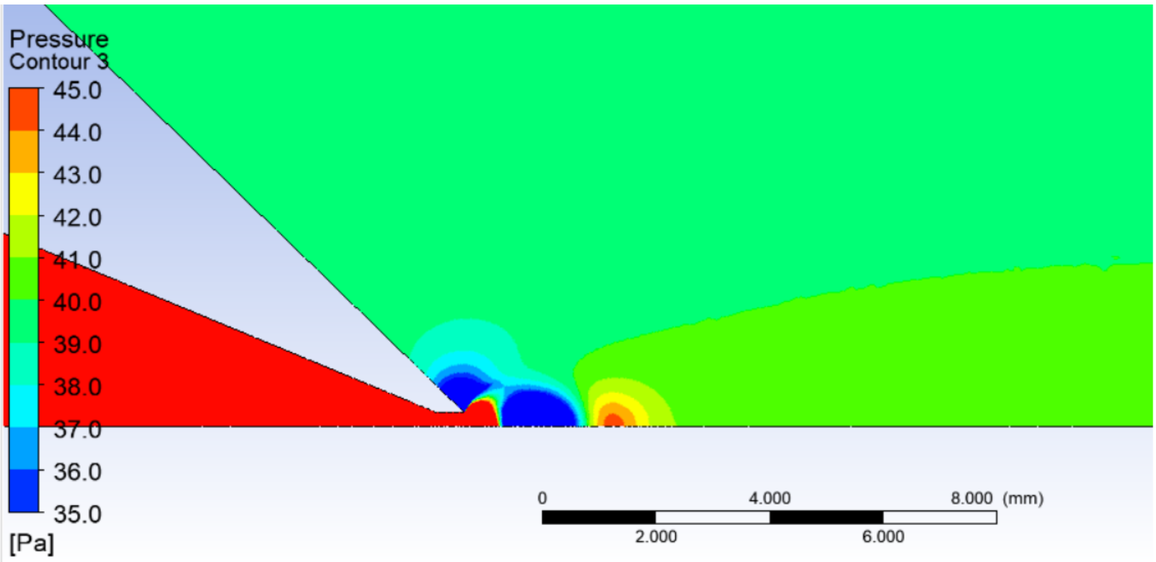

Figure 3. *Pressure layout for variant of 2000 Pa in the specimen chamber*

The gas flow behind the aperture with the sharp pressure gradients are characteristic also with the sharp temperature gradients, this is shown in fig. 5. The obvious Mach cone which is placed at the end of the supersonic flow and the diffusion of the oblique shock wave from the Mach cone, which will be possible to observe using Schlieren optic methods, this is shown in fig. 4 (5 ,6, 7). The control calculations for the critical temperature and critical velocity were made:

$$T_{kr} = \frac{P_{kr}}{R\rho_{kr}} \qquad [1]$$

Temperature of the entering gas to the aperture:

$$T_0 = \frac{P_0}{R\rho_0} \qquad [2]$$

Critical velocity: $$v_{kr} = \sqrt{\frac{2k}{k+1}RT_o} \qquad [3]$$

Where: P_{kr} – critical pressure, R – universal gas constant, ϱ_{kr} – critical density, P_o – input pressure, ϱ_{kr} – input density, k – Boltzmann constant

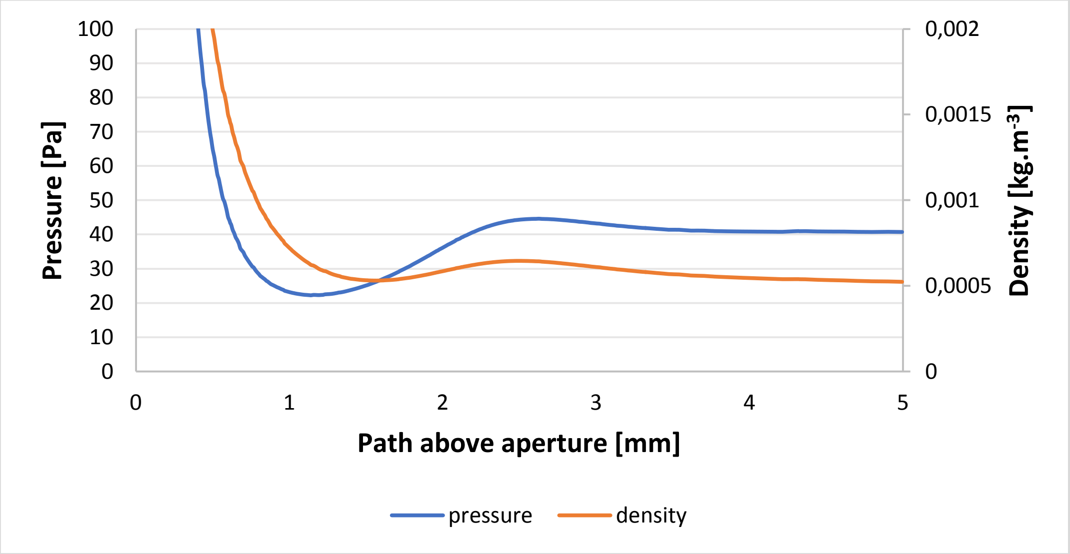

Figure 4. *Pressure and density running above the aperture*

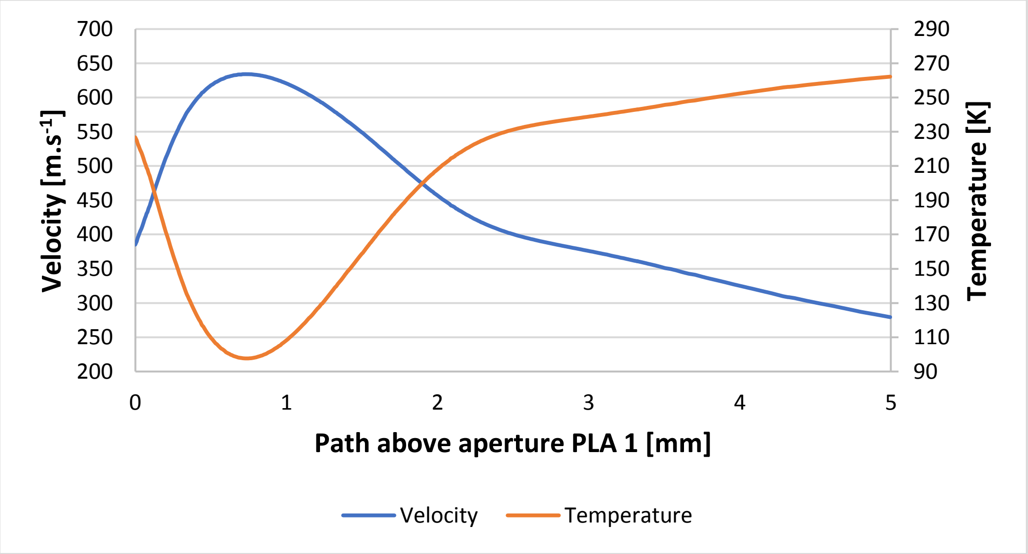

Figure 5. *Velocity and temperature running above the aperture*

Acknowledgments

This research has been carried out in the BUT specific research programme (project No. FEKT-S-17-4595).

References

1. P. Vyroubal; J. Maxa; V. Neděla; J. Jirák and K. Hladká, Apertures with Laval Nozzle and Circular Orifice in Secondary Electron Detector for Environmental Scanning Electron Microscope, Advances in Military Technology, vol. 8, no. **1**, p. 59-69, (2013).
2. J. Maxa; V. Neděla; J. Jirák; P. Vyroubal and K. Hladká, Analysis of gas flow in a secondary electron scintillation detector for ESEM with a new system of pressure limiting apertures. Advances in Military Technology, vol. 7, no.**2**, p.39-44, (2012).
3. J. Maxa and V. Neděla, The Impact of Critical Flow on the Primary Electron Beam Passage through Differentially Pumped Chamber. Advances in Military Technology, , vol. 6, no. **1**, p. 39-46. ISSN 1802-2308, (2011).
4. J. Maxa; M. Bílek; P. Hlavatá; P. Vyroubal and K. Lepltová, Comparisons Using Methods of Continuum Mechanics and Monte Carlo at Differentially Pumped Chamber. Advances in Military Technology, vol. 11, no. **2**, p. 143-150. ISSN: 1802-2308. (2016).
5. V. Neděla; E. Tihlaříková; J. Runštuk; J. Hudec, High-efficiency detector of secondary and backscattered electrons for low-dose imaging in the ESEM. Ultramicroscopy, p. 1-11. ISSN 0304-3991, (2018).
6. V. Neděla; I. Konvalina; M. Oral; J. Hudec. The Simulation of Energy Distribution of Electrons Detected by Segmental Ionization Detector in High Pressure Conditions of ESEM. Microscopy and Microanalysis, p. 264-269.
7. M. Daněk, Aerodynamika a mechanika letu, p. 83, VVLŠ SNP, Košice (1990).

Materials for Biodegradable Implants Prepared by Powder Metallurgy

M. Sedlaříková[a], J. Hrabovský, M. Růžička[b] and J. Vondrák[a]

[a] Faculty of Electrical Engineering and Communications,
Brno University of Technology, Brno, Czech Republic

[b] Technical Institute of Fire Protection, Prague 4, 143 01, Czech Republic

Preparation of metal components by a modified powder technology was checked. Iron powder and a suitable binder are used for manufacturing of an object of arbitrary form. Its final treatment occurs in nitrogen at 1100 °C. Polystyrene dissolved in toluene served as the binder.

Tailored Preparation of Special Components

The idea of biodegradable metallic implants in surgery is promising. For example, Wegener et al [1] described the manufacturing of implants by powder metallurgy enabling production of special tailored objects for medical purposes. We have used the modification of powder metallurgy for this purpose as well [2, 3]. We have introduced a method, which uses a similar polymeric substrate or binder for preparation of precursors. In this paper, we compare three polymer additives for preparation of iron based materials from the viewpoint of their morphology. On the contrary to the paper quoted above, we decided to use polyurethane, polypropylene and polystyrene as binders.

Materials and Methods

As the starting material, we have used commercially available iron prepared by the reduction of iron oxides by hydrogen. Alternatively, also carbonyl iron and/or powdered ferosilicium served for the same purpose. In the case of polyurethane (PUR), the material BULPREN was used and in the case of polypropylene (PPY), the polypropylene 500 g/m^2 has been used. For good soaking, wetting angles for different liquids were measured. The best soaking had toluene, so it was used to prepare a suspension with powdered iron. Then, a foam from PUR or PPY was added to the suspension and all parts were mixed together.

Finally, polystyrene (PS) was dissolved in toluene and the powder of iron was saturated by this solution. A PTFE mold was further filled by PS iron containing paste; the solvent was removed by evaporation. Finally, the product was annealed in argon first to 400 °C with the aim of de-bonding and removal of polymer. Finally, the temperature was increased to 1100 °C.

The morphology of the product was investigated by microscopy, either optical or SEM. The behavior of iron powder with the polymer was studied also by DTA with attaches mass spectrometric detection of products formed in stream of argon.

Results

DTA Investigations

The process of sample preparation by DTA was investigated. Obtained DTA curves are shown in Fig. 1 for the PS binder. Figure 2 shows the rate of gaseous decomposition products during the experiments. The later were obtained by mass spectrometric analysis. Their composition is listed in Tab. 1. According to the results of MS analysis, on the contrary to DTA of other binder materials used for preparation of the starting samples, there is no evidence of any exothermic reaction in intermediate range of temperatures. The gases obtain toluene and cleavage fractions having structure of smaller hydrocarbons only. Hence, only thermal degradation of PS occurs.

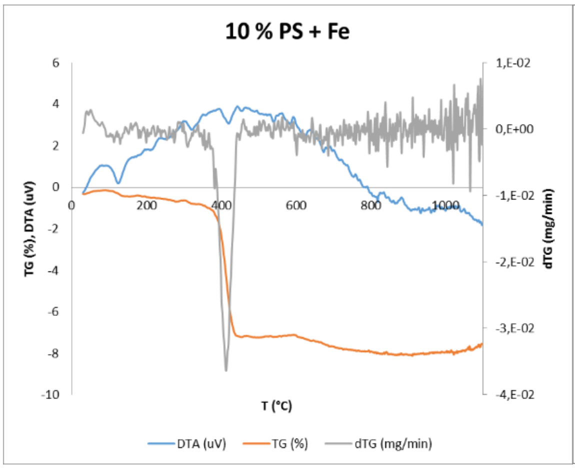

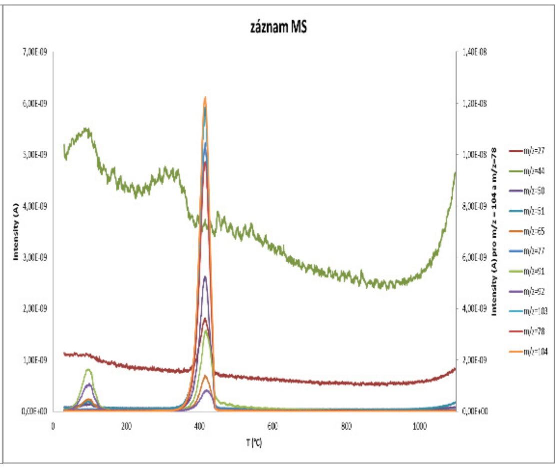

Figure 1. *(left) DTA of a PS bonded sample*
Figure 2. *(right) Formation of decomposition products*

Figure 3. *Appearance of the PS bonded sample after annealing*

Table 1. *Composition of fragments obtained from the PS sample*

ionic mass	formula of fragment
104	C_8H_8
103	C_8H_7
77	C_6H_5
78	C_6H_6
51	C_4H_3
50	C_4H_2
27	C_2H_3

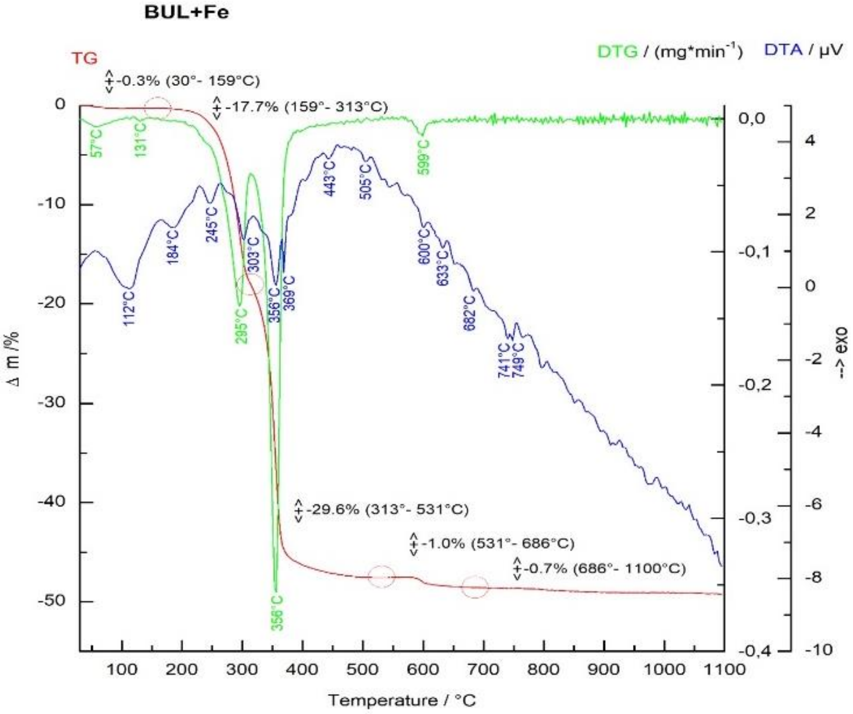

Figure 4. *DTA of a PUR bonded sample*

On the contrary to that, the DTA curve of a sample containing PUR as binder exhibits a marked exothermic reaction with the maximum at 400 °C indicating a vivid reaction of elemental iron with the PUR (see Fig. 4).

We suppose that this process is a kind of oxidation of Fe by the oxygen atoms in the structure of PUR yielding in coverage of metal surface by iron oxides as it was shown by XRD.

Morphology of Products

The following figures 5 and 6 show enlarged views of the morphology of reaction products. As we see, PS bonded product is much more homogenous than that bonded by PUR, products are porous, while the product prepared by the use of PS is rather homogenous and the creation of smooth metallic parts seems to be promising.

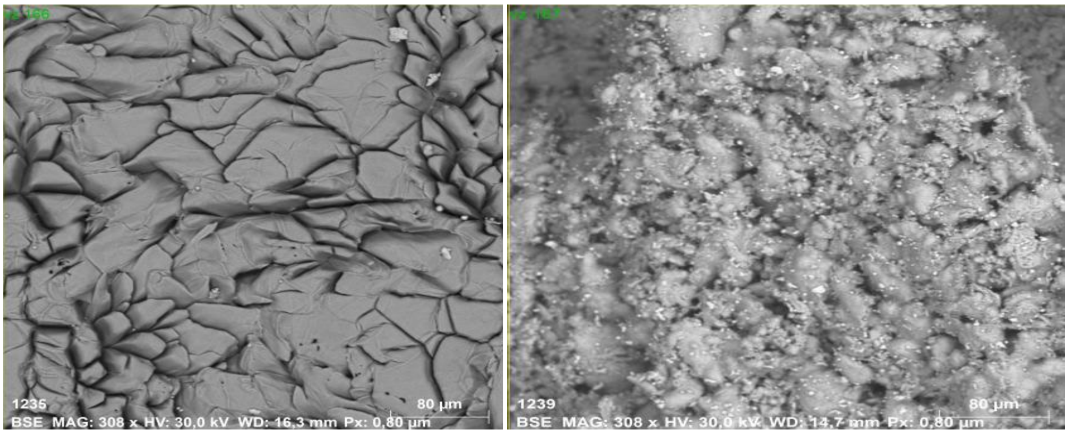

Figure 5. *(left) and* ***Figure 6****. (right) Morphology of a PS bonded product and a product bonded with PUR.*

Corrosion and Degradation of Samples

To monitor the degradability and the effect of body fluids, annealed samples were placed in physiological body stimulating solutions. There were classical NaCl solution, Ringer's solution and SBF (simulated body fluid, prepared according to [3]). Samples placed in these solutions were maintained at 37 °C (body temperature) and their monthly corrosion potentials, weight loss and solution conductivity were measured.

The greatest weight loss for PP samples occurred during the first measurements, when corrosive products were released into solutions. In the last measurement, the weight loss was the smallest, probably due to alkalization of solutions and the inability to dissolve the corrosion products. The weight losses correspond to the measured corrosion potential.

For PS samples in combination with Ringer’s solution or NaCl solution, weight gain was noted, which could be caused by the deposition of corrosion products in the sample structure. In combination with simulated body fluid, smaller weight gain was observed than other solutions. The small weight gain could be due to the presence of different ions, which allowed releasing of corrosion product to the solution (SBF turned reddish-brown in color).

Discussion

The production of biodegradable components by powder metallurgy seems promising. However, the role of a binder necessary for their formation prior to thermal treatment is important. The binder must not contain any oxygen atoms, which would cause oxidation of metal to metal oxide and, thanks to purity of the product, reasonably looking components can be manufactured in this way. The ideal properties of implants should be obtained by combining different powder metals. Also the technology of 3D printing could be utilized for the production of rather complex shapes.

Acknowledgements

This work was supported by the grant FEKT-S-17-4595 "Materiály a technologie pro elektrotechniku III"

References

1. B. Wegener, B. Sievers, S. Utzschneider, P. Müller, V. Jansson, S. Rößler, B. Nies, G. Stephani, B. Kieback, P. Quadbeck, *Microstructure, cytotoxicity and corrosion of powder-metallurgical iron alloys for biodegradable bone replacement materials,* p.1789-1796 Materials Science and Engineering: B 176 (2011)
2. J. Vondrák, M. Sedlaříková, A. Košíček, M. Hávová and J. Kadlec, *ECS Trans.*, 2018 87(1): 415-421
3. J. Vondrák, M. Sedlaříková, Z. Galánová, P. Čudek and T. Binar, *ECS Trans.*, 2018 87(1): 423-429

The passability of the track vehicle

Milan Chalupa

The vehicle passability is one part of the vehicle handling. The vehicle passability simulation calculations can help to come up with the answers on basic and supplementary questions on design influence changes in the area of car properties testing. Terrain vehicle passability given by stair step up ability, ditch traverse ability, by the ability vehicles to surmount definite angle of gradient, fordability or deep fording ability is given by vehicle design. It is usefull to have some more information that influence might change the ability of vehicle overrule definite angle uphill for example. It can be information how is possible the best to affect the vehicle ability to fetch through obstacle with low adhesion or else. These items of vehicle driveability can be influenced by height of vehicle centre of gravity, vehicle weight, by the high of the track rib shape or invasive speed of the vehicle by riding to climb. The vehicles ability to surmount a climb will be influenced by adhesion coefficient betwen the track and the ground by the vehicle riding. We can find the answers cheaply and quickly by usage of computational simulating systems, as it the Adams AVT is.

The main aim of the article is to acknowledge the possibility of usage results simulation calculations of the vehicle construction. This simulation results are gained by the help of computing simulating system Adams AVT. The simulating calculations were done to find out influences of the vehicle construction parts changes or operation conditions. The operation conditions are represented by invasive car speed, the angle of roadway gradient uphill or values adhesion coefficient. Under investigation are for example possibilities of vehicle to achieve the biggest angle at ride of vehicle into slope uphill or the travelling of the biggest distance by uphill riding.

Corrosion Resistance of Plasma Nitriding and Zinc Phosphating Duplex System for C45 Steel

D. Kusmič[a], P. Faltejsek[a], O. Čech[b]

[a] Department of Mechanical Engineering, University of Defence in Brno, Brno, 61200 Czech Republic

[b] Brno University Of Technology, Department Of Electrical And Electronic Technology, Brno, Czech Republic

This study is focused on corrosion resistance of plasma nitrided and duplex treated (plasma nitrided and additionally zinc phosphate conversion coating) C45 carbon steel, using the NSS tests. The duplex treatment was compared to untreated, plasma nitrided (PN) and simple zinc phosphate (Znph) steel. The steel samples were plasma nitrided at a temperature of 500 °C for 15 h in the nitriding atmosphere ratio of $3H_2:1N_2$ (l/h), the case depth reached 0,324 mm and the compound layer 6,4 μm. The additionally crystalline Znph layer composed by hopeite $Zn_3\ (PO_4)\ 2.H_2O$ and by a smaller quantity of phosphophyllite $Zn_2Fe\ (PO_4)\ 2.H_2O$ reached approximately 6,2 μm (for all treated steel samples). The NSS tests (1000 h) proved slight corrosion improvement of PN steel (vcorr = 1.26 $g/m^2.h$) and distinct improvement for simple Znph coating on steel (vcorr = 0.7 $g/m^2.h$), compared to untreated one (vcorr = 1.36 $g/m^2.h$). Very distinctive corrosion resistance was found for duplex treated steel (vcorr = 0.36 $g/m^2.h$). Results were completed and confirmed with very good agreement by weight loss and visual evaluation.

Renewable Energy System Combined with Hybrid Energy Storage Devices

K. Lota, R. Mańczak, Ł. Kolanowski, I. Acznik, K. Kopciuch, G. Lota

Division in Poznan, Łukasiewicz Research Network - Institute of Non-Ferrous Metals Central
Laboratory of Batteries and Cells, Poznan 61-362, POLAND

katarzyna.lota@claio.poznan.pl

The growing demand for electricity as well as the depletion of fossil fuel resources affect the research and development of new solution for energy generation and storage. One of these solution is the construction of independent renewable energy sources which can be combined with different energy storage devices. The aim of this study was to determine the electrical properties of the selected commercial power sources (Li-ion batteries) for hybrid energy storage in renewable energy system. For this purpose the dependence of capacity vs. discharge current, internal resistance, cycling stability and nail penetration test were performed.

Introduction

Taking into account the population growth and industrial development it can be observed a significant increase of world`s energy demand. In this case, our ecosystem is polluted due to the emission of gases derived from burning of fossil fuels. Therefore, there is an increasing interest to develop more efficient renewable energy systems. Renewable energy is produced from renewable resources such as sunlight, wind or waves. Apart from the efficiency and construction of renewable energy devices, energy storage in such systems play a significant role to maintain reliable all electrical devices. The research and development of renewable energy systems have caused the interest for new, efficient and low cost energy storage devices. This kind of power sources play an important role in renewable energy plants because they ensure proper power supply, adjust power variations and enables energy storage/conversion which is produced by variable weather conditions (1,2).

Various energy storage system can be implemented for renewable energy devices such as lead-acid or lithium-ion (Li-ion) batteries. Lithium-ion batteries are very common and widely used due to their high energy density, long cycling stability and high efficiency (3). It should be noted that this kind of system should work together with battery management systems (BMSs) which quarantee a reliable operation. All of Li-ion batteries require the presence of BMS, because it prevents the damage, protect the battery from overcharging/discharging etc. Moreover, an effective BMS apart from the prevention of any damages it is important to control the state of charge (SOH) and state of health (SOH) by measuring the voltage, current and temperature during working (4,5).

In this study, the commercial Li-ion batteries (prismatic and cylindrical cells) with CMC and LFP technology were investigated in order to operate with other power sources in hybrid system for renewable energy purposes.

Experimental

All of the investigated accumulators were conducted for the broad electrical analysis. At the first step the nominal capacity was measured, for this purpose the constant current (0.5C) charging up to 4.2V was applied and then the accumulator was kept at this voltage until the current droped to a value of 0.02C. After that, the discharge at 0.5C was applied to 2.5V. Moreover, the discharge at different current load (0.1C-5C) was also provided. The current-voltage characteristic was also studied at different temperatures (-20°C; -10°C; 0°C; +20°C; +40°C; +60°C). At the next step, the internal resistance test was carried out using alternating current (1 kHz) method according to the PN-EN 61951-2:2011 standard. The test was performed at a temperature of 20°C for accumulators in a charged and discharged state. Measurement of internal resistance was performed using a certified tester 3554-type (Hioki E.E. Corporation). In addition, a nail penetration test was carried out in order to simulate internal shor-circuit.

Summary and Conclusions

All of the commercial Li-ion batteries were characterized by high charge-discharge efficiency, about 99%. Based on the voltage-current characteristics, the increase in current the capacity decreases, but it should be noted that all of the examined accumulators were characterized by good charge propagation. During the charge/discharge processes provided at different temperatures, the increase in temperature causes a decrease in the cell capacity, which is related to the decrease in electrolyte conductivity. Structural analysis showed a typical cell structure for Li-ion systems. No structural defects were found. Nail penetration analysis caused cell explosion due to internal short circuit of electrodes, which is typical for this type of systems. At a later stage, the best selected cells will be tested in a series and parallel together with the designed BMS for hybrid systems combined with other electrochemical power sources like lead-acid battery and electrochemical supercapacitors.

Acknowledgments

The authors acknowledge the financial support from the European Regional Development Fund - Grant no POIR.04.01.02-00-0099/17-00.

References

1. D. Connolly, H. Lund, B.V. Mathiesen, *Renew. Sust. Energ. Rev.*, **60**, 1634 (2016).
2. N. Kannan, D. Vakeesan, *Renew. Sust. Energ. Rev.*, **62**, 1092 (2016).
3. C. A. Vincent, B. Scrosati, *Modern batteries. An introduction to electrochemical power sources,* Butterworth-Heinemann, Oxford, 1997.
4. R. Xiong, L. Li, J. Tian, *J. Power Sources*, **405**, 18 (2018).
5. M.A. Hannan, M.S.H. Lipu, A. Hussain, A. Mohamed, *Renew. Sust. Energ. Rev.*, **78**, 834 (2017).

Numerical Simulation of Galvanic Corrosion

M. Mačák[a], P. Vyroubal[a]

[a] Department of Electrical and Electronic Technology, Brno University of Technology, Brno 616 00, Czech Republic

The presented article describes a numerical approach for investigating the galvanic corrosion. The main equations of the model were described and implemented into Ansys Fluent. The model was then used to investigate a general case of the galvanic corrosion.

Introduction

Galvanic corrosion occurs due to the electrochemical coupling between two metals with a different corrosion potential in a common electrolyte. The metal with a lower corrosion potential acts as an anode and is dissolved, while the other metal acts as a cathode, and so its reaction is either an oxygen reduction or a hydrogen evolution. Experimental investigations of corrosion phenomena can be often time consuming, difficult to perform and subsequently expensive, as it is necessary to build prototypes for testing. An alternative method to experiments is the application of numerical simulations, which solve relevant partial differential equations. The simulations give better overview on the phenomenon as they can capture values of quantities, which are difficult to obtain experimentally (such as distribution of species concentrations in the electrolyte). This leads to a better understanding of the phenomenon, which results in speeding up the designing and optimizing new corrosion resistant materials. (1, 2)

Numerical model

In order to capture the phenomenon of a galvanic corrosion, a new custom electrochemical model was created and implemented into Ansys Fluent. The model is built on User-Defined Scalars, for which general transport equations are solved. These equations were then adjusted by User-Defined Functions, to properly describe the electric potential in electrodes, in the electrolyte and the transport of media in the electrolyte. The charge transfer in the solid phase (the electrode) follows the Ohm's law (Eq. [1]), whereas the current density in the electrolyte is related to the flux of the species due to diffusion, migration and the convection (Eq. [2]) (3):

$$\nabla \cdot \left(-\sigma \nabla \varphi \right) = 0 \qquad [1]$$

$$\boldsymbol{j} = z \cdot F \left(c_i \boldsymbol{v} - D_i \nabla c_i - \mu c_i \nabla \varphi \right) \qquad [2]$$

Where σ is the electric conductivity, φ is the electric potential, $\boldsymbol{j}$ is the current density, z is the charge number, F is the Faraday's constant, c_i is the molar concentration, $\boldsymbol{v}$ is the velocity, D_i is the diffusion coefficient and μ is the mobility.

Usually, the full description of the electrolyte current is too complex, while it is not always necessary to resolve every term. Depending on the application, it is possible to neglect certain terms. The most common assumption is the electroneutrality, which removes the convection term. (3, 4)

For galvanic corrosion, it possible to assume a constant concentration of the electrolyte, and so the diffusion term can be also neglected. This means that the electrolyte potential can be also described by the Ohm's law, but the finite rate of the reactions is still considered. The kinetics of reactions are driven by the difference of the potential between the electrode and the electrolyte and is described by the Butler-Volmer equation:

$$j_{far} = j_0 \left[\exp\left(\frac{z \cdot F \cdot \alpha_A}{RT} \eta \right) - \exp\left(-\frac{z \cdot F \cdot \alpha_C}{RT} \eta \right) \right] \tag{3}$$

Where j_0 is the exchange current density, η is the overpotential, R is the molar gas constant, T is the thermodynamic temperature and $\alpha_{A,}$ α_C are charge transfer coefficients.

As a large overpotential can be expected due to the high conductivity, either the anodic or the cathodic term (depending on the reaction) prevails and the other can be neglected. (4) Still, the full description of the Butler-Volmer equation was implemented, as it is more general and captures the whole range of overpotentials.

Results and discussion

A general analysis of galvanic corrosion, involving one-electron reactions, was carried out. The parameters of the reactions were the same, as reported in (5), so the results could be compared, and the model validated.

Fig. 1 show the computational geometry, which consist of an electrolyte domain and two electrodes, which were considered only as a boundary condition. The boundary conditions for electrolyte potential at the electrodes were defined by the Butler-Volmer equation. Fig. 2 show the potential distribution inside the electrolyte domain and at the electrodes. These results are in an excellent agreement with the results reported in (5). As expected, the highest current density is situated at the contact of the metals.

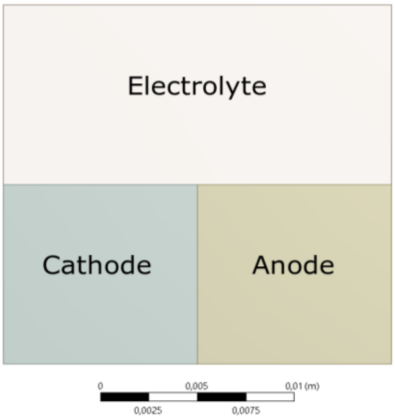

Figure 1. *Geometry*

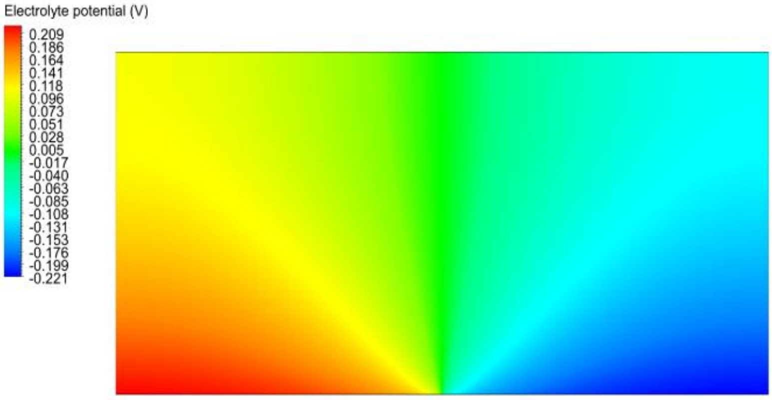

Figure 2. *Distribution of the electrolyte potential*

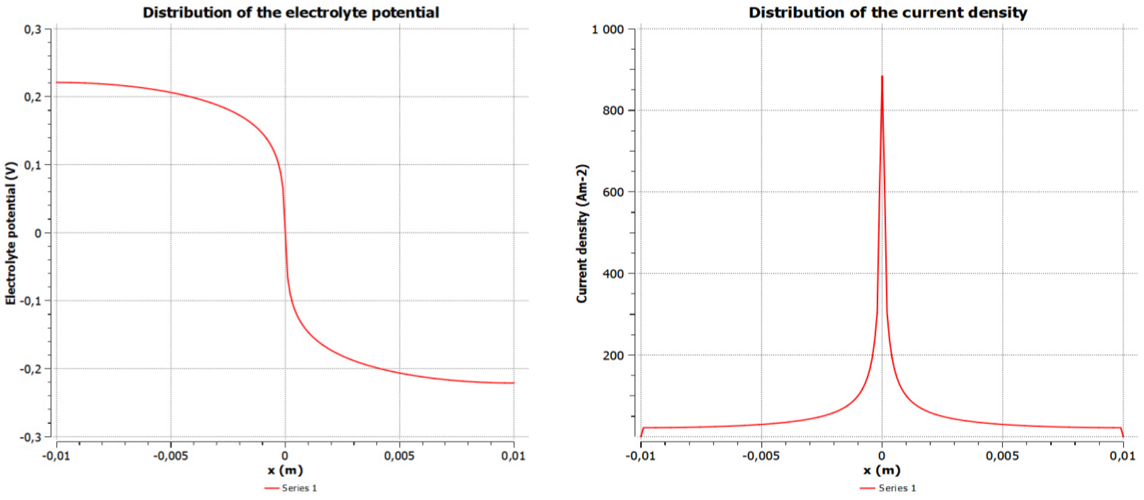
Distribution of the electrolyte potential

Distribution of the current density

Figure 3. *Distribution of the electrolyte potential (left) and the current density (right) near the electrodes*

Acknowledgments

This work was supported by the BUT specific research programme (project No. FEKT-S-17-4595).

References

1. R. Radouani, Y. Echcharqy and M. Essahli. *International Journal of Corrosion*. **2017**, p. 1-10 (2017).
2. A. Balamurugan, S. Rajeswari, G. Balossier, A. H. S. Rebelo and J. M. F. Ferreira. *Materials and Corrosion*. **59**(11), p. 855-869 (2008).
3. W. Mai and S. Soghrati. *Electrochimica Acta*. **260**, p. 290-304 (2018).
4. S. R. Cross, S. Gollapudi and Ch. A. Schuh. *Corrosion Science* **88**, p. 226-233 (2014)
5. P. Doig. *Journal of The Electrochemical Society*. **126**(12) (1979).

Analyzing Discharging and Charging Performance of a Lithium-ion Battery

S. S. Madani[a]

[a] Department of Energy Technology, Aalborg University, Aalborg, DK-9220, Denmark

Lithium-ion batteries are indispensable parts in electric vehicles, owing to their high energy density, discharge and charge efficiency. Therefore, it is essential to investigate their charging and discharging behavior at different current rates. The purpose of this investigation was to determine and analyses the discharge and charge behavior of a lithium-ion battery at different conditions. In addition, the relationship between cycle number, current and capacity during discharging and charging were analyzed. It was concluded that the extracted charge declined nonlinearly with the amount of the discharging current.

Introduction

The big number of automobiles presently are consuming fuels around the world, which causing significant problems such as global warming and reduction of primitive energy resources. In addition, the air quality was affected by these pollutions. So, it is essential to develop clean and safe energy sources.

Rechargeable batteries are kind of batteries in which electrical energy could be accumulated as chemical energy. This chemical energy could be transformed to electrical energy when needed. Among rechargeable batteries, lithium-ion batteries are providing a bigger market owing to their high energy density.

Lithium-ion batteries have been accepted extensively for electric vehicle applications because of several reasons such as no memory effect, long lifetime and high-power density [1].

The Grey System Theory (GST) effectiveness to be implemented to the anticipation of the parameters of battery cell performance attribution to their discharge and charge cycles was investigated [2].

Usage analysis and lithium-ion battery cell cycling were studied [3]. The aim of this investigation was to age battery cells in an environment for hybrid electric vehicle and to identify appropriate methods for determining cell ageing [3].

In this investigation we introduced a detailed and comprehensive analysis of discharge and charge parameters of a commercial lithium-ion battery, whilst submitted to continuing discharging and charging cycles under constant charge and discharge currents of 0.2 C, 0.4 C, 0.6 C and 0.8 C.

Experimental

The studies were accomplished on a lithium-ion battery, with standard discharge capacity equal to 3350 mA h and a nominal voltage equal to 3.6 V. The PEC battery tester was employed in the discharge-charge tests, by connecting the corresponding cables to the positive and negative battery cell poles, respectively. Figure 1 shows that the battery cell was being charged and discharged at different rates. In addition, the corresponding voltage and temperature are illustrated.

Table 1 demonstrate the test matrix which was designed for the battery discharging and charging experiments. Charging generally includes periods of constant voltage and constant-current charging. The discharge and charge could be controlled by voltage or current. The terminal voltage decreases and increases during discharging and charging. The discharge and charge dynamics of lithium-ion batteries could be defined by voltage measurement under constant discharge and charge current inputs.

The charge and discharge curves of the lithium-ion battery are illustrated in Figure 2 and 3 correspondingly. The low and high rate of discharge cases demonstrate that the voltage decreases slowly and quickly correspondingly. Similarly, the low and high rate of charge cases demonstrate that the voltage increases slowly and quickly correspondingly. The battery cell was cyclically discharged and charged at a specific current and among lower and upper voltage limit.

Notwithstanding, this pattern during discharge is different. As could be seen from the figure, the slope of the final stages of the discharging cases have almost same profile except for 0.2 C which is higher.

The variation in the battery cells voltage among two points which voltage quickly varies is due predominantly to Li^+ extraction and insertion during the increases and decreases in the voltage correspondingly [4]. Great currents exert rapid variations in the concentration of Li^+ ions into the cathode structure [5].

As it was mentioned before at the beginning part of the charge graphs, the rate of increase in voltage is more than the rest. The rapid voltage rise in the region which voltage quickly varies at the commencement of battery cell charging is owing to fast polarization of overvoltage [6].

Similar to the charge curves in the discharge curves also there are regions which voltage decrease more. During discharge, the rapid variation in the battery cell voltage in the region which voltage quickly varies, happens because of approximately complete maintenance of the lithium ion [7].

For each of the twenty discharging currents, the battery was charged under the same currents, leading to 20 discharge-charge cycles for each current rate. It could be observed that there is a considerable variation in the final voltage and initial voltage during each cycle and test, due to the capacities decline quickly during the cycles, to finally settle to almost 2194 mAh and 2201mAh for discharge and charge capacities correspondingly after the 20 cycles. It could be seen that the amount of declined capacities is not the same between different consecutive cycles.

Several load profiles were applied to the battery cell. These were accomplished under the constant current protocol. The obtained results are illustrated in Table 2. The studied variables were: the discharging and charging currents, the corresponding discharging and charging times, the charge and discharge capacity. The capacity curves at different cycles of the lithium-ion battery is illustrated in Figure 6.

Table 2 demonstrates that throughout the time discharged at 0.2 C, the battery cell average discharging capacity for twenty cycles is 3163.4 mAh which is 239.4 mAh greater than throughout the time discharged at 0.4 C. Notwithstanding, following being discharged by 0.6C and 0.8C the battery cell average discharging capacities are 2549 mAh and 2364 mAh correspondingly. The battery cell average discharging capacity for the 0.4 C cycles is 375 mAh higher than 0.6C cycles and for 0.6C cycles compared to 0.8 C this amount is 184.7 mAh. In addition, Table 2 demonstrates that throughout the time charged at 0.2 C, the battery cell average charging capacity for the cycles is 3124.2 mAh which is 195.4 mAh higher than throughout the time charged at 0.4 C. Notwithstanding, following being charged by 0.6C and 0.8C the battery cell average charging capacities are 2553 mAh and 2371 mAh correspondingly. The battery cell average charging capacity for the 0.4 C cycles is 375.7 mAh which is higher than 0.6C cycles and for 0.6C cycles compared to 0.8 C this amount is 182 mAh. The required time to charge the battery cell from 2.6 to 4.2 V and to discharge it from 4.2 to 2.6 V is considerably reliant on the current intensity as demonstrated in Table 2 and Figures 4 and 5.

Conclusion

To comprehend the charge and discharge behavior for the individual lithium-ion battery cell different charge and discharge cycles with various current rates were applied to the battery cell. In addition, dependence and impact of the discharging charging and time, on the charge and discharge capacity was studied. The battery cell charge capacities equal to 3124.2, 2929, 2553 and 2371 mAh, were achieved for charging at 0.2 C, 0.4 C, 0.6 C and 0.8 C. Similarly, the battery cell discharge capacities equal to 3163.4, 2924, 2549 and 2364 mAh, were gained for discharging at 0.2 C, 0.4 C, 0.6 C and 0.8 C. A nonlinear reduction of the discharge and charge capacity with the intensity of the discharging and charging current was achieved. It was concluded that both, the discharging and charging times, decline with the current intensity. In addition, the discharge and charge time rely on the discharge and charge current intensity.

Reference

1. Zhao, R., Zhang, S., Gu, J., et al.: 'An experimental study of lithium ion battery thermal management using flexible hydrogel films', Journal of Power Sources, 2014, 255, (0), pp. 29-36.
2. W. Lin, B. Ji, L. Chen, B. Tian, J. Li, and H. Pan, “Analysis and prediction of the discharge characteristics of the lithium–ion battery based on the Grey system theory,” *IET Power Electron.*, vol. 8, no. 12, pp. 2361–2369, 2015.
3. P. Svens, M. Behm, and G. Lindbergh, “Lithium-ion battery cell cycling and usage analysis in a heavy-duty truck field study,” *Energies*, vol. 8, no. 5, pp. 4513–4528, 2015.
4. Scrosati, B.; Garche, J.; *J. Power Sources* **2010**, *195*, 2419.
5. Reimers, J. N.; Dahn, J. R.; *J. Electrochem. Soc.* **1992**, *139*, 2091.
6. Bernardi, D. M.; Go, J.-Y.; J. Power Sources 2011, 196, 412.
7. S. P. Da Silva, P. R. C. Da Silva, A. Urbano, and J. Scarminio, “Analysis of a commercial portable lithium-ion battery under low current chargedischarge cycles,” *Quim. Nova*, vol. 39, no. 8, pp. 901–905, 2016.

Hybrid Tree Harvester Machine with Battery Powered Hydro-electric Drive

P. Prochazka[a], I. Pazdera[a] , R. Cipin[a]

[a] Department of Power Elecrtical and Electronic Engineering, Brno University of Technology, Brno 61600, Czech Republic

The paper describe design of battery powered drive unit intended for tree harvester application. Battery powered hybrid drive unit in working machine is currently quite common (1). The battery capacitance is not sufficient to realize harvester as an only battery powered machine. Nevertheless, the hybrid concept of electric drive is useful to cover short power peaks demands during the harvester standard operation. In harvester application there is typical high ratio between short power peak and average demanded power. The development in batteries increases of significance and possibility of electric drive utilization in three harvesters.

Conception of tree harvester hybrid drive

Battery powered hydro-electric drive unit in tree harvester application is useful as an auxiliary power source covering power peak demands during harvester standard operation. Implementation of battery powered drive allows to design harvester diesel motor with lower power (2, 3). It leads to lower consumptions which is beneficial in terms of environment pollution. The total weight of the harvester is reduced which is friendly to forest land and vegetation. Battery powered drive unit provides additional energy to harvester to be able to easily operate in difficult terrain.

The basic concept of hydro-electric drive is shown in Fig. 1. The combustion engine *7* is connected via transmission *8* with electric motor *6* and two hydro-generators *9*,*10*. Hydro-generators delivers power to wheels trough valve blocks *11* and hydro-motors *12*. The electric motor is chosen as a salient permanent magnet synchronous motor (PMSM) due to its good torque/volume(weight) ratio. Salient motor can operate in wider velocity range in comparison with classical PMSM. It has also better control performance in comparison with induction machine. The motor can operate in motor of generator mode to be able to charge the battery during lower power demands on consumption engine. The synchronous motor is controlled via three – phase inverter *4* which ensures proper energy flow from battery *1* to motor and vice versa. Battery is based on sealed lead acid technology. Battery is protected by power fuse *2* and it is possible to disconnect it from circuit by circuit breaker *3*. The power is transmitted to harvester wheel via hydro-motors *12*. The whole drive system is controlled via main processor which gathers data from sensors and controls proper energy flows in the system according to actual power demands.

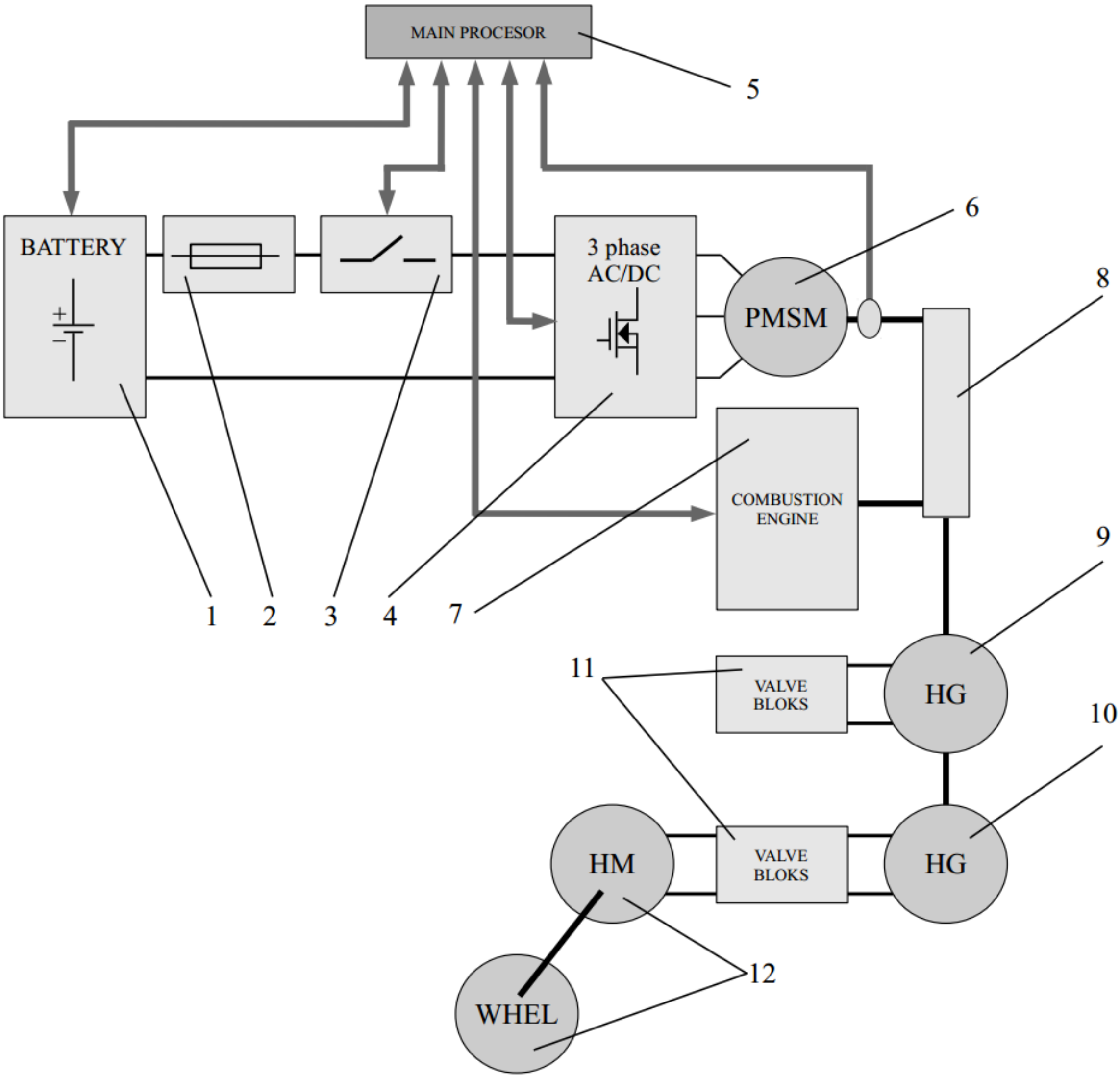

Figure 1. *Basic concept of hydro–electric drive.*

Electric drive component design

Design of each component is driven by power demands during tree harvester operation. There is defined torque profile during typical harvester operation and nominal speed derived from hydraulic component. Torque and velocity profile of harvester with combustion engine during operation cycle is shown in Fig. 2. It is possible to choose appropriate PMSM according to this profile. The parameters of chosen salient PMSM motor are summarized in Table I.

TABLE I. *PMSM motor parameters.*

Physical quantities	Value	Unit
Nominal Power	23	kW
Nominal speed	1500	RPM
Maximal speed	4500	RPM
Nominal current	650	A
Nominal phase-phase voltage	48	V

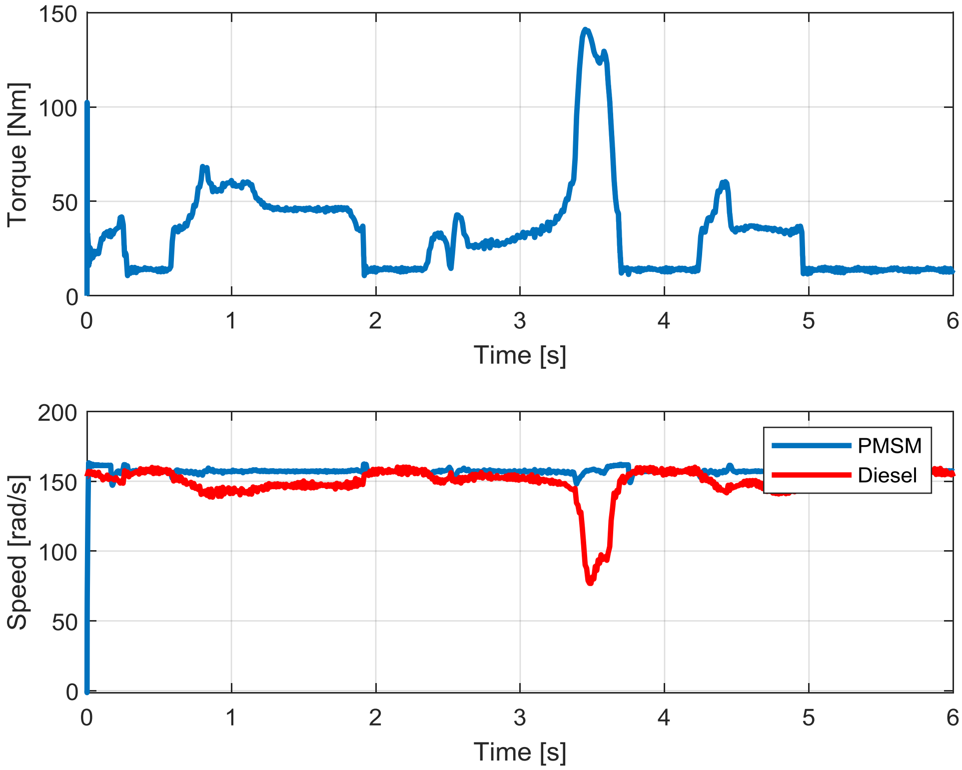

Figure 2. *Torque and velocity profile of harvester with combustion engine (red) and alternatively with electric drive (blue) during operation cycle.*

The simulation model of the whole drive unit was created in MATLAB/Simulink environment. The model is useful for estimation of other component parameters which are difficult to calculate. The control stability and dynamic performance is also verified thank to this model. The block diagram is shown in Fig. 3. The simulation result will be discussed more in detail in full paper.

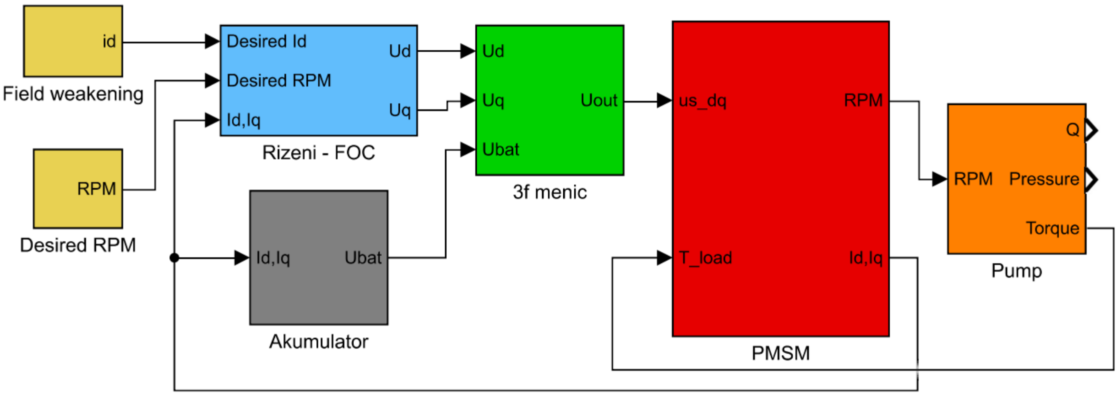

Figure 3. *Basic block diagram of simulation model of hybrid harvester drive.*

The tree-phase DC/AC inverter from SiliXcon company was chosen according to simulation results. The inverter is based on power MOSFET technology. The inverter parameters are summarized in Table II.

TABLE II. *SiliXcon SL inverter parameters.*

Physical quantities	**Value**	**Unit**
Voltage range	24-80	V
Nominal current	340	A
Maximal short-time current	500	A
Power nominal/peak	24/36	kW

The battery pack was determined according to harvester operation cycle (Fig. 2), which is quite different to operation cycle in typical electric traction application. There is high difference between peak and average value of power. Simultaneously there is put significant attention to robustness and reliability of the whole drive unit. Due to this fact the lead acid based batteries are chosen for this application. Six packs are connected in series. The voltage level of the whole pack is 72V and capacity 92 Ah (6,6 kWh). The capacity is given especially due to demand on high value of instantaneous power for a short time. The battery parameters are summarized in Table III.

TABLE III. *Battery parameters.*

Physical quantities	**Value**	**Unit**
Nominal voltage	12	V
Nominal capacity	82	Ah
Short-circuit current	2300	A
Inner resistance	7	mΩ
Dimensions (L x W x H)	417x105x156	mm

Acknowledgments

This research work has been carried out in the Centre for Research and Utilization of Renewable Energy (CVVOZE). Authors gratefully acknowledge financial support from the Ministry of Education, Youth and Sports of the Czech Republic under NPU I programme (project No. LO1210).

References

1. L. Immonen, M. Laurila, Rilla and J. Pyrhonen, *Modelling and simulation of a parallel hybrid drive system for mobile work machines*, IEEE EUROCON 2009, St.-Petersburg (2009). DOI: 10.1109/EURCON.2009.5167736
2. S. Rong-Feng, Z, Xiaozhen, Z. Chengjun, *Study on Drive System of Hybrid Tree Harvester*. ScientificWorldJournal (2017). doi:10.1155/2017/8636204
3. K. Einola, *Prestudy of a Power Management of a Cut-To-Length Forest Harvester with a Hydraulic Hybrid System*, 13th Scandinavian International Conference on Fluid Power,Linköping, Sweden (2013). DOI: 10.3384/ecp1392a8

The influence of alloying elements on surface hardness of ferritic nitrocarburizing layers of barrels

Z. Pokorny, D. Dobrocky

Department of Mechanical Engineering, University of Defence, Brno, Czech republic

The article deals with a chemical composition of saturated layers after ferritic nitrocarburizing process. Experiments are focused on using of gas ferritic nitrocarburizing processes for surface treatment due to increasing of surface hardness with low influence on the dimensional accuracy. Ferritic nitrocarburizing processes were applied to steels 31CrMoV9 (sample B3), ČSN 41 5330 (sample B3) and 32CrMoV12-10 (sample B4) used for weapon manufacturing, which were subsequently evaluated by electron microscopy, GDOES and microhardness methods. The results of measurement showed high influence of alloying elements on surface hardness of created carbide-nitride layer after chemical-heat treatment process. Main task was to compare microhardness after ferritic nitrocarburizing in accordance with chemical composition.

Introduction

The aim of this paper is to achieve an enhanced of surface hardness, better wear resistance and reduced friction coefficient connected to specific surface morphology. During chemical heat-treatment process primarily the interstitial phases of nitrides and carbides of iron are created. The initial nitrides and carbides phases are created in grain boundaries, in biggest defects well known as an area defects. Generally, these type of nitrides and carbides caused only low increasing of microhardness. The surface hardness after chemical heat treatment depends on two fundamental phenomenon. The surface hardness of created carbide and nitride phases depends on microstructure and finally on content of suitable alloying elements in steel. Generally, the fundamental elements caused increasing of mechanical properties are alloying elements as molybdenum, vanadium, aluminum or chrome. The mechanical properties of layer are dependent on the proportion of created individual phases in steel. The created compound layer has been very hard and brittle with good friction and anticorrosion properties. The thickness and hardness of γ'-Fe_4N (diffusion layer) depends on quantity and suitability of alloying elements for mentioned treatment process. Therefore, this paper demonstrates the influence of selected alloying elements on increasing of surface hardness. This optimized used technology called ferritic nitrocarburizing. After chemical heat treatment application, special semi-diffusion area (part) of heterogeneous layers are created in the surface. This part of created layer has another different characteristics than layer established after standard nitriding processes. For comparison with standard nitriding process chemical composition of steel was verified by GDOES/Bulk method on LECO SA 2000 spectrometer and local measurement of composition was carried out on SEM microscope Hitachi Tabletop 3000 equipped by XRD Oxford Instruments Stream-2. Microstructure was evaluated by using SEM method on Hitachi Tabletop 3000. Thickness and microhardness of nitrided layers were measured by microhardness method in accordance with DIN 50190 standard on automatic microhardness tester LECO LM 247 AT. Thickness of compound layer was evaluated by electron microscopy. The evaluation of influence of alloying elements on depth and surface hardness was performed by using microhardness indentation test.

Intelligent routing algorithms in the complex sensors network for control energy storage

Krzysztof Stankiewicz, Jerzy Jagoda

Institute of Mining Technology KOMAG

Intelligent routing algorithms in the complex sensors network possible to be used for construction of intelligent cells and energy storage are presented. The concept of Internet of Things (IoT) assumes connecting the possible highest number of objects (devices, machines, sensors, etc,), present in the given work environment, to ICT network to increase volume and quality of acquired data. Taking into account more common use of energy storages consisting of high number of secondary cells, supervised by BMS, the authors presented the concept of the intelligent cell equipped with voltage and temperature sensors, passive balancing system and a wireless communication system enabling the connection with the network of mesh topology. Due to that, construction and supervision of big energy storage will be significantly simplified. Self-organization and multi-redundant communication network will secure operational reliability, flexible configuration and operational safety. In the presented analysis of intelligent routing algorithms, information on the requirements put to them (in relation to e.g. number of nods, energy saving, work environment) is included. The results of analyses are summarized as well as directions of further research work on implementation of the selected solutions in the sensors network controlling the cells and energy storage operation, are indicated.

Introduction

The literature survey indicates a significant advantages of using the reactive algorithms for IoT use (opposite to the proactive algorithms), due to higher energy savings (lack of necessity for cyclic refreshing of routing tables). No necessity of collecting data on routing also significantly simplifies construction of a single network nod.

However, from the literature survey it results that of proactive and reactive routing algorithms in the sensors network has a lot of limitations associated with the following:

- decreasing the transmission capacity with the increase in the number of network nodes,
- decrease in the efficiency of data delivery to the addressee (PDR) along with the increase in the number of network nodes,
- decrease in network capacity along with the increase of speed of the network nodes movement.

Reactive algorithms are applicable in small sensors network. The IoT concept assumes constructing the sensor networks with hundreds and thousands of nodes.

The authors suggest using the extended routing protocols based on Swarm Intelligence (SI) in the expanded sensor networks. Use of the routing algorithm, built on the basis of SI, eliminates the need to remember routes by each network node, and also maintains high capacity and stable data transmission in networks of many nodes.

Hardware implementation

In the paper it has been emphasised that the simulation tests are not enough to verify the routing algorithm operating on the SI basis and their implementation in the proper hardware solution is indispensable for validation. The authors indicated several hardware solutions that can be used to implement the selected routing algorithms. The results obtained on the basis of program simulation are promising (Fig. 1).

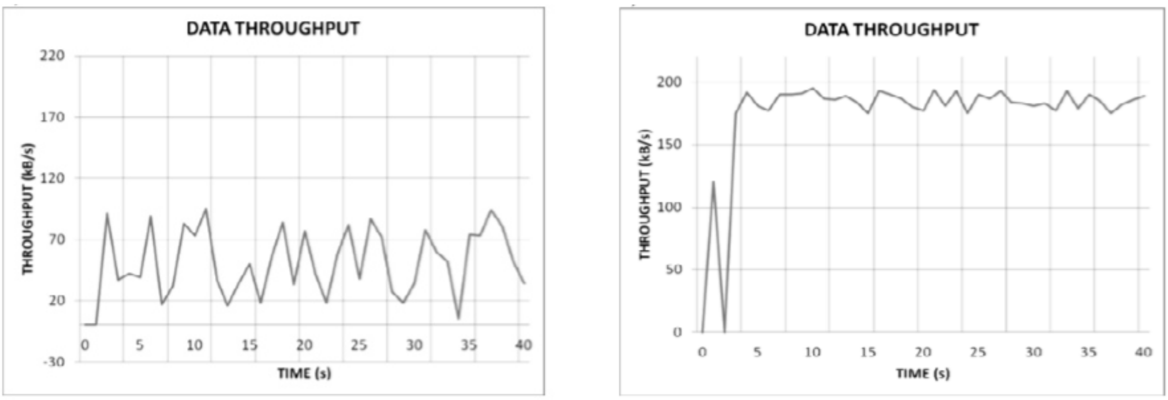

a) b)

Figure. 1. *Transmission capacity in the networks of 500 nods (AODV algorithm (a) and algorithm developed on the basis of SI (b)).*

Within the current research work, it is planned to implement SI routing in dispersed BMS systems with passive balancing, which in turn can be used in construction of energy storage sites consisting of hundreds or thousands of links. Each link will be equipped with an individual BMS with passive balancing, and data exchange between the cells will be carried out in the wireless network of mesh topology. Such an approach, in principle, will significantly simplify and speed up the construction of energy storage.

The suggested structure of the integrated cell is given in Fig. 2

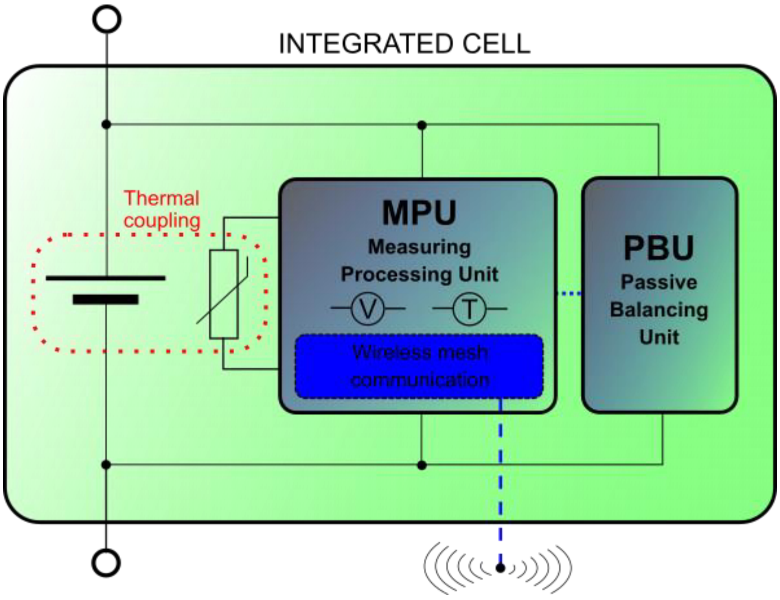

Figure 2. *Single integrated cell*

Response of the human musculoskeletal system when driving in a passenger car

Martin Svoboda, Milan Chalupa, Karel Jelen, Petr Kubový, Igor Žuravský, Josef Ponikelský

Vertebrogenic disorders are one of the most common causes of pain that afflict today's man. Nowadays it is clear that long-term exposure to the body causes an adverse response in the human body, which can lead to irreversible damage. We are exposed to such vibrations when driving in vehicles. The damping of these dynamic effects is solved by the vehicle suspension system. All this is then reflected in the driving safety, driving characteristics of the vehicle and also in the response to the locomotive apparatus of the vehicle crew. In the relationship between head and neck, neck injuries are mostly caused by the inertia of the head. Although the product of speed and weight (kinetic energy) are proportional to the values that increase the likelihood of neck or head injury. It is surprising that significantly more injuries occur at slow speeds. The force effects that are transmitted to the cockpit always affect the body of the person controlling the vehicle. In the long run, one-sided strain on the body has a negative impact on human health, in exceptional cases it can lead to death. The main aim of the article was to measure the dynamic effects that are transmitted to the driver (passenger) when driving in a passenger car over obstacles. The measurement was performed experimentally in a real environment on a defined path at different driving speeds and vehicle excitation. The magnitude of the accelerations generated on the driver / passenger seat structure, under the buttocks, head and cervical vertebrae C7 was recorded. The result of the work was to find out how much dynamic effects are transmitted from the vehicle structure to the driver / passenger body, respectively. the head and vertebrae of the cervical spine C7 as the vehicle crosses obstacles.

Dynamic Thermal Model of a Cylindrical Battery Cell

M. Toman[a], R. Cipin[a], P. Vorel[a], D. Cervinka[a]

[a] Department of Power Electrical and Electronic Engineering, Brno University of Technology,
Technicka 12, Brno 616 00, Czech Republic

This paper describes a thermal model of a cylindrical battery cell usable for calculation of instantaneous temperature distribution during discharging. The thermal model is based on a thermal network considering the thermal capacity. The functionality of the model was verified by simulation using the finite element method and a very good coincidence was achieved.

Introduction

Thermal calculations of single battery cells or complex battery packs are usually based on the use of the finite element method. The main advantage of these models consists in their accuracy. On the other hand, the computational complexity and consequently relatively long calculation time can be considered as a major disadvantage. In some applications, for example to estimate the instantaneous battery temperature using a microcontroller in a battery management system, the simplicity of the calculation can play an important role. In this case, it is advisable to use a thermal model based on a so-called thermal network. Description of a simple but very accurate dynamic thermal model of a battery cell based on the use of a thermal network is the aim of this article. The procedures described in this article are based on the author's previous work (1) in which a thermal model of a battery cell was introduced, however without the possibility to perform transient simulations.

Thermal Network of a Cylindrical Battery Cell

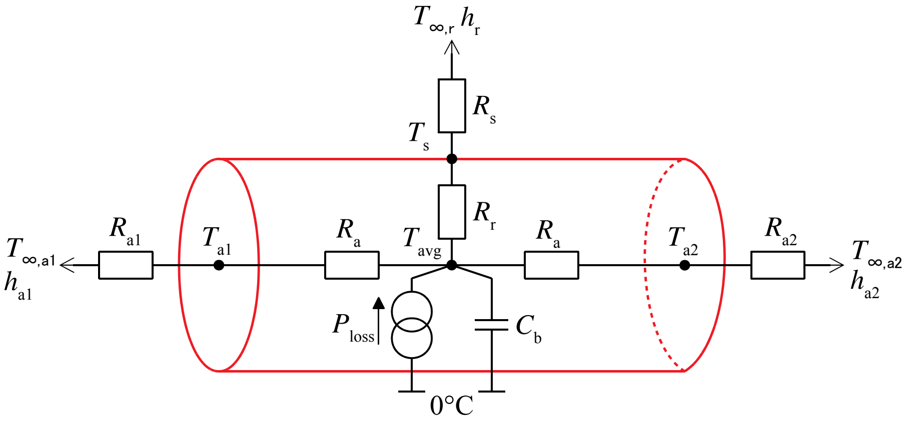

Figure 1. *Considered thermal network of a cylindrical battery cell.*

In the following section, the calculations of the individual thermal resistances and nodal temperatures are shown, see Fig.1. In this figure, all parameters related to the radial direction are indicated by "r" in the subscript and the parameters related to the axial direction are indicated by "a".

Surface thermal resistances are classically determined as thermal resistances by convection, see (2):

$$R_{\mathrm{a1}}=\frac{1}{h_{\mathrm{a1}}A_{\mathrm{a}}},\ R_{\mathrm{a2}}=\frac{1}{h_{\mathrm{a2}}A_{\mathrm{a}}},\ R_{\mathrm{s}}=\frac{1}{h_{\mathrm{r}}A_{\mathrm{r}}} \qquad [1]$$

where R_{a1} is the convection thermal resistance of the left end surface, R_{a2} is the convection thermal resistance of the right end surface, and R_{s} is the convection thermal resistance of the main (cylindrical) surface of the battery, and A_{a}, A_{r} are given surfaces.

Under the assumption that the temperature distribution is parabolic in the axial and radial directions, the internal resistances are calculated according to equations:

$$R_{\mathrm{a}}=\frac{L}{6k_{\mathrm{a}}A_{\mathrm{a}}},\ R_{\mathrm{r}}=\frac{1}{6\pi Lk_{\mathrm{r}}} \qquad [2]$$

where R_{a} is the internal thermal resistance in axial direction, R_{r} is the internal thermal resistance in radial direction, k_{a} and k_{r} are the battery thermal conductivities in radial and axial directions respectively, and L is the length of the battery.

From the previous equations, it is possible to express the total resistances in individual directions as:

$$R_{\mathrm{total,a1}}=R_{\mathrm{a}}+R_{\mathrm{a1}},\ R_{\mathrm{total,a2}}=R_{\mathrm{a}}+R_{\mathrm{a2}},\ R_{\mathrm{total,r}}=R_{\mathrm{r}}+R_{\mathrm{s}} \qquad [3]$$

All these resistances are in parallel, see Fig. 1. The resulting parallel resistance R_{p} is calculated according to the equation:

$$R_{\mathrm{p}}=\frac{1}{\dfrac{1}{R_{\mathrm{total,r}}}+\dfrac{1}{R_{\mathrm{total,a1}}}+\dfrac{1}{R_{\mathrm{total,a2}}}} \qquad [4]$$

The average temperature T_{avg} of the battery cell is calculated according to the differential equation:

$$\frac{\mathrm{d}T_{\mathrm{avg}}(t)}{\mathrm{d}t}=\frac{1}{C_{\mathrm{b}}}\left(P_{\mathrm{loss}}(t)+\frac{T_{\infty,\mathrm{r}}}{R_{\mathrm{total,r}}}+\frac{T_{\infty,\mathrm{a1}}}{R_{\mathrm{total,a1}}}+\frac{T_{\infty,\mathrm{a2}}}{R_{\mathrm{total,a2}}}-\frac{T_{\mathrm{avg}}(t)}{R_{\mathrm{p}}}\right) \qquad [5]$$

where C_{b} is the total thermal capacity of the cell. Other nodal temperatures can now be calculated using the following equations:

$$T_{\mathrm{a1}}(t)=T_{\infty,\mathrm{a1}}+\frac{R_{\mathrm{a1}}\left(T_{\mathrm{avg}}(t)-T_{\infty,\mathrm{a1}}\right)}{R_{\mathrm{total,a1}}},\ T_{\mathrm{a2}}(t)=T_{\infty,\mathrm{a2}}+\frac{R_{\mathrm{a2}}\left(T_{\mathrm{avg}}(t)-T_{\infty,\mathrm{a2}}\right)}{R_{\mathrm{total,a2}}} \qquad [6]$$

$$T_{\mathrm{s}}(t)=T_{\infty,\mathrm{r}}+\frac{R_{\mathrm{s}}\left(T_{\mathrm{avg}}(t)-T_{\infty,\mathrm{r}}\right)}{R_{\mathrm{total,r}}} \qquad [7]$$

where T_{a1} is the average temperature of the left end surface, T_{a2} is the average temperature of the right end surface, and T_{s} is the average temperature of the cell surface (cylindrical surface). The maximum temperature T_{max} of the cell is calculated according to the equation:

$$T_{\mathrm{max}}(t)=T_{\mathrm{s}}(t)+\frac{h_{\mathrm{r}}D\left(T_{\mathrm{s}}(t)-T_{\infty,\mathrm{r}}\right)}{4k_{\mathrm{r}}} \qquad [8]$$

Calculations

Using the mentioned equations, temperatures of Li-Ion 18650 battery cell were calculated. The course of power loss according to the red curve, see Fig. 2, was considered for the calculation. Cooling conditions are as follows: $T_{\infty,\mathrm{r}} = T_{\infty,\mathrm{a1}} = T_{\infty,\mathrm{a2}} = 25$ °C, $h_{\mathrm{a1}} = 5\ \mathrm{W{\cdot}m^{-2}{\cdot}K^{-1}}$, $h_{\mathrm{a2}} = 15\ \mathrm{W{\cdot}m^{-2}{\cdot}K^{-1}}$, and $h_{\mathrm{r}} = 10\ \mathrm{W{\cdot}m^{-2}{\cdot}K^{-1}}$. In the Fig. 2, the resultant courses of the surface temperature and the maximal temperature are plotted by blue lines. To verify the calculations, a simulation using a finite element method was performed in ANSYS. The obtained results are plotted by black dashed lines. It can be seen that the results obtained using the thermal network and using ANSYS are in perfect agreement each other.

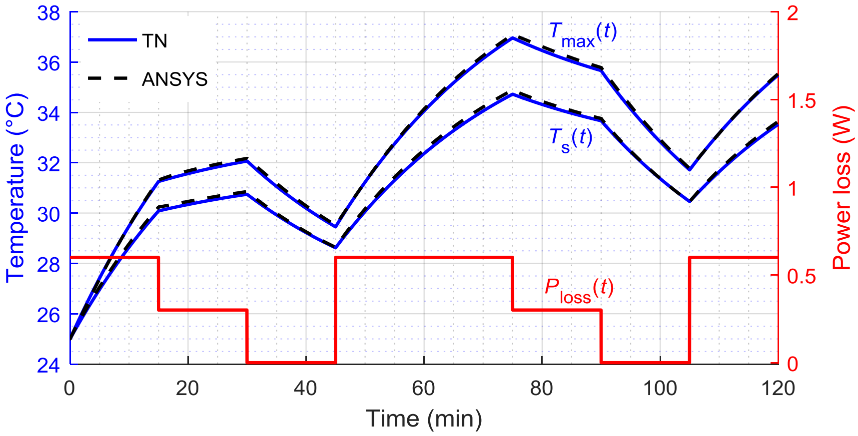

Figure 2. *Comparison of results obtained using the thermal network (TN) and using simulation in ANSYS.*

Conclusion

The paper deals with the dynamic thermal model of a battery cell based on a thermal network. Firstly, the calculation of the average temperature of the cell was performed. Then knowing this average temperature, it is possible to calculate surface temperatures and also the maximal temperature of the cell. The model is relatively simple, but the simulation in ANSYS has proven that it is very accurate.

Acknowledgment

This research work has been carried out in the Centre for Research and Utilization of Renewable Energy (CVVOZE). Authors gratefully acknowledge financial support from the Ministry of Education, Youth and Sports of the Czech Republic under NPU I programme (project No. LO1210) and BUT specific research programme (project No. FEKT-S-17-4374).

References

1. M. Toman, R. Cipin, P. Vorel, *Thermal Network for Battery Cell Temperature Modeling*, ECS Transaction, vol. 87, p. 285-290, (2018).
2. Y.A. Cengel, A.J. Ghajar, *Heat and Mass Transfer*, McGraw-Hill Education, Fifth Edition, ISBN: 978-007339818, (2015).

Simple BMS circuit and charger for a Li-ion battery pack 12 V

P. Vorel[a], J. Martis[a], M. Toman[a]

[a] Department of Power Electrical and Electronic Engineering, Brno University of Technology, Brno, Czech Republic

Introduction

A simple analogue BMS circuit and a charger with a fly-back converter were designed for a battery pack containing 3 Li-ion cells (1) connected in series (ca. 12 V / 9 Ah). The pulse transformer of the converter ensures the galvanic separation of the charged battery pack from the mains. The control circuits of the charger co-operate with the BMS circuit to avoid an overvoltage of any cell during the charging.

TABLE I. *Basic charger and BMS parameters*

Number of series Li-ion cells	3
Discharge cut-off voltage (per cell)	3.1 V
Final charging voltage (per cell)	4.1 V
Maximum voltage of the battery pack	12.3 V
Maximum power / current of the charger	30 W / 2.4 A
Supply	230 V / 50 Hz
Switching frequency	200 kHz

The voltage of each cell is monitored (not only the pack voltage) because any over-charging strongly influences the safety and life-time of the cells (2), (3), (4). A relatively simple device with an analogue control was constructed. Although no microprocessor and no software were used, a reliable and robust system was constructed. The main idea of this solution was to provide an inspiration to “intermediate” electronics constructors (like students). As they don´t need to write and debug any software, they can better focus on basic principles of power electronics, analogue electronics and feedback control.

BMS circuit

The BMS circuit is in Fig. 1. Two differential amplifiers with gains equal to 1 are used to shift the voltages of the middle and upper cell to the common ground (minus terminal of the down cell). This way three voltage signals related to the same ground are obtained.

The overvoltage of any cell is detected this way: If any of the three mentioned voltages increases over 4.1 V then the voltage on pin 1 of the IO3 increases over 2.5 V and so the IO3 opens (short circuit between its anode and cathode). The IO3 (type TL431, originally designed as a parallel voltage stabilizer) is used as a comparator here. Then the transistor T3 is switched-off and a logic 0 appears at the BMS output CON2-2. If the voltage of all three cells is lower than 4.1 V then the logic 1 is at this output CON2-2. This signal is used for the charger current control.

The under-voltage of any cell is detected this way: If any of the three cell voltages decreases under 3.1 V then the voltage on pin 1 of the IO2 decreases under 2.5 V and so the IO2 closes (open circuit between its anode and cathode). Then the transistor T1 and power MOS-FET T2 are switched-off and the T2 disconnects the load of the battery pack. The R19 represents a positive feedback which creates a hysteresis for the comparator IO2. The hysteresis avoids oscillations between switched-on and -off states.

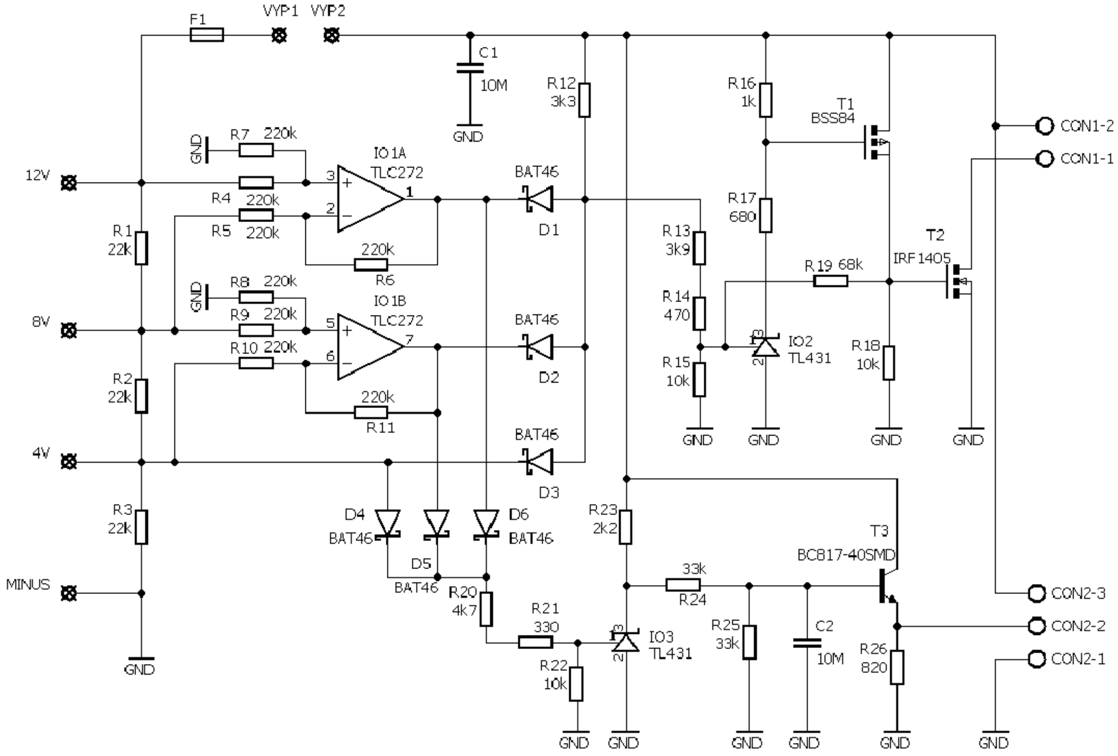

Figure 1. BMS circuit

Charger design

The complete circuit of the charger is in Fig. 2. There is an EMC filter on the input. The single-phase bridge rectifier B1 produces the DC link voltage for the DC/DC converter. The capacitors C1 and C2 reduce the DC link voltage ripple. The resistor R1 limits the initial charging current peak of the capacitors C1 and C2 when switching-on the charger. The DC/DC converter is created with the power MOS-FET, pulse transformer, secondary rectifier diode, output capacitors (C10 and C11) and additional circuits. The standard fly-back topology is used. The third winding of the transformer is used to create the DC supply voltage for the control circuits (together with the diode D2 and capacitor C4). The circuit D1, R3, C3 represents a standard snubber circuit decreasing the switching-off voltage overshoots of the power transistor caused by the leakage of the pulse transformer.

The control circuits are based on the integrated circuit UC3844. This circuit provides PWM for the MOS-FET. A slave current control loop is present in the system. The actual current is sensed from the shunt resistor connected in the source of the MOS-FET. The required current value is obtained from a non-traditional master voltage controller which ensures that no cell can be over-charged. The common over-voltage logic signal CON2-2 from the BMS is galvanically separated with the optocoupler OK2 and then it is filtered by a low-pass filter with a long time constant. If any cell is already near to the full voltage then the over-voltage signal oscillates between 0 and 1. Then the variable average value of this pulse signal serves as the required current.

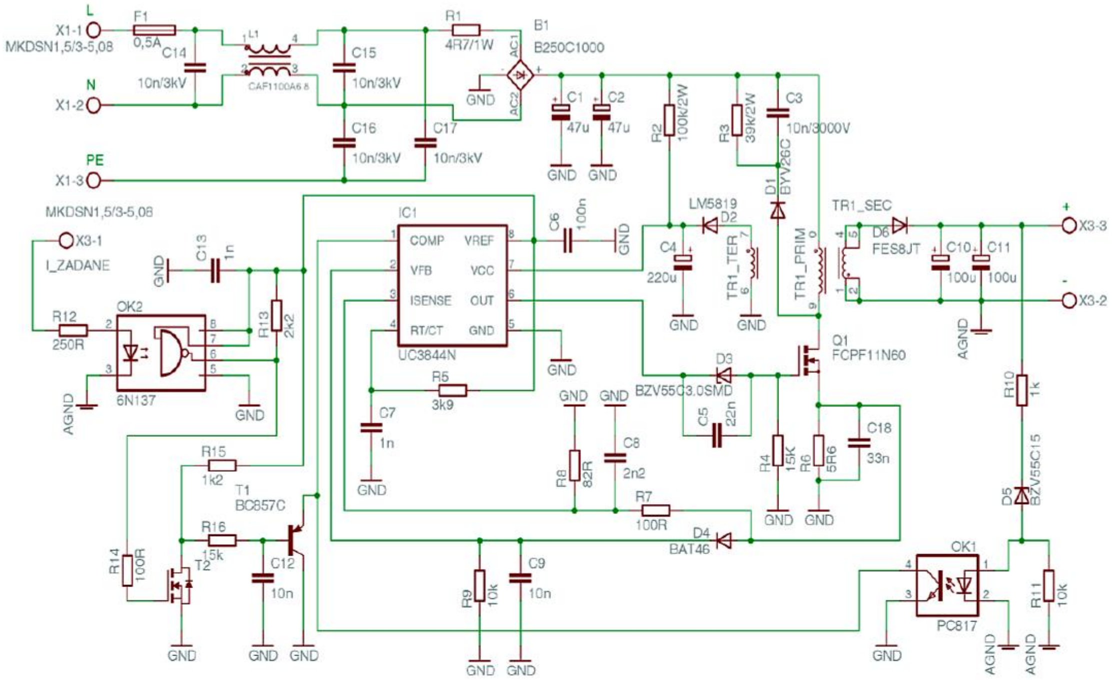

Figure 2. *Complete circuit of the charger*

Conclusions

A very simple BMS circuit and charger were designed and proven in a regular use. The system is used for a battery pack mounted on a city bike (for lighting purposes). As the circuits are simple the system can be also constructed by technicians with lower skills. The reliability of the system is high but no monitoring data are present (like SOC etc.).

Acknowledgment

This research work has been carried out in the Centre for Research and Utilization of Renewable Energy (CVVOZE). Authors gratefully acknowledge financial support from the Ministry of Education, Youth and Sports of the Czech Republic under NPU I programme (project No. LO1210).

References

1. Panasonic CGR18650C Cell Datasheet. http://www.rosebatteries.com/pdfs/Panasonic%20CGR18650C.pdf
2. Y. Li and L. Zhen, "Battery Management System," 2010 International Conference on Measuring Technology and Mechatronics Automation, Changsha City, 2010, pp. 739-741.
3. C. Lan, S. Lin, S. Syue, H. Hsu, T. Huang and K. Tan, "Development of an intelligent lithium-ion battery-charging management system for electric vehicle," 2017 International Conference on Applied System Innovation (ICASI), Sapporo, 2017, pp. 1744-1746.
4. A. Zhang, S. Song, C. Wang, J. Zhang, K. Wang and L. Li, "Research of battery management system for integrated power supply," 2017 Chinese Automation Congress (CAC), Jinan, 2017, pp. 3178-3181.

Monitoring Of Temperature Influence On Properties Of Lead-acid Accumulators

J. Zimáková[a], P. Bača[a], P. Musil[a]

[a] Brno University of Technology, Technická 10, 616 00 Brno, Czech Republic

This work offers a measurement scheme for automated measuring workstation. Furthermore, the practical section presents results of measurements on parameters of chosen lead-acid battery types. It also contains long-term deep battery cycling measurements results and datasheet values is included. Conclusion sums up parameters of chosen lead-acid battery types and their feasibility for further usage in power backuping.

Introduction

The use of batteries is currently the only available way to store energy in the longer term. The primary function of the accumulator is its ability to receive, behave and emit electrical charge. Electrical energy is stored in the form of chemical energy. Accumulators find a wide range of applications. It is included at every mobile electrical equipment or used as a power source to power electric vehicles. Recently, there has also been a significant increase in the use of accumulators in the area of electricity storage; they are used both in off-grid systems and in facilities serving as backup energy sources.

The article examines primary parameters of selected types of accumulators and influence of operating temperature on individual parameters of cells. The aim is to select a suitable type of accumulators for back-up of electrical equipment. The selected lead-acid batteries will be subjected to a similar mode that is typical for uninterruptible power supplies - keeping the battery fully charged and then discharging to the final voltage. In addition, the measurement scheme is designed for both standard and elevated temperatures, which are typical for the operation of these accumulators in backup systems. The main aim of this work is to verify whether the selected batteries really meet the values set whether they are suitable for the selected application.

Experiment

The following lead accumulators will be used for the experiments proposed:

- Panasonic (LC-R127)
- EnerSys (NP7-12T)
- CTM (CT7-12L)
- CTM (CTV7-12)

The selected batteries are 6-cell, the nominal capacity is 7.2 Ah.

Measurement design:

1. Verification of function parameters of accumulators in comparison with catalog ones values.

Assumed number of cells: 3 batteries in set, 4 sets (battery types), 12 batteries in total.

a) Discharge with a constant current of 0.25 C (1.75 A) to a voltage of 10.2 V.
b) Charge at a constant current of 0.35 C (2.5 A) with voltage limitation 14.7 V and the condition of termination of the charging phase on delivery of 104% charge issued in a previous discharge phase.
c) Evaluation of measured values.

2. Long-term test: verification of battery life (cycling to full discharge).

Assumed number of cells: 3 batteries in set, 4 sets (battery types), 12 batteries in total. The battery packs will be freely placed in a fume cupboard at standard temperature. Stability of ambient temperature will be ensured by air conditioning of the entire laboratory room.

a) Discharge with a constant current of 0.25 C (1.75 A) to a voltage of 10.2 V.
b) Charge at a constant current of 0.35 C (2.5 A) with voltage limitation 14.7 V and the condition of termination of the charging phase on delivery of 104% charge issued in a previous discharge phase.
c) Evaluation of measured values.

3. Verification of battery operating parameters at different temperatures.

Number of cells: 2 batteries in the set, 4 sets (battery types), 8 batteries in total.

a) Cells placed in the annealing furnace, temperature set to: 30, 45, 60 and 75 ° C.
b) Temperature stabilization and temperature min. 2 hrs
c) Evaluation of measured values.

Measuring workplace

A modern workplace for automated measurement of parameters and processes for various types of electrochemical articles. The diagram of the measuring workplace is shown in Figure 1.

The measuring workplace consists of:

- two Agilent 34980A control panels,
- four Agilent N6700B power supplies,
- Two desktop computers
- two connecting terminals,
- switch,
- measuring cabling.

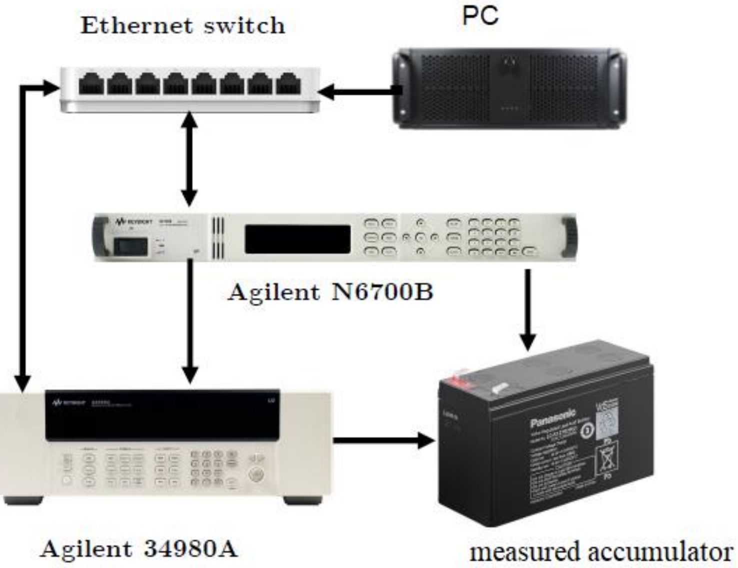

Figure 1. *Simplified scheme of measuring workplace.*

According to the mode shown in the 1st, a standard cycle was performed, followed by the long-term test, point 2 of the measurement scheme, was launched. Long-term battery measurement took 30 days. Capacity values are shown in table 1. The table shows that after the start of cycling the LC-R127 type by Panasonic and the CTV7-12 type by CTM tended to capacity increase. This trend reached its maximum between the 20th - 40th cycle of both types of accumulators.

Table 1. *Capacity table after 1st, 10th and 100th cycle of accumulators of different types*

producer	Panasonic			EnerSys			CTM			CTM		
type	(LC-R127)			(NP7-12T)			(CT7-12L)			(CTV7-12)		
accumulator number	1	2	3	4	5	6	7	8	9	10	11	12
capacity [Ah] 1. cycle	6,78	6,63	6,50	6,85	6,87	6,82	6,77	6,82	4,68	5,69	5,48	5,57
capacity [Ah] 10. cycles	6,79	6,74	6,71	6,07	6,30	5,97	6,55	3,68	2,56	5,83	5,62	5,72
capacity [Ah] 100. cycles	6,77	5,72	4,30	4,37	4,03	3,99	5,83	1,72	1,55	6,05	5,70	5,38

Experiment 3 is primarily focused on battery parameters at elevated temperatures. The aim of the measurement is to examine the influence of temperature on the battery parameters and on its overall functionality.

For the measured cells, 3 cycles were performed to verify the functionality of the battery and to eliminate the manufacturing defect. The primary parameters of the batteries and their capacity were subsequently measured at 30, 45, 60 and 75 ° C. To compare whether the internal structure of the accumulators was deformed, a comparative measurement was performed again at 30 ° C. The measured capacitance values are shown in the table 2.

Table 2. *Battery capacity of different types at 5 different temperatures*

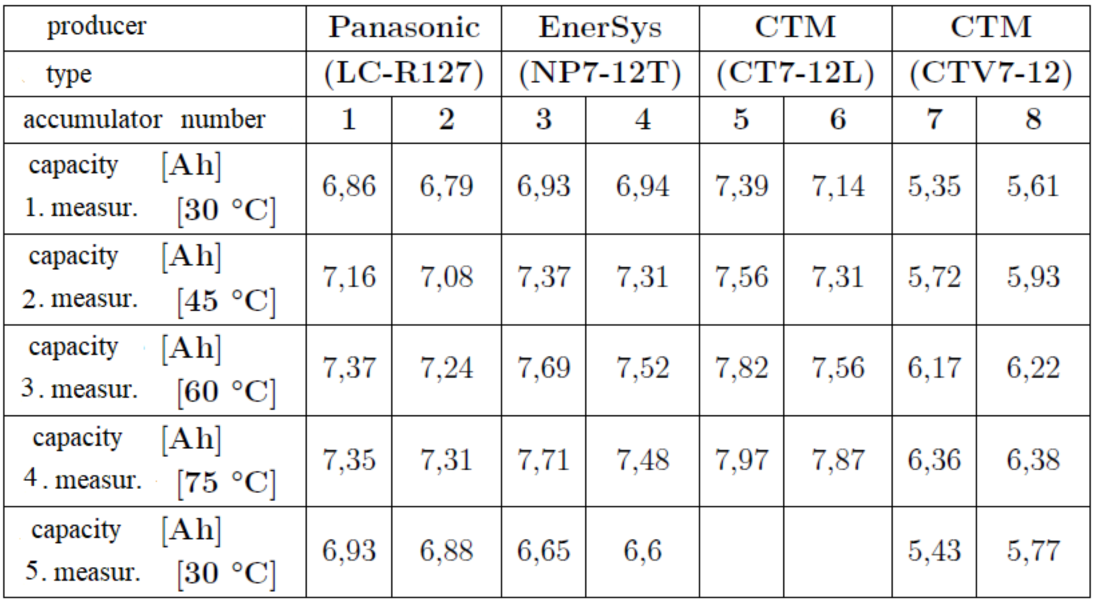

producer	Panasonic		EnerSys		CTM		CTM	
type	(LC-R127)		(NP7-12T)		(CT7-12L)		(CTV7-12)	
accumulator number	1	2	3	4	5	6	7	8
capacity [Ah] 1. measur. [30 °C]	6,86	6,79	6,93	6,94	7,39	7,14	5,35	5,61
capacity [Ah] 2. measur. [45 °C]	7,16	7,08	7,37	7,31	7,56	7,31	5,72	5,93
capacity [Ah] 3. measur. [60 °C]	7,37	7,24	7,69	7,52	7,82	7,56	6,17	6,22
capacity [Ah] 4. measur. [75 °C]	7,35	7,31	7,71	7,48	7,97	7,87	6,36	6,38
capacity [Ah] 5. measur. [30 °C]	6,93	6,88	6,65	6,6			5,43	5,77

Acknowledgements

This work was supported by the specific graduate research of the Brno University of Technology No. FEKT-S-14-2293.

References

1. J. Jung, Boca Raton (2016)
2. H. Kiehne, *Battery technology handbook*. 2nd ed. New York: Marcel Dekker, c2003. ISBN 0-8247-4249-4.
3. B. Culpin, J. Power Sources 133 (1), 79-86

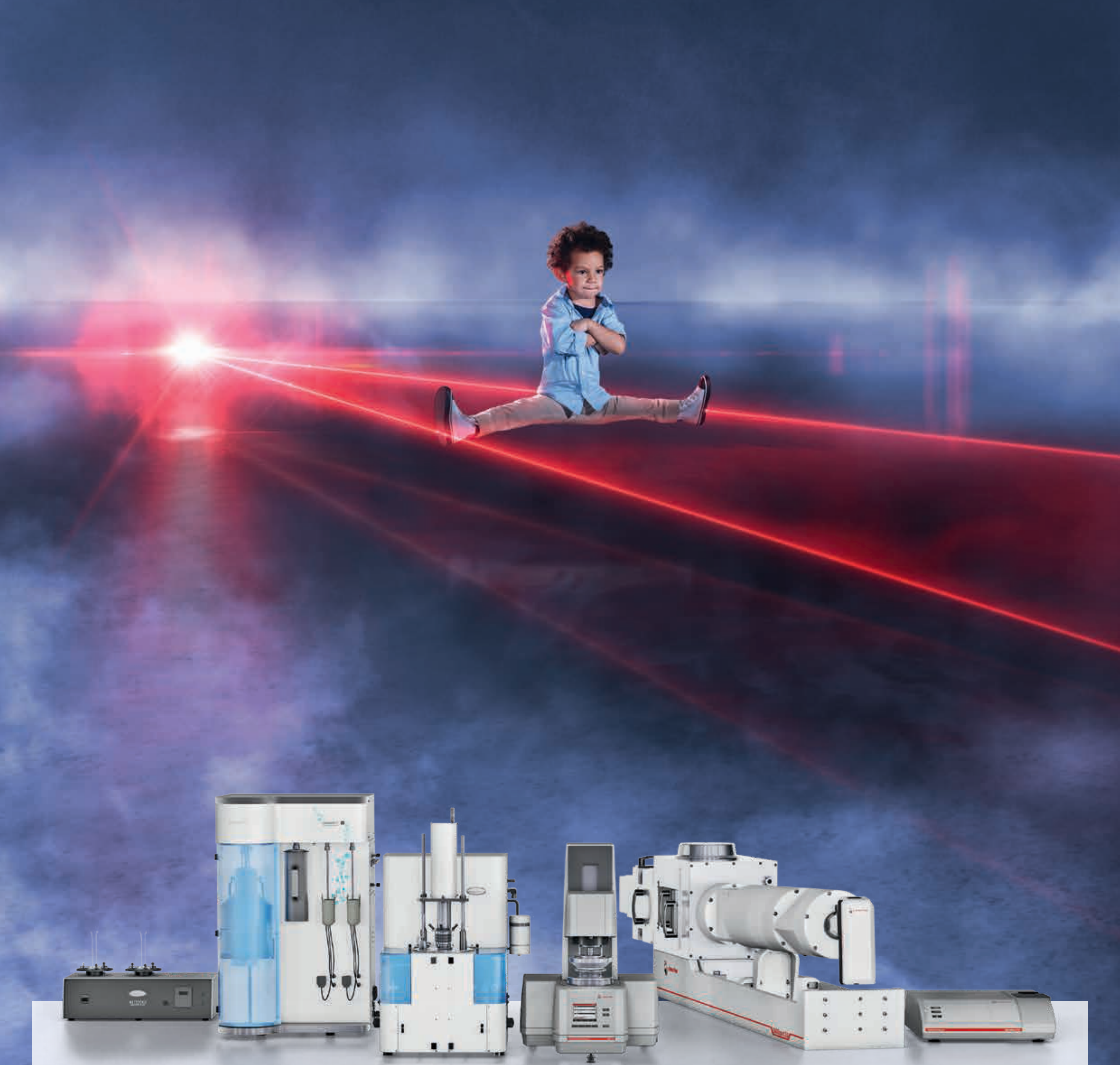

LABIMEX CZ **www.labimexcz.cz**

TESTOVACÍ KOMORY

PRO ENVIRONMENTÁLNÍ ZKOUŠKY V LABORATOŘÍCH

korozní solné a kondenzační komory

⇐ truhlové a skříňové komory
objemy 300, 400, 1000, 2000 litrů

truhlové, objemy 640 a 1100 litrů ⇒
jednoúčelové i kombinované
testy lakovaných a galvanizovaných
povrchů

komory pro sluneční simulace Xe světlem ⇒

s pevnou zkušební plochou
nebo otočným držákem,
regulace osvitu, teploty
a relativní vlhkosti
INDOOR a OUTDOOR zkoušky

⇐ UV testery ultrafialovým zářením

osvit, kondenzační podmínky,
simulace deště

⇐ klimatické a teplotní komory

rozsahy -40 resp. -70°C až +180°C, 10
- 98% RH, komory bez chlazení
až 300°C, objemy 53 - 720 litrů

prachové a ostřikové (spray) komory ⇒

stanovení odolnosti výrobku vůči
vniknutí vody nebo prachu, odolnost
vůči působení abrazivního prachu
stanovení stupně krytí IP

Komory odpovídají plnění zkušebních norem ČSN, ISO, EN, DIN, SAE, ASTM

Zajišťujeme prodej, servis, dodávky, instalace, zaškolení, poradenství, kalibrace.

LABIMEX CZ s.r.o.

Počernická 272/96
108 00 Praha 10 - Malešice
Česká republika
info@labimex.cz
www.labimexcz.cz
tel : +420 241 740 120

Dr. Ing. Milan Pražák

prazak@labimex.cz
+420 602 366 407

Ing. Jan Kolačný
kolacny@labimex.cz
+420 727 835 669

Ing. Jozef Maco

ingjozefmaco@gmail.com
+421 327 798 346
+421 910 970 699
Rakoľuby 697
916 31 Kočovce
Slovensko

LABIMEX CZ s.r.o.

VYBAVENÍ LABORATOŘÍ A ZKUŠEBEN

Počernická 272/96, 108 00 Praha 10, Malešice tel. +420-241 740 120, fax +420-241 740 138
prazak@labimex.cz, +420 602 366 407; kolacny@labimex.cz, +420 727 835 669

Q-LAB Corporation

- ✓ korozní komory pro zkoušky v solné mlze
- ✓ korozní komory pro cyklické i kombinované solné a kondenzační zkoušky
- ✓ korozní komory pro zkoušky s řízenou rel. vlhkostí a samočisticím ostřikovým systémem
- ✓ komory pro testy UV zářením kombinované s kondenzačními testy
- ✓ komory pro sluneční simulaci xenonovým světlem – xenotesty
- ✓ standardizované testovací plechy – zkušební panely
- ✓ možnost testování vzorků na venkovních expozicích – Florida a Arizona

Liebisch

- ✓ korozní komory pro zkoušky v solné mlze
- ✓ korozní komory pro kondenzační zkoušky s možností doplnění zkoušek s SO_2 (Kesternich testy)
- ✓ korozní komory pro cyklické i kombinované solné a kondenzační zkoušky

PTL Dr. Grabenhorst

- ✓ prachové komory pro zkoušky odolnosti proti vniknutí standardního prachu do výrobků – testy stupně krytí IP
- ✓ sprayové komory pro zkoušky odolnosti proti vniknutí vody do výrobků – testy stupně krytí IP
- ✓ ruční sprchy a trysky pro zkoušky odolnosti proti vniknutí vody do dílů, výrobků - testy stupně krytí IP
- ✓ žhavá smyčka – přístroj pro testování požární bezpečnosti (hořlavosti materiálů)
- ✓ přístroj na testování plazivých proudů – testování tvorby vodivých cest na povrchu materiálů
- ✓ sondy na zkoušky vniknutím cizího předmětu – testy stupně krytí IP 0-4X

Binder

- ✓ klimatické komory s řízenou teplotou i vlhkostí
- ✓ teplotní komory s řízenou teplotou
- ✓ sušárny s přirozenou i nucenou cirkulací vzduchu

ELASTOCON

- ✓ přístroje na mechanické a fyzikální zkoušky plastů a pryží (testy stárnutí, relaxace, creepu, fogging test)

ELCOMETER, BYK GARDNER

- ✓ přístroje pro hodnocení povrchových vrstev a barev, barevnost, lesk, tloušťka vrstvy

BETTERSIZE

- ✓ analyzátory tvaru částic, laserové granulometry

SOBRIETY

THE ULTIMATE STRAIN ANALYSIS SYSTEM

MERCURY RT
REAL-TIME TRACKING SYSTEM

MATERIAL TESTING

The measuring system is applied for complex material testing analysis in 2D or 3D and is based on non-contact measurement using digital cameras. It is designed for maximum flexibility to comply with any requirements of our customers. It is suitable for measurement of components of all sizes, consisting of practically any material at temperatures as high as 1400°C. Both static and dynamic events can be evaluated.

- optical non-contact measuring system
- complex analysis of strains and displacements in 3D space
- analysis of material properties and component testing for product development
- goes beyond standard tensometers and extensometers
- based on digital image correlation technology (DIC) with high sub-pixel accuracy
- designed for quick and easy set-up
- suitable for test rigs, test centres and academic purposes
- visually represented data for simple interpretation
- enables measurement in climate chambers

VIBROGRAPHY

The system performs vibration measurement and analysis, vibration diagnostics of harmonic and transient processes. It allows for analysing events in the frequency domain (FFT).

The output is data – e.g. deflection size, velocity and acceleration. Other outputs are diagrams – frequency diagram, phase diagram, operational deflection shape (mode shapes), Campbell diagram.

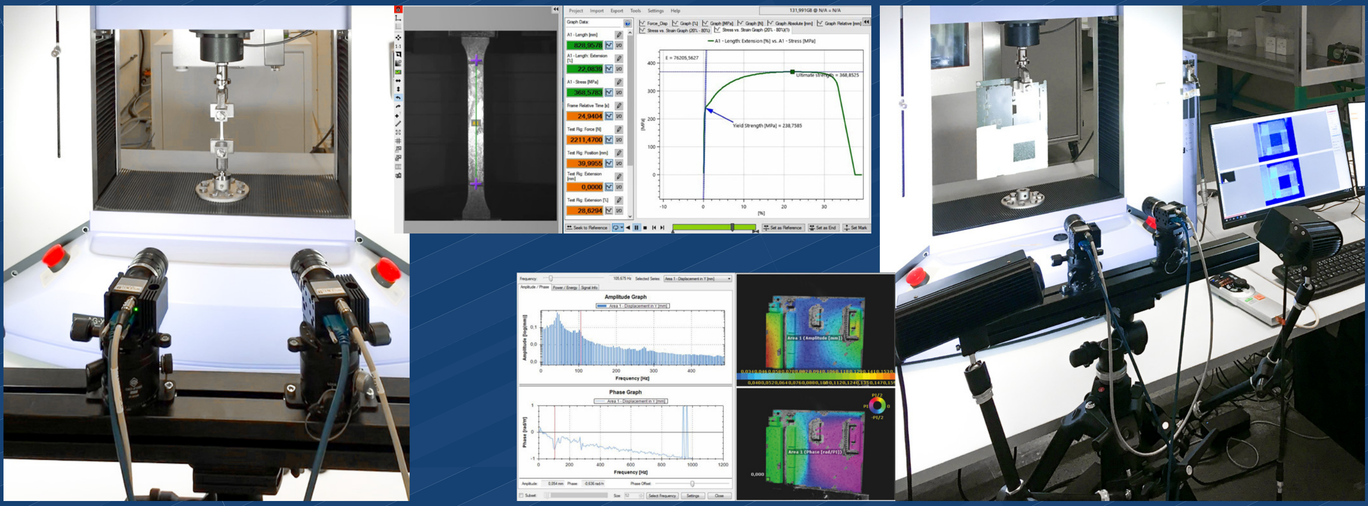

Sobriety s.r.o., Blanenská 1288/27, 664 34 Kuřim, Czech Republic, T: +420 541 231 696, E: sales@sobriety.cz, www.sobriety.cz

SVOS, spol. s r.o. Chrudimská 1663, Přelouč 535 01, Czech Republic
www.armsvos.cz, tel. +420 466 955 743, email svos@armsvos.cz

Founded in 1992 and located in Přelouč, Czech Republic, **SVOS is one of the leading European producers of armoured vehicles** for various applications. Since its establishment, the company has delivered **more than 3200 vehicles to 100 operators in 60 countries** including the most prestigious diplomatic corps, top-equipped law enforcement agencies and widely deployed armed forces. Today the company provides not only design, development and production of armoured vehicles, but also own production of ballistic glass.

The SVOS portfolio includes:

- **Armoured VIP limousines**
- **Armoured vans and trucks**
- **Armoured cross-country vehicles**
- **Cash-in-transit vehicles**
- **Law-enforcement vehicles**
- **Special military vehicles**
- **Own design multipurpose military vehicles**

The **top product called Perun**, a multipurpose military vehicle, was developed in order to address the global demand for vehicles with new standards in troops protection. SVOS introduced on the market a brand-new vehicle truly redefining the operators´ safety expectations. The safety concept of the vehicle includes several patent-protected solutions and presents a sophisticated complex of matters allowing survivability of the vehicle after multiple blast or ballistic impact. Carefully selected material with the V-hull shaped vehicle body and special blast deflecting and distribution shaping and blast-resistant seats allow to the crew to withstand even multiple blast threats, while the state-of-the-art body armouring utilizing in-house produced ballistic glazing allow the highest possible protection against rifle bullets. It has to be mentioned the Perun vehicle was in its open-top variant tested for threats no other vehicle was tested I the world yet and therefore pioneers and defines the new standard of the blast and ballistic tolerance.

Conference Sponsors:

Anton Paar

SKUPINA ČEZ

BioLogic
Science Instruments

pragolab

BOGGES

CHROMSPEC
SPOL. S R.O.

EVC

EV Battery

LABIMEX CZ

SOBRIETY

SVOS

tart®

Title: Advanced Batteries Accumulators and Fuel Cells – 20th ABAF

Edited: Jiří Vondrák
Marie Sedlaříková
Vítězslav Novák
Petr Bača

Publishing Office: Jiří Vondrák
Marie Sedlaříková
Vítězslav Novák
Petr Bača

Deadline: August 1st 2019

Publisher: Brno University of Technology
Faculty of Electrical Engineering and Communication
Department of Electrical and Electronic Technology

Year: 2019

ISBN 978-80-214-5774-4